Structural Analysis of Brno's New Main Station's Entrance hall's timber roof

MSc Graduation Thesis Structural Engineering and Design (7K45M0)

J.J. (Job) Niessen

1507680

Graduation Committee:

Ir. A.P.H.W. (Arjan) Habraken (Tu/e)

Dr. Ir. S.P.G. (Faas) Moonen (Tu/e)

Ir. K. (Karsten) Nefs (Tu/e)

Final version

Graduation date: Eindhoven, May 12, 2023

PREFACE

The motivation for choosing this project comes from several reasons. First of all, the subject of parametric design was discussed during several courses of the master track Structural Engineering and Design. Using software like Grasshopper to efficiently analyse different design variants and optimize a structure is something that really appeals to me. This project gives the opportunity to learn and apply this technique. Next to that is the structure and architectural design very remarkable and interesting. Due to its unique design and importance it is set to become a landmark for the city of Brno. All together this made it a very interesting project to work on.

First of all I would like to thank Arjan Habraken for his guidance and feedback throughout the project. Then I would like to thank Faas Moonen and Karsten Nefs for their role on my committee. Finally I want to thank my family and friends for their support during the project.

Job Niessen
Tilburg, May 2023

ABSTRACT

The city of Brno is set to receive a new main train station designed by Benthem Crouwel Architects. The entrance hall of the station consists of five barrel vault-shaped segments which have a timber grid roof structure. This project is focussed on the structural design of the timber grid structure of the entrance hall's roof. Multiple design options such as the arch shape, grid pattern, support conditions, barrel vault variants and different connections are analysed.

For long-spanning structures, the own weight of the structure may become determining for the cross-section's dimensions. However, timber is a lightweight material which means it may be more vulnerable for effects due to snow and wind. It was discovered that the largest bending moments in the structure are caused by wind, for which a parabolic shape is favourable over the catenary line and ellipse.

The grid pattern in the architectural design is a flat grid which is vertically projected onto a base surface that defines the structures shape. This grid pattern can be shifted resulting in the elements being connected differently at the supports. Next to that can the base surface be divided into equal parts. The latter was found to result in slightly lower internal forces than the other grid patterns.

Different support conditions such as hinged, semi-rigid and rigid are analysed. Next to that, the combination of hinged supports at one side and rigid at the other side is considered. Semi-rigid supports, which can be created by connecting the adjacent arches, results in the lowest bending moment in the structure. In addition, it significantly reduces the deformation of the structure and increases the stability compared to hinged supports.

The barrel vault shaped segments depicted in the architectural design have a single-curved monoclastic shape. Applying a second curvature by creating a height difference along the vault will result in a saddle-like shape (anticlastic) or dome-like shape (synclastic). The double curvature may lead to more stiffness to the structure. Another possibility is incorporating the facades in the structural system. This will restrain the structure from the sideways movement caused by wind. It was found that the facades and the anticlastic shape will both reduce the deformations and maximum bending moment. The restraining of the facades will however result in significantly larger normal forces.

Three joint mechanisms are considered to be interesting for the timber grid structure. A segmented system in which the elements span from node to node, a lattice system in which the elements more or less have a woven structure and considering the structure to exist from individual arches with secondary beams in between. Because the secondary beams have hinged ends they only experience normal forces. The different joint mechanisms are compared to each other, first on their structural behaviour. Then a variant study is conducted in which their complexity in the manufacturing process and their potential material cost is analysed. The elements in the two different directions do not experience an equal magnitude of the internal forces. Therefore it is expected that considering the structure as individual arches with secondary beams leads to a design that requires the least amount of timber. Furthermore is it considered to be a relatively practical variant to realise. In the lattice system the elements are build-up from different layers with shear blocks, and twist along their length. The segmented system requires a relatively large amount of steel because each node exists from long steel slice plates with many bolts and a long steel tube to which the slice plates are connected.

A vertical load on an arch causes horizontal reaction forces at the supports. Because the roof is supported by a long-spanning structure, the supports are not restrained from moving horizontally. The beam of the long-spanning structure can however be used to create a truss-like structure and preventing the supports from moving horizontally. To obtain this truss effect, the supports in the corners of the roof need to be restrained from horizontal movement by the use of for example the facades or tie rods.

Based on the results from the analysis conducted during the project, a final structural system was chosen for which the detailing is worked out. The structure has an anticlastic shape, a catenary shape for the arches, semi-rigid supports and a grid pattern created by dividing the base surface into equal parts. Furthermore is the structure considered to exist from individual primary arches with secondary beams

in between. The detailing includes the supports, connections between the segments of the arches and the connections of the secondary beams to the arches. A criterium for the maximum allowable horizontal deformation was mostly determining for the final appearance and properties of the structure.

CONTENT

LIST OF FIGURES

LIST OF TABLES

1 INTRODUCTION

The city of Brno in the Czech Republic is set to receive a new main train station, designed by Benthem Crouwel Architects. The station's entrance hall, which serves as the main entrance, has a unique design consisting of five barrel vault-shaped parts. The roof structure consists of timber arches which span in two different directions, resulting in a timber grid structure. This goes along with the trend that has been going on in recent years towards the use of timber as a structural material. The increasing popularity of timber is due to a variety of factors. One reason is that it is a renewable (biobased) resource, which means it can be replenished over time through reforestation. Timber is also a lightweight material, making it more suitable for long-spanning structures. Different factors such as the size of the structure and orthotropic behaviour of timber make it that this structure requires careful design considerations. This project will cover the structural design of the entrance hall's roof. Different shapes and detailing options will be analysed and compared, leading to a final proposed structural design.

Figure 1 Architectural design for the new entrance hall, illustration from: Benthem Crouwel Architects (2020)

Several timber grid shells and structures such as the roof of the entrance hall have been made in the past. With the use of an appropriate form finding method in combination with the high strength-to-weight ratio of timber, long-spanning structures can be achieved. Therefore, these structures are often used in the construction of public buildings, such as exhibition spaces. Especially the development of digital design and fabrication has significantly influenced how timber grid-structures structures are build. The structures are more complex and diverse, and have gained an increasing interest (Chilton & Tang, 2017). On the other hand, the nodes can be geometrically complex and have to take into account the orthotropic behaviour of the timber. The nodes are especially important, as the mechanisms of the connections can greatly influence the structural behaviour.

Aside from the type of connections between the timber elements, there are some other design options which can be varied, and influence the distribution of the internal forces and deformations in the structure. These design options are:

- Shape of the arches: There are several options for the shape of the arches of the structure. Three possible shapes are an ellipse, parabola or catenary arch. Also, an optimization method can be used to obtain a shape which is optimal for the loads which act on the structure.
- Grid pattern: The grid pattern can be adjusted without creating a very different design. The grid pattern in the architectural design is a flat grid which is vertically projected on a surface which defines the shape of the structure. The flat grid can be slightly shifted which changes for example how the timber elements are connected at the supports. When a flat grid is vertically projected on a shape, the elements will have varying lengths. Another grid pattern can be created by

dividing the base surface of the structure into equal parts. This will result in a pattern in which all elements have the same length.

- Support conditions: The supports can be hinged, rigid or semi-rigid. This can be important for the overall stability of the structure and the distribution of the internal forces. Semi-rigid supports can be achieved by connecting adjacent arches at the supports, which will cause the arches to work together. Also, a combination of rigid and hinged supports will be considered.
- Barrel vault variants: Most of the parts in the architectural design have a monoclastic barrel vault shape. A second curvature could be added which may lead to greater structural stability and smaller internal forces. The middle part of the structure can be lowered resulting in a saddle-like (anticlastic) shape. The middle part could also be heightened which results in a dome-like (synclastic) shape. Something which will also be included in this part of the project is including the facades as part of the structural system. By applying rigid facades, lateral deformation of the structure is partially restrained. This could lead to a significantly different structural behaviour.

As could be seen in Figure 1 does the entrance hall exist from five different parts. These parts vary in sizes and are not all exactly barrel vault variants. One part in the corner has more of a triangular shape than a barrel vault shape. The outer part on the other side is an overhang. In the middle of the entrance hall, the largest part is located. Because this part has the largest span and height it may be determinate for the structural system which will eventually be used for all parts of the entrance hall. Therefore, this part will be used for the analysis of the above-described design options. The final product of this project will be a final design which can then function as an example for the remaining parts of the entrance hall.

1.1 Project phasing and scope

The project is divided in three different phases. The first phase is a preliminary study in which an overview of several structures, similar to the entrance hall's roof will be described. This will result in different ideas of how the roof could be made and may be leading for the remaining process of the project.

In the second phase the effect of the different design options will be analysed. The design possibilities are the shape of the arches, grid pattern, support conditions, double curvature and joint mechanism (type of connection). This analysis will be performed within the parametric design environment Grasshopper. Parametric design has the advantage that many different variants can be analysed in an efficient manner. Next to that can a plug-in called Karamba3D be used for the structural analysis. This way the variants can be created and structurally analysed in the same environment. For the structural analysis, a Grasshopper script is made for both a 2D and 3D model. The 2D model includes an arch which can be analysed with Karamba3D on the load combinations which are applicable to the structure. With this model some of the design possibilities explained above can be analysed including the shape, support conditions and stiffness of the joints between the elements. This model may help to explain why certain results are as they are in the 3D analysis.

The third and final phase includes a variant study and the applicable detailing. The different types of connections may affect certain factors such as transportation limits, practicality, manufacturing process, durability and costs differently. Therefore, different variants which are created following the analysis from the second phase will be partially worked out and compared to each other. The variants will be worked out such that they can be compared well on the criteria mentioned above. The variant study will lead to a final variant for which the most important detailing will be worked out. After the detailing, the final design will be given.

1.2 Architectural design and starting points

As illustrated in the architectural design in Figure 1 does the entrance hall exist from five barrel vault-shaped segments. Figure 2 provides a clearer overview of the various layers that make up the structure of the entrance hall. The figure shows the roof covering, timber grid structure, facades and the long-spanning structures that support the roof of the entrance hall.

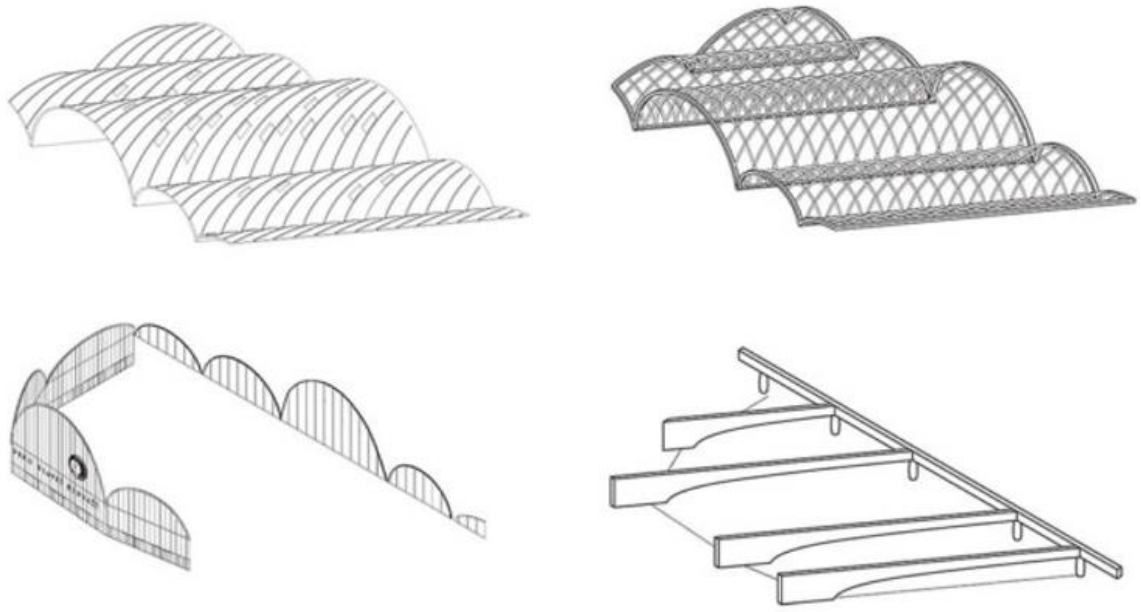

Figure 2 Different layers of structure entrance hall, illustration from: Jongtien et al. (n.d.)

The determination of the load cases and combinations applied to the structure is added in Appendix A. Due to the unique shape of the entrance hall, a Computational Fluid Dynamic (CFD) analysis is performed in order to obtain a realistic estimation of the wind load on the structure. The results of this CFD analysis can be found in Appendix B. For the different analysis in this project, often the load combinations in the Ultimate Limit State (ULS) are applied. Each load combination includes a specific load case. These load cases are schematically depicted, together with the corresponding load combination in the figure below. Load combination ULS-2 to 4 include load cases resulting from snow, and ULS-5 to 9 load cases resulting from wind. Load combination 1, which is not added to the figure only includes an equally distributed permanent load, for which a value of 0,5 kN/m2 is assumed.

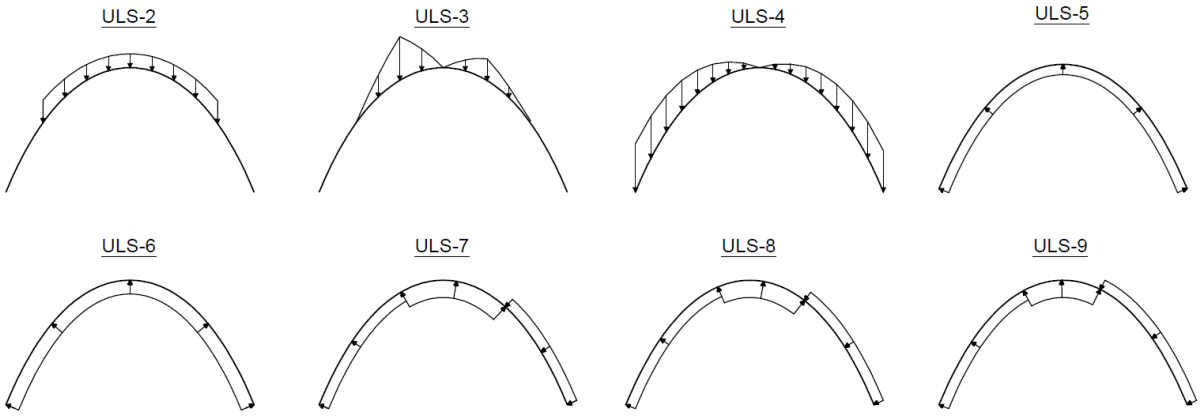

Figure 3 Schematic overview load cases applied for the analysis

The dimensions assumed for this project were derived and estimated from a catalogue (Jongtien et al., n.d.). The dimensions of the top view of the entrance hall, and for the large part of the roof are presented in the figure below.

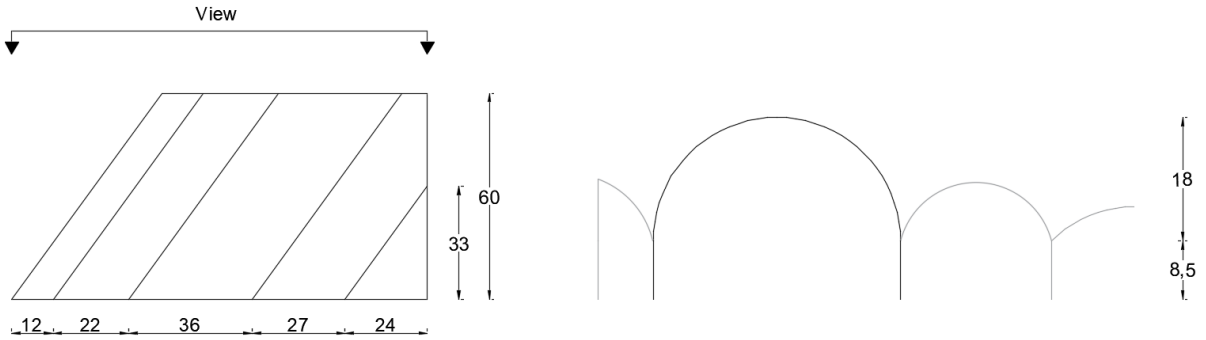

Figure 4 Assumed dimensions of the entrance hall structure

2 PRELIMINARY RESEARCH

A preliminary research was conducted on existing timber grid structures such as shells and domes. This was done in order to gain an overview of the various types of connections and form-finding methods that can be applied to the timber grid structure of the entrance hall. From the research, several structural systems became apparent that utilize specific connection types and manufacturing processes. The different connection types lead to specific structural systems as described by Larsson (2018). An overview of the different structural systems will be provided in this chapter including examples of structures that have implemented them in their design.

2.1 Zollinger roof system

The Zollinger roof system is a type of construction that consists of timber lamellas arranged in a diamond pattern. These lamellas are connected to each other at the middle of the crossing lamellas. It can therefore be seen as a type of reciprocal frame. This system was invented by German architect Friedrich Zollinger in a response to the shortage of timber in Germany after World War I. The low material cost, use of standardized elements and possibility for efficient dismantling made it a popular type of construction at that time. From today's perspective however, this system is considered to require a large amount of effort to realize. In addition, deformations caused by creep can weaken the connections over time and affect the durability of the structure (Franke et al., 2017). Despite its limitations, the Zollinger system remains a notable example of a system to create a timber grid structure.

The Toskana Thermal springs in Bad Sulza, Germany is a timber grid-shell that uses the Zollinger principle, but with a different type of connection that results in a rectangular grid pattern instead of a diamond pattern. Timber dowel connectors are used to prevent corrosion in the connections. The form-finding process for this structure involved digitally simulating a hanging model to determine a shape that is ideal for the load resulting from its own weight (Chilton & Tang, 2017).

a) b)

Figure 5 (a) Zollinger roof (Glentleiten Open Air Museum, n.d.), (b) Close-up of connection Toskana Thermal springs (Chilton & Tang, 2017)

2.2 Actively bend grid-shells

Actively bent grid shells are a type of structural system that uses a grid of timber beams that are actively bent into a desired shape. The process starts by bending a flat grid into a desired shape and then constraining it in that shape. The beams can be single-layered or double-layered. When the elements are double-layered, shear blocks are applied to create a composite effect, allowing the laths to function as a single cross-section. The principle of the actively bent grid shell was developed by Frei Otto. The first large scale application of this principle was in the construction of the Mannheim Multihalle pavilion, for which Otto used a physical hanging model as a form-finding method. Since then, the design and form-finding methods for timber actively bent grid shells have been refined and improved through the development of digital software. The stresses that occur during the deployment of flat grids must be carefully estimated to prevent breaking of the laths, while still allowing them to remain flexible enough for the bending process (Chilton & Tang, 2017).

Figure 6 Frei Otto's Mannheim Multihalle grid-shell, both pictures from: Wooddays (2020)

2.3 Lattice grid-shells

The principle of multi-layered elements crossing each other can also be applied with prefabricated elements. In this case the thickness of the laths is not limited by the manufacturing process. This is for example done for the roof of Centre Pompidou-Metz designed by architect Shigeru Ban. The digital advancement together with a CNC milling machine made it possible to prefabricate the complex glulam elements for the grid. The pre-fabricated parts can only have a limited length. Therefore, individual parts of the grid were connected to each other through two steel plates per lath with a thickness of 5 mm, connected with bolts. At the nodes the layers were connected through a single M24 bolt. The bolts were prestressed through 125 mm spring washers (Chilton & Tang, 2017).

Another interesting example is the Waitomo Caves visitor centre in New Zealand (Figure 7). The structure has a span of 28 meters and has a grid which is drawn onto a toroid shape in a diagonal way. The structure itself has an arched cross-section making it similar to the entrance hall's roof parts. The elements are twisted along their lengths such that the elements remain oriented according to the base surface normal. Each 28 m long layer is made from three pre-fabricated Laminated Veneer Lumber (LVL) sections. These sections were jointed and screwed together on-side. In between the layers glued-laminated shear blocks are placed. At the nodes, the layers are connection through a single 20 mm bolt. The structure is stabilised through stainless steel diagonal ties (Chilton & Tang, 2017).

a) b)

Figure 7 (a) Waitomo cave visitor centre (Picture from: Vector Foiltec, 2023), (b) Centre-Pompidou Metz (Picture from: L'Express, 2010)

2.4 Segmented grid-shell

In a segmented system, the beams are discontinuous and span from node to node. The timber elements themselves are straight, and the curvature of the structure is created by the nodes. Structures that utilize this system, such as the CrossRail place at Canary Wharf in London, often have a single-layered construction and custom steel nodes. This structure, with a barrel vault shape and a span of 12 meters, consists of 1418 Glulam elements of varying lengths, grades, and depths. The straight elements are oriented according to the normal of the base surface of the structure, with the twisting realised through

the connections. These steel connections are geometrically complex, and many of the nodes are unique (Chilton & Tang, 2017). Other examples of this principle can be found in timber reticulated domes, such as the Tacoma Dome in Washington, USA, the Saldome 2 in Aargau, Switzerland, the Odate dome in Akita, Japan, and the wooden domes in Brindisi, Italy (Shu et al., 2020).

Several types of connections have been developed for these structures, with three steel connectors for a segmented system shown in Figure 7. The first is a tendon embedded timber joint, similar to the joint used in the CrossRail place at Canary Wharf. The second is a steel plate splint joint, used in one of the domes in Brindisi. These joints provide some rotational stiffness and are suitable for large spans, but their torsional resistance is weak. Shu et al. (2020) examined another type of joint, a slotted steel plate joint, which connects the steel plate to the timber elements using bolts. The different connections can be seen in the figure below.

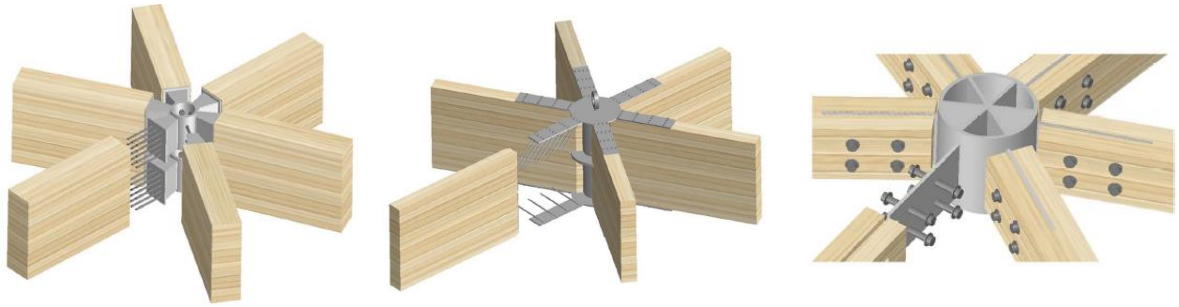

a) b) c)

Figure 8 Connection types for the segmented system (Shu et al., 2020): (a) embedded timber joint, (b) plate splint joint, (c) slotted in steel plate joint

2.5 Ribbed grid-shell

The ribbed grid-shell, developed by Julius Natterer, is an innovative variation on Frei Otto's actively bent grid-shell. It is constructed using multi-layered thin laths, which are filled with short-length laths rather than shear blocks and are then nailed together. Unlike Frei Otto's method of bending a flat grid into shape, the ribbed grid-shell is built directly into its final shape using a temporary scaffolding. This allows for the use of thinner laths that are more flexible and less prone to breaking during construction. Additionally, the ability to easily insert more laths if additional bending stiffness is needed is a benefit of this system. The short-length laths that fill the spaces between the layers create a single layer of crossing elements (Chilton & Tang, 2017).

Several structures have been built using the ribbed grid-shell system, including the boat house in Morges, Switzerland, which has a barrel vault shape and measures 60 meters in length, 20 meters in span, and 12 meters in height. Another example is the polydome in Ecublens, Switzerland, which has a 27,5 meter radius spherical profile and a rectangular plan of 25x25 meters. This structure was constructed by laying laths over a temporary scaffolding and then building them up into the final grid-shell elements. One unique aspect of the polydome is that the element density is higher in the middle to accommodate the distribution of forces (Chilton & Tang, 2017). The freedom in the grid pattern allowed by the ribbed grid-shell system is demonstrated by these examples, which are shown in the figure below.

a) b)

Figure 9 (a) Boat house Morges, Switzerland, (b) Polydome Ecublens, Switzerland. Both from Chilton & Tang (2017)

2.6 Other systems

Next to the systems described above there are some other more unique structural systems other than the ones described in this chapter. One example is the roof of the Swatch Headquarters in Biel, Switzerland by Shigeru Ban. The grid exists from pre-fabricated glulam elements which fit into each other like a puzzle by the use of halving lap joints. Another example is the Cambridge mosque, produced by Blumer Lehmann, which is fully parametrically designed by Marks Barfield Architects. The structure exist from 2746 elements with 145 variations (Blumer-Lehmann AG, n.d.).

a) b)

Figure 10 (a) Cambridge mosque (Carlson, 2022), (b) Swatch headquarters (Gonchar, 2019)

3 SHAPE OF THE ARCHES

The first design option of the roof structure that will be analysed is the shape of the arches. In older structures which were made out of stone, also arches were used. Because these structures were made out of stone, the own weight of the structure was the most important load and would therefore be determinate for the shape. The ideal shape for an equally distributed load is the catenary line. This is the shape obtained when a rope is suspended between two fixed points. By doing so the rope will deform in the most optimal shape for its own weight. In this shape the rope will only experience normal tension forces and no bending moments due to its own weight. If this shape would somehow be fixated and turned upside down the rope will only experience normal compression forces instead of tensile forces. The main structure of the entrance hall's roof will however be made with timber which is a relatively lightweight material. Therefore, wind and snow loads may have a greater impact on the internal forces than the weight of the structure, which means that the catenary shape may not be the optimal shape for the arches.

In this study, different variants of arch shapes will be analysed and compared based on all load combinations. The variants include standard arch shapes such as an ellipse, catenary, and parabola, as well as an optimized shape determined using the Particle Spring Method. The analysis of the different shapes will be performed using a 2D and 3D Grasshopper model, with Karamba3D for the structural analysis. The load cases and combinations can be found in Appendix A.

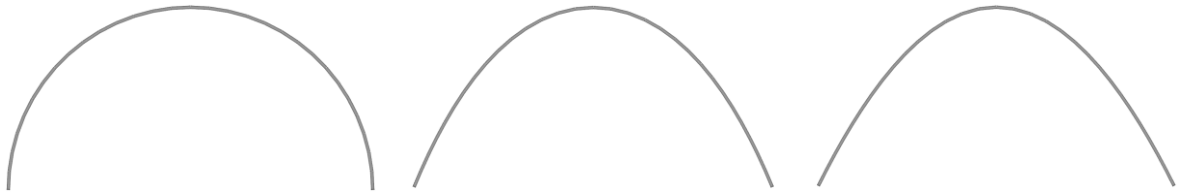

Figure 11 Possible shapes for the arches: (a) ellipse, (b) catenary line, (c) parabola

3.1 Arch shape analysis 2D

First, a 2D analysis is performed to get a first impression of the differences of the internal forces between the standard shapes. The standard shapes were as described in the introduction an ellipse, catenary line and parabola (Figure 11). The structure was given hinged supports, a rectangular cross-section of 300x450 mm and GL24h as material with the properties according to EN 14080.

The results of the analysis can be seen in the table below. For each shape the bending moment, normal force and shear force can be seen for every load combination in the Ultimate Limit State (ULS).

Table 1 Internal forces with hinged supports (2D analysis)

	Ellipse			**Catenary**			**Parabola**		
	M [kNm]	N [kN]	V [kN]	M [kNm]	N [kN]	V [kN]	M [kNm]	N [kN]	V [kN]
ULS_1	42,02	41,21	9,77	0,97	41,50	2,11	10,69	41,35	3,35
ULS_2	75,62	62,26	17,07	6,82	64,70	3,75	16,93	67,15	5,67
ULS_3	83,80	62,69	17,29	28,63	65,44	8,52	37,10	68,61	11,30
ULS_4	87,03	139,03	22,71	49,44	128,14	12,74	71,86	124,87	18,10
ULS_5	37,27	20,17	9,80	21,12	21,32	4,95	17,73	21,43	4,06
ULS_6	37,01	18,52	10,92	37,53	17,73	9,45	39,41	17,56	9,13
ULS_7	59,24	16,42	10,28	56,70	18,30	9,65	51,66	17,86	9,73
ULS_8	93,04	14,23	12,32	74,40	14,65	11,80	67,80	14,16	11,65
ULS_9	110,87	15,58	19,76	95,37	19,43	15,14	89,87	19,87	14,10

Considering the load combinations which include snow load cases (ULS-2, 3 and 4), the catenary line seems to be the shape with the lowest bending moments. This would be expected since the snow load acts vertically like the gravity load of a structure. Looking at the wind loads however (ULS-5 to 9), the parabola seems to result in the lowest bending moments. Especially the last three of these load combinations generally cause the highest bending moments. These load combinations include wind load cases in which wind pressure acts on one side of the arch and wind suction on the other side.

3.2 Optimization of arch

As previously discussed in chapter 2, various form-finding methods have been used to determine the shapes of past timber grid-shell structures. For example, the shape of the Multihalle Mannheim by Frei Otto was obtained by the use of a hanging model, a method that finds a shape that experiences only normal tensile forces. By flipping this shape, a shape is obtained that only experiences normal compressive forces. Today, computer-aided software is available for the form-finding of structure shapes, including methods such as the Force Density Method, Particle Spring Method, and Dynamic Relaxation. Alongside the standard shapes, an additional variant will be considered which is an arch shape optimized using the Particle Spring method.

For this project a form-finding method will be used which utilizes a combination between the Particle Spring Method and a generic solver. This method is described by van Vooren (2018) for the optimization process of 3D concrete printed arches. The main advantage of this method compared to a hanging model is that it takes into account all load combinations. The arch is thus optimized for the loads resulting from snow and wind as well instead of only it's own weight as is the case for a hanging model. To explain this form-finding method, first a brief explination of the Particle Spring Method and generic solver is given. Then an explination will be given on how they are used together to find an optimized shape.

3.2.1 Particle spring method

The particle spring method is used to create physical simulations. The Particle Spring system is a model which exists out of a chain of masses which are called particles. These particles are connected with each other by axial springs. Each spring is given a length, constant axial stiffness and a damping coefficient. The damping coefficient is needed to prevent oscullation of the system. In the springs, no bending is allowed. Therefore the system will only experience pure tensile forces. The particles are given a position, mass and a velocity. Next to that can an external force be applied to them. This results in a summerized vector which is based on all forces acting on the particles. The particles can furthermore be restrained in any direction. The system will change the length of the axial springs untill static equilibrium is reached (Kilian & Ochsendorf, 2005).

3.2.2 Generic solver

Galapagos is a generic solver that is available as a component for the 3D modelling software Rhino3D. It can be used to find solutions for a wide range of problems by using an optimization process. A set of variables or so-called genes is adjusted in order to find the best possible solution to a given problem. The problem is basically a number depending on these variables which has to be maximized or minimized. Galapagos works by iteratively adjusting the variables to try to find a solution that is most likely to be optimal (Rutten, 2013). Galapagos is used in combination with Grasshopper which allows users to define and adjust the variables that are used by the solver. This can be helpful for tasks such as optimizing the shape of a structure.

If the particle spring system is a chain in which the particles at the ends are restrained in any direction, and no horizontal external forces are applied this will result in a catenary arch. As explained in the introduction of this chapter, a caternary arch is the ideal shape for a equally distributed load. When horizontal forces are applied to the particles, the resulting forces will change, and therefore the shape of the arch will change as well. As explained above does the generic solver require a problem to maximize or minimize and genes which can be adjusted for the maximization or minimization process. In this case

the horizontal forces will function as the genes for the generic solver Galapagos. Everytime the horizontal forces are adjusted the shape changes, and Karamba3D will calculate the maximum bending moment resulting from all load combinations. This bending moment will be given to the Galapagos componant as goal to be minimized. The initial height of the system is determined by the vertical forces which are applied to the particles and the initial length and stiffness given to the springs. By adjusting these variables the required height can be obtained. To ensure that the final shape is symmetrical, the script is made such way that the horizontal force on one particle is always equal to the horizontal force on the opposite particle but in the opposite direction.

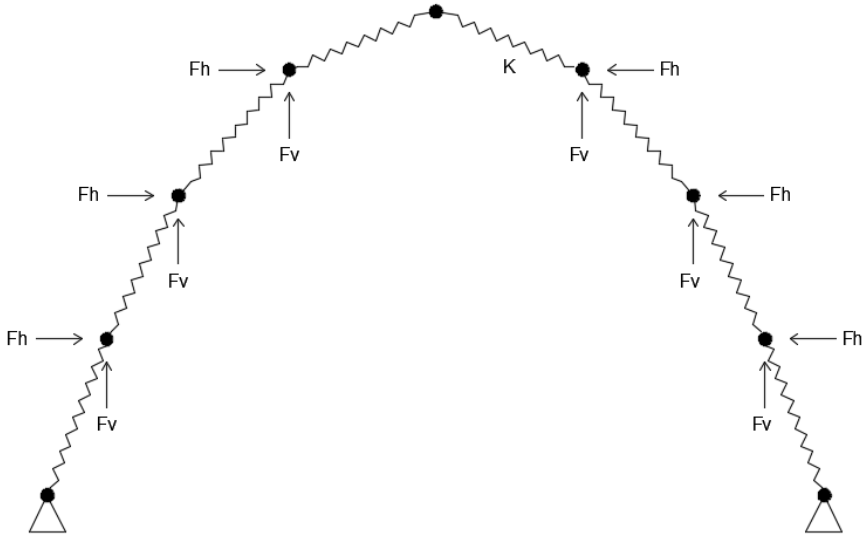

Figure 12 Optimization with Particle spring method

3.2.3 Optimized arch

The optimization process can be done in 2D and in 3D. In both cases Karamba3D will calculate the maximum bending moment in the structure resulting from all load combinations. In a 3D model it will however change the arch which defines the base shape of the structure. For this analysis it is decided to perform the process in a 2D model. Then this shape will be applied to the 3D model. The main reason for this is that the 3D model is much slower. Therefore, Galapagos will need a lot of time to obtain a good result. The final shape which resulted from the optimization process is shown in the figure below. In the next paragraph the standard shapes together with the optimized shape will be compared using the 3D model.

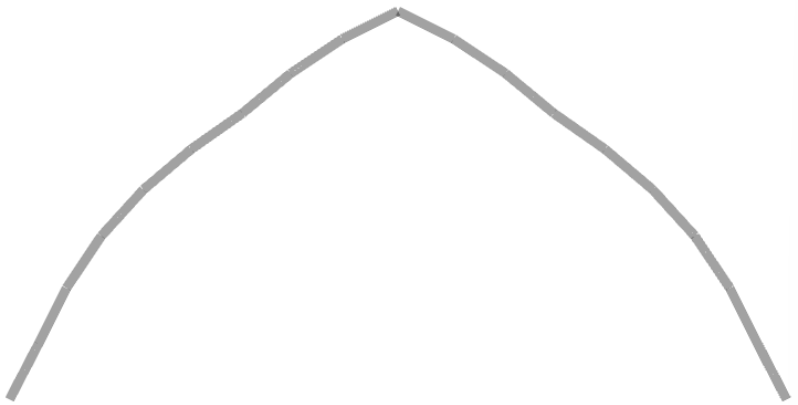

Figure 13 Optimized shape

3.3 Arch shape analysis 3D

The shapes which were analysed in 2D will be compared again in a 3D model. Also, the optimized shape will be taken into account as a fourth variant. This will be done to check if the conclusions about the shape in 3D are the same. If this is not the case the optimization process is to be done another way in 3D. The 3D model which is used for this analysis is the biggest part of the entrance hall's roof. The grid pattern which is applied is a pattern created by dividing a base surface into equal parts. In the next chapter this will be explained in more detail. This grid variant is then referred to as grid pattern 3.

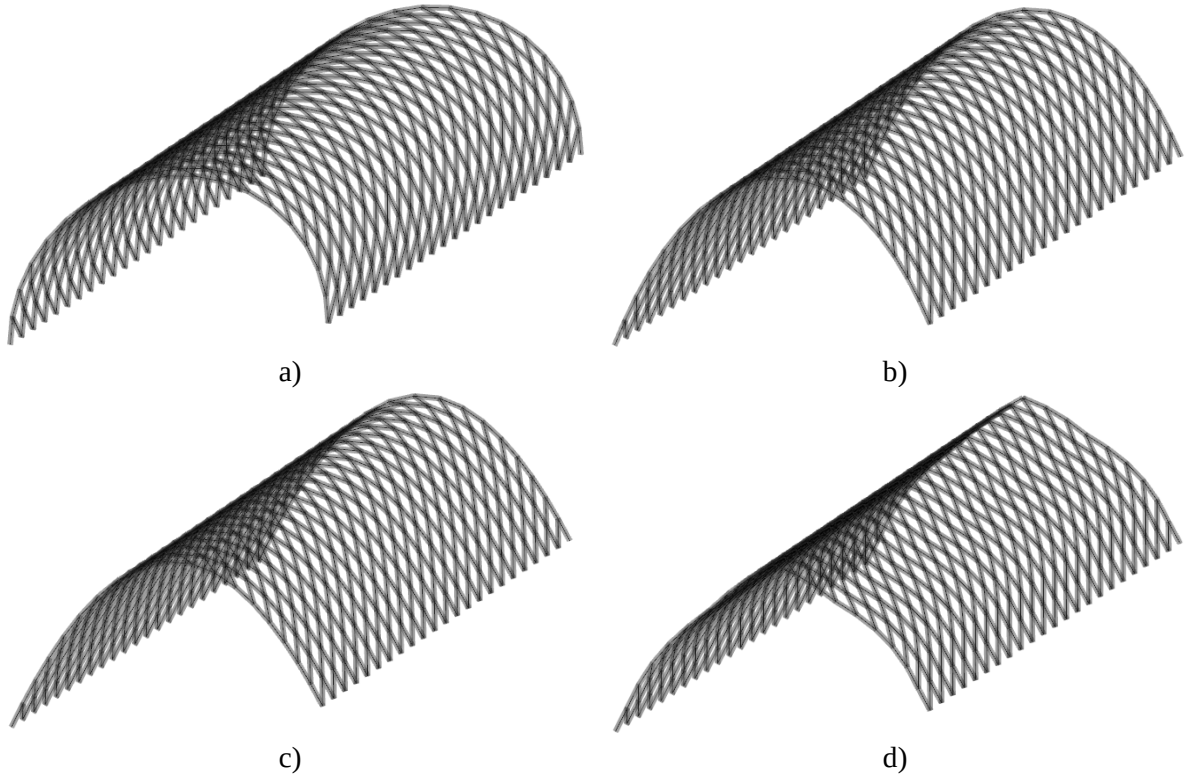

Figure 14 3D model with: a) ellipse; b) catenary; c) parabola; d) optimized shape

The supports in the 3D model are hinged and the properties for the elements are the same as in the 2D model. This means that the cross-section dimensions and material properties are the same. Furthermore, are only elements applied in the two directions as shown in the architectural design which are rigidly connected at the nodes. This means no bracing elements or joint properties have been applied yet.

Table 2 Maximum internal forces for different arch shapes (3D analysis)

	Ellipse	**Catenary**	**Parabola**	**Optimized**
M_y [KNm]	250,99	221,7	210,88	176,87
M_z [KNm]	27,28	56,31	47,85	51,61
M_t [KNm]	10,34	9,28	8,99	7,91
V_z [KN]	17,31	34,78	30,06	26,89
V_y [KN]	52,42	46,65	44,38	46,28
N_c [KN]	436,73	348,33	346,65	326,71
N_t [KN]	247,71	215,35	198,27	192,50

In the table above the maximum internal forces resulting from all load combinations are given for each shape. The maximum bending moments are caused by wind while the highest normal forces are caused by snow accumulation. Between the standard shapes, the parabola results in the lowest bending moment. The 2D analysis already showed that the wind loads cause a lower bending moment when a parabolic

shape is applied. The optimized shape however results in an even lower bending moment due to wind as it would be expected. The optimized arch shape looks very similar to a gothic arch. This type of arch is used in older structures such as cathedrals but also for greenhouses, and is shown to better resist lateral loads resulting from wind than more circular arches (Nafisi Poor & Javid, 2021). It seems that a more pointed shape helps to resist the lateral wind loads, which also explains why the parabola resists the wind load best out of the standard shapes. It should be mentioned that the differences between the shapes decrease if the supports are semi-rigid or rigid. The bending moment is more concentrated at the supports instead of in the arch itself in this case.

3.4 Effect of increasing permanent load

Adding more permanent load to an arch can help to decrease the effect of the wind load by increasing the overall stiffness of the structure. This is because a more heavily loaded arch will be more resistant to deformation under such loads. The added permanent load can be in the form of additional dead load on the structure resulting from the weight of roofing material. This will increase the total load that the structure must support, and the increased stiffness might help the structure to better resist the wind load. First, the maximum horizontal and vertical deformation is presented in the table below for each shape variant resulting from the SLS load combinations. In this table the horizontal deformation in mm is depicted by H and the vertical deformation with V. The left column of the table shows the permanent load in kN/m^2.

Table 3 Effect permanent load on horizontal and vertical deformation per arch variant

	Ellipse		**Catenary**		**Parabola**		**Optimized**	
	H	V	H	V	H	V	H	V
0,0	537,28	217,63	378,48	194,24	340,56	195,97	270,32	167,98
0,5	549,87	228,41	380,01	194,45	336,63	194,20	269,51	158,98
1,0	568,96	250,12	381,46	195,36	335,58	194,67	268,78	167,74
1,5	593,79	274,00	382,91	196,26	334,66	195,24	266,98	176,79
2,0	618,17	309,60	384,25	197,11	333,81	197,71	273,96	185,83

The table shows that increasing the permanent load has a different effect on each shape variant. For the ellipse it has a negative effect as both the horizontal and vertical deformation increase as the permanent load increases. For the catenary shape the effect is almost negligible, for which the explanation may be that the maximum bending moment of the catenary shape remains unchanged, as a uniformly distributed load does not result in a bending moment. For the parabolic shape the effect is very small as well. It does have a slight positive effect on the horizontal deformation, and almost no effect on the vertical deformation. For the optimized shape it can mainly affect the vertical deformation negatively if the permanent load is significantly increased. The effect of the increasing permanent load on the bending moment is given for each load combination per shape variant in the table below.

Table 4 Effect increasement of permanent load on bending moment for different arch shape variants

Ellipse									
	ULS-1	*ULS-2*	*ULS-3*	*ULS-4*	*ULS-5*	*ULS-6*	*ULS-7*	*ULS-8*	*ULS-9*
0,5 [kN/m²]	88,66	173,29	181,93	171,95	128,60	150,12	220,73	250,18	250,99
1,0 [kN/m²]	143,73	217,35	225,98	216,00	172,65	194,17	232,55	227,57	287,67
1,5 [kN/m²]	198,79	261,40	270,03	260,05	216,70	238,22	269,23	250,71	324,35
2,0 [kN/m²]	253,86	305,45	314,02	304,13	261,03	282,77	311,55	293,54	360,96
Catenary									
0,5 [kN/m²]	5,53	23,55	53,65	102,19	85,00	127,83	149,09	191,31	221,70
1,0 [kN/m²]	9,41	22,10	52,40	103,75	83,55	126,38	150,35	192,56	220,45
1,5 [kN/m²]	13,30	20,65	51,15	105,42	82,10	124,92	151,60	193,81	219,20
2,0 [kN/m²]	17,19	19,20	49,90	107,08	80,65	123,47	152,85	195,06	217,95
Parabola									
0,5 [kN/m²]	21,89	21,78	51,04	144,09	76,32	121,66	133,98	171,54	210,88
1,0 [kN/m²]	35,59	32,74	54,50	154,04	66,36	111,70	143,57	181,14	201,28
1,5 [kN/m²]	49,29	43,70	60,99	164,00	56,40	101,73	153,17	190,74	201,90
2,0 [kN/m²]	62,98	54,66	68,24	173,95	46,44	91,78	162,77	200,34	208,53
Optimized shape									
0,5 [kN/m²]	42,66	61,14	97,89	173,50	76,78	136,73	94,37	114,66	176,87
1,0 [kN/m²]	68,22	81,60	113,19	193,99	78,70	133,68	89,15	114,97	176,57
1,5 [kN/m²]	93,79	102,11	128,48	214,11	80,74	135,25	95,60	118,24	177,33
2,0 [kN/m²]	119,36	122,57	143,78	234,56	82,66	137,18	100,77	123,41	185,13

The only significant positive effect occurs for the parabolic shape for ULS-5 and ULS-6. These load combinations contain a wind load case in which only wind suction acts on the arches. The bending moment resulting from the permanent load in the parabola most likely counters the bending moment resulting from wind suction. It should furthermore be noted that the normal compressive force increases significantly in the structure. This can eventually have a negative effect on the stability of the structure, as well as the amount of material. The Eurocode takes into account a combination of bending moments and normal forces. A very high normal force can therefore lead to bigger cross-sections. Another reason not to apply extra permanent load on the large part is because the horizontal reaction forces increase as the permanent load increases. The arches are placed on a large long-spanning beam and therefore these horizontal forces cannot be transferred to the foundation easily. It could therefore be useful to increase the permanent load on the smaller adjacent parts to balance the horizontal forces out as much as possible. In Chapter 9 the effect of the horizontal movement at the supports is analysed further.

3.5 Conclusion on the arch shape

The analysis has shown that a wind load case with wind pressure at one side of the arch and wind suction at the other side results in the highest bending moments. Considering the standard shapes, the parabolic arch gives the lowest maximum bending moment. Looking at the bending moments occurring from snow, it should be mentioned that the catenary arch is favourable. The moment can be decreased further by applying the optimized shape. This results in a shape which looks similar to a gothic arch, a shape known to help resist lateral loads due to wind. This shape however, deviates significantly from the architectural design. In addition, certain detailing or design options may be required for specifically this shape. It will therefore not be considered in the remaining part of this project. Finally, other properties such as the radius of curvature and the use of hinges, which can affect the distribution of internal forces and ultimately the maximum bending moment, should also be taken into consideration in the final shape selection.

4 GRID PATTERN

In the architectural design, the grid structure of the entrance hall's roof parts has elements spanning in two different directions. The grid of the main building is extended to the entrance hall, resulting in the first direction (secondary direction) for the elements. The other arches span in a direction perpendicular to the first direction (primary direction), as shown in the figure below. From above, the grid seems to have a simple rectangular pattern. However, from the side, it can be seen that the elements have varying lengths. There are many other different grid patterns that can be applied, such as triangular and even honeycomb patterns, which can influence the structural behaviour. However, it is not the intention to deviate too much from the architectural design. Smaller adjustments can be made that won't result in a completely different structure, but these small adjustments can still have a significant influence on the structural behaviour. In this chapter, three different variants for the grid pattern will be analysed. First, an explanation will be given on how the variants are created and some practical issues will be discussed. Then, the variants will be compared on the internal forces resulting from different load combinations.

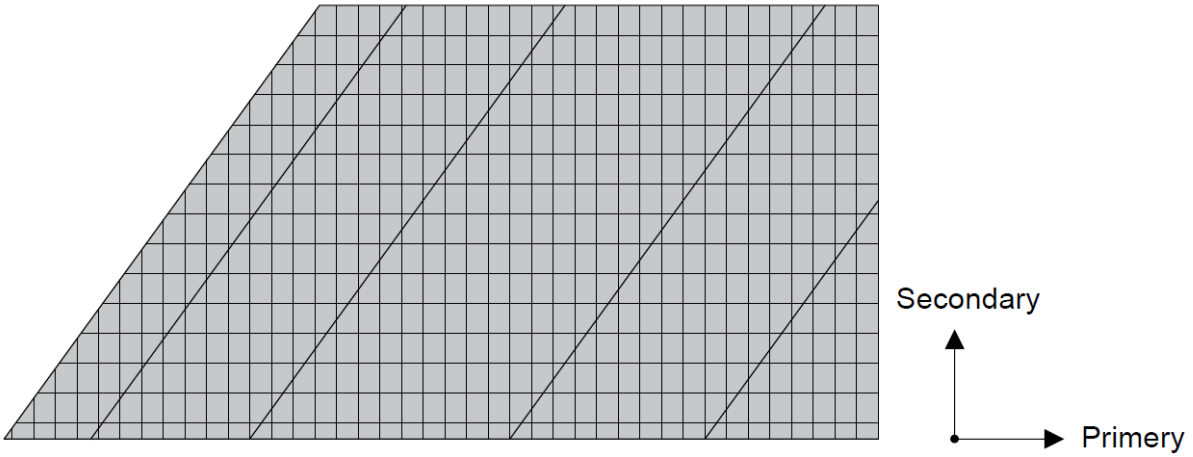

Figure 15 Grid element directions

4.1 Pattern variants

There are different methods to create a grid pattern on a base shape. For this analysis two different methods have been used to create three different grid patterns. These methods and the corresponding patterns will be briefly explained.

4.1.1 Vertically projected grid pattern

A grid can be created by drawing a flat grid and vertically projecting it onto a base surface, resulting in elements with varying lengths. At the edges where the surface is steep, the elements will be long. In the middle, where the shape has a small radius, the elements will be much shorter. This can also be seen in the architectural design. This method is shown in the figure below.

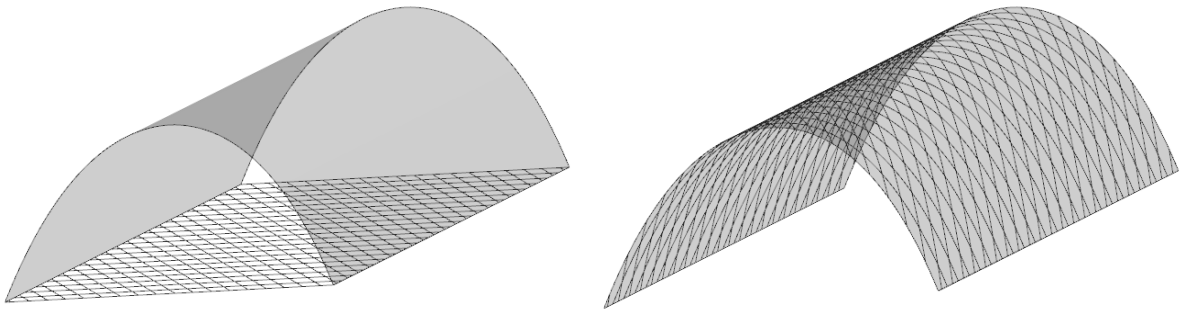

Figure 16 Grid created by vertical projection

This method is used to create two different patterns. The difference between the two patterns is how the elements are connected at the supports. In the architectural design, the elements in the primary and

secondary direction do not connect at the supports. However, the grid can be slightly shifted over the base surface, such that the elements do connect at the supports. The first two patterns will be one in which the elements do not connect, and one in which the elements do connect at the supports.

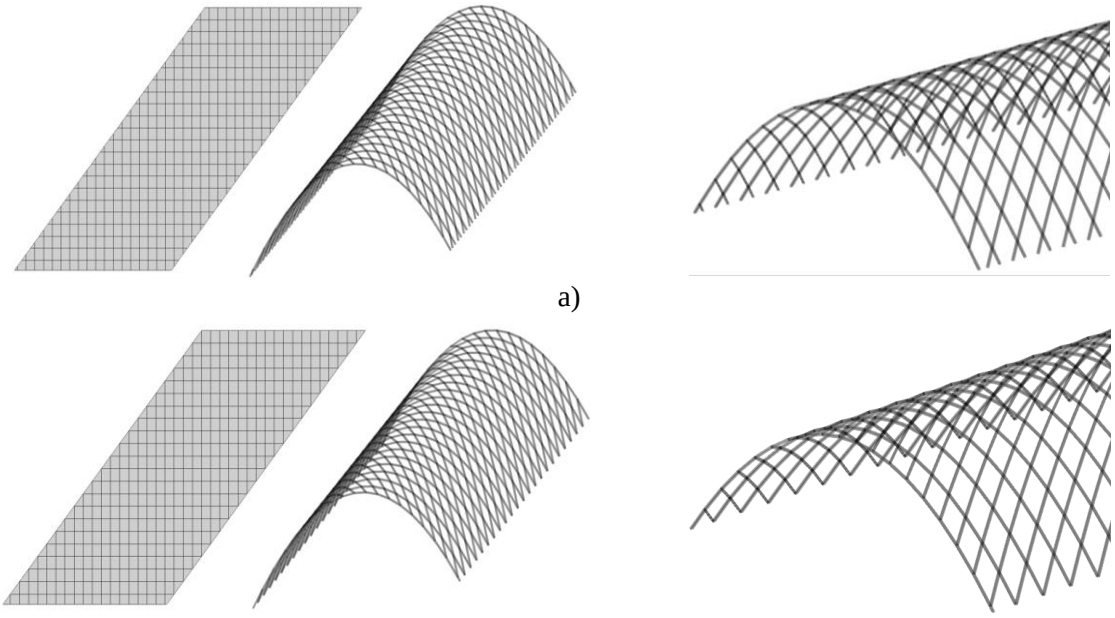

a)

b)

Figure 17 Grid patterns created by vertical projection (a) pattern 1, (b) pattern 2

4.1.2 Grid pattern by dividing surface

Aside from vertically projecting a flat grid on a base surface, the base surface can be divided into equal parts. This will result in elements with an approximately equal and constant length. This is what is done for the third grid pattern, which can be seen in Figure 19. To create this grid in Grasshopper, a plug-in called Mesh+ is used. Similarly to the first variants, this grid pattern consists of arches spanning in the primary direction. However, in this case, these arches are divided into equal parts. By connecting the nodes created by the division of the arches, the base shape is divided into equally large parts. This method is shown in the figure below.

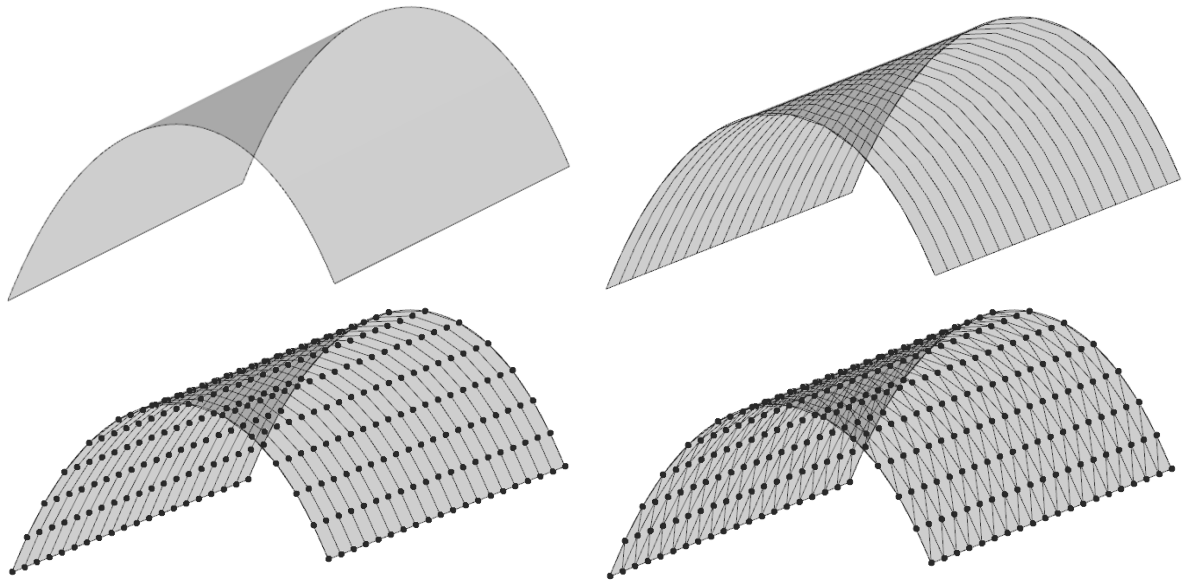

Figure 18 Grid created by equal division of base shape

With the above described method the third and final pattern is created and can be seen in the figure below.

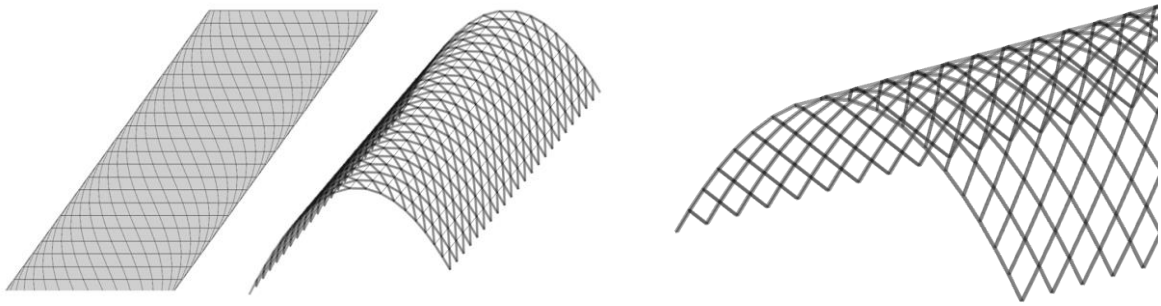

Figure 19 Grid pattern 3

The two entrance hall parts on the right in Figure 20 do not have a barrel vault shape like the other parts of the structure. In both of these parts, the upper right corners are cut off. Mesh+ does not create feasible meshes for these surfaces. Therefore, the meshes are created by creating a full surface of a barrel vault and then trimming the meshes at the boundaries of the real surfaces. This, however, causes a practical issue. When the meshes are trimmed at the edges of the surfaces, some very small elements smaller than 50 mm are left over. The lengths of these elements will be too small to create the connections between the elements. The small elements caused by trimming the mesh can be seen in the figure below, where they are highlighted in red. This problem could be solved by locally drawing a custom mesh with longer elements. However, this causes another problem. If this is not done carefully, the mesh does not follow the base surface of the parts anymore. This is an aesthetic disadvantage but might also cause practical issues concerning the roof covering. The first two patterns don't have this problem because all elements are vertical or horizontal. Since the mesh is trimmed vertically, only the horizontal elements are trimmed at the location pointed out in the figure. If the grid patterns shown in Figure 17 are continued to the two parts on the right, this will not result in very small elements.

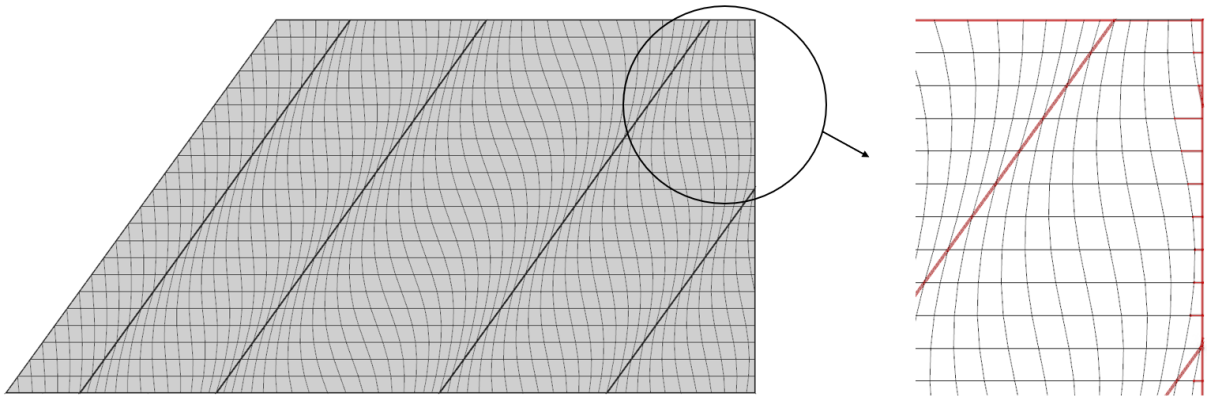

Figure 20 Practical issue due to trimming of grid

For the entrance hall segment which is highlighted above, a custom mesh is drawn. Every element which is smaller than 1 meter has been removed from the mesh together with the connecting elements. It should be mentioned that this in turn results in longer elements. The custom mesh is shown in the figure below.

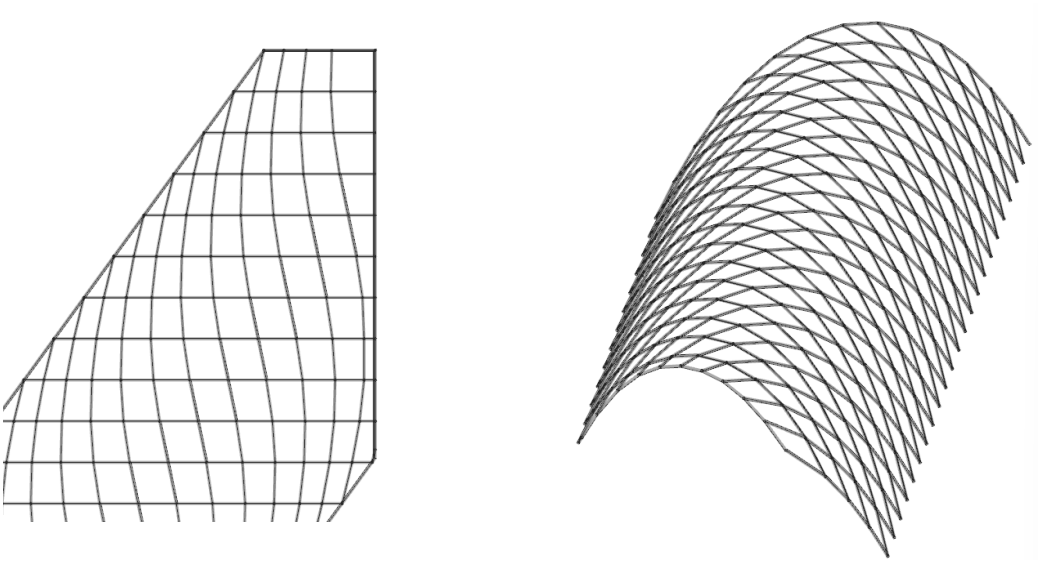

Figure 21 Adjusted grid pattern at trimmed part

4.2 Grid size

An important factor in the grid patterns that are vertically projected on the base shape is how the elements connect at the supports. The elements are only connected correctly at the supports with certain grid sizes, which can be seen in the figure below. For other divisions, the elements will connect differently along the length of the structure, which can cause the same practical issue that occurs for grid pattern 3 meaning that very small elements are created. However, grid pattern 3 does not have this problem regarding the grid size, as it can be created with all kinds of grid sizes. This means that if grid pattern 3 is eventually applied to the structure, material density optimization is possible (Chapter 13). Among the grid sizes shown in the figure, a grid size of 2 x 2.75 m is considered to be the most suitable one. The first division is very coarse, leading to very high internal forces, while the last division is very dense and is expected to result in the highest total amount of timber. Finally, to ensure a fair comparison between the grid patterns, the total length of grid elements is measured. Grid pattern 1 and 2 have the same total length, while the total length of grid pattern 3 is 99.6% of the total length of the other patterns.

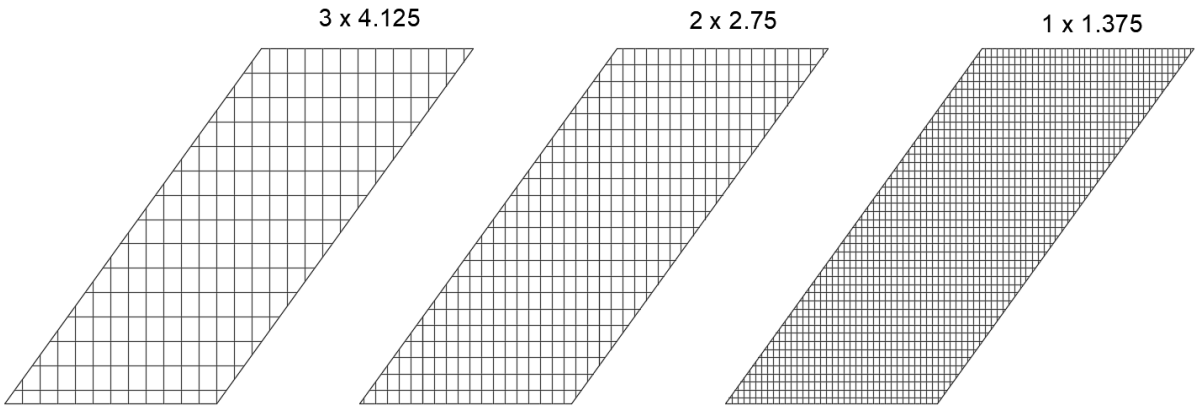

Figure 22 Possible grid sizes for grid pattern 1 and 2

4.3 Effect grid pattern on internal forces

The three grid patterns are compared with the 3D Grasshopper model together with Karamba3D. Again, for this analysis all load combinations are applied to the structure. Below the bending moment distribution caused by wind pressure on one side of the arch and suction on the other side is shown for the different patterns. In Table 5 the maximum internal forces resulting from all load combinations are given.

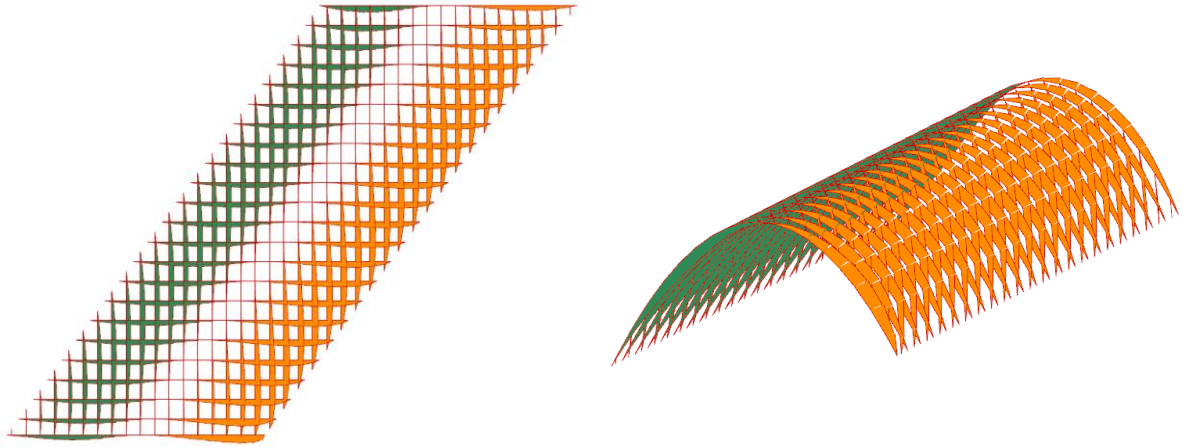

Figure 23 Moment distribution caused by wind – grid pattern 1

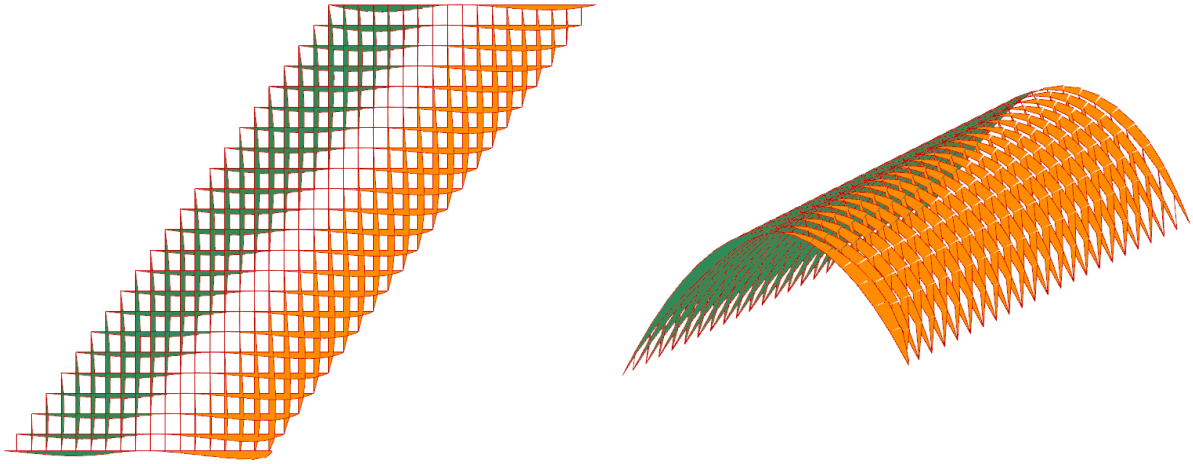

Figure 24 Moment distribution caused by wind – grid pattern 2

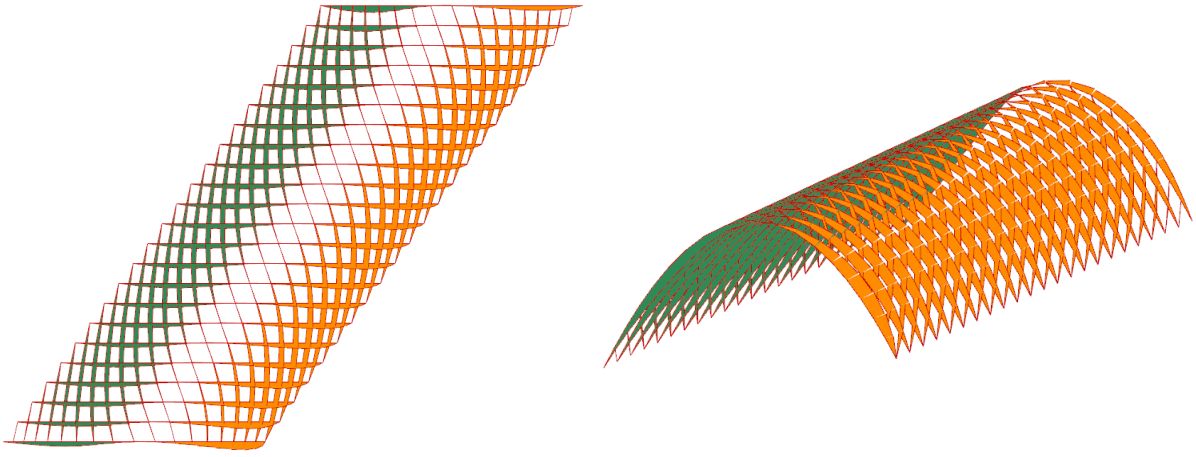

Figure 25 Moment distribution caused by wind – grid pattern 3

The bending moment distributions are very similar for all three grid patterns. The bending moments in the strong direction (M_y) are also close to each other. The main difference is found in the bending moment in the weak direction (M_z). For grid pattern 2 this moment is significantly larger than for the other patterns. Grid pattern 2 has relatively long elements at the supports, meaning that they are less laterally restrained by the elements in the secondary direction. This could be the cause of the larger bending moments in the weak direction.

Table 5 Effect grid pattern variants on internal forces - hinged supports

	Pattern 1	**Pattern 2**	**Pattern 3**
M_y [KNm]	216,59	232,2	212,85
M_z [KNm]	45,65	83,33	55,11
M_t [KNm]	9,25	9,71	8,38
V_z [KN]	31,45	103,48	34,27
V_y [KN]	46,54	62,58	44,66
N_c [KN]	346,96	345,09	330,67
N_t [KN]	187,52	185,47	168,10

5 SUPPORT CONDITIONS

The support conditions of a structure can significantly influence its internal forces, deformations, and stability. While hinged and rigid supports are commonly used, it is also possible to apply a combination of hinged and rigid supports. Additionally, connecting arches of adjacent parts can lead to semi-rigid supports. In this chapter, the stiffness values of semi-rigid supports will be determined, and then the influence of various support conditions on the internal forces will be analysed. Furthermore, the effect of support conditions on deformations and stability will also be examined in the final section of this chapter.

5.1 Cooperation between adjacent arches

The semi-rigid support stiffness values are determined using a 2D Grasshopper model with the Karamba3D plug-in. The model consists of the main arch of the entrance hall's roof and one of the smaller adjacent arches. The arches are rigidly connected at their intersection. Hinged supports are placed at the ends of the arches. The arches are subjected to a load combination including a wind load case, where wind pressure acts on one side of the main arch and wind suction on the other side, while only wind suction is applied to the smaller arch. In addition, one of the load combinations incorporating a snow load case is applied. The deformation caused by these load combinations results in a varying stiffness at the connection, with some load combinations causing the arches to move away from each other and others causing them to move closer together.

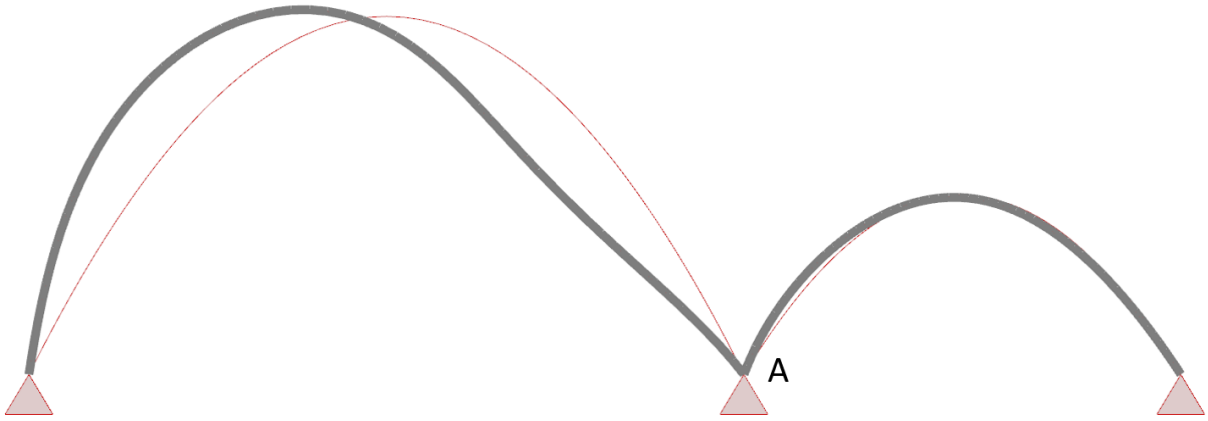

Figure 26 Cooperation adjacent arches

The stiffness is greater while the snow load or only the permanent load is applied, than while the wind load is applied. The CFD analysis showed that only wind suction acts on the smaller arch. In this case, the smaller arch will deform in the same direction as the larger arch, providing less resistance and therefore resulting in less stiffness. Another factor that greatly affects the rotational stiffness is the cross-section dimensions (bending stiffness) of the smaller arch. To show its effect, two different cross-section sizes have been applied. The stiffness is calculated by dividing the bending moment at point A by the rotation at this point (Figure 26). The table below shows the stiffness values determined by this model, along with the corresponding load combinations and cross-section dimensions. From the results, it can be seen that the cross-section's dimensions play a crucial role in the resulting rotational stiffness. The range of stiffness values for this analysis is approximately 1000 to 13.000 kNm/Rad.

Table 6 Stiffness values semi-rigid supports

Load combination	Height [mm]	Width [mm]	Stiffness [kNm/Rad]
ULS-1: Permanent	300	200	1874,70
ULS-1: Permanent	450	300	13107,60
ULS-2: Snow	300	200	1654,90
ULS-2: Snow	450	300	11712,60
ULS-9: Wind	300	200	1320,40
ULS-9: Wind	450	300	9122,20

5.2 Effect support conditions on internal forces

The effect of the support conditions on the internal forces is analysed with a 3D model with grid pattern 3 and a parabolic shape for the arches. The results are presented in the table below. The table mentions two support combinations: combination 1, in which one side has hinged supports and the other side has rigid supports, and combination 2, in which the support conditions are reversed. These combinations must be considered separately because some load cases are not symmetrical. The results shown for semi-rigid supports are based on an average stiffness value of 7000 kNm/Rad considering the stiffness range. The effect of the support stiffness on the internal forces will be presented as well.

Table 7 Internal forces for different support conditions

	Hinged	Rigid	Combination 1	Combination 2	Semi-rigid
M_y [kNm]	210,88	203,53	231,79	254,85	155,07
M_z [kNm]	47,85	21,08	51,64	46,77	31,13
M_t [kNm]	8,99	4,51	7,03	6,22	4,79
V_z [kN]	30,06	13,07	27,16	24,77	19,25
V_y [kN]	44,38	42,27	40,48	44,24	42,87
N_c [kN]	346,65	313,38	344,00	341,56	323,13
N_t [kN]	198,27	87,22	137,13	134,65	116,11

The results indicate that the use of semi-rigid supports results in the lowest bending moment in the strong direction (M_y) with the applied stiffness value. The internal forces within the range of the stiffness values are also analysed, as depicted in Figure 27. In the graph, the results are normalized.

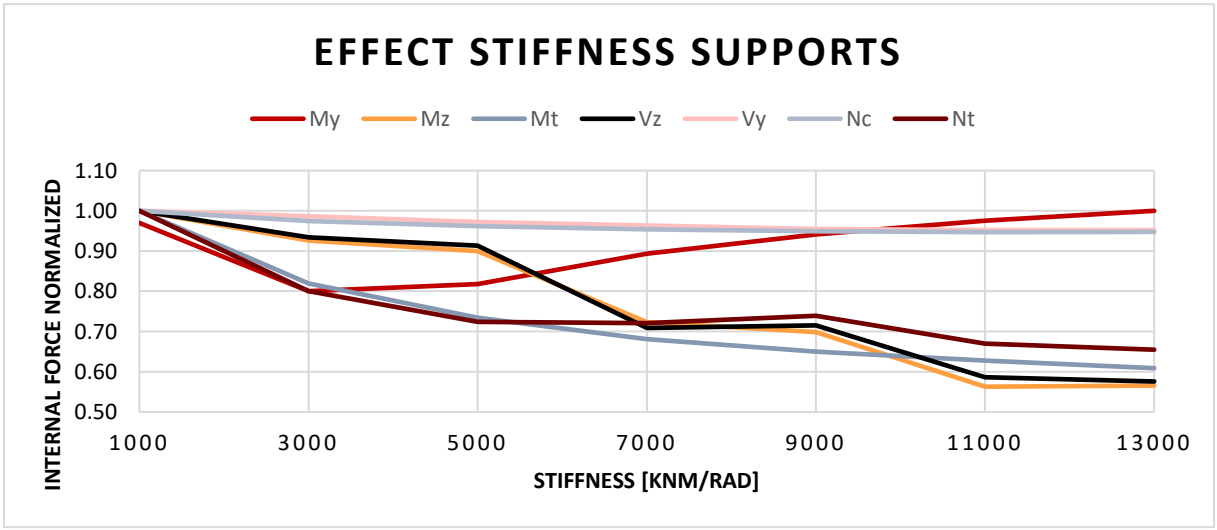

Figure 27 Effect rotational stiffness supports on internal forces

From the graph it can be seen that all internal forces decrease when the stiffness is increased, except for the bending moment in the strong direction (M_y). This bending moment decreases until the stiffness

becomes 3000 kNm/Rad. Thereafter it starts to increase again while the maximum bending moments is caused by the same load combination within the range. The highest bending moment occurs when the stiffness is 13.000 kNm/Rad. With this stiffness the bending moment is 173,5 kNm. This is still significantly lower than the maximum bending moments with other support conditions. The reason why semi-rigid supports lead to lower bending moments is because the semi-rigid supports allow for a redistribution of the bending moment along the arch. For hinged supports, the bending moment is fully distributed along the arch and with rigid supports it is concentrated at the supports. In this case, the distribution of the bending moment seems to be optimal when the rotational stiffness at the supports is approximately 3000 kNm/Rad. The redistribution of the bending moment along with the increasement of the rotational stiffness is visualized in the figure below.

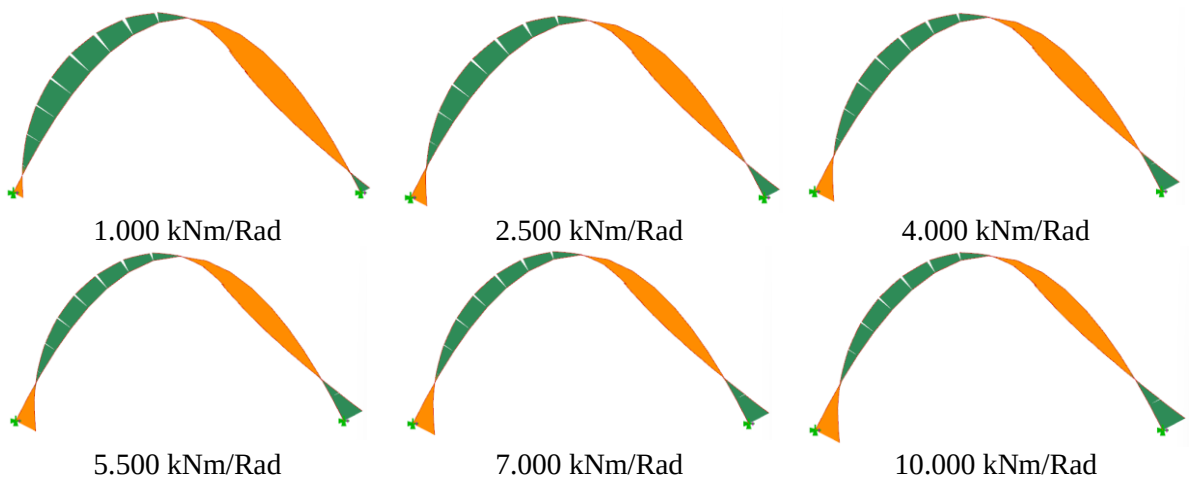

Figure 28 Redistribution of bending moment due to support stiffness

5.3 Effect support conditions on stability

In this section, the effect of the support conditions on the stability of the structure is analysed. The effect on deformations and stability is first shown for the 3D model. The table below presents the deformation in the x, y, and z directions, as well as the Buckling Load Factor (BLF). The BLF is the ratio of the critical buckling load to the acting load, and as long as it is greater than 1, buckling will not occur. The BLF is not only affected by the support conditions but also by the dimensions of the cross-section and the stiffness of the joints between the elements.

Table 8 Deformation and stability for different support conditions

	Hinged	Rigid	Combination 1	Combination 2	Semi-rigid
U_x [mm]	313,05	115,54	221,45	182,04	187,02
U_y [mm]	233,69	85,99	162,51	133,25	140,51
U_z [mm]	182,53	70,43	127,31	106,78	111,80
BLF	2,21	8,43	3,68	3,66	4,71

In addition to the support conditions, the joints between the elements play a crucial role in the stability of a structure like a grid-shell. Using a 2D model, the joint stiffness is increased for each support condition and the BLF is plotted for each joint stiffness. This can be seen in Figure 29, which includes a line for Semi-rigid_1 and Semi-rigid_2. The first line represents a stiffness value of 1000 kNm/Rad for the supports, while the second line represents a stiffness of 10.000 kNm/Rad. These values are based on the results presented in Table 6.

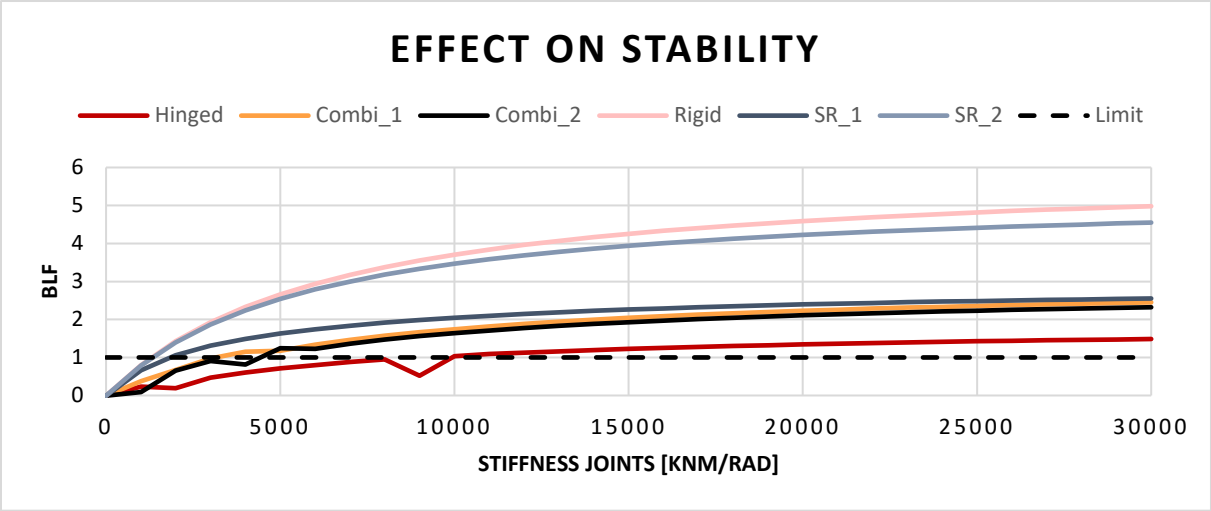

Figure 29 Influence joint stiffness and support conditions on stability

The graph clearly shows the effect of the support conditions on buckling. Rigid supports have the advantage that the joints require less joint stiffness to prevent buckling in the structure. When the supports are hinged, it takes much longer before the BLF exceeds 1. In this example, the joints have to be almost ten times stiffer in order to prevent buckling. When a combination of hinged and rigid supports is used, the required stiffness falls between that of only rigid or hinged supports. Semi-rigid supports have a positive effect on the stability of the structure as well. The line for the semi-rigid supports with a stiffness of 10.000 kNm/Rad is almost identical to that of rigid supports. With semi-rigid supports with a stiffness of 1.000 kNm/Rad, stability is achieved relatively fast. Semi-rigid supports result in a decreased maximum bending moment in the structure compared to hinged or rigid supports, which may explain why stability is achieved relatively quickly. At a certain stiffness value, the BLF stops increasing. At this point, the joints behave as rigid joints. The zone where the BLF is increasing is where the joints show semi-rigid behaviour. A joint classification is derived by Fan et al. (2011) which shows that the bending stiffness and length of the elements influence when a joint behaves rigid or not as well.

5.4 Conclusion on support conditions

The analysis suggests that connecting arches from adjacent parts with each other to create semi-rigid supports is beneficial. First of all, it is likely to result in a relatively low bending moment in the structure. Additionally, it was shown that stability can be achieved relatively quickly, even with the minimal stiffness within the determined range. It is worth noting that the roof parts are placed on long-spanning structures, making it difficult to create rigid supports. Connecting arches of adjacent parts seems to be a more practical solution in this case.

6 BARREL VAULT VARIANTS

In the architectural design, the entrance hall segments have a single-curvature (monoclastic) shape which is not ideal for resisting asymmetric external loads, resulting from snow and wind. To improve the resistance against external loads and increase the overall stability, a shape with a double-curvature could be applied resulting in a shell-like structure. This can be achieved by creating a saddle-like shape (anticlastic) by decreasing the height at the middle of the structure, or a dome-like shape (synclastic) by increasing the height at the middle. Another way to increase overall stability is by incorporating rigid facades into the structural system. These facades can limit lateral displacements and improve the stability of the structure. In this chapter, four variants will be compared: a monoclastic design with and without facades, as well as an synclastic and a anticlastic variant. An overview will be given of the displacements and internal forces resulting in each variant.

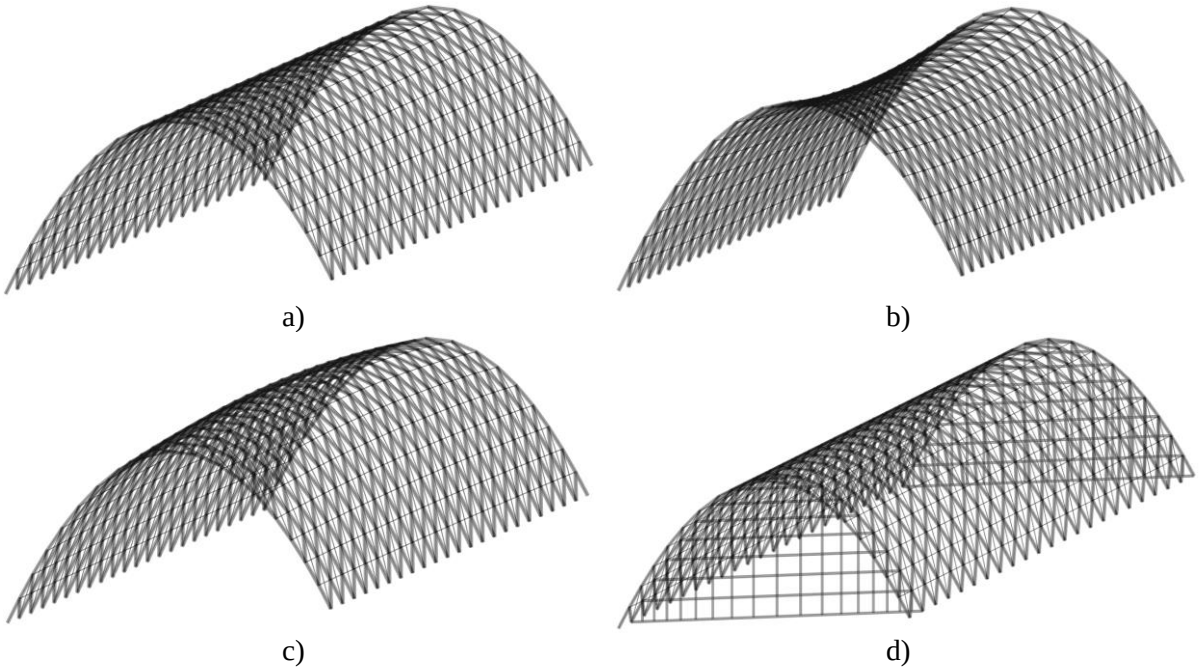

Figure 30 (a) barrel vault, (b) anticlastic, (c) synclastic, (d) rigid façade

6.1 Modelling of barrel vault variants

The variants were modelled and analysed using a 3D Grasshopper model and the Karamba3D plug-in. For the anticlastic and synclastic shapes, the height at the middle of the base surface was adjusted by 1/10 of the height of the outer arches. This height difference was chosen to ensure that the design would not deviate significantly from the architectural design. However, it should be noted that if the height difference were increased, the effect on internal forces would likely be more significant. Additionally, it should be noted that the CFD simulations were performed using a model in which the parts have a single-curvature shape (monoclastic). Significant changes in the shape may result in wind loads which do not fit the different variants. The purpose of this analysis is to demonstrate the effect of double-curved shapes in comparison to a single-curved shape. A larger height difference could be applied if this is deemed necessary in a later stage of the project.

The rigid façades are modelled as a steel frame connected to the nodes of the timber grid using steel HEA profiles for the façade elements. The dimensions were chosen to prevent buckling of the façade itself. One façade was connected to the second arch at the front of the structure, consistent with the architectural design. A second rigid façade was connected to the outer arch at the back of the structure. The connections between the façades and the main timber grid were designed as hinged connections.

6.1.1 Bracing elements

In this analysis, the role of bracing elements becomes important. In particular, for the variant with rigid facades, the structure must act as a cohesive system. Without bracing, the effect of the rigid façade may be limited to only the areas near the facades. To achieve this, bracing elements are placed transversely between the primary and secondary elements. For this project, it is assumed that the bracing elements will be tension-only elements, such as cables. This is modelled by disabling the bending stiffness for these elements and using a component from the Karamba3D plug-in to eliminate any elements that experience compressive forces. This leaves only bracing elements with a tensile normal force in the model. Additional information can be found in Appendix F.

6.2 Structural analysis barrel vault variants

The variants of the structure are analysed with Karamba3D to determine the internal forces and deformations. The effect on stability will be further examined in the next chapter, where different joint mechanisms will be compared and the impact of double-curvature and the rigid façade will also be considered. The supports are hinged and the arches have a parabolic shape for this analysis. In the figure below the displacements resulting from wind are plotted for each variant. The magnitude of the displacements is given in Table 9.

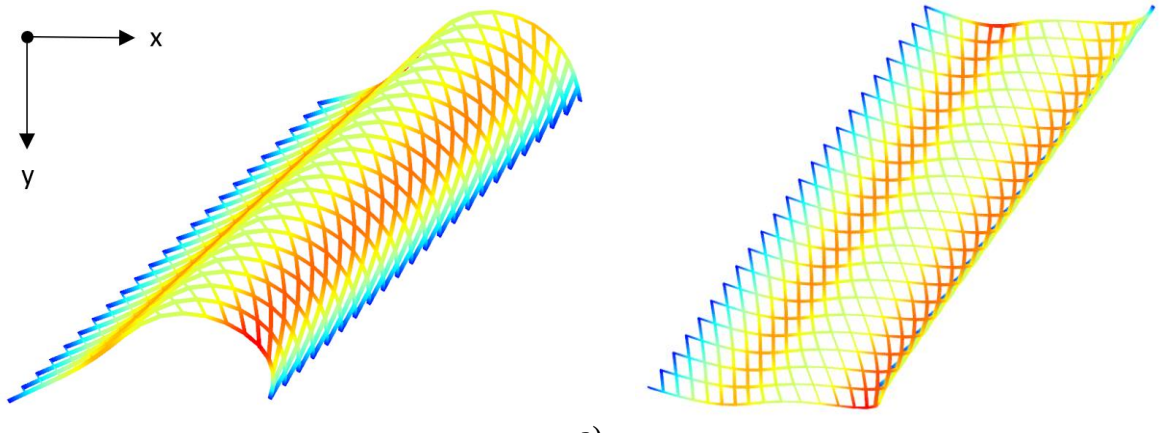

a)

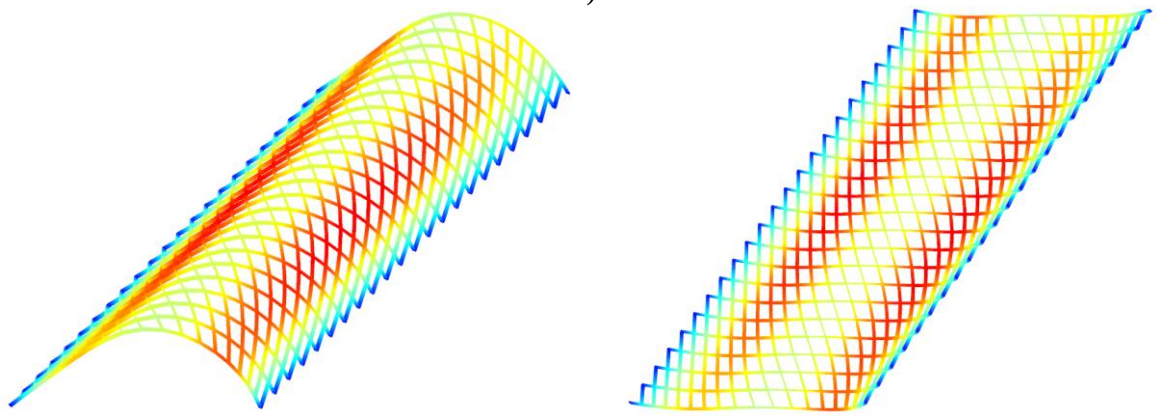

b)

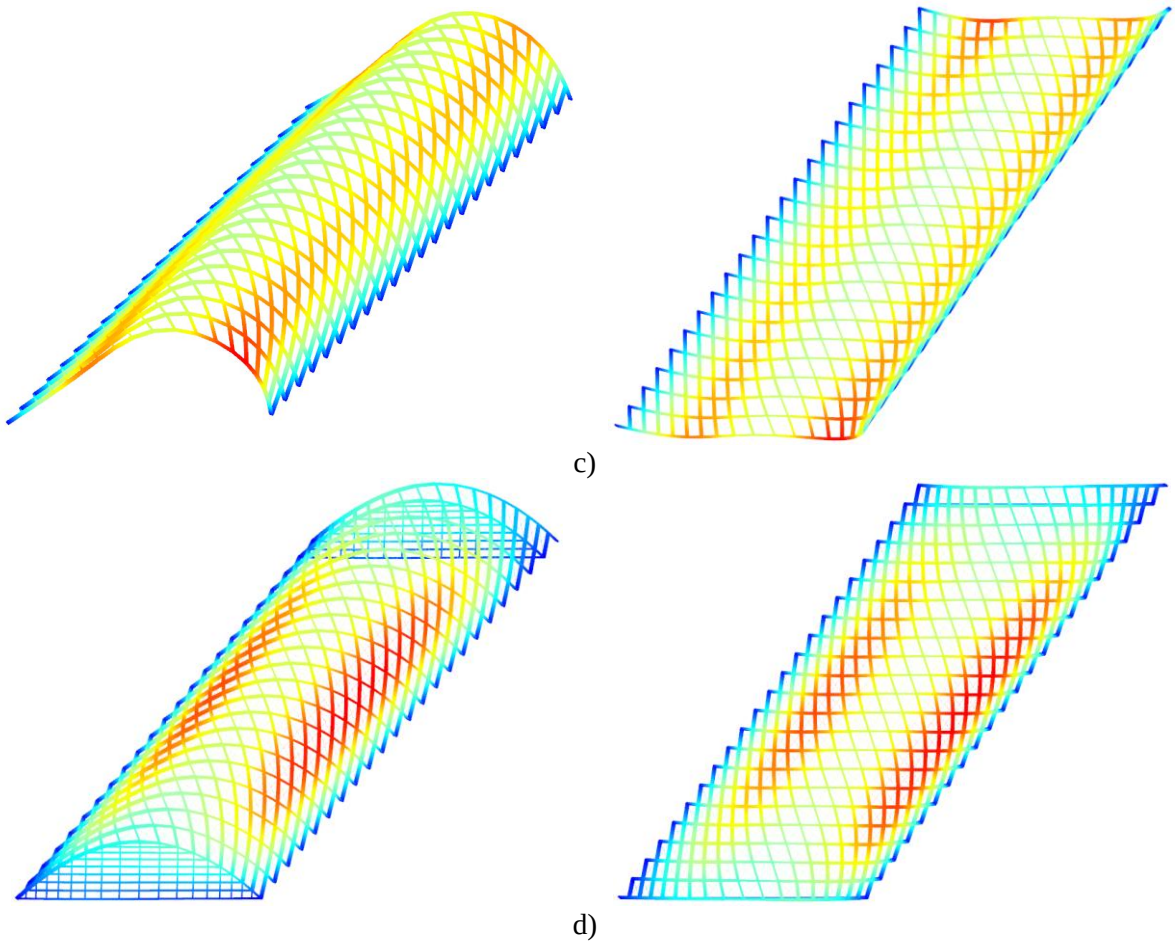

Figure 31 Deformed models due to wind of barrel vault variants: (a) monoclastic, (b) anticlastic, (c) synclastic, (d) rigid facades

Table 9 Results deformations of barrel vault variants

Deformation [mm]	Monoclastic	Anticlastic	Synclastic	Rigid facades
x-direction	183,08	144,09	232,48	77,16
y-direction	127,96	101,66	168,87	55,48
z-direction	105,60	91,85	134,11	44,39

Compared to a monoclastic shape does the anticlastic shape have a positive effect on the deformations of the structure. The anticlastic shape results in a more horizontal truss structure in the middle, providing extra stiffness in the horizontal direction. The synclastic shape does not have this advantage and results in larger deformations compared to the monoclastic variant. Next to that do the arches in the middle get a different height/span ratio. The wind acts perpendicular to the surface. Because the arches in the anticlastic shape get more flat, the wind load acts overall more vertically. For the synclastic shape it means that the wind acts more horizontally. Next to that may the arches in the synclastic shape be more vulnerable to lateral deformation due to their increased height. These factors may as well contribute to the difference in the deformation compared to the monoclastic shape. Incorporating rigid facades in the structural system seems to reduce the deformation due to wind significantly. This would be expected as sidewards deformation is restrained at the location at which the facades are applied.

Aside from the deformations do the different variants influence the internal forces in the structure. In the table below the maximum internal forces resulting from all load combinations are presented.

Table 10 Results with cable bracing elements

	Monoclastic	Anticlastic	Synclastic	Rigid facade
M_y [kNm]	210,88	162,73	263,46	120,15
M_z [kNm]	47,85	39,95	60,43	109,95
M_t [kNm]	8,99	6,84	11,32	4,91
V_y [kN]	30,06	27,76	37,48	69,10
V_z [kN]	44,38	37,53	55,02	37,28
N_c [kN]	346,65	329,67	396,30	653,77
N_t [kN]	198,27	181,11	203,70	806,62

Comparing the different variants to each other it can be concluded that the anticlastic shape significantly decreases the bending moment compared to a monoclastic shape. Looking at the synclastic shape it is clear that this variant results in the highest bending moment. It was expected that both the anticlastic and synclastic shape would be advantageous compared to the normal barrel vault variant due to their second curvature. However, as mentioned previously are the middle arches simply smaller and bigger. This could also explain why the difference in the bending moment between the anticlastic and normal variant is approximately the same as the difference between the synclastic shape and the normal variant.

Another notable result are the large normal forces in the variant with the rigid facades. These normal forces are located in the main timber grid elements and are almost twice as high compared to the other variants. The big normal forces result from the load combinations with wind pressure at one side of the structure and wind suction at the other side. What could be happening is that due to this wind load the structure wants to move sideways, but this is prevented by the facades. This causes the elements at and right after the facades to be pulled and pressed. This is clearly visible in the figure below which shows the normal force distribution in the structure. The tensile normal forces are depicted in blue and the compressive normal forces in pink, as depicted by the legenda. On the other hand does incorporating the facades lead to the lowest bending moment out of the different variants.

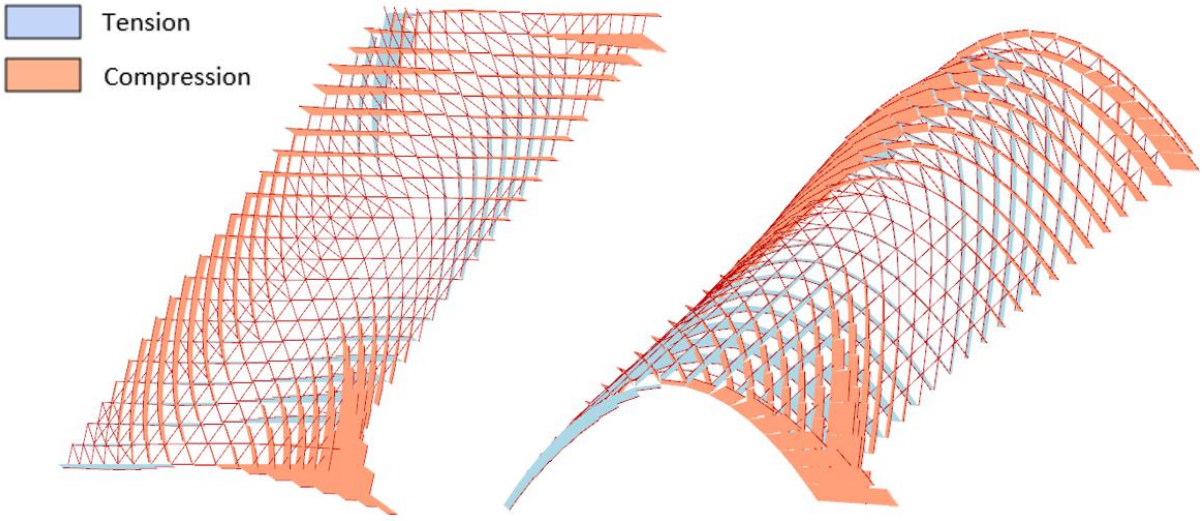

Figure 32 Normal force and displacement in variant with rigid facade

6.2.1 Rigid façade and the shape of the arches

Because the moment distribution with rigid facades deviates significantly from the other variants, the conclusions about the shape of the arches given in Chapter 3 may differ in this case. From the analysis conducted for the shape of the arches it became clear that a load combination with wind pressure on one side of the arch, and wind suction on the other side results in the largest bending moments. Due to the

sideways deformation being restraint however, it may be possible that the maximum bending moment in this case is caused by for example a snow load. In this case the catenary shape would most likely be better than a parabola as became clear in Chapter 3. An additional analysis is therefore performed to check if this is the case. The results can be seen in the table below.

As can be seen in the results in the table below are the conclusions about the arch's shape completely different with the facades incorporated in the structural system. First of all, does the parabolic shape now seems to be the least favourable shape for the combination of wind pressure and suction, considering the bending moment in the strong direction compared to the other shapes. Without the facades the parabola was the most favourable shape in this case. For the ellipse and the parabola, the snow accumulation between the arches has become more relevant. For the ellipse this load combination (ULS-4) now causes the largest bending moment.

Table 11 Influence rigid facade on arch shape effect

	ULS-1	ULS-2	ULS-3	ULS-4	ULS-5	ULS-6	ULS-7	ULS-8	ULS-9
Ellipse									
M_y [KNm]	54,55	104,00	112,19	117,88	66,33	81,98	58,27	70,41	72,97
M_z [KNm]	30,05	57,93	55,75	57,27	35,33	49,47	66,77	79,81	68,45
M_t [KNm]	1,73	3,23	3,85	3,23	2,00	2,56	1,84	2,17	2,31
V_y [KN]	15,30	29,19	27,67	31,17	22,03	26,02	40,15	48,04	40,60
V_z [KN]	17,51	31,56	32,48	39,78	23,48	33,94	21,29	20,29	27,84
N_c [KN]	363,08	535,37	511,04	605,95	453,92	434,33	610,78	567,41	725,42
N_t [KN]	27,33	49,67	54,70	68,38	77,67	166,74	447,80	538,90	364,18
Catenary									
M_y [KNm]	11,24	18,21	30,67	74,48	56,89	83,73	80,22	106,21	104,76
M_z [KNm]	3,41	7,67	18,13	26,18	23,33	32,35	56,09	72,97	85,22
M_t [KNm]	0,33	0,78	0,97	2,48	1,89	3,77	2,42	3,22	4,45
V_y [KN]	2,54	6,07	11,80	19,73	15,36	20,32	35,50	45,79	52,73
V_z [KN]	6,50	9,15	13,43	24,27	19,92	33,24	24,10	31,56	33,88
N_c [KN]	248,84	315,34	287,80	462,69	290,84	339,83	551,16	625,53	910,98
N_t [KN]	2,63	7,53	12,34	175,50	23,07	89,00	393,25	510,34	570,76
Parabola									
M_y [KNm]	17,24	19,27	30,90	115,42	52,71	86,67	82,66	109,14	123,45
M_z [KNm]	7,36	7,51	17,41	37,85	20,13	32,22	49,19	64,68	84,77
M_t [KNm]	0,60	0,57	1,12	4,08	1,74	3,87	2,42	3,23	5,22
V_y [KN]	4,97	5,20	13,72	24,70	13,54	20,98	31,70	41,24	53,11
V_z [KN]	9,69	10,35	16,84	36,61	18,06	32,79	24,77	32,15	36,30
N_c [KN]	250,01	287,66	277,11	489,87	253,91	312,46	491,38	561,24	858,26
N_t [KN]	17,99	6,05	28,83	240,26	23,82	75,50	354,37	464,37	583,62

6.3 Conclusions on barrel vault variants

Applying an anticlastic shape or incorporating the facades in the structural system were both found to be effective for decreasing the deformation and bending moment. The facades however, have a drawback which are the large normal forces due to the restraining of the deformation due to wind. The facades also change the conclusions about the arch shape variants concerning the maximum bending moment. In this case a lower bending moment can be obtained by applying a catenary shape.

7 JOINT MECHANISMS

The joints between the elements in a grid-structure are crucial for its overall stability and structural behaviour. In a 2D model, the effect of the joint stiffness together with the support conditions on the stability of an arch was previously discussed (Chapter 5). However, in a 3D model, joints have additional Degrees of Freedom (DOF) due to their ability to translate and rotate in three different directions, resulting in a total of six DOF's. Different types of joint mechanisms can result in varying combinations of restraints and DOF, each with different stiffness values. To avoid comparing all possible combinations, the preliminary research was used to identify the most common structural systems used in existing timber grid structures. Three systems are considered to be particularly promising for the grid structure of the entrance hall's roof which are a lattice system with prefabricated elements, a segmented system, and a system using arches as primary beams with secondary beams in between. These systems will be further analysed and compared in terms of their effect on internal forces, stability and deformations.

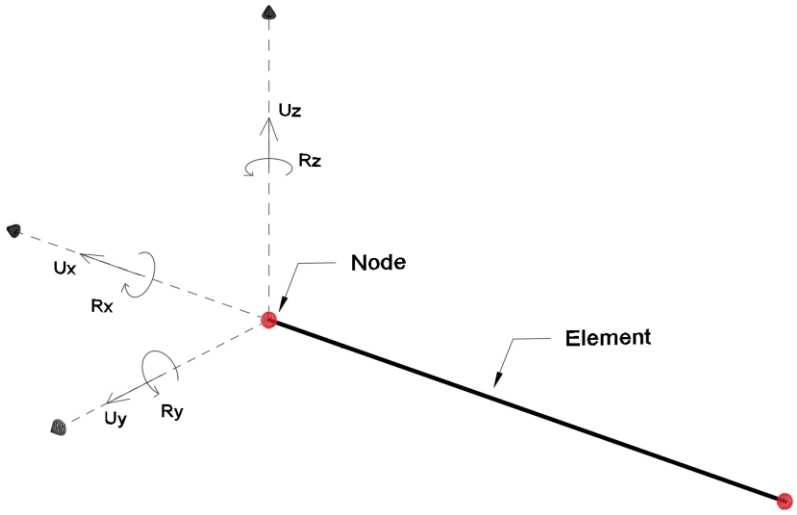

Figure 33 Degrees of Freedom in a 3D model

7.1 Structural systems

In the preliminary research in Chapter 2 the more commonly different types of systems for grid-structures were described. Each system has different types of connections between the elements, has a different manufacturing process or requires certain properties of the grid pattern. The Zollinger roof system for example requires a limit for the angle between two crossing lamellas of approximately 45° when the original joint-type are used. Furthermore, was sagging of the roof an issue with this system. Also does the structure of the entrance hall roof experience large compressive forces. With the reciprocal type of grid pattern, large stresses perpendicular to the grains may occur in the timber elements. The Toskana Thermal springs in Bad Sulza, Germany had a different type of connection which requires the elements to be connected perpendicular to each other. This limitation is a disadvantage compared to other systems that allow for the realization of the grid pattern from the architectural design. For this reason and the mentioned structural issues, it is decided not to continue with the Zollinger roof system.

Another system that will not be further analysed is the ribbed grid-shell. This system is similar to the lattice grid-shell, with the main difference being the manufacturing process. Unlike Frei Otto's actively bend grid-shell, the ribbed grid-shell is constructed directly in its final shape. However, there are also lattice grid-shells that are constructed using prefabricated elements. As discussed in the preliminary research, the ribbed grid-shell requires temporary scaffolding on which the elements are assembled on-site. In situations where large cross-sections are required, it is expected that the use of prefabricated elements would result in a less complex manufacturing process than that of a ribbed grid-shell. For this reason, and because the joint mechanism is very similar, it has been decided to focus on the lattice grid-

shell with pre-fabricated elements. However, because the joint mechanism is the same, the ribbed grid-shell will be considered in this chapter to some extent, but not included in the remaining part of the project.

Another system that will be considered in this chapter is the segmented grid-shell. This system has been successfully used in large-scale projects, particularly in the construction of timber domes. It allows for creating the grid pattern variants which are discussed in Chapter 4. Therefore, the segmented system will be included in this chapter. Compared to the lattice grid-shell, the joints in the segmented grid-shell have different DOF and specific rotational and axial stiffnesses. The analysis of the structural performance of these systems will be described in the following sections.

7.1.1 Segmented system

In the segmented system the elements span from node to node. A joint is therefore applied at each node of the timber grid. The preliminary research identified several different types of joints that can be used in this system. One commonly used joint is the slotted in steel plate joint. This joint consists of a central circular component, which is connected to steel plates on either side to connect the elements. These steel plates are inserted into the middle of the timber elements and fixed in place with connectors such as bolts or dowels. The connectors are arranged in a rectangular pattern (see figure below)

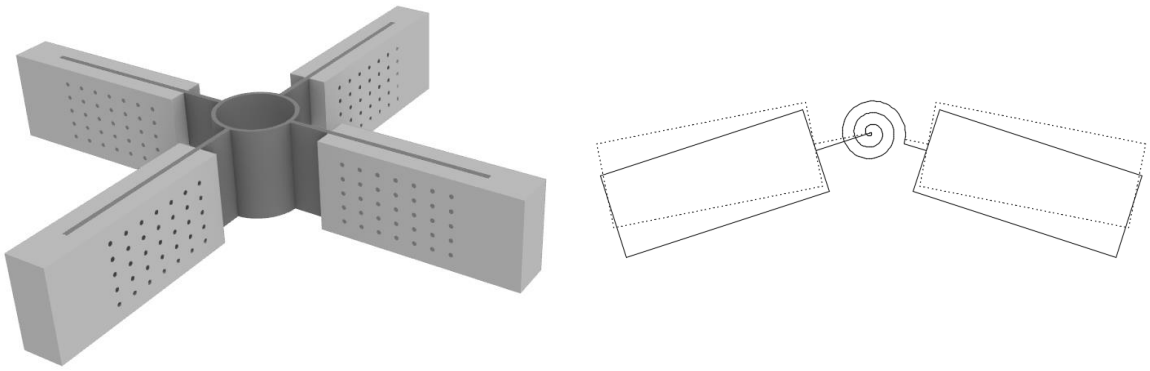

Figure 34 Concept of slotted in steel plate joint

When analysing the segmented system, it is important to accurately estimate the rotational stiffness of the joints. A method exists for determining the stiffness of the slotted in steel plate joint in a timber frame, but as pointed out by Shu et al. (2020), this method should not directly be used when large axial forces are present. In their research, they analysed the structural performance of timber domes with this type of joint, and provided an analytical method to estimate the rotational stiffness and ultimate moment capacity. Using this analytical method, a range for which the segmented system will be analysed is established. This range is presented in Table 12. Additionally, it is important to consider the rotational stiffness in the z-direction. No analytical method is currently available for determining the stiffness in this direction. However, Shu et al. (2020) provided a moment-curvature diagram from a test which indicates the rotational stiffness in this direction is relatively low (approximately 87 kNm/Rad) for their sample. Therefore, the joint will be modelled as hinged in this direction. The axial stiffness and strength of the joint can be determined according to Eurocode 5. The calculation procedure for determining the stiffness values and force capacities of the joint can be found in Appendix C.3.

The rotational stiffness of the joint mainly depends on the amount of bolts, their diameter and the cross-section width. The range presented in Table 12 is established by varying these factors, resulting in different joint layouts (J1 to J7). The minimum bolt spacing according to EC5 is taken into account for the design of these joints. The results of this analysis can be found in Table 12. The table also includes a height, which indicates the minimum height of the cross-section required to create the corresponding joint, taking into account the minimum bolt distance as presented in Appendix C.3 as well.

Table 12 Properties for different joint layouts

Joint	Rows x columns	Diameter [mm]	Width [mm]	Height [mm]	C_r [kNm/Rad]	C_t [kN/m]	N [kN]	M_u [kNm]
J1	2x2	10	200	100	41,70	46053,63	21,96	2,04
J2	4x5	16	200	288	2229,53	368429,03	193,74	102,22
J3	5x5	20	200	440	5149,13	575670,35	312,72	225,77
J4	4x7	22	200	396	8502,23	709225,87	379,39	364,29
J5	5x8	20	200	440	11232,91	921072,56	477,38	492,52
J6	5x8	20	300	440	14769,64	921072,56	627,68	647,59
J7	6x8	20	300	520	18899,14	1105300,00	753,22	828,65

7.1.2 Lattice system

The elements in a lattice grid-shell are continuous and can rotate freely along their length at the crossing point of the elements. This mechanism is similar to that of a pair of scissors, where the two blades can also rotate freely from each other. Therefore, this mechanism will be referred to as a scissor mechanism from now on. The figure below illustrates this mechanism. To analyse the effect of the scissor mechanism on the internal forces, an adjusted model is used in Karamba3D. Unlike the other systems, which can be modelled using hinges with or without specific stiffness values, this system requires a different approach. An adjusted calculation model is created to simulate this mechanism and is explained in Appendix F.4.

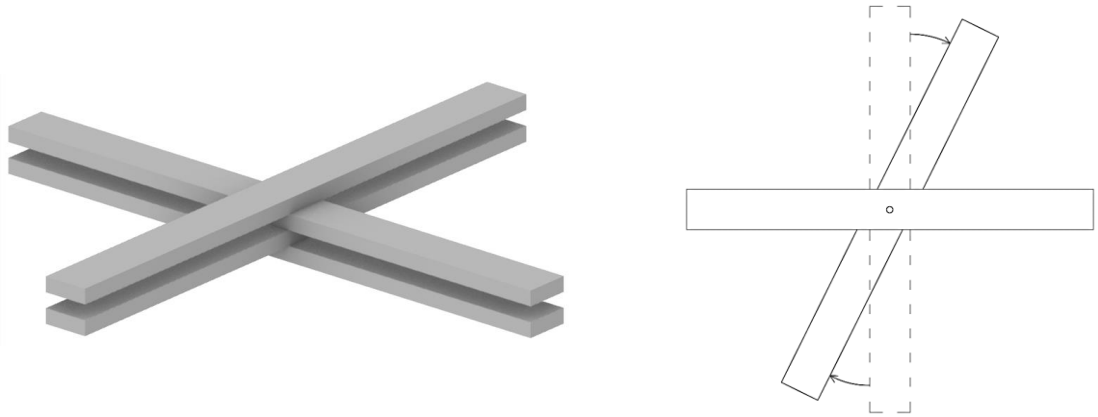

Figure 35 Concept of node in a lattice system

7.1.3 Arch system

In the lattice system and the segmented system, the elements in all directions are assumed to experience an equal magnitude of internal forces, and therefore have the same cross-section dimensions. It is however likely that the internal forces in the primary beams are significantly larger than in the secondary beams. The structure can therefore also be viewed as consisting of primary arches that are laterally supported by secondary beams in between. These secondary beams can be connected to the primary beams using custom cold-formed connectors such as angled joist hangers for example, and have hinges at their starting and ending points. The arches themselves are assumed to be continuous for this chapter and no hinges or springs are applied to them. It is possible to give the arches and secondary beams different cross-sections in a later phase, but for this chapter the same cross-section will be applied to all elements.

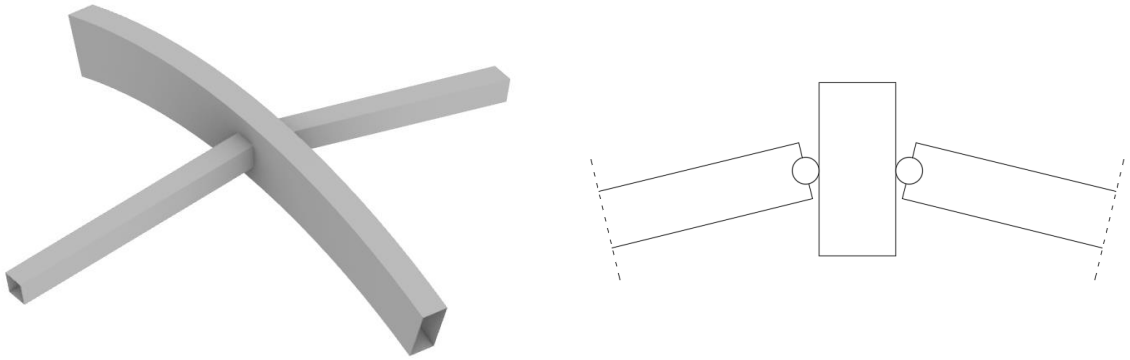

Figure 36 Concept of node in arch system

7.2 Effect joint mechanisms on internal forces

In this section of the chapter, the effect of different joint mechanisms on the magnitude and distribution of internal forces will be analysed. The results for the three joint mechanisms described earlier in this chapter, as well as a variant with fully rigid joints, will be presented. This will provide a better understanding of how the joint mechanism affects the internal forces. The analysis includes all load combinations, including those from snow and wind. The maximum internal forces resulting from all load combinations will be provided.

Several design options have been discussed in previous chapters, but not all of them are expected to have an significant impact on the conclusions of the analysis in this chapter. These include design options such as the shape of the arches and grid pattern. Therefore, for each result presented in this chapter, a catenary shape and grid pattern 3 will be applied. Additionally, the supports will be assumed to be hinged, unless otherwise stated. However, there may be other parameters that do influence the internal forces and have different effects for different joint mechanisms. These variables include the stability elements and the rigid facades. The stability elements are modelled as cables or tension-only elements (Appendix F.3), as described in the previous chapter, which is why the grid patterns visible in the following figures are irregular.

The next two pages present the maximum internal forces for different variants of the structure. The two variants are a monoclastic variant with and without bracing elements, and a variant with rigid facades, also with and without bracing elements. Results for each variant with the different joint mechanisms are given. The moment distribution for load combination ULS-9 is also provided for the different joint mechanisms, to determine if there are any significant variations in the bending moment distribution. Additionally, the effect of the element orientation on internal forces is analysed, noting that this variable does not apply to the lattice system, as elements must follow the normal vector of the base surface for this system. For the results on the next two pages, the elements are orientated according to the base surface normal for each joint mechanism. Finally, the difference in the internal forces for elements in the primary and secondary direction (Chapter 4) are also presented.

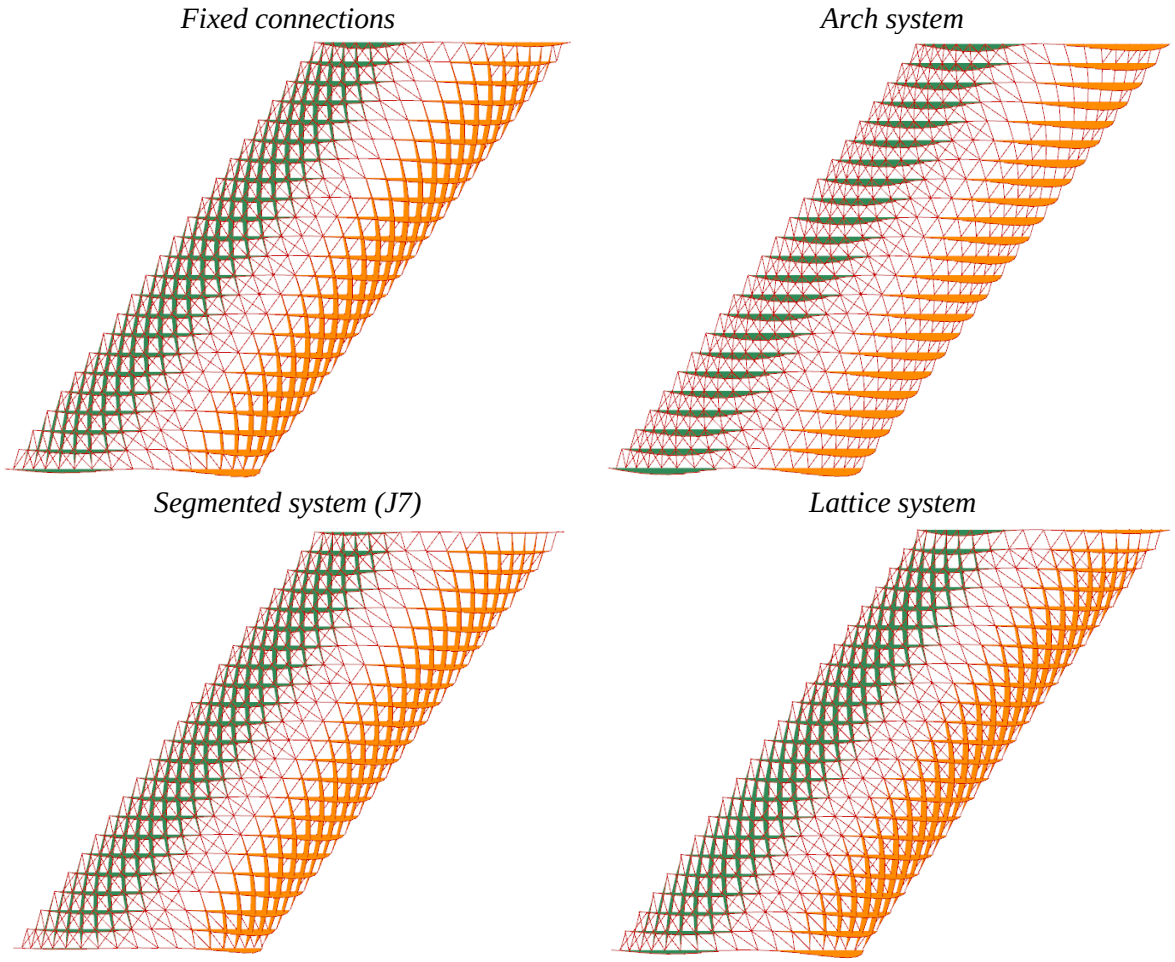

Figure 37 Moment distribution due to wind for monoclastic variant with different joint mechanisms

Table 13 Internal forces monoclastic variant without bracing elements

	Fixed connections	Arch system	Segmented system (J7)	Lattice system
My [kNm]	222,66	318,66	230,83	231,07
Mz [kNm]	53,24	113,90	141,47	55,59
Mt [kNm]	8,60	29,17	71,60	9,77
Vy [kN]	32,78	30,66	47,81	17,20
Vz [kN]	46,62	48,16	59,03	46,16
Nc [kN]	336,76	346,96	324,65	315,18
Nt [kN]	195,72	116,91	164,30	88,55

Table 14 Internal forces monoclastic variant with bracing elements

	Fixed connections	Arch system	Segmented system (J7)	Lattice system
My [kNm]	220,62	229,79	187,48	209,8
Mz [kNm]	21,74	75,66	9,28	50,91
Mt [kNm]	8,34	24,90	42,87	7,93
Vy [kN]	12,97	14,53	6,66	10,29
Vz [kN]	46,28	42,16	38,77	44,15
Nc [kN]	343,46	342,39	373,70	338,48
Nt [kN]	256,14	179,64	336,16	142,96

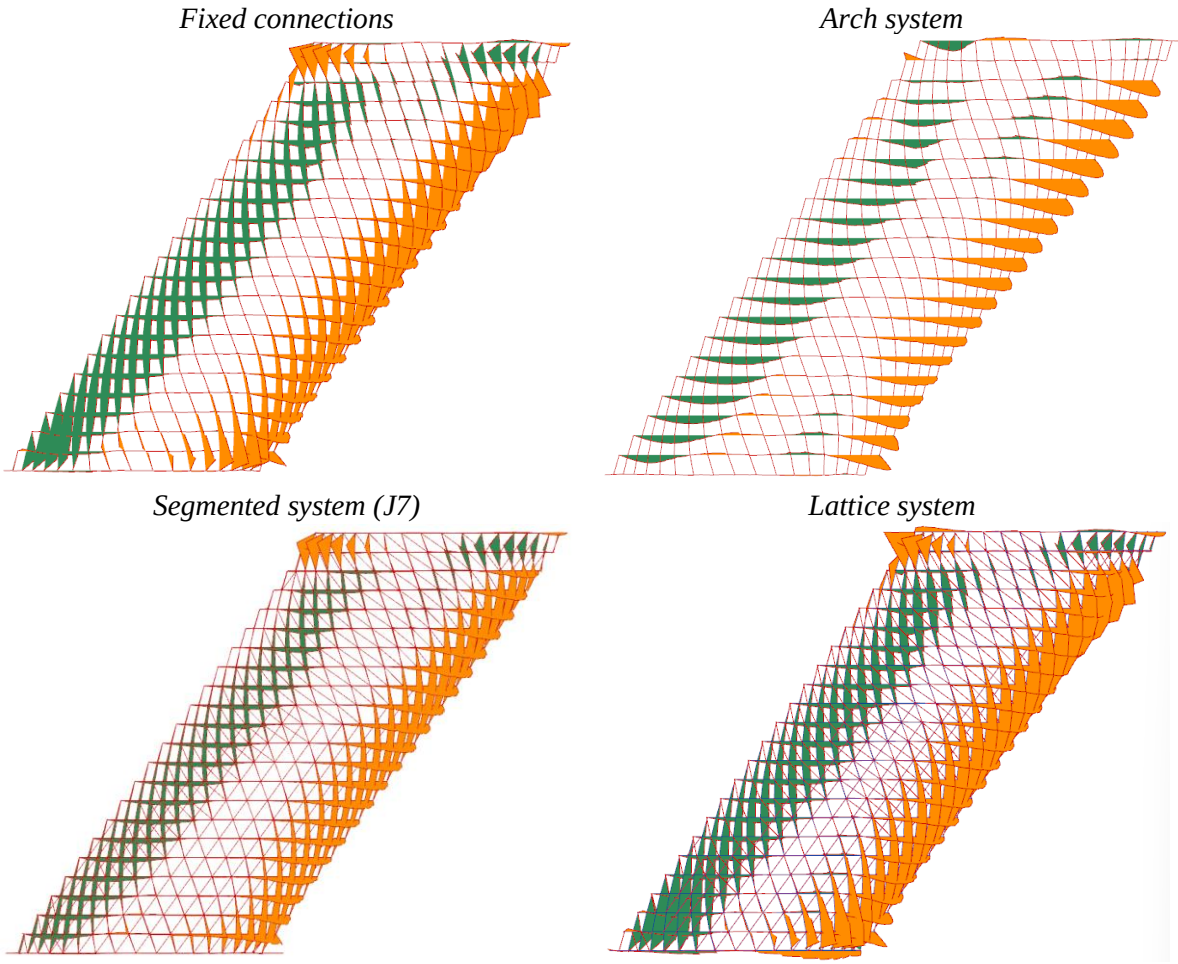

Figure 38 Moment distribution due to wind for variant with facades with different joint mechanisms

Table 15 Internal forces variant with facades without bracing elements

	Fixed connections	Arch system	Segmented system (J7)	Lattice system
My [kNm]	151,08	267,47	274,56	294,18
Mz [kNm]	120,75	123,77	159,36	58,56
Mt [kNm]	5,21	29,18	25,50	6,38
Vy [kN]	73,72	37,29	53,79	19,65
Vz [kN]	40,38	50,23	76,58	75,13
Nc [kN]	540,91	527,85	582,54	440,64
Nt [kN]	721,02	290,29	302,22	518,63

Table 16 Internal forces variant with facades with bracing elements

	Fixed connections	Arch system	Segmented system (J7)	Lattice system
My [kNm]	76,55	132,16	80,48	105,40
Mz [kNm]	45,76	27,21	31,08	35,03
Mt [kNm]	3,19	9,53	6,52	4,25
Vy [kN]	28,98	11,25	10,91	10,69
Vz [kN]	29,87	29,92	25,30	32,10
Nc [kN]	1172,26	1591,17	1337,84	619,00
Nt [kN]	458,46	582,25	431,29	436,42

7.2.1 Element orientation

The element orientation is the alignment of the elements in relation to the base surface of the structure. While the elements can be positioned to have their upper face following the surface normal, they can also be arranged such that they are always vertical, as illustrated in the figure below. The element orientation is considered in this chapter as it is dependent on the specific joint mechanism. As explained before, in a lattice grid-shell, the elements must be oriented according to the surface normal to allow the elements in the primary and secondary direction to cross each other.

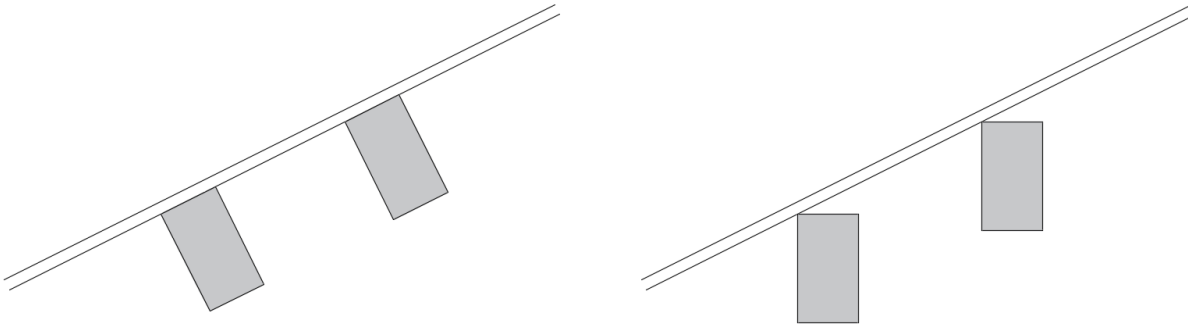

Orientation according to surface normal Vertical orientation

Figure 39 Different orientations for the grid elements

Segmented system

The internal forces for the segmented system with elements oriented both according to the surface normal and vertically are presented in Table 17 and 18. It can be observed that, in terms of the bending moment in the weak direction (M_z) and the torsional moment (M_t), a relatively stiff joint is beneficial. As the joint's stiffness increases, these internal forces decrease. The bending moment in the strong direction (M_y) slightly increases with an increasing stiffness. Both the bending moments in the y- and z-direction are larger with a vertical element orientation. For the z-direction this would be understandable when considering the direction in which the wind load acts on the structure, which is perpendicular to the base surface of the structure. When the elements are oriented according to the surface normal, the wind load acts directly in the strong direction of the cross-section. However, when the elements are vertical, the wind load partially acts in the z-direction of the cross-section. Additionally, the torsional moments are relatively high with an orientation according to the surface normal, which may affect the moment distribution. As the rotational stiffness of the joints increases, the torsional moments decrease.

Table 17 Internal forces with vertical orientation

Joint	M_y [kNm]	M_z [kNm]	M_t [kNm]	V_y [kN]	V_z [kN]	N_c [kN]	N_t [kN]
J1	205,87	208,21	209,49	59,75	81,42	935,43	482,10
J2	189,50	65,23	47,76	16,54	51,74	373,71	223,47
J3	202,95	39,84	27,63	10,10	47,82	352,58	232,80
J4	208,66	30,72	20,60	8,67	46,42	346,92	228,04
J5	210,96	27,03	17,79	8,09	45,98	345,68	230,75
J6	212,90	24,17	15,66	7,66	45,49	342,96	222,36
J7	214,28	22,08	14,11	7,33	45,25	342,20	222,23

Table 18 Internal forces with orientation according to the surface normal

Joint	M_y [kNm]	M_z [kNm]	M_t [kNm]	V_y [kN]	V_z [kN]	N_c [kN]	N_t [kN]
J1	102,82	43,05	217,78	14,91	50,85	976,52	212,62
J2	178,37	22,70	54,80	8,11	50,22	432,66	374,49
J3	175,44	13,76	50,96	6,76	43,58	400,53	352,45
J4	180,44	11,41	47,76	6,71	40,16	382,98	338,98
J5	182,56	10,53	45,92	6,68	38,42	382,40	342,39
J6	185,25	9,85	44,31	6,67	38,53	372,34	331,84
J7	187,48	9,30	42,89	6,66	38,78	371,68	333,31

The torsional moments are not only affected by the joint stiffness, but also by the support conditions and grid pattern. The results presented in the tables above are for grid pattern 3 (Chapter 4). The maximum torsional moment with an orientation according to the surface normal is around the 50 kNm. For grid variant 1 and 2 however, this increases to around 75 kNm. Torsional moments of this magnitude can be very problematic for the dimensioning of the structure. The maximum torsional moment can be decreased significantly by applying (semi-)rigid supports.

Arch system

In this analysis the elements for the arch system were oriented according to the normal of the surface. It is possible but the twisting of the glulam arches results in a more expensive manufacturing process. Therefore, the maximum internal forces for this system with vertically oriented elements are given as well in the table below.

Table 19 Maximum internal forces for arch system with different element orientations

	Orientation surface normal	Vertical orientation
M_y [kNm]	229,79	219,92
M_z [kNm]	75,66	35,45
M_t [kNm]	24,90	14,00
V_y [kN]	14,53	10,41
V_z [kN]	42,16	38,52
N_c [kN]	342,39	339,26
N_t [kN]	179,64	153,93

7.2.2 Differences in element directions

For the arch system the beams are divided in primary and secondary beams. The arches are in this case the primary beams. The moment distributions in Figure 37 and 38 for this system show that there are no bending moments in the secondary beams. For the other systems this is the case, however the magnitude in both primary and secondary beams is not equal. Table 20 shows the maximum internal forces in the primary beams. Then Table 21 shows the maximum internal forces in the secondary beams.

Table 20 Internal forces in primary beams

	Fixed connections	Arch system	Segmented system	Lattice system
M_y [kNm]	220,62	229,79	187,49	209,80
M_z [kNm]	16,63	75,66	9,29	50,91
M_t [kNm]	5,28	24,90	42,89	7,93
V_y [kN]	11,36	14,53	6,66	10,29
V_z [kN]	46,28	42,16	38,78	44,15
N_c [kN]	343,46	342,39	371,68	338,48
N_t [kN]	256,14	179,64	333,31	142,96

Table 21 Internal forces in secondary beams

	Fixed connections	Arch system	Segmented system	Lattice system
M_y [kNm]	115,00	0,54	114,97	126,73
M_z [kNm]	21,74	0,59	9,30	21,96
M_t [kNm]	8,34	6,41	15,70	1,58
V_y [kN]	12,97	0,62	3,01	6,54
V_z [kN]	25,93	0,74	29,42	22,88
N_c [kN]	232,81	277,29	216,37	187,51
N_t [kN]	46,66	35,44	32,23	39,20

7.2.3 Conclusion on internal forces

Comparing the joint mechanisms on the bending moment in the strong direction in a monoclastic variant, it is clear that the highest bending moment appears in the arch system. This would be expected since the arches are supposed to take all the force. The differences with the other joint mechanisms however becomes small when bracing elements are applied. Especially for the arch system these bracing elements reduce the bending moment significantly. The bending moment in the weak direction is also much larger in the arch system. The bracing elements significantly reduces this bending moment as well, but together with the lattice system remains high compared to the other joint mechanisms. Both systems have continuous arches which do not get rotational restraints in the weak direction from the elements in the other direction. This could explain why the bending moment in the weak direction is large in this direction. For the segmented system the torsional moments are notably larger than for the other joint mechanisms.

In the segmented system the bending moment in both the strong (y) and weak (z) direction is larger with a vertical element orientation. The differences might be caused by how the loads are applied on the cross-section. Wind for example acts perpendicular on the base shape of the structure. With a vertical element orientation, it will logically result in larger bending moments in the weak direction. This is because the wind load does not exactly act in the strong direction of the elements. For the permanent load and snow loads this is the other way around. For the arch system however, is the bending moment in the weak direction particularly high with an orientation according to the surface normal. This bending moment becomes significantly smaller with a vertical orientation.

The difference in the primary and secondary beams is especially important for the arch system. Due to their hinged ends, the only bending moment in the strong (y) and weak (z) direction in the secondary beams is due to their own weight. Small torsional moments are present because the secondary elements are restrained in this direction and not all loads act in the strong direction of the cross-section. Particularly the normal forces are relevant for the secondary beams. For the other systems the forces are clearly much smaller in the secondary beams than in the primary beams.

7.3 Effect joint mechanisms on stability

As presented in Chapter 5, the joint stiffness and support conditions are important factors for the stability of the structure. Therefore, the stability is analysed again but now for the joint mechanisms of the structural systems. Furthermore, is the stability analysed for both a monoclastic variant as a variant including rigid facades. The distributions of internal forces were shown to alter due to the inclusion of rigid facades, and this is the case for the stability of the structure as well.

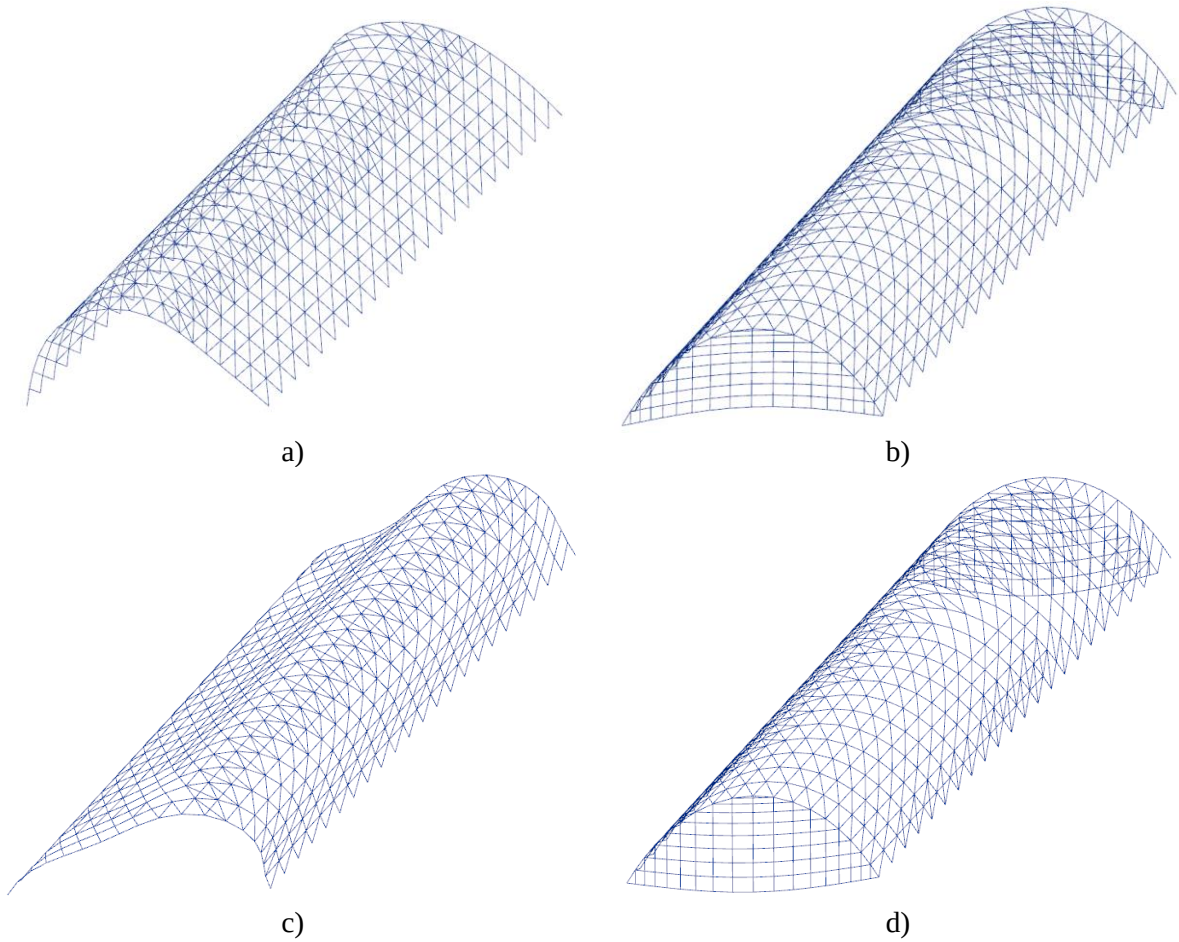

Figure 40 (a) 1st eigenmode monoclastic and hinged supports, (b) 1st eigenmode facades and hinged supports, (c) 1st eigenmode monoclastic and rigid supports, (d) 1st eigenmode facades and rigid supports

Table 22 BLF joint mechanisms for a monoclastic variant

	Fixed connections	Arch system	Segmented system	Lattice system
Hinged supports	1,73	0,88	0	1,42
Rigid supports	12,60	7,68	3,46	4,98

Table 23 BLF mechanism for a variant including the facades

	Fixed connections	Arch system	Segmented system	Lattice system
Hinged supports	4,28	2,81	2,94	4,69
Rigid supports	10,69	7,72	5,69	9,09

The buckling modes looks the same for the different joint mechanisms. But as mentioned above are the buckling modes influenced by the rigid facades. For a monoclastic variant, an in-plane buckling mode appears which is typical for an arch. The lowest BLF in this case results from snow drift between the entrance hall's roof parts. This would be expected since this this load combination results in the largest compressive normal forces in this variant. For the variant with rigid facades however, the facades

themselves buckle. The facades prevent the sideways movement of the structure due to wind, causing them to be pressed. The lowest BLF in this case is therefore caused by wind (ULS-9) instead of snow.

For the segmented system, the BLF for the monoclastic variant is noted as 0. The BLF for this analysis is calculated using Karamba3D's second order analysis component. The results are exact for small deformations. For the monoclastic variant with a segmented system the deflections are however very large compared to the other systems. The sideways translation is more than one meter. It is therefore assumed that the BLF given by Karamba3D in this case is incorrect. The results in Table 22 indicate that for the arch system and segmented system stability is not reached with a monoclastic variant and hinged supports. The rigid facades and rigid supports both significantly increase the BLF. There are however other factors that may help to increase the BLF as well. One option would be to increase the height of the cross-section and/or apply an anticlastic shape. Furthermore, is the highest rotational stiffness of the range showed earlier used. It may be interesting to see what happens with the BLF if the rotational stiffness is increased until the joints show rigid behaviour. Finally, the effect of the element orientation on stability will be analysed as well.

In the graph below the effect of the joint stiffness on the BLF is presented for semi-rigid and rigid supports. For the semi-rigid support, the analysis is conducted once with a stiffness of 1000 kNm/Rad, and once with a stiffness of 9000 kNm/Rad. This analysis is conducted to show the effect of the joint stiffness and support conditions on the BLF for the segmented system. Then in Table 24 the BLF with a cross-section height increased from 450 mm to 600 mm is given for both the segmented and arch system. Furthermore does the table show the difference between the monoclastic and anticlastic variant, as well as both element orientations.

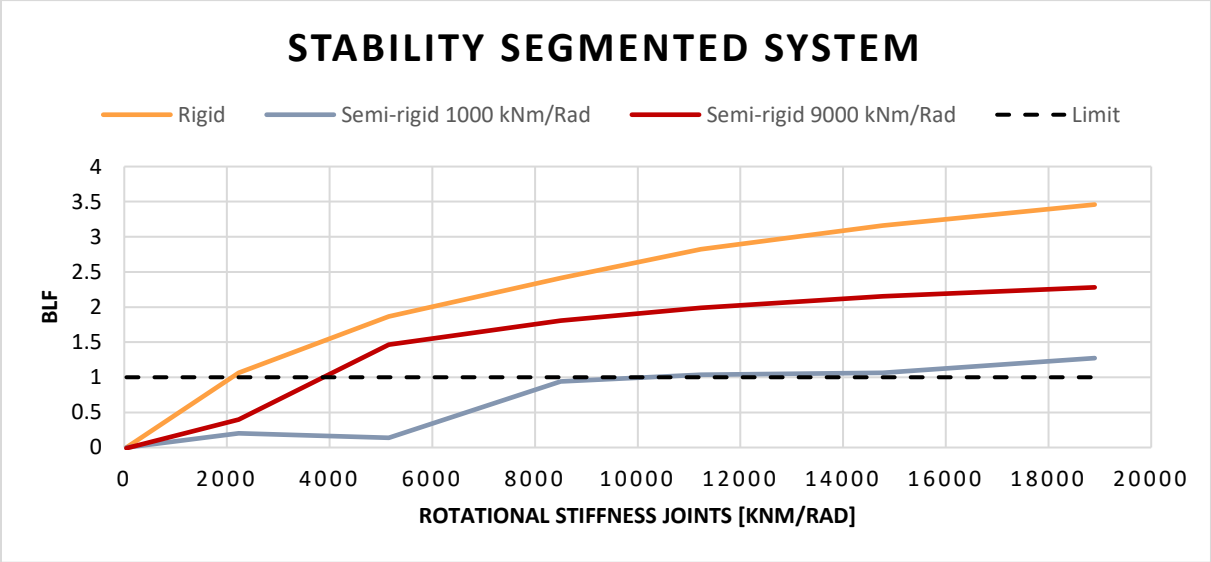

Figure 41 Effect joint stiffness and support conditions on the BLF in segmented system

Table 24 Effect double curvature on BLF

	Monoclastic (600 mm)		**Anticlastic (600 mm)**	
	Surface normal	*Vertical*	*Surface normal*	*Vertical*
Segmented system	1,44	0,97	1,57	1,13
Arch system	1,74	2,09	1,93	2,32

The anticlastic shape seems to increase the BLF for both the segmented system as the arch system. As explained in the previous chapter does the anticlastic shape result in a structure that has more stiffness in the lateral direction compared to a monoclastic variant. This is due to the structure becoming more flat in the middle, resulting in a more horizontal truss-structure. The effect of a vertical element

orientation is different for both systems. Earlier it was shown that for the segmented system the maximum bending moment and normal forces become larger with a vertical orientation. Therefore, the decrease of the BLF is as it would be expected. For the arch system the effect of the vertical element orientation on the internal forces was the opposite. The same happens with the BLF.

For the segmented system with a monoclastic variant and vertical element orientation, an error is given that the nodal displacement increments did not converge. A BLF of 0,97 is given in this case which would imply that the system buckles under the applied load. Due to the error which is given by Karamba3D it is however not certain if this is indeed the correct BLF for this variant.

7.4 Effect joint mechanism on deformation

As shown in the previous chapter does the wind load cause a large sideways deformation of the roof structure. Different shapes such as an anticlastic and synclastic shape, next to incorporating the facades in the structural systems were applied to analyse their effect on the deformation. In this section of this chapter the effect of the different joint mechanisms on the deformations is looked at. For this analysis a monoclastic variant with hinged supports is used. For all joint mechanisms an equivalent bending stiffness is maintained. The results are presented in the table below.

Table 25 Deformations of different joint mechanisms

	Fixed connections	Arch system	Segmented system (J7)	Lattice system
Horizontal	225,72	427,16	669,89	332,70
Vertical	159,84	310,09	459,30	236,40

From the three different joint mechanisms, the lattice system results in the least deformations both in the vertical as horizontal direction. This would be expected because in this system, the elements are continuous and contain no hinges in the y-direction. Based on the results the lattice system seems to result in the stiffest system, which already became apparent from in the previous section of this chapter. Furthermore, does the segmented system with Joint 7 (Table 12) lead to the largest deformation. The reason for this is that the many joints that are located in the arches significantly reduce their stiffness. This system does however have the possibility to create joints with more rotational stiffness, leading to smaller deflections. The reason that the arch system deforms more than the lattice system is because the secondary beams have hinges at their ends. Therefore, they will not add stiffness to the arches.

7.5 Conclusions on stability and deformation

The results of the stability and deformations would imply that the lattice system results in the structure with the most stiffness. The segmented system seems to result in the structure with the least stiffness. There are however several important factors which are not taken into account in this chapter. The primary arches in the arch system and all elements in the lattice system are assumed to be continuous. In reality this is not possible due to transportation limits, causing these elements to be segmented. These segments will have to be connected resulting in joints with a certain rotational stiffness within the structure. This will decrease the overall stiffness of the structure. In addition does the segmented system have the possibility for the application of joints with a larger rotational stiffness. The differences in deformation may therefore not be as much as shown in the results.

8 VARIANT STUDY

In the previous chapter different joint mechanisms corresponding to the potential connection types for the timber grid were analysed on their effect on the internal forces and stability of the structure. However, there are additional considerations to take into account when comparing the different structural systems. For example, when dimensioning the cross-sections according to Eurocode 5, it becomes apparent that curved timber elements require additional stresses to be considered. Additionally, specific details for certain systems can affect the dimensions of the cross-sections. For example, the lattice system utilizes shear blocks for which a composite factor needs to be taken into account, and the segmented system requires a certain amount of bolts with a minimum distance. Other factors such as practicality and the manufacturing process can also influence the choice between the analysed design options. To make a more substantiated comparison between the structural systems discussed in the previous chapter, variants will be worked out for each system. The dimensions of the cross-sections will be determined based on the ULS criteria, important detailing, practical issues, and the influence of the manufacturing process will be taken into account. For each design option (arch shape, grid pattern, etc.), reasoning will be given to determine which is the best option based on the above described factors. Finally, they will be compared based on material cost and practicality. For the criterium material cost, the variants will be compared based on their estimated required amount of timber and steel. For the criterium practicality, an elaboration will be given about the complexities of each variant, from which will be estimated what the more practical variant to manufacture will be. The variant that scores the highest on these criteria will be developed further for the final design. Relevant calculation procedures for cross-sections and detailing can be found in Appendix C, along with corresponding spreadsheets in Appendix E.

Detailing of the supports and connections that may be necessary due to transportation limits are not worked out in this chapter yet. The variants are furthermore worked out assuming hinged supports. In addition is a maximum width of 240 mm assumed for the cross-sections. This is the maximum width indicated by different manufacturers within the standard sizes for Glulam elements.

8.1 Variant segmented system

The segmented system exists from individual straight timber elements that are connected by slotted in steel plate joints. To provide sufficient rotational stiffness, normal force, and bending moment capacity, does the joint require a specific number of bolts. According to Eurocode 5, a minimum distance between the bolts must be maintained. To achieve this, a minimum height of the timber element is required, which can be determinate for the dimensions of the cross-sections. Therefore, it is important to include this detailing in the design of this variant. The considerations for the design options for the segmented system will be described first. Then the final dimensioning including the detailing of the joints will be provided.

8.1.1 Element orientation – segmented system

As previously discussed does the segmented system allow for the elements to be oriented either vertically or according to the surface normal. However, the vertical orientation results in a practical issue, as illustrated in Figure 42. The image on the left shows a joint that corresponds to a vertical orientation, which could be located in one of the arches near a support. In addition to the two timber elements that are connected to this joint and shown in the figure, there are other timber elements that are connected to this joint that come from a direction perpendicular to the figure. Since these elements are also oriented vertically, the joint must also be oriented vertically. When the elements have a height of 0,6 m for example, the joints near the supports must be almost 1,5 m long in order to connect all the elements. On the other hand, when the elements are oriented according to the surface normal, as shown in the figure on the right, the joint need to be as long as the height of the elements. This practical issue leads to a significant additional amount of required steel. Therefore, it is decided to create a variant in which the elements are oriented according to the surface normal.

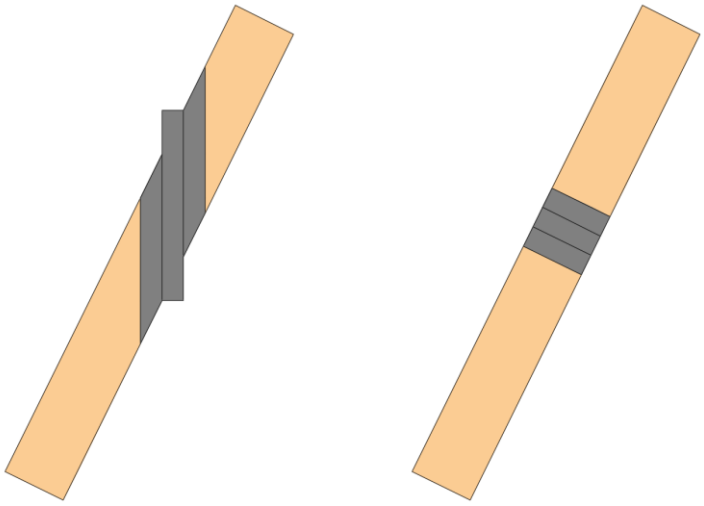

Figure 42 Practical issue joint segmented system concerning element orientation

8.1.2 Barrel vault variant – segmented system

The use of rigid facades at the ends of the structure was found to increase the stability of the structure and reduce torsional bending moments for both element orientations. However, as previously shown in Chapter 6, including the rigid facades also leads to very large normal forces in the elements, caused by wind pressure acting on one side and suction on the other side of the arches. These normal forces are especially large when the facades are placed in the outermost arches of the structure. The magnitude of these normal forces is such that the height of the cross-sections depends on the normal force resistance of the joints, requiring an increase in height to add more bolts to the connections. However, by placing the facades one arch inwards, the normal forces decrease significantly, but it will still be a deciding factor for the dimensioning. On the other hand, the torsional moments that occur in the structure are a bigger concern than the normal forces. Therefore, the smallest cross-section is achieved by incorporating the facades into the structural system. Additionally, in terms of stability, the facades have a significant advantage. Therefore, this variant will include the rigid facades in the structural system.

8.1.3 Grid pattern – segmented system

As shown in Chapter 4, the differences in internal forces between grid pattern 1 and grid pattern 3 are minimal. Grid pattern 1 is a flat grid, which is vertically projected on a shape and closely resembles the architectural design, while grid pattern 3 is created by dividing the shape into equal parts. It was found that the normal forces in grid pattern 1 are significantly larger with rigid facades than for grid pattern 3. As previously discussed, the normal forces are a deciding factor in determining the dimensions of the cross-sections. Given this, it has been decided to apply grid pattern 3 for this system.

8.1.4 Arch shape – segmented system

In Chapter 6 it was shown that the catenary shape results in the lowest maximum bending moment when rigid facades are applied. Given this advantage, it has been decided to apply a catenary shape for this variant.

8.1.5 Final variant segmented system

As previously mentioned, the detailing of the joint can be determinate for the dimensions of the cross-sections of the timber elements. Calculations have shown that this is indeed the case for this system. To resist the normal forces that are a result of wind when facades are incorporated into the structure, the joints requires a sufficient amount of bolts. The joints must have at least 7x8 bolts with a diameter of 22 mm. The rotational stiffness corresponding to this bolt layout has also been included in the calculation model to determine the internal forces. The cross-sections themselves are 240 x 660 mm. A 3D model of this variant is shown in the figure below.

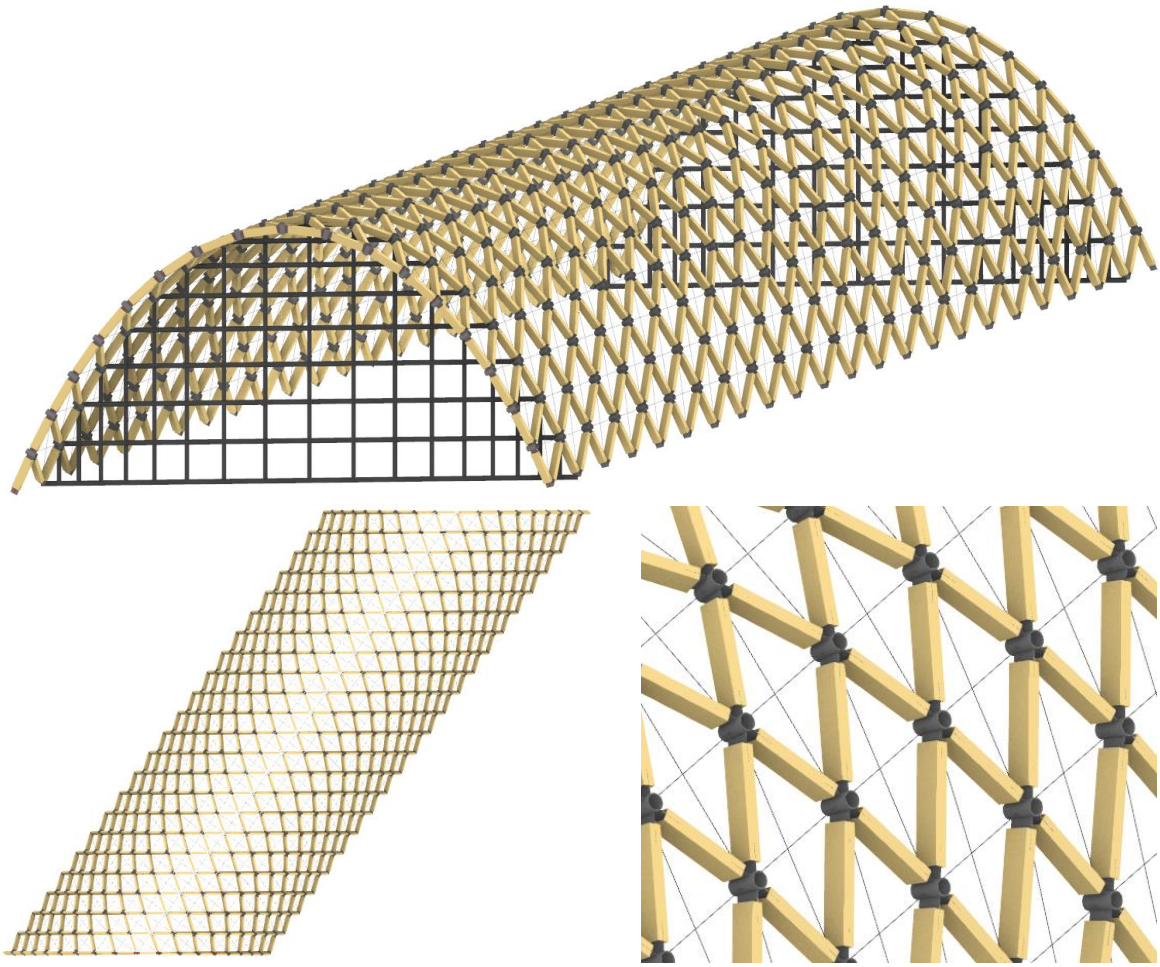

Figure 43 Design variant with segmented system

The figure below presents the final geometry of the slotted in steel plate joint. The joint contains 7x8 bolts at each side. The steel plates are 660 mm in height and have to be at least 924 long. The spreadsheet which is used for determining this geometry can be found in Appendix E.

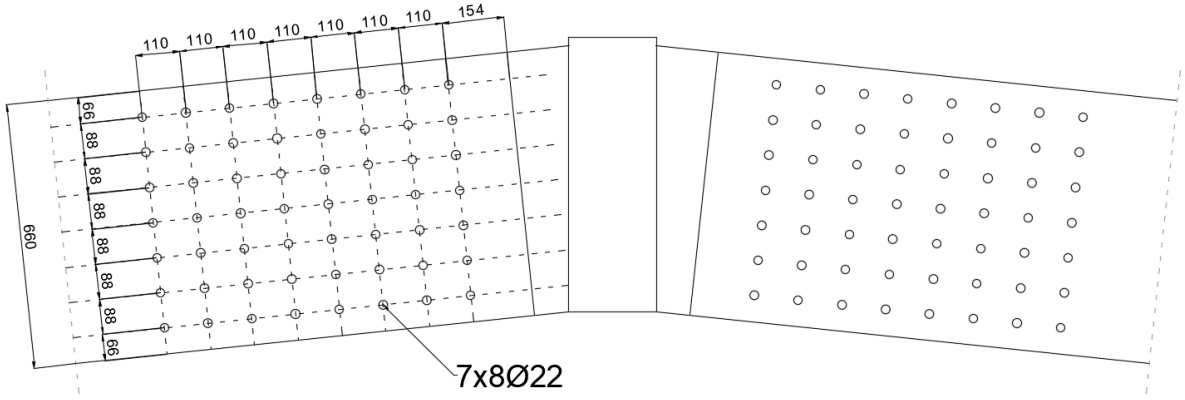

Figure 44 Layout joint for variant with segmented system

8.2 Lattice system

In the lattice system, the elements are continuous and have a woven-like structure. The cross-section consists of two outer layers with shear blocks in between. The elements can therefore be considered as build-up elements or mechanically connected beams (as described by Eurocode 5). A composite factor

affecting the stress distribution in the cross-section must be taken into account. The lattice system utilizes pre-fabricated curved elements, unlike the segmented system which utilizes straight elements. The dimensioning of the cross-sections in the lattice system is different due to the curvature of the timber elements, causing additional stresses. The bending stresses in this case are not linearly distributed over the height but have a parabolic distribution. Additionally does a positive bending moment in a curved element result in stresses perpendicular to the grains of the timber. The calculation procedure for such build-up elements can be found in Appendix C.

8.2.1 Element orientation – lattice system

As explained in the previous chapter, it is necessary for this system that the elements are oriented according to the surface normal. This is because elements from different directions must be able to cross each other.

8.2.2 Grid pattern – lattice system

The elements in the secondary direction in grid pattern 1 and 2 have two curvatures, a vertical and a torsional curvature. In grid pattern 3 these elements have an additional horizontal curvature. In order to realize this third curvature, blocked glue laminated timber or a CNC milling machine has to be applied. Utilizing a CNC milling machine will however result in cut fibres, which leads to stresses perpendicular to the grains of the timber. This technique is for example used in the manufacturing process of Centre Pompidou Metz. Due to the cut fibres, a reduction of the material strength had to be considered (Chilton & Tang, 2017). For this reason, together with the results from Chapter 4 it is decided to apply grid pattern 1 for this variant.

8.2.3 Barrel vault variant – lattice system

In the previous chapter, it was demonstrated that a variant including the facades with a lattice system significantly reduces the maximum bending moment compared to a monoclastic variant. The analysis was conducted using grid pattern 3. The backside facade was connected to the outermost arch, while the frontside facade was positioned one arch inward, similarly to the architectural design. However, grid pattern 1 has a grid pattern that is cut off at one side of the structure, making it impossible to place the backside facade in the outer arch. Thus, this leads to a different moment distribution compared to what was shown in the previous chapter. The difference in maximum bending moment for this case is minor (2 kNm) between a variant with facades and an anticlastic shape. Applying an anticlastic shape instead of the facades will therefore save both steel and timber.

8.2.4 Arch shape – lattice system

As stated in the introduction of this paragraph does a curvature in the elements result in additional stresses, including stresses perpendicular to the grains of the timber. The radius of curvature of the elements is an important factor in determining the stresses perpendicular to the grains of the timber. A larger radius of curvature reduces these stresses. Among the analysed shapes, the parabolic arch and the catenary arch contain the smallest radius of curvature located at the peak, with decreasing values towards the ends of the arch. The ellipse on the other hand, has a much larger and constant radius of curvature along its length.

It may be overly conservative to apply the lowest radius of curvature for the cross-section dimensioning in combination with the maximum bending moment, as this bending moment resulting from wind typically occurs at the sides of the arches, where the radius of curvature is much higher. However, positive bending moments do occur at the peak for several load combinations. This can be seen in Appendix A where the bending moment distribution is plotted for all load combinations for a 2D catenary arch. In a 3D model the moment distributions are very similar. An analysis is performed in which the tensile stresses perpendicular to grains are determined for each load combination. For each load combination the largest positive bending moment is applied in combination with the radius of curvature of the location where this bending moment occurs. It became clear that load combination ULS-6 results in the largest tensile stresses perpendicular to grains. This load combination includes a wind load that causes a positive bending moment in the peak of the arch.

The most advantageous shape to apply is the catenary shape, as it results in the smallest cross-section due to the optimal combination of radius of curvature and maximum positive bending moment. Therefore, this shape will be applied for the arches in the variant with the lattice system.

8.2.5 Final variant lattice system

The dimensioning of the cross-sections resulted in three layers with a height of 250 mm and a width of 240 mm. The total amount of required timber, including the shear blocks, will be provided in the final section of this chapter. Additionally, the figure shows steel connectors at each node for the bracing elements, which have been modelled after the connectors used in the Waitomo Caves Visitor Centre (Chapter 2). It should be mentioned that if this system will be applied for the final variant, the structure has to be segmented due to transportation limits. The connections between the segments can have a certain rotational stiffness depending on their detailing. This can alter the internal forces in the structure. For this analysis it was assumed that the elements are continuous, as the detailing for these connections has not been worked out so far.

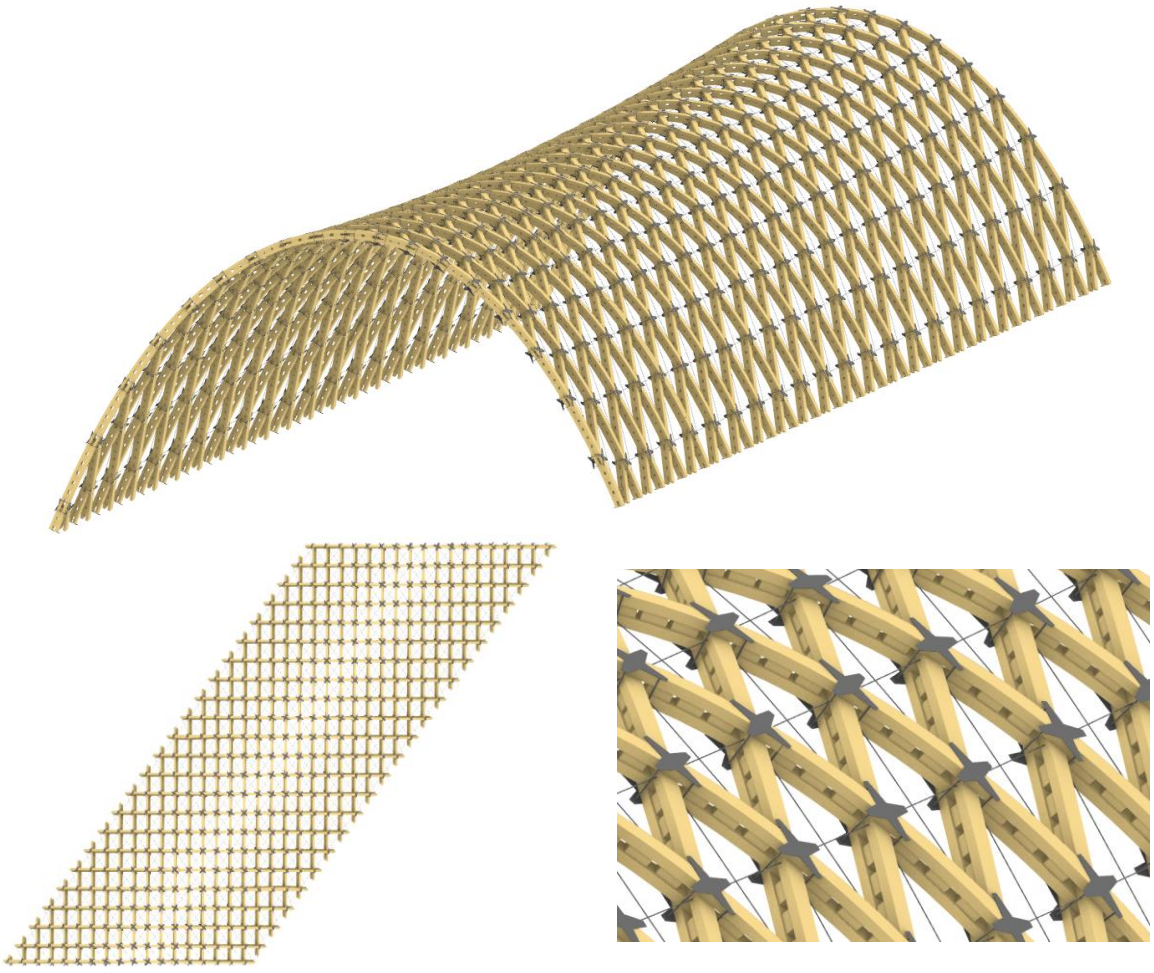

Figure 45 Design variant with lattice system

8.3 Arch system

It was assumed for the segmented and lattice system that all elements are equal, meaning that regardless of the direction, all elements have the same cross-section dimensions and are either all straight or all curved. In this system, the primary beams and secondary beams are considered independently. As previously stated, the secondary beams only experience normal forces, whereas primary beams experience significant bending moments. Furthermore, are the primary beams curved, whereas the secondary beams are straight. This results in a different calculation procedure between primary and secondary beams.

8.3.1 Element orientation – arch system

In this system, elements can be oriented either according to the surface normal or vertically. However, orienting the arches according to the surface normal would require them to be twisted along their length, making them more costly and most likely leading to more complicated detailing. The previous chapter's analyses showed that a vertical orientation decreases the internal forces and increases the stability of the structure. Therefore, all elements in the system will be oriented vertically.

8.3.2 Barrel vault variant – arch system

In this variant, the primary beams being curved and experiencing significant bending moments means that the stresses perpendicular to the timber grains are decisive in determining the cross-section dimensions. Decreasing the maximum bending moment is therefore most important. This can be achieved by applying the rigid facades or an anticlastic shape. For this variant the facades are more effective in decreasing the maximum bending moment. However, the normal forces are significantly larger than those resulting with an anticlastic shape. These large normal forces also occur in the secondary beams. For this system, a connection has to be created by which normal forces can be transferred through the primary arches without causing stresses perpendicular to the grains of the primary arches. If the normal forces are very large this may result in a very complex connection. Furthermore, it could be possible that the cross-section of the secondary beams has to be significantly increased because the detailing requires sufficient normal force capacity, as became clear in the variant utilizing the segmented system. It is therefore expected that an anticlastic shape is the better option.

8.3.3 Grid pattern – arch system

Since the secondary beams are not curved, does the grid pattern not affect the manufacturing process of the beams like it did for the lattice system. The choice of grid pattern is solely based on which one results in the lowest maximum bending moment. As demonstrated in Chapter 4, this occurs when using Grid Pattern 3, which divides the structure into equal parts. Therefore, this grid pattern will be applied in this variant.

8.3.4 Arch shape – arch system

The reasoning for the shape of the arches in this system is similar to that of the lattice system. The stresses perpendicular to the timber grains determine the cross-section dimensions, making the radius of curvature an important factor to consider. A catenary shape offers an optimal combination of the radius of curvature and maximum positive bending moment.

8.3.5 Final variant – arch system

As expected, are the cross-sections for the primary beams (arches) much larger than those of the secondary beams. For the primary beams the cross-section is 240 x 610 mm, while the cross-section for the secondary beams is 120 x 120 mm. The secondary beams only experience normal forces and the cross-section’s dimensions are therefore determined by the critical buckling load. A 3D model of this variant can be seen in the accompanying figure.

As explained in the previous section of this chapter do certain size limits have to be taken in consideration due to transportation. In this chapter the arches are assumed to be continuous, but will be segmented in a possible final variant. As explained for the lattice system can the detailing of the connections between the segments alter the bending moment values.

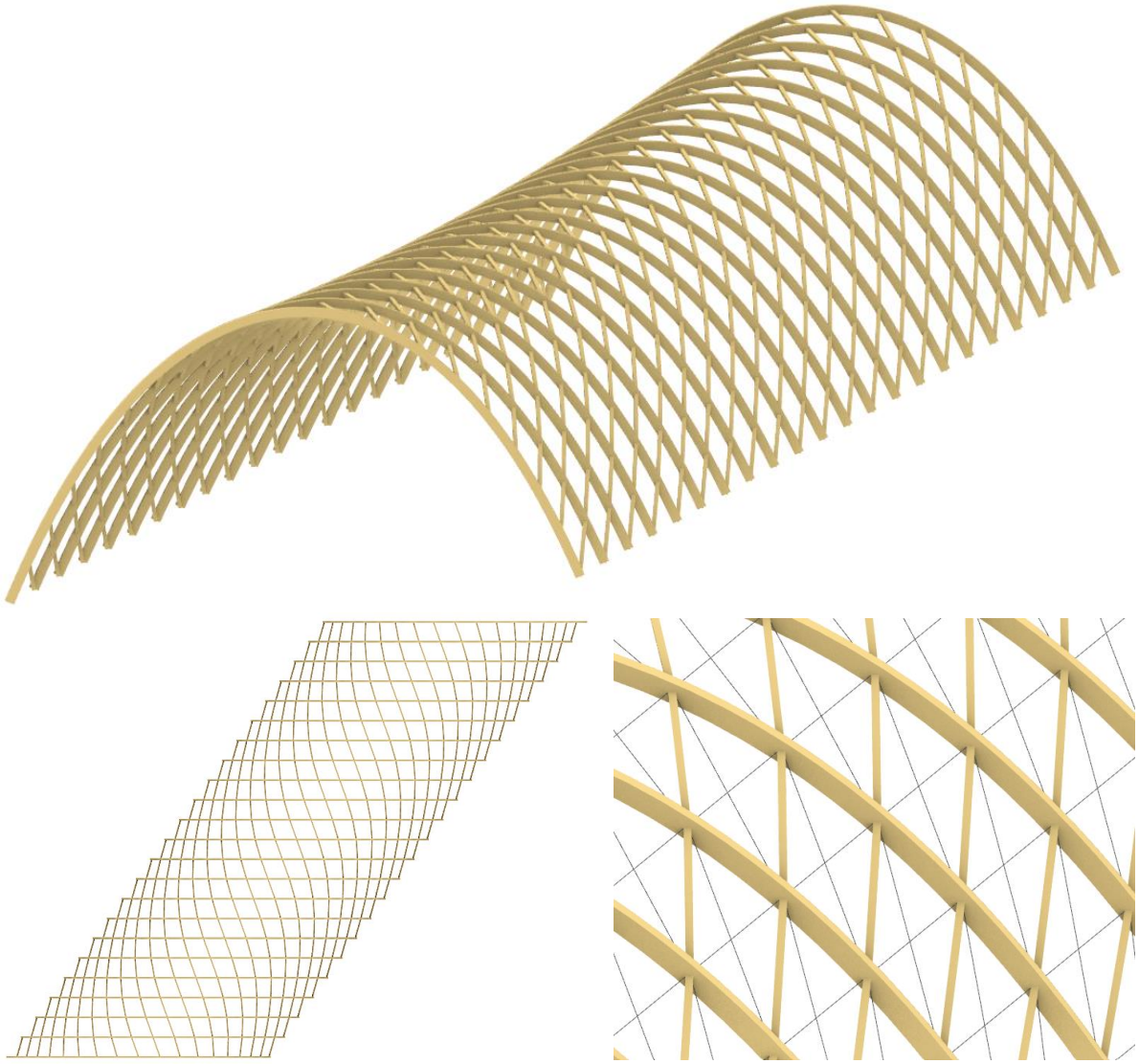

Figure 46 Design variant with arch system

8.4 Comparison variants

By developing a variant for each structural system to some extent, a more reasoned comparison can be made based on the criteria material cost and practicality. Although the detailing is not worked out completely, a better overview is obtained on the effect the connection types have on these criteria.

Due to the relatively small size of the secondary beams in the arch system compared to elements in other variants, the total amount of timber required for this system is significantly lower. An estimation of the total required timber for each variant can be found in the table below.

Table 26 Required timber for each variant

	Segmented system	Lattice system	Arch system
Timber (m^3)	415,8	338,7	196,0

The amount of steel required for the segmented system is significantly higher compared to the other variants. This is due to the required number of bolts, which requires a certain height for the cross-section, and therefore also increasing the height of the connection's steel parts. Additionally, the length of the steel plates required is based on the number of columns and the diameter of the bolts. According to the

calculations, the plates are estimated to have a length of nearly 1 meter on each side of the joint. This results in a usage of approximately 4 meters of steel plates, 224 bolts, and a steel tube of at least 0,66 meters in height for each joint. Given the number of joints in the structure, this leads to a substantial amount of steel compared to the other variants.

The curvature in the segmented system is realised through the geometry of the joints, which vary in angle depending on their location in the structure. This leads to complex and diverse joints, in addition to the large amount of required steel, making this variant less favourable. The lattice system has to be build-up from outer layers and shear blocks on-site. Furthermore, it is complex due to the geometry of the elements which vary and are both curved and twisted along their length. Additionally, the amount of required timber is significantly more than the total amount of timber for the arch system. The use of steel connectors for bracing elements may also result in a large amount of steel. On the other hand, the secondary beams in the arch system require complex custom steel connections that can transfer normal forces through the arches and prevent compressive stresses perpendicular to the grains. The elements themselves however, have a simple rectangular cross-section.

In terms of practicality, the lattice system results in timber elements that are complex to manufacture, while the nodal connections are relatively simple. For the arch system this is the other way around. It is therefore hard to point out the more favourable variant in terms of practicality. Based on the ULS-criteria, a significant amount of timber can be saved applying the arch system. The SLS-criteria however, may have an great impact on the amount of timber. This will be discussed in the next section.

8.5 Performance of variants on serviceability criteria

As mentioned in earlier chapters, does the structure greatly deform due to the wind acting on it. The sideways deformation makes it challenging to meet the criterium for the horizontal deformation which is provided by the Eurocode (Appendix C). In this chapter, the detailing of the variants is not fully worked out. Designing supports that have a rotational stiffness will help to decrease the deformation and may be necessary for each joint mechanism. The segmentation in the lattice and arch system will however most likely cause an increase of the deformation. For the arch system, only the primary beams need to be segmented. For the lattice system this applies for the elements both in the primary as in the secondary direction. In the table below the maximum horizontal deformation is given for each variant, caused by the load combinations corresponding to the SLS (Appendix A). The criterium states that this deformation should not be larger than 1/300 of the height, which comes down to 60 mm.

Table 27 Maximum horizontal and vertical deflection for each variant

Deformation [mm]	Segmented system	Lattice system	Arch system
Horizontal	115,57	117,2	256,92
Vertical	58,19	79,38	153,91

As can be seen by the results are the variants far from meeting the criterium for the horizontal deflection. It can therefore be concluded that the cross-section dimensions will most likely be greatly increased for all variants. This will impact the practical issues which are described in this chapter as well. The nodes in the segmented will become larger leading to more steel. The layers of the lattice variants will become thicker or even a third layer is needed, leading to an even more complex manufacturing process. This variant however still has the possibility for rigid facades to be applied, or the height difference for the anticlastic shape should be greatly increased. For the arch system incorporating rigid facades was not considered to be strategic due to the normal forces that have to be transferred through the primary arches. Therefore, also for this variant the height different of the anticlastic shape should be greatly increased.

8.6 Conclusions on variant study

The segmented system requires both the largest amount of steel and timber. In addition, it utilizes complex steel nodes which require to be manufactured very accurately. The lattice system exists out of elements build-up from two pre-fabricated layers and shear blocks. The elements twist along their length

as they are required to be oriented according to the surface normal. In terms of the ULS criteria it requires a significant larger amount of timber compared to the arch system. This variant is however much closer to meeting the SLS criterium for the horizontal deformation. This difference in the total amount of timber may therefore not be as big when they are designed to fulfil all SLS requirements. The arch system is however still considered to be the favourable variant. The elements in the secondary direction are straight. The primary arches are curved but do not need to be twisted along their length. The nodal connections however are more complex compared to those in the lattice system. Given it's potential to be the variant that requires the least amount of timber, it is decided that the variant utilizing the arch system will be worked out to a final design.

9 HORIZONTAL MOVEMENT OF ARCHES

When a vertical force is applied to an arch, the ends of the structure tend to move outward, as illustrated in the figure below. This behaviour also occurs at the supports of the roof arches. The roof is supported by long-spanning structures, which can make it difficult to manage the horizontal reaction forces that result from the loads on the roof. This is because these forces cannot be directly transferred to the foundation. The long-spanning structures can however be used to create a truss-like system to prevent horizontal movement at the supports. The focus of this chapter will be on a possible solution and its effect on the internal forces in the structure.

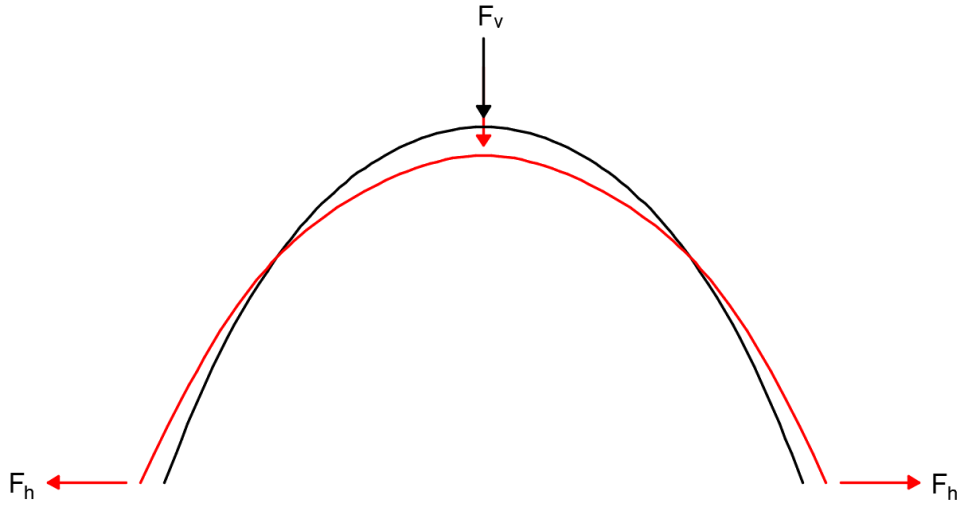

Figure 47 Horizontal reaction forces arch

For arches that are not situated at ground level, one possible solution is to apply a tension rod between the supports. This creates a horizontal equilibrium and prevents horizontal movement of the supports. However, adding tension rods to every arch can be visually unappealing. An alternative approach is to strategically use the long-spanning structure to create a truss-like structure restraining the horizontal movement of all supports. For this truss to be active, only the supports at the corners need to be restrained.

In similar structures which contain segmented arches, tension rods may not be necessary, since the adjacent arches create a horizontal equilibrium themselves. The arches from different parts in the entrance hall are however not the same size and therefore will not have equal horizontal reaction forces. Nevertheless, may the smaller arches still decrease the resulting horizontal force at the supports.

In this chapter three different situations will be covered to obtain an overview of the effect of the horizontal movement on the structural behaviour. The three situations that will be analysed are:

- Situation A: All supports in the structure are horizontally restrained.
- Situation B: All supports at one side can move horizontally. Also, the effect of a smaller adjacent arch will be included.
- Situation C: All supports at one side can move horizontally except for the corners. In addition, elements at the outer sides between the supports are placed that represent the long-spanning structure.

This study will use a single load combination that takes into account snow accumulation between the different roof parts, as this load combination results in the largest horizontal reaction forces and may therefore be crucial for the results. Additionally, all joint mechanisms will be considered to determine if they have any effect on the outcome of the different situations.

9.1 Situation A

The figure below presents the bending moment distribution (M_y) for situation A, where all supports are hinged and horizontal movement is restrained. The results for the internal forces are given in Table 28.

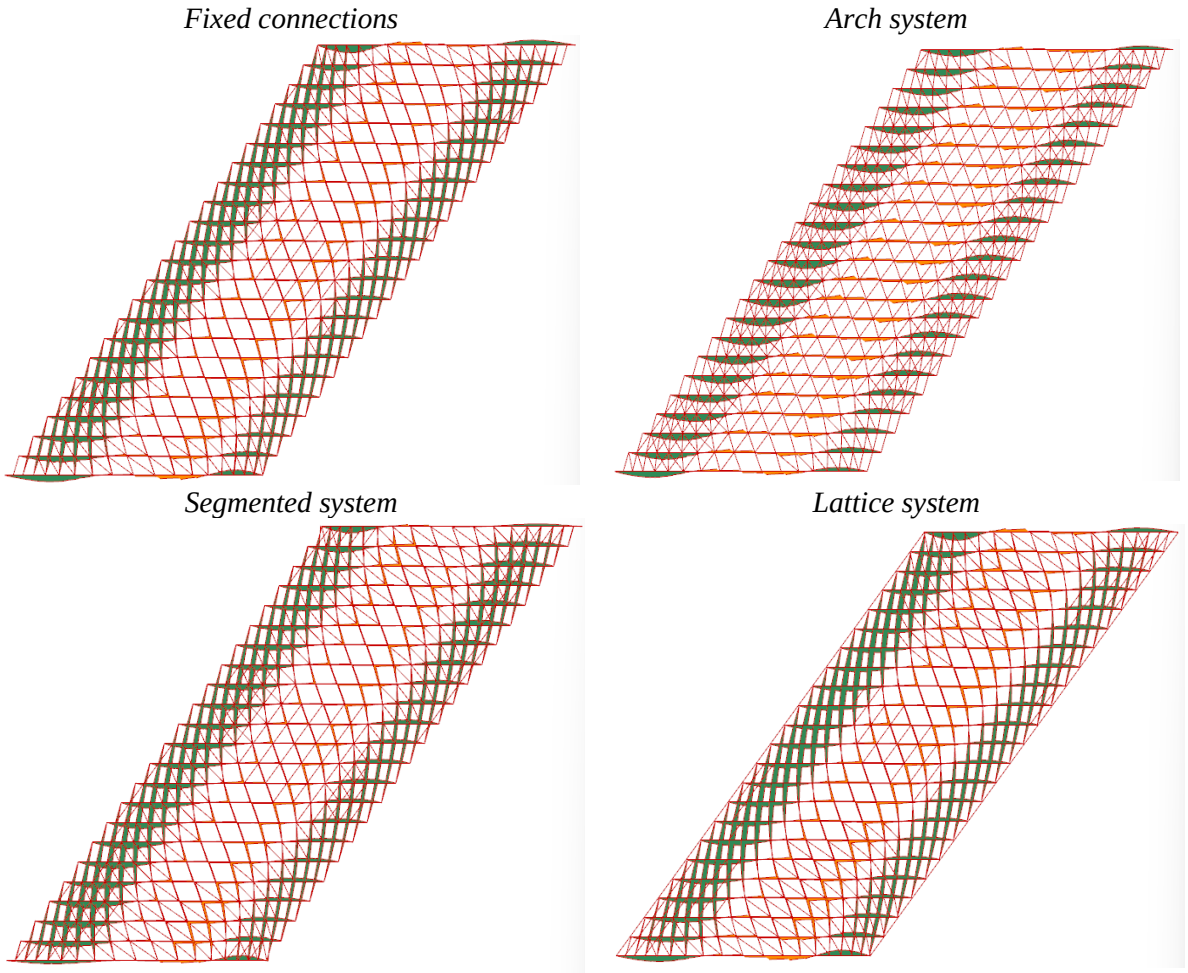

Figure 48 Moment distribution (M_y) situation A per joint mechanism

Table 28 Internal forces situation A resulting from snow accumulation

	Fixed connections	Arch shape	Segmented	Lattice
M_y [kNm]	97,47	136,12	96,39	105,21
M_z [kNm]	12,35	19,45	4,49	18,25
M_t [kNm]	3,44	12,06	26,94	3,99
V_y [kN]	9,56	9,22	6,68	8,30
V_z [kN]	26,95	30,47	27,75	28,70
N_t [kN]	39,88	12,04	34,04	29,22
N_c [kN]	348,97	349,64	354,9	338,18

9.2 Situation B

The figure below presents the bending moment distribution (M_y) for situation B, where all supports on the right side are able to move in the horizontal direction. No resistance from the adjacent arch is taken into account yet. As can be observed, the moment distribution differs greatly from that of situation A and the internal forces are significantly larger. This conclusion is consistent for all joint mechanisms.

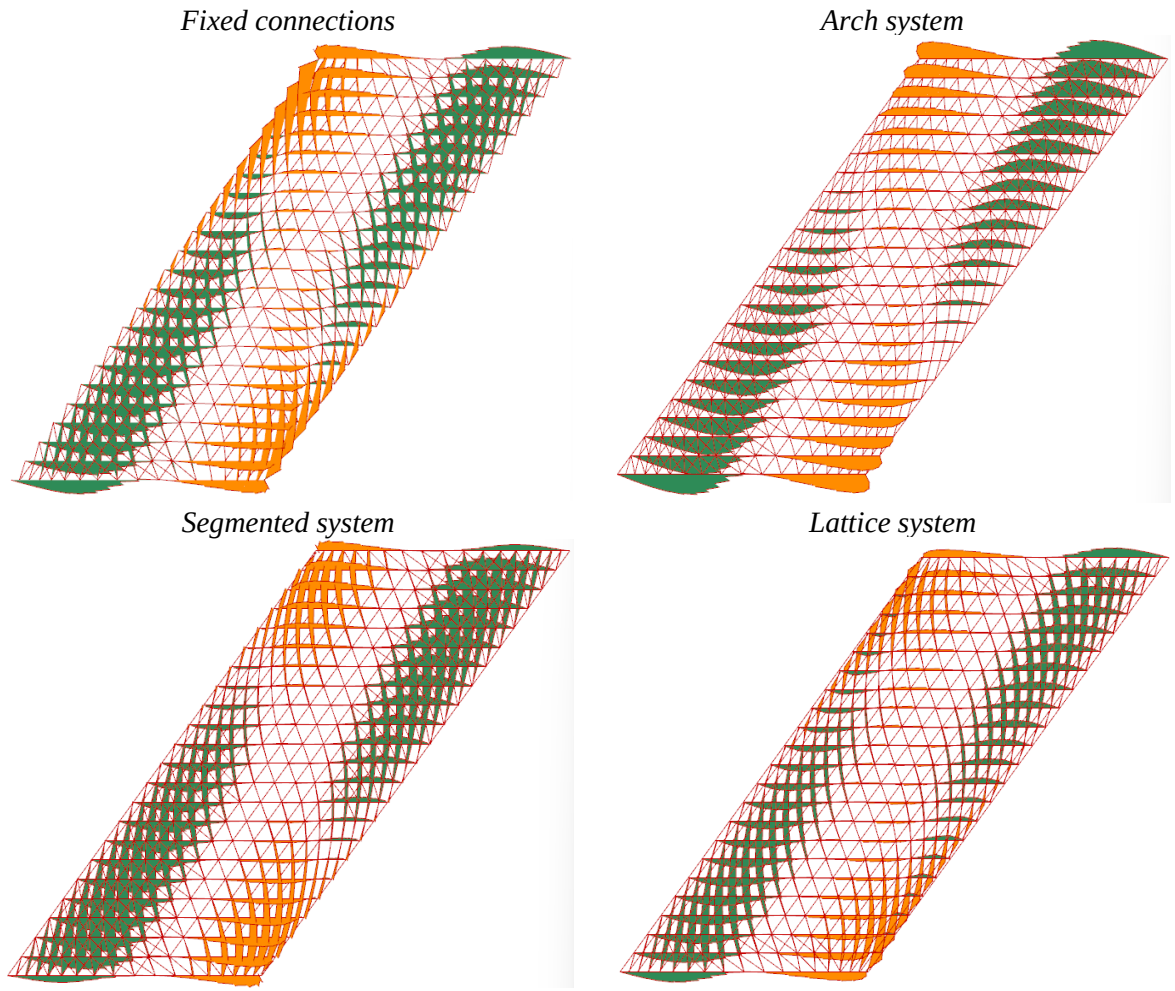

Figure 49 Moment distribution (M_y) situation B per joint mechanism

Table 29 Internal forces situation B resulting from snow accumulation

	Fixed connections	Arch	Segmented	Lattice
M_y [kNm]	400,92	603,06	416,39	304,00
M_z [kNm]	37,80	191,44	15,87	82,91
M_t [kNm]	20,63	69,31	98,24	26,78
V_y [kN]	27,42	26,47	8,15	18,82
V_z [kN]	94,62	87,80	98,78	58,84
N_t [kN]	207,70	113,25	334,08	241,87
N_c [kN]	938,64	1042,08	995,72	871,47

The horizontal movement at the supports of the large arch is countered by the smaller adjacent arches. This is due to a smaller horizontal reaction force resulting from the smaller arch, and the force required to deform the smaller arch. The smaller arch essentially acts as a horizontal axial spring at the supports of the larger arch. To determine this axial stiffness and the horizontal reaction force of the smaller arch, a 2D Grasshopper model is used.

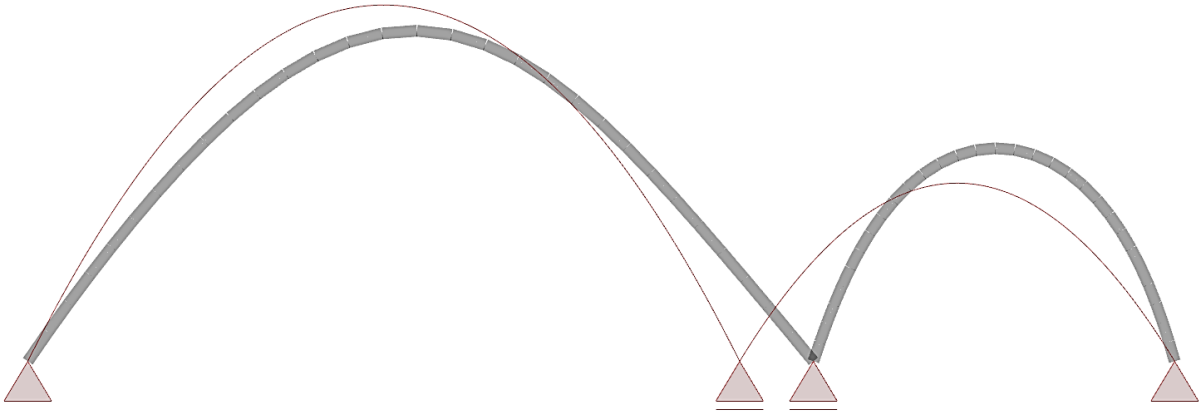

Figure 50 Axial resistance of smaller arch

The axial stiffness of the small arch is mainly determined by the cross-section assigned to it, as illustrated in the graph. For a cross-section of 300x600 mm, the corresponding stiffness is approximately 55 kN/m. However, when the cross-section is significantly smaller (200x400 mm), the stiffness is only 11 kN/m.

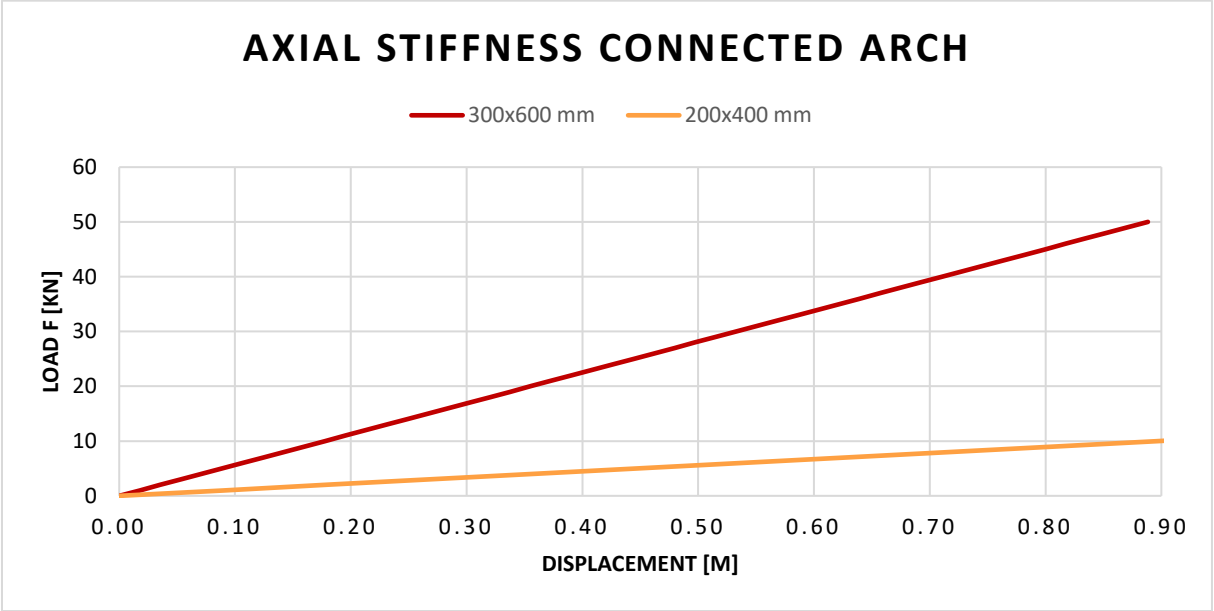

Figure 51 Axial stiffness smaller adjacent arch

To account for the resistance provided by the smaller arch in the 3D model, a horizontal axial spring and a horizontal point load with the magnitude of the reaction force of the smaller arch are applied at the supports. The distribution of moments will remain similar, but the values of the internal forces will differ, as shown in the table. The effects on the bending moment in the weak direction (M_z) and the compressive normal force may vary depending on the joint mechanisms. Across all joint mechanisms, the bending moment in the strong direction (M_y) decreases, but remains significantly higher than in situation A.

Table 30 Internal forces situation B resulting from snow accumulation including effect adjacent arch

	Fixed connections	Arch shape	Segmented	Lattice
M_y [kNm]	316,69	416,40	303.41	269,27
M_z [kNm]	29,13	192,67	11.05	73,60
M_t [kNm]	18,32	46,86	77.05	22,80
V_y [kN]	22,04	55,58	7.21	17,01
V_z [kN]	80,79	71,20	58.6	50,88
N_t [kN]	128,09	50,16	194.43	190,73
N_c [kN]	592,94	597,37	660.11	732,26

9.3 Situation C

The figure below presents the bending moment distribution (My) for situation C, in which now the supports in the corners are restrained from moving horizontally. In addition are elements placed at the outer right side between the supports that represent the supporting long-spanning structure.

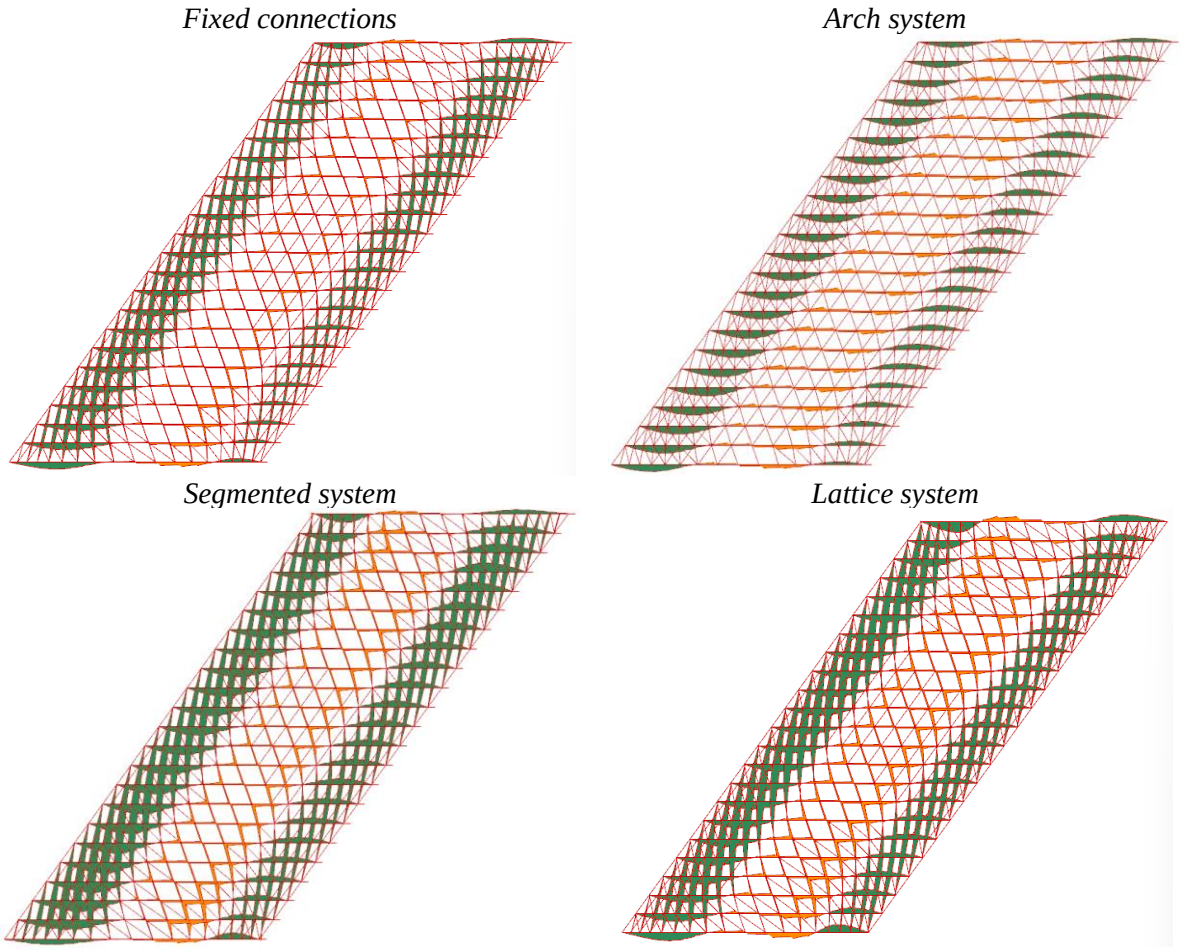

Figure 52 Moment distribution (My) situation C per joint mechanism

Table 31 Internal forces situation C resulting from snow accumulation

	Fixed connections	Arch	Segmented	Lattice
M_y [kNm]	99,12	134,79	100,90	100,35
M_z [kNm]	11,34	23,05	6,36	19,13
M_t [kNm]	3,88	12,64	25,82	4,17
V_y [kN]	10,40	9,23	7,55	8,21
V_z [kN]	25,18	30,64	26,54	27,47
N_c [kN]	1450,52	1457,52	1521,81	1475,79
N_t [kN]	1346,56	1411,52	1396,46	1392,79

Examining the bending moment distribution, it is clear that it is very similar to that of situation A. The values of the bending moments and shear forces are also nearly identical. However, the normal forces are significantly larger when compared to the case where all supports are restrained. These normal forces are present in the elements located between the supports, as illustrated in the figure below.

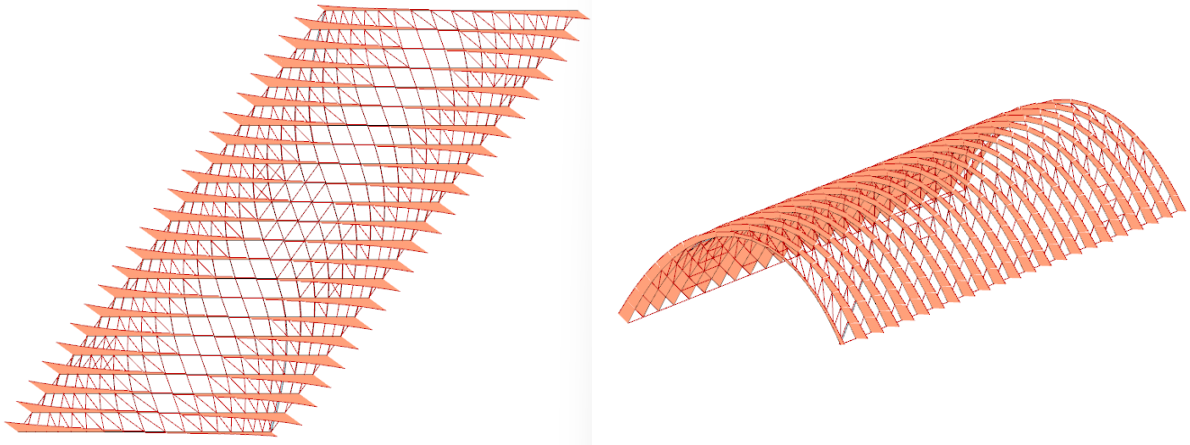

Figure 53 Normal force distribution situation A

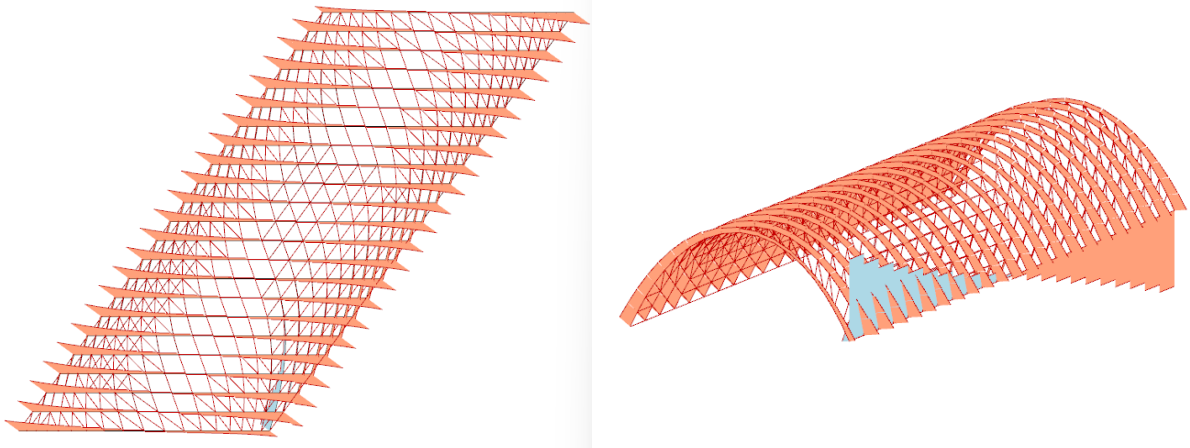

Figure 54 Normal force distribution situation C

Furthermore, the normal forces are also greater in the main structural elements, as can be seen in the table below, which excludes the normal forces in the side beams. The large tensile normal force occurs in the secondary beams near the restrained supports.

Table 32 Normal forces in primary and secondary beams situation C

	Situation A	Situation C
N_t [kN]	39,88	209,90
N_c [kN]	348,97	382,25

9.4 Horizontal restraint through facades

As previously discussed, preventing horizontal displacement at the supports can be achieved through the use of tension rods. Incorporating the facades into the structural system can however also be used to restrain the supports of the arches to which the facades are applied. In Chapter 6 it was shown that the facades will however greatly affect the distribution and magnitude of the internal forces. The results presented below do not aim to compare situations that include or exclude facades. Instead, they demonstrate the differences between a situation where all supports are restrained from moving horizontally (left) and one where all supports on the right side are free to move horizontally.

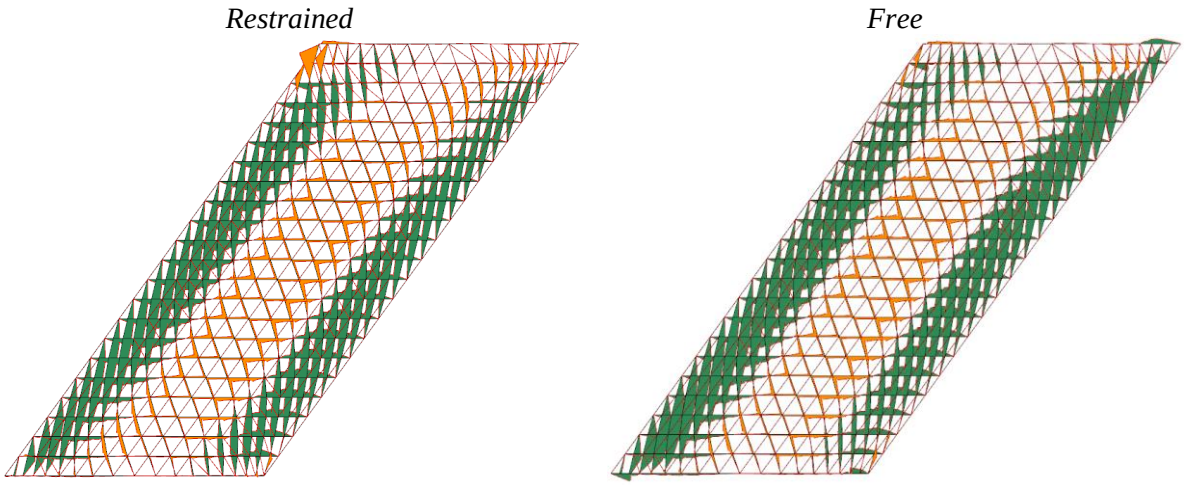

Figure 55 Effect horizontal movement supports on moment distribution for a variant incorporating facades

Table 33 Effect horizontal movement supports on internal forces for a variant incorporating facades

	Restrained	**Free**
M_y [kNm]	68,05	77,47
M_z [kNm]	11,16	18,02
M_t [kNm]	2,21	3,31
V_y [kN]	11,76	13,16
V_z [kN]	23,43	24,42
N_c [kN]	118,8	1036,57
N_t [kN]	412,31	1298,46

The differences in the internal forces are slightly bigger between both situations than for a variant without the facades. Generally, the same conclusions could be given as for the differences between situation A and C.

In a previous analysis (Chapter 8) it was shown that without considering the horizontal DOF of the supports, the normal forces already become very large if certain wind loads act on the structure, and the facades are incorporated in the system. For the segmented system and the arch system, the normal forces can be problematic. For the segmented system the cross-section height of the elements had to be increased to create a joint with sufficient normal force capacity. If the normal forces increase further this could therefore lead to an even larger amount of required timber and steel than shown in the variant study. For the arch system, normal forces that occur in the secondary beams have to be transferred through the arches. Therefore, if the normal forces become very large this may lead to very complex detailing. The normal forces in the primary and secondary beams are checked for free and restrained horizontal movement of the supports. The results are given in the tables below.

Table 34 Normal forces in primary and secondary beams with supports restrained from horizontal movement

	Primary beams		Secondary beams	
	N_c [kN]	N_t [kN]	N_c [kN]	N_t [kN]
ULS-1	196,88	0,00	11,74	0,73
ULS-2	290,50	0,00	55,47	5,83
ULS-3	333,05	0,00	127,30	12,25
ULS-4	376,25	0,00	53,11	86,86
ULS-5	221,44	3,40	130,97	18,46
ULS-6	407,44	138,00	229,97	0,81
ULS-7	615,62	169,10	278,75	235,77
ULS-8	709,14	253,40	330,88	303,90
ULS-9	1113,32	361,81	508,30	328,90

Table 35 Normal forces in primary and secondary beams with supports free of horizontal movement

	Primary beams		Secondary beams	
	N_c [kN]	N_t [kN]	N_c [kN]	N_t [kN]
ULS-1	347,95	0,00	114,62	2,37
ULS-2	542,13	0,00	221,12	4,57
ULS-3	462,55	17,44	291,87	4,71
ULS-4	651,28	92,83	180,06	7,30
ULS-5	225,32	8,99	146,18	16,52
ULS-6	367,14	126,61	233,86	0,82
ULS-7	568,39	152,85	302,11	229,35
ULS-8	630,23	228,87	350,35	309,71
ULS-9	1045,29	369,82	557,67	296,99

Allowing the supports to move horizontally does not affect the normal forces much when a wind load is applied, but drastically increase for the snow loads and the load combination that only contains the permanent load. These load combinations create the largest horizontal reaction forces. The normal force distribution in the primary and secondary beams for both situations is plotted in the figures below for the load combination containing snow accumulation between the different roof parts.

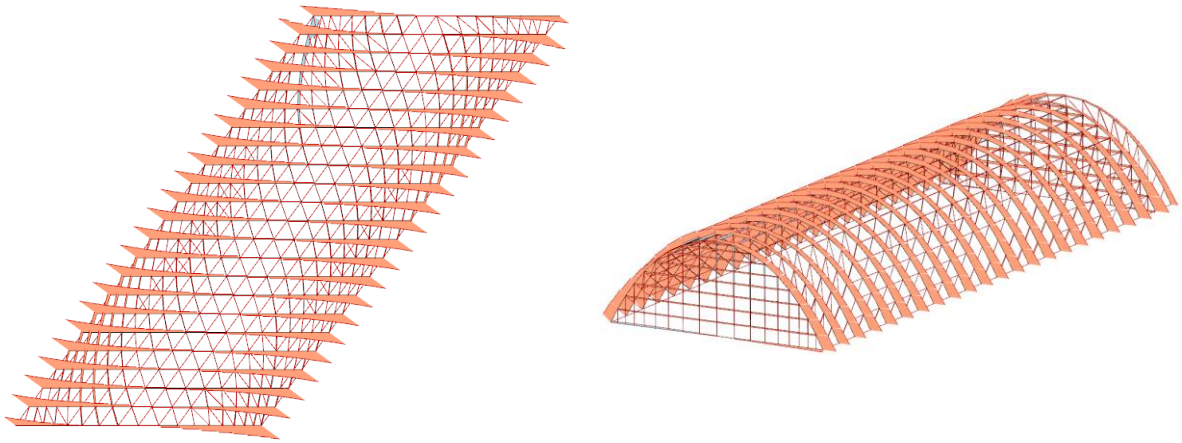

Figure 56 Normal force distribution with supports restrained of horizontal movement

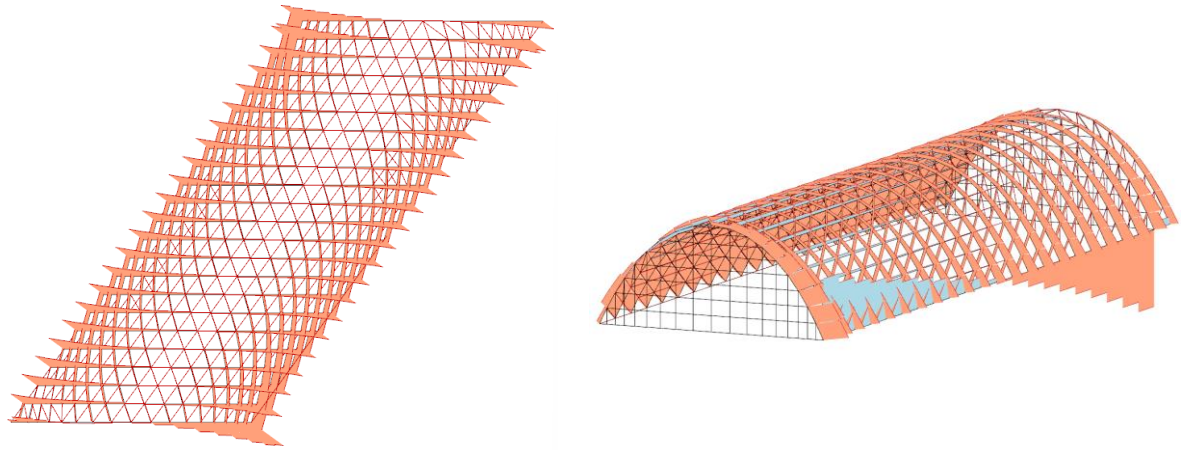

Figure 57 Normal force distribution with supports free of horizontal movement

It seems that the normal forces especially increase in the arches to which the facades are connected, and the secondary beams that are connected to these arches.

9.5 Conclusions on horizontal movement of arches

It was initially expected that because the roof is supported by a long-spanning structure, the horizontal reaction forces of the arches could be problematic. However, the analysis conducted in this chapter has shown that the long-spanning beam can strategically be used to create a truss-like structure that prevents the arches from sliding horizontally. To obtain this truss effect the corners of the structure have to be restrained from moving horizontally by the use of for example a tie rod or the facades. By doing this, the bending moments and shear forces barely change in the structure. The normal forces however, especially resulting from snow increase significantly. This is also occurs in case the rigid facades are used to restrain the corners from moving horizontally.

10 DETAILING AND FINAL DESIGN

In this chapter, the final detailing and dimensioning of the roof structure will be presented. First, the structural system will be chosen based on the results from previous chapters. With the final structural system known, the appropriate detailing can be determined. The detailing process will include the following:

- Connections between arch segments;
- Connections arches at supports;
- Connections secondary beams at supports;
- Connections secondary beams to arches.

Once the final detailing is determined, the dimensioning of cross-sections and the exact layouts of the connections will be determined, such that the final design meets the Ultimate Limit State (ULS) and Serviceability Limit State (SLS) criteria. The calculation procedure of the elements and detailing, next to the ULS and SLS criteria can be found in Appendix C. The corresponding spreadsheets are added in Appendix E.

10.1 Final structural system

In the previous chapters, various design options have been analysed and compared. Based on the results, a combination of design options will be chosen that is expected to result in the least amount of material and more practical variant. It was previously concluded that the elements in the primary and secondary direction did not need to resist the same magnitude of internal forces. In Chapter 8, one system consisting of primary arches with secondary elements in between was found to require significantly less material than other systems analysed considering the ULS criteria. On the other hand, it did not get close to the criterium which is provided by the Eurocode for the maximum horizontal deflection. However, for the reasons given in the conclusion of Chapter 8 it is still considered to be the favourable variant in terms of material cost and practicality.

In Chapter 8, an anticlastic shape was applied to the variant utilizing this system, and the supports were assumed to be hinged. The anticlastic shape was applied to decrease the maximum bending moment in the structure. Instead of the anticlastic shape, the facades could be added to the system to decrease the maximum bending moment. However, in the previous chapter, it was discovered that releasing the supports, except for those in the corners, from horizontal movement did not affect the bending moments or shear forces in the structure, but did affect the normal forces. When snow acted on the structure and the facades were included, the normal forces increased significantly in both primary and secondary beams. Large normal forces were already present due to the wind load on the structure. To ensure the detailing has sufficient normal force capacity, the cross-sections of the secondary beams may become significantly larger than shown in the variant study. Therefore, it is decided to decrease the maximum bending moment and deflections of the structure in another way. This will be achieved by maintaining the anticlastic shape. The height difference between the middle arch and the outer arches will however be increased from 1/10 to 1/3 of the height. This changes the appearance but also drastically decreases the horizontal deformation of the structure. Additionally, the supports will be semi-rigid instead of being hinged as was assumed in the variant study. The shape for the arches will be a catenary arch, and grid pattern 3 will be applied for the reasoning given in Chapter 4. Finally, the supports at both sides of the structure are allowed to move horizontally except for those at the four corners of the structure. Elements between the supports are taken into account to create the truss effect as described in the previous chapter.

10.2 Connections between arch segments

The timber arches cannot be transported as a single part, so they have to be divided into segments that will be connected together on-site. In most European countries, including the Czech Republic, the maximum length of a standard vehicle is 16,5 m and the maximum height is 4 m (EPSRauthor, 2014). While it is possible to transport larger elements, it may require special permits and escort vehicles,

making it more expensive. Therefore, the size limits for a standard vehicle will be used, resulting in the arches being divided into four segments as shown in the figure. In the figure the dimensions for the outer arches are given, which have the longest total length. The connections will be made using steel slice plates, similar to the slotted steel plate joints described in Chapter 7. In this case, only two elements have to be connected since the joints are not located at the nodes of the structure.

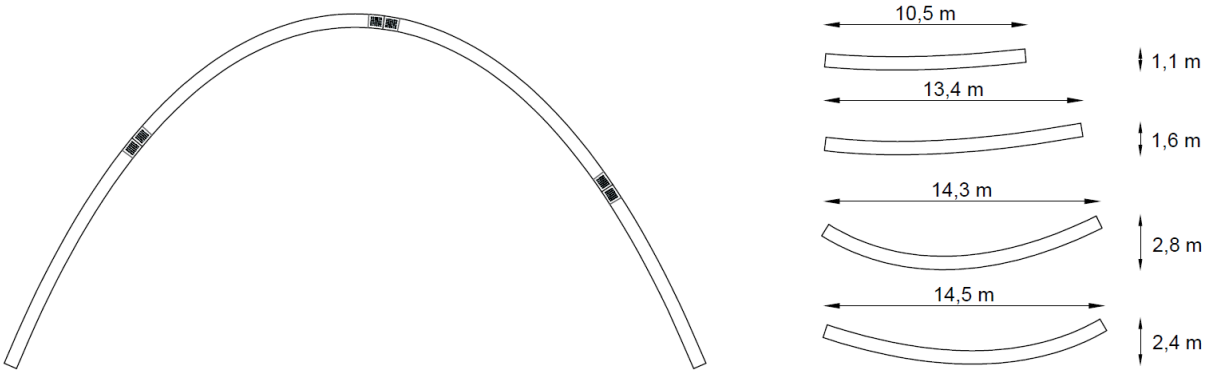

Figure 58 Arch segments with sizes of outer arches

The connections between the arch segments and the supports will have a certain level of rotational stiffness, which will affect the moment distribution in the arches and its deformation. Ideally, the rotational stiffnesses should be chosen to achieve the lowest maximum bending moment. However, it may be necessary to apply a larger rotational stiffness due to the large deformation of the structure. A preliminary analysis is performed to demonstrate the effect of the rotational stiffness on the maximum bending moment. A range for the joint stiffness of 1000 to 20.000 kNm/Rad is considered. The analysis is conducted four times, with a rotational stiffness of 1000, 4000, 5000 and 7000 kNm/Rad for the supports. These values are based on possible joint layouts that have sufficient normal force capacity. The results are presented in the graph below.

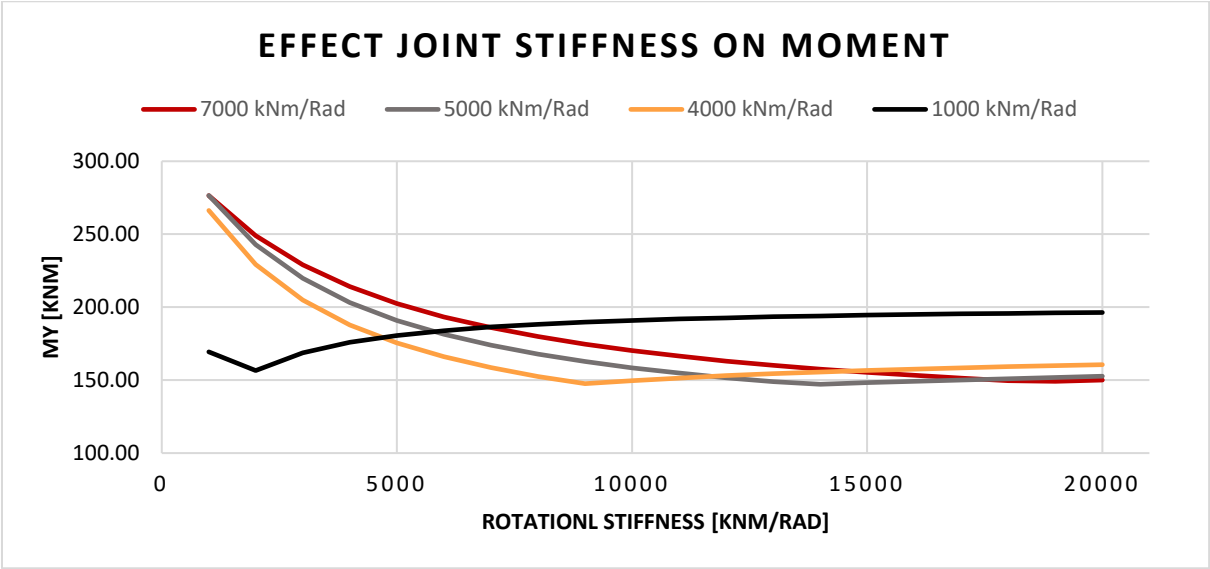

Figure 59 Graph showing the effect of rotational stiffness ratio on max. bending moment

The bending moment distribution depends mostly on the ratio between the rotational stiffness of the joints between the segments, and the stiffness of the supports. From the results it seems that if the stiffness at the supports is relatively small, and the stiffness of the connections between the segments is large, the bending moment is less concentrated in the supports. On the other hand, if the rotational stiffness in the supports is relatively large compared to the joints in the arch, the bending moment is concentrated much more in the supports and less in the arches themselves. The bending moment

distribution shifts as the ratio between the stiffness values changes. This means that the magnitude of the maximum bending moment mostly depends on the ratio between the different stiffnesses, and therefore it is not necessary to apply very large stiffness values. However, the joints require a certain normal force capacity and thus a minimum number of rows and columns of bolts. As a result, both joints have a minimum rotational stiffness. The above-described occurrence is depicted in the figure below. In this figure the bending moment is plotted for two different combinations of the rational stiffness values on the same scale. The corresponding stiffness values are given in Table 36.

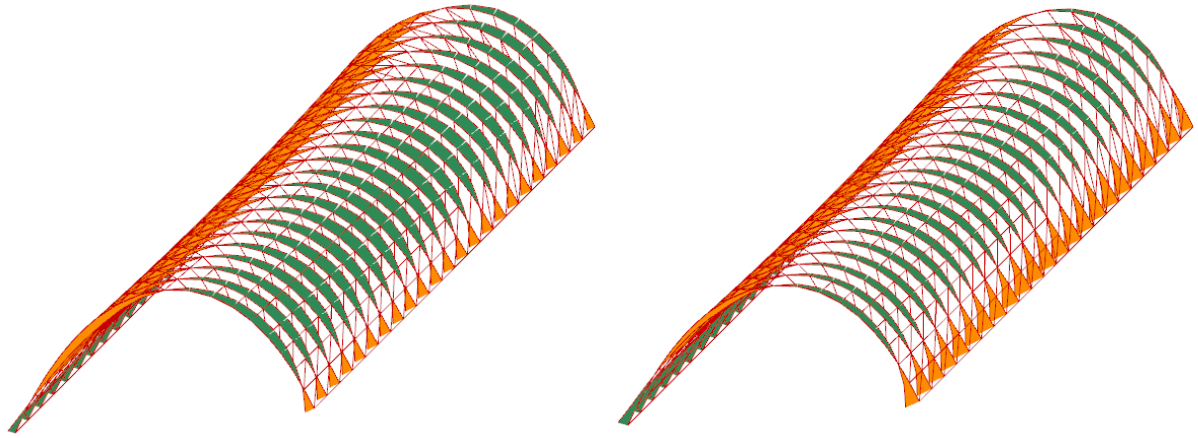

a b

Figure 60 Shifting of bending moment distribution due to different stiffness ratios

Table 36 Rotational stiffness values corresponding to Figure 60

Situation	Supports	Connections segments
a	4000 kNm/Rad	20.000 kNm/Rad
b	4000 kNm/Rad	2000 kNm/Rad

As explained before do the connections require a minimum number of bolts to obtain sufficient normal force capacity, and therefore have a minimum rotational stiffness. The rotational stiffness of the supports depends on a variety of factors that will be explained in the next section. The final layout of the connection is given in the final section of this chapter.

10.3 Supports

At the supports, two primary arches and two secondary beams are connected. The supports are situated on a large, long-spanning beam that prevents horizontal movement of the supports (Chapter 9). The arches are connected to a custom steel component by the use of slotted in steel plates, while the secondary beams are connected using steel pin joints. These joints are located on an elevated section so that it is not connected to the custom steel component of the arches. This node is depicted in Figure 61. This section of the chapter will provide the detailing of the connections of the arches and secondary beams to these components.

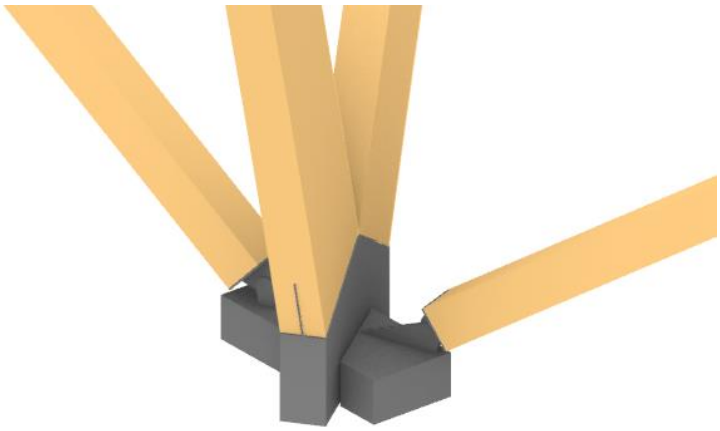

Figure 61 Layout of the supports

10.3.1 Connections arches at supports

As described earlier will the supports be semi-rigid to decrease the maximum bending moment and deflections of the structure. In Chapter 5, the semi-rigid behaviour was realised by fixing the arch to one of the smaller adjacent arches. It was shown that this stiffness depends on the cross-section dimensions of the arches and the load combination. Now a third factors comes in which is the rotational stiffness of the joint itself. The same 2D model will be used for this analysis as in Chapter 5, but in this case a rotational stiffness will be applied at the connection between the two arches.

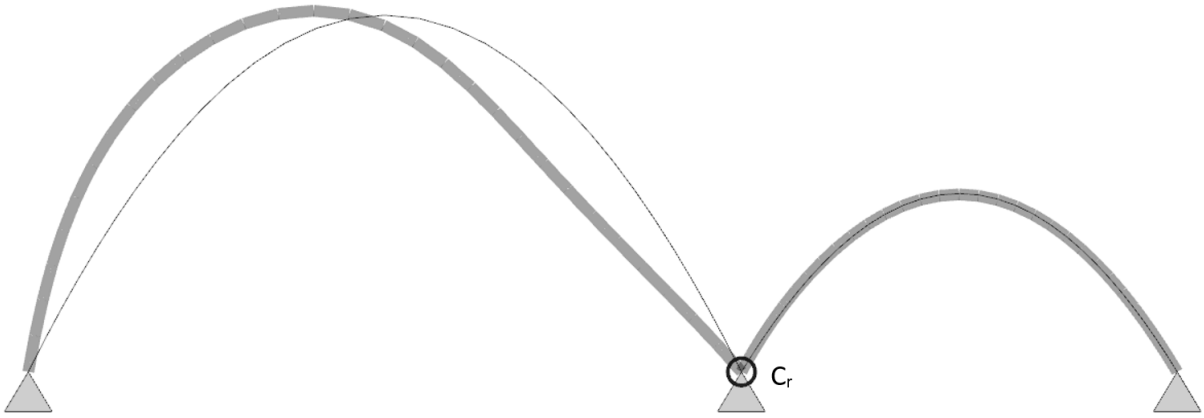

Figure 62 2D scheme of arches working together including joint stiffness

For this analysis, a range for the joint stiffness is estimated. For many different joint layouts, the rotational stiffness, normal force capacity and moment capacity is determined based on the analytical method given by Shu et al. (2020). Given that the maximum normal force at the supports is approximately 350 kN, a stiffness range of 7000 to 40000 kNm/Rad will be used for this analysis. Next to that is the cross-section size for the smaller arch varied. The width is fixed on 200 mm and the heights will be 450, 600 and 750 mm. The load combination will be ULS-9 which results in the largest bending moment and deformation and is therefore determinate.

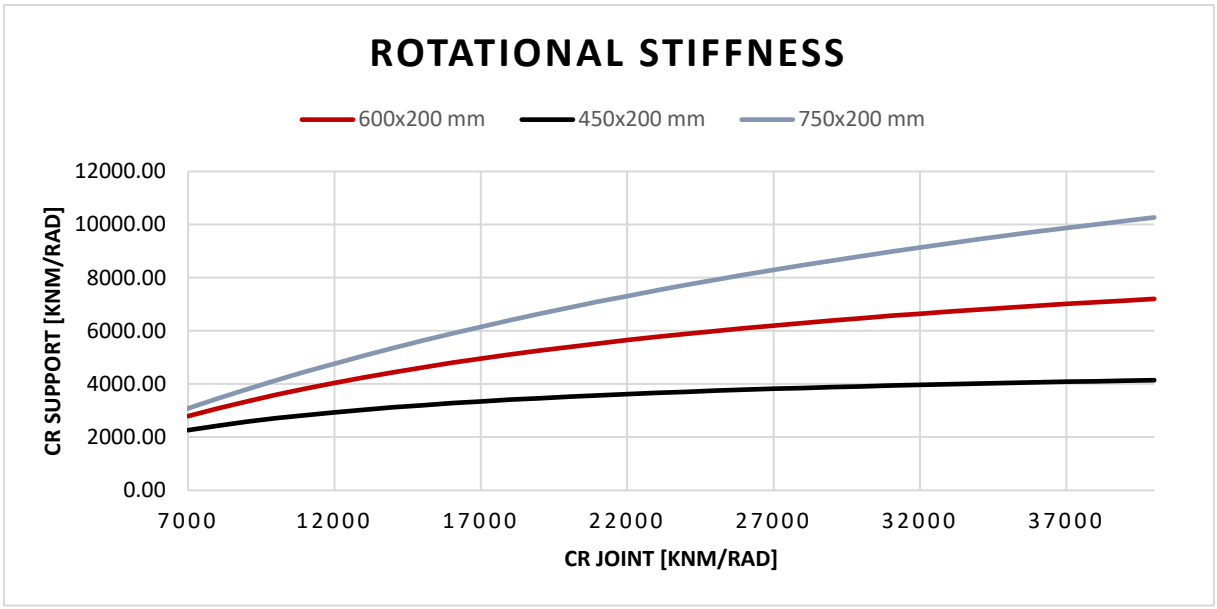

Figure 63 Rotational stiffness supports due to cross-section and joint stiffness

The results show the importance of the cross-section the smaller arch is given. With a lower joint stiffness, the differences are relatively small but increase as the joint stiffness increases. As explained by Fan et al. (2011) do the cross-section dimensions partially determine if a joint in a grid structure behaves rigidly. For larger cross-section dimensions, the joint stiffness has to be larger in order for the joint to behave rigidly. Therefore, the rotational stiffness at the supports will keep increasing longer in case a larger cross-section is applied to the smaller arch. In this project the adjacent parts will not be fully analysed, and therefore their final dimensions will remain unknown. A conclusion that was made in the previous section of this chapter is that the lowest maximum bending occurs at certain ratios between the rotational stiffness values of the connections at the supports and between the arch segments. For the cross-section dimensions, the SLS criteria will however most likely be determinate. Therefore, for the final design it is not the aim to find the such a ratio but rather achieve sufficient rotational stiffness.

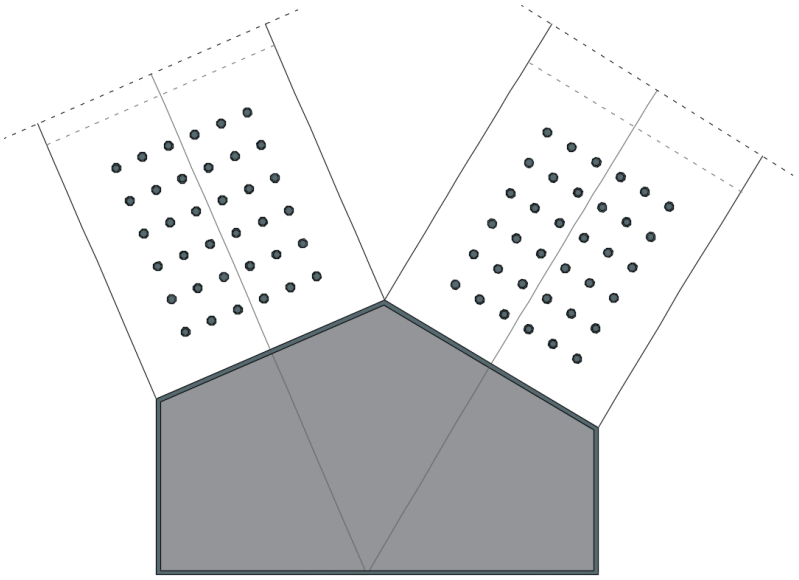

Figure 64 Concept layout of connection between arches

10.3.2 Connections secondary beams at supports

The connections of the secondary beams to the supports will be hinged like the connections to the arches. By doing so, no bending moments except for those caused by the own weight will occur in the secondary beams. This hinged connection can be achieved through a steel pin joint. In this case the joint layout solely depends on the normal force capacity. The layout for this joint is presented in Figure 65 and Table 37.

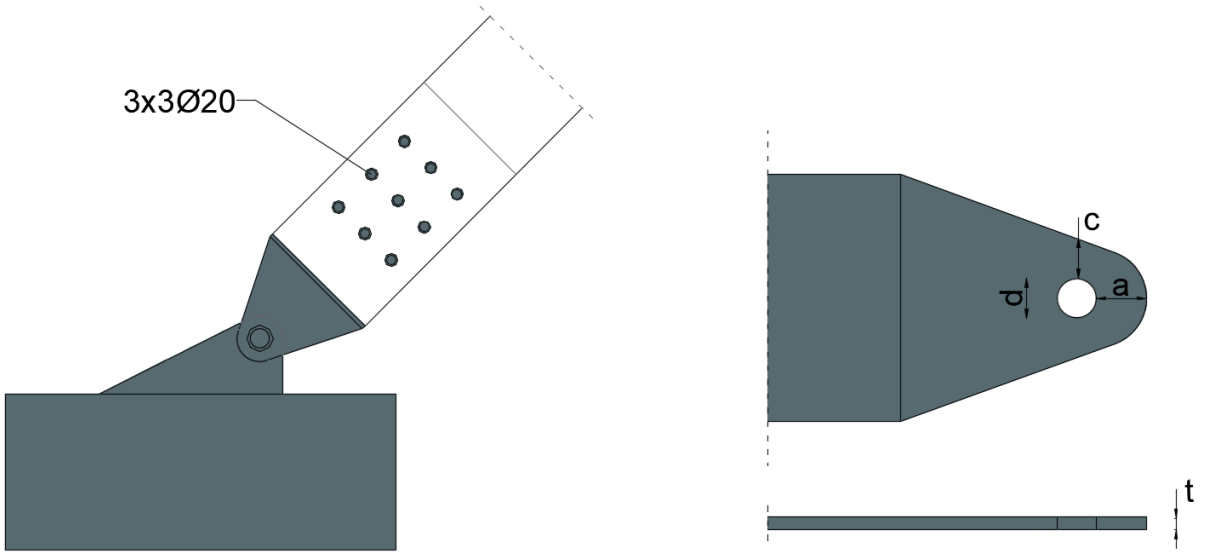

Figure 65 Layout of connection secondary beams at supports

Aside from the layout of the bolts, the dimensions of the steel pin have been determined. The procedure and spreadsheet for determining these dimensions are added in the appendixes mentioned in the introduction of this chapter.

Table 37 Minimum measurements of the dimensions of the steel pin joint

Dimension	Minimum measurement
a	51 mm
c	37 mm
d	40 mm
t	10 mm

10.4 Connections between arches and secondary beams

The connection of the secondary beams to the arches is complex due to several factors. First of all are normal forces present in the secondary beams with the maximum compressive force being 102,8 kN. To avoid stresses perpendicular to the grains of the arches, these normal forces have to be somehow transferred through the arches. In addition are the secondary beams not connected exactly perpendicular to the arches, but at a certain horizontal and vertical angle that varies for each node. Finally at each corner of the connection, stability elements have to be connected. Also, for these elements the horizontal and vertical angle varies. This is visualized in Figure 68. These connections are considered to be hinged and therefore it is not required that this node has rotational stiffness. In this section, a proposal is given for the detailing of a node that takes into account the above-mentioned factors.

To transfer the normal forces through the arches, a steel tube with sufficient normal force capacity will be applied through the arches at each node. The steel tube has to be connected to a custom steel part which is similar to a joist hanger. This joist hanger has a U-shape that hides the connection to the steel tube. In addition, it gives the opportunity to hang the beam on the arch and provides space to which the stability elements can be connected. To both the joist hanger as the steel tube, plates have to be welded

which can then be connected with bolts. The joist hanger has to remain open at the top in order for the connection between the tube and the joist hanger to remain accessible. Finally, the secondary beam is connected to the joist hanger by the use of a slotted in steel plate.

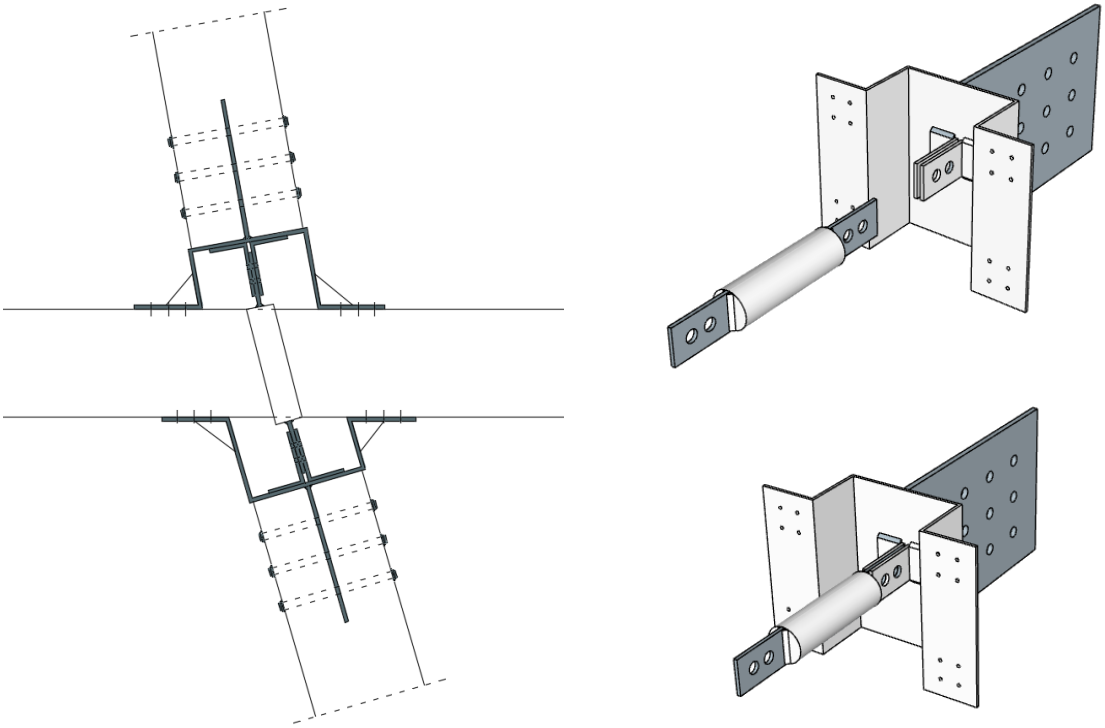

Figure 66 Concept layout connection secondary beams to arches

Another adjustment that will be made compared to the variant shown in chapter 8, is the orientation of the secondary elements. Earlier, a vertical orientation was applied for both the arches as for the secondary beams. This will however result in several practical issues. When the secondary beams are oriented vertically the tension rods will reach the connections at inconvenient places, especially at the ends of the arches. The tension rods may have to be connected right above or below the secondary beams instead of in the middle. When the secondary beams follow the surface normal this problem does not occur. This problem is illustrated in the figure below.

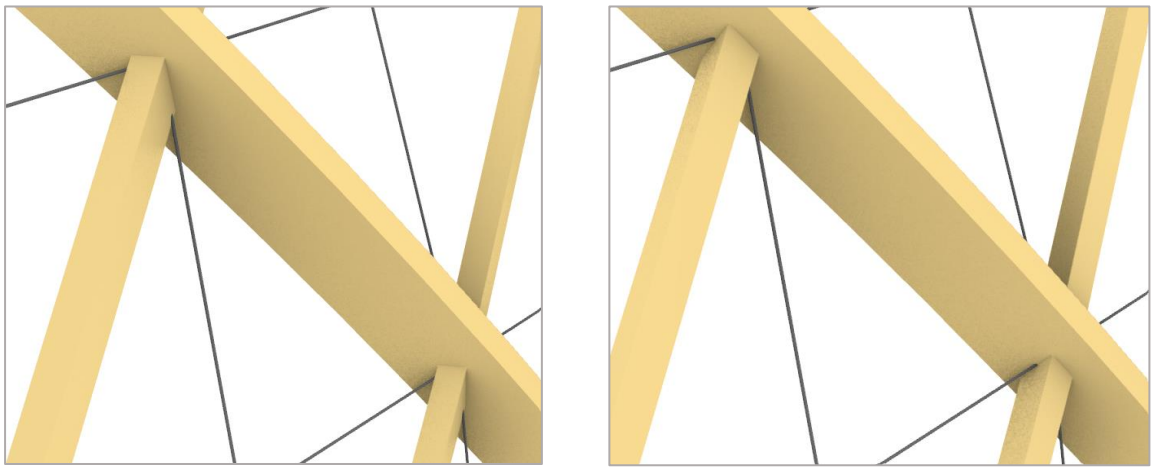

a) b)

Figure 67 Effect orientation on connectivity tie rods: a) vertical orientation; b) orientation according to surface normal

Furthermore, does a vertical orientation result in larger joist hangers which is a problem that also occurred in the segmented system and is described in Chapter 8. To make the detailing less complex and

keep more consistency between the different nodes, it would be advised to not apply a vertical orientation for the secondary beams. Because only normal forces occur in the secondary beams, this does not influence the internal forces or structural behaviour of the roof. The disadvantage is that the secondary beams do not reach the supports vertically anymore. Therefore, the pinned steel joint has to be attached to the elevated part in an angled manner. As explained in the beginning of this section, vary the angles between the stability elements and the secondary beams per node in two directions. Generally, a tie rod is connected to a steel plate and can rotate in one direction. This steel plate would have to be welded to the joist hanger in the exact other angle to be able to connect the tie rods correctly between the nodes. To keep the detailing consistent as much as possible between the different nodes, it would be advised to connect the tie rod to a steel part that can rotate in the other direction. This can be done by connecting a vertical steel plate with a hinged end by connecting it for example with a pin to a horizontal steel plate that is welded to the corners of the joist hanger. This concept is illustrated in the figure below.

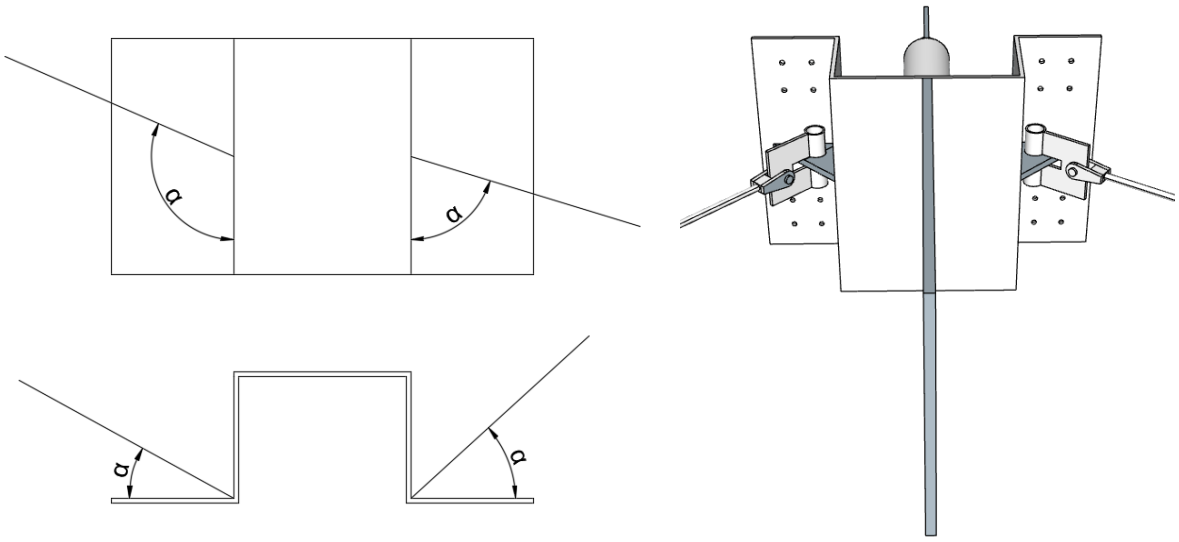

a) b)

Figure 68 a) Varying angles tie rods; b) Concept double hinged connection tie rods

Although the double hinged ends of the tie rods make the nodal connections more consistent. It seems inevitable that each node has a unique layout for the connection. At each node the secondary beams are connected to the arch with a different angle. For example, if the joist hanger would be given the same layout at each node, the plates for the connection with the tube and secondary beams would have to be welded to the joist hanger in the exact correct angle. Adjusting the shape of the joist hanger to the angle at which the secondary beam is connected to the arch, as was done in Figure 66 will ensure that the plates can always be welded exactly perpendicular to the joist hangers. This is expected to be more practical. For the nodes, one in the peak of an arch and one at the end of an arch are drawn and presented in Figure 69. This will provide an idea of what the nodes will look like and what the geometrical differences are between the nodes.

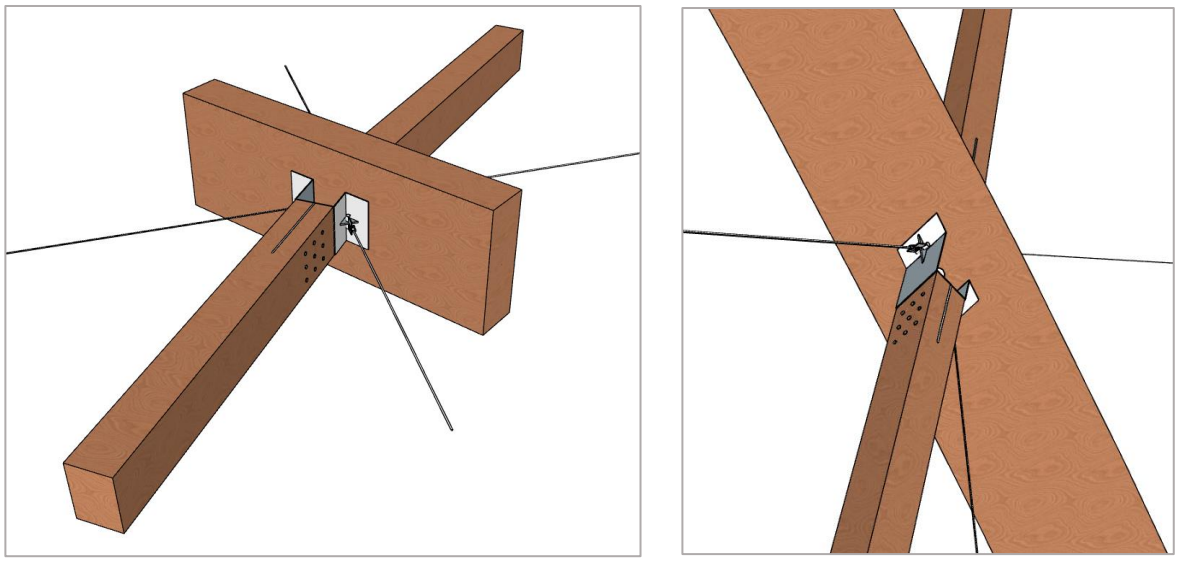

Figure 69 Concept of connection secondary beam to arch in peak and end of arch

Calculations have been conducted for the main parts of this node using the largest normal force that occurs in the secondary beams. The parts which have been calculated are:

- The slotted in steel plate connection of the secondary beam to the joist hanger
- The connection between the joist hanger and the steel tube
- The steel tube

The spreadsheet that has been used for this calculation can be found in Appendix E and the calculation procedure in Appendix C. The minimum dimensions, number of bolts and material strengths are presented in the figure below.

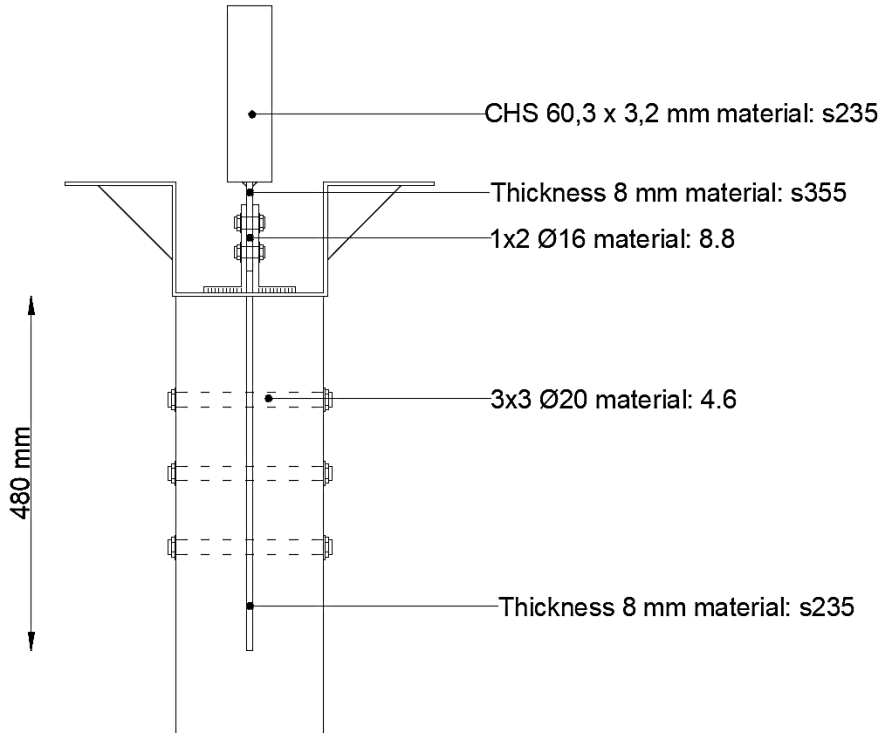

Figure 70 Dimensions of connection secondary beams to arches

10.5 Final design

With the detailing and design options (arch shape, grid pattern, etc.) known, a final design has been created that meets the ULS and SLS criteria. As explained in the introduction of this chapter is the sideways deflection of the arches due to wind a determining factor for the final design of this structure. A significant height difference between the middle and outer arches had to be applied to drastically decrease the horizontal deformation. Next to that were the joint layouts for the supports and segment-connections chosen such that their rotational stiffness is as large as possible, while the columns and rows of bolts still fit within the size limits the arches have. What is meant by size limits is that a minimum height of the cross-section is required, and there is a limited space between the nodes. The joint layout for the supports and segment-connections together with their stiffness and strength properties is given in the table below. For the rotational stiffness of the supports, the assumption is made that the adjacent arches have the same cross-section dimensions. Finally, the material for the arches was set to GL28h which is a higher material grade than the GL24h which was assumed so far. GL28h has a higher modulus of elasticity which causes the arches to have a greater bending stiffness. For the secondary beams a material grade of GL24h is maintained.

Table 38 Joint layout and properties supports and segment-connections

Rows x columns	Diameter [mm]	Width [mm]	Height [mm]	C_r [kNm/Rad]	C_t [kN/m]	N [kN]	M_u [kNm]
7x8	24	240	720	34136	1.89E+06	1016,34	1428,46

As expected, did the cross-dimensions need to be significantly increased compared to the variant shown in Chapter 8. The most determining factor for the arches is the criteria for the horizontal deflection which states that it should not be more than 1/300 of the height. For this structure this means that the maximum allowed horizontal deflection is 60 mm. As described in the introduction of this chapter did the height difference between the outer and middle arches need to be increased to at least 1/3 of the height of the outer arches. In the final design the height of the outer arches is 18 m while the middle arch has a height of 11 m. This is slightly more than the height difference of 1/3 that was described earlier, but necessary to meet the deformation criterium. The cross-section of the secondary beams is also significantly larger compared to that of the variant from chapter 8. This is an effect of the detailing of the node. The minimum bolt spacing required the height to be at least 280 mm. The deformations resulting from the SLS load combinations can be seen in Table 39. The directions which are given in this table can be seen in Figure 71. The final cross-section dimensions are presented in Table 40. The maximum lamella thickness concerning the manufacturing process is added as well in this table. Explanation about the determination of this thickness is provided in Appendix C.

Table 39 Deformation in SLS of final design

	Deformation [mm]
x-direction	59,34
y-direction	42,17
z-direction	58,34

Table 40 Cross-section dimensions of final design

Element	Profile	Material
Primary beam	240x720 mm	GL28h
- Lamella thickness	33 mm	
Secondary beam	200x280 mm	GL24h
Stability elements	Ø12 mm	S355

The figure below presents the final design of the structure. The total amount of timber is 259,2 m^3. Comparing this to the total amount of timber shown in chapter 8 it seems that with the arch system still a lot of timber can be saved compared to the other systems. When an anticlastic shape is applied the lengths of the arches get shorter, but the total length of the secondary beams increases. Because the cross-sections of the secondary beams are small, the total amount of timber remains relatively low. This could be an extra reason to apply an anticlastic shape for this specific variant. A drawback of the anticlastic shape is that the connection at each node in the structure is unique. For a monoclastic shape, the connections along an arch are unique. However, the same array of nodes is repeated for each arch. In case the anticlastic shape would be adjusted to a monoclastic shape, maintaining the stiffness properties of the detailing, the cross-section height of the arches would have to be approximately 1600 mm in order to meet the horizontal deformation criterium.

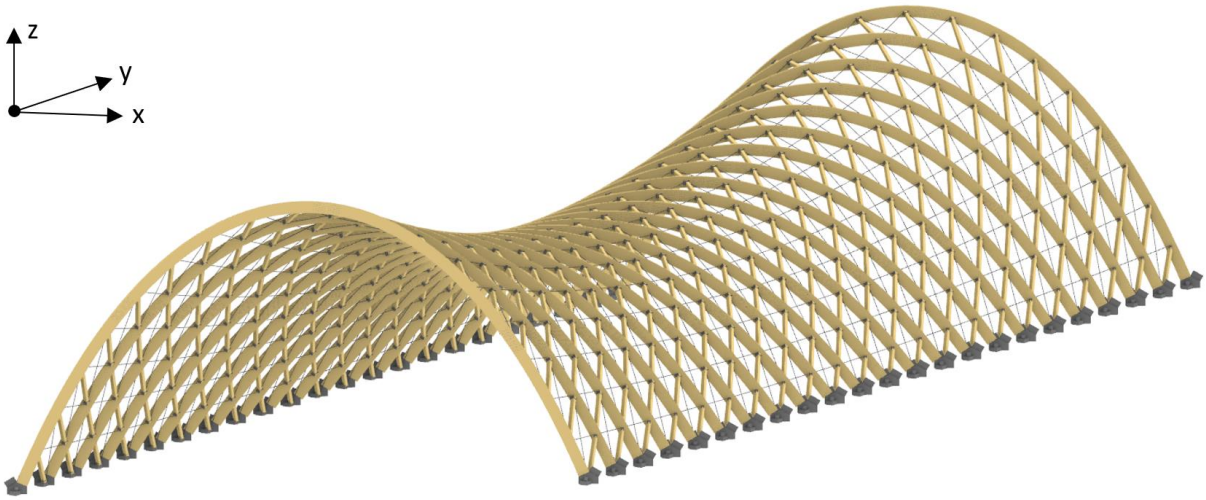

Figure 71 Final design of large part Brno's new main station's entrance hall roof

11 DISCUSSION

During the project, various assumptions and estimations were done that may cause errors in the results of the different analysis and final design. In this chapter an overview is provided of assumptions that might have caused significant errors in the results given in this project.

Effect of adjacent parts

For the final design of the structure, the supports were designed in such way that there is cooperation between the adjacent arches. The rotational stiffness at the supports due to this cooperation was estimated using a 2D calculation model with two connecting arches. In reality, the large part of the entrance hall, which has been analysed during this project is connected to two smaller parts. The height and span of these parts are different, and will therefore have a different effect on the rotational stiffness of the supports. Next to that is one of the parts cut-off at the corner creating a cantilevered part. Not all supports of the large part are therefore connected to a complete arch. These factors cause the rotational stiffness to vary between the supports. Because the rotational stiffness is important, not only to reduce the maximum bending moment but also to decrease the large deformation due to wind, a more thorough 3D analysis may be necessary.

Wind loads

Different shapes have been analysed for the arches. Next to that are an anticlastic and synclastic shape considered. The wind loads that have been used for the analysis were determined according to a Computational fluid Dynamic (CFD) analysis with a student version of Ansys Fluent. For this CFD analysis, a simple 3D model containing a monoclastic variant with a catenary shape for the entrance hall parts is used. During the project it is assumed that the wind loads remain unchanged between the various analysed shapes. In reality this would however not likely be the case.

Rigid facades

The rigid facades were modelled as a steel frame, connected to the nodes of the timber grid. A wind load on the facades will cause a great deformation of the façade itself. The deformation of the facades may cause them to be less rigid, and not restrain the sideways deflection of the roof as much as shown in this project. In the actual final design of the entrance hall, the facades may be connected with elements between the foundation and the roof. Also, a cable truss structure for example may be necessary to prevent the large deformation of the facades. The wind load on the facades has been taken into account, but was imposed on the nodes at which the façade in the front of the structure was connected. Therefore, the effect of the deformation of the facades, resulting from wind has not been taken into account.

Further analysis of detailing

The detailing for the final design has been worked out to a certain extent. For the steel parts of the supports only a proposed shape has been given to which the arches can be connected. This steel part could for example have a truss-like structure existing from steel plates. A Finite Element Method analysis would be required to examine the stresses that occur from its connection with the arches. This stress analysis is not included in this project and therefore the internal structure of this part is not determined. How these parts are connected to the long-spanning structure that supports the roof may also affect the rotational stiffness at the supports, depending on how much it lifts up due to rotational deformation of the arches. Furthermore, do the steel tubes of the connections of the secondary beams to the arches result in holes in the cross-section of the arches. As explained by Dröscher, Augustin & Schickhofer (2016) does the sudden interruption of the cross-section caused by the hole result in a disturbed stress distribution. This leads to stress-concentration at the edges of the holes, and normal stresses perpendicular to the grains of the timber. Due to these stresses, it might be necessary to apply additional reinforcement around the holes to prevent failure of the timber. Another potential problem that may requires additional analysis results from the angles at which the secondary beams are connected to the arches. There is a vector change between the two secondary beams that are connected at one node. Although the angle differences are small between the two secondary beams it may cause the steel tube to slightly rotate, and therefore may require additional analysis as well.

12 CONCLUSION

In this project various different design options for Brno's new main train station's entrance hall have been analysed and compared to each other on the base of internal forces, deformations, stability and practicality. The design options included the shape of the arches, grid pattern, support conditions, double curved shapes, incorporating the facades and different possible connections between the primary and secondary grid elements. The analysis for the different design options were conducted for the large part of the entrance hall, as it is expected to be determining for the structural system. Following the results of these analyses it became clear that to realize the roof structure of the entrance hall, some great challenges have to be overcome. First of all is the structure vulnerable to large deformations due to wind. The CFD analysis conducted with Ansys Fluent showed that wind loads can occur on the roof in which wind pressure acts on one side of the arch while wind suction acts on the other side. This causes a large sideways deflection of the arches, especially if the roof has a single-curved monoclastic shape as depicted in the architectural design. Next to that causes the combination of geometrical complexity and the orthotropic behaviour of the timber the detailing to become very complex. At each node the geometry is different and the detailing has to be made such that it prevents stresses perpendicular to the grains of the timber elements.

The project started with identifying potential systems that could be used to create the timber grid structure of the entrance hall's roof. Three types of connections between the timber elements were found to be most interesting, which were the segmented system, lattice system and arch system. The elements in the primary and secondary connections do not experience the same magnitude of internal forces, as these are much larger in the primary elements (arches). Therefore, it was expected to have a great advantage in terms of the total amount of required timber. Next to that is it considered to have a less complex manufacturing process compared to the other systems.

Based on the results of all the analysis performed during this project, a final design was created. In the final design the shape of the arches has a catenary shape. Analysis showed that a parabolic shape leads to a slightly lower maximum bending moment which results from wind. However, because the arches are curved, stresses perpendicular to the grains of the timber resulting from a positive bending moment have to be considered. A lower radius of curvature leads to larger stresses perpendicular to the grains. This radius of curvature is lower for the parabola than for the catenary shape. The combination of the radius of curvature and the maximum positive bending moment resulting with a catenary line was found to be favourable. From the three analysed grid patterns, one in which the base shape of the structure is divided in equal parts showed to result in lower bending moments compared to the grid patterns which are vertically project. Therefore, this grid pattern was selected for the final design. From the different support conditions and combinations of support conditions it was found that applying semi-rigid supports had several great advantages. It reduces the maximum bending moment, makes the structure significantly more stable and reduces the deformation compared to hinged supports. This semi-rigid behaviour can be achieved by connecting the arches to the smaller adjacent arches, resulting in a cooperation between the arches. Rigid supports would have had more effect on the stability and deformation. Fully rigid behaviour is however hard to achieve due to the roof being supported by a long-spanning structure. Finally, it was decided to apply an anticlastic shape for the structure. This shape decreases the deformation of the structure compared to a monoclastic shape. Incorporating rigid facades to the system does this too, but it will result in significantly larger normal forces in the structure, including the secondary beams. Since normal forces have to be transferred through the arches it was expected that it could be problematic for the detailing of the structure.

The horizontal deformation was most determining for the final shape and dimensions of the final design. The height difference for the anticlastic shape between the middle and outer arches had to be significantly increased up to 7 m. Furthermore, did the cross-section height of the arches become larger than initially expected. The total amount of timber became 259,2 m^3 which is still lower than the variants

with the other systems shown in the variant study. It can therefore be concluded that this system leads to the most durable design.

13 RECOMMENDATIONS

During the project various design options and optimization processes have been left out to maintain a manageable scope for the project. Based on the results of this project it is expected that some of these design options and optimization processes may lead to a design which is more durable and closer to the architectural design. This chapter will give an overview of recommended studies that could lead to a better design considering these criteria.

Application of the rigid facades

Due to the large sideways deformation of the structure due to wind, an anticlastic shape with a large height difference between the outer arches and middle arch had to be applied. A more effective way to reduce this deformation was by applying rigid facades. This however resulted in large normal forces in the structure, which could be problematic for the detailing and could in turn result in larger required cross-sections. It is expected that if the facades would be more flexible, the normal forces would not be as large. Making the façades more flexible could however make them more vulnerable to buckling. It could be interesting to analyse what happens to the structure if the two outer arches themselves would be significantly stiffer than the other arches. This could be done by for example giving these arches a steel-timber composite cross-section. Doing this for the adjacent outer arches could result in a larger rotational stiffness at their supports as well in case there is a cooperation between the arches. The outer arches might behave less rigid than the facades and the normal forces could therefore be less severe.

In this project the structural system incorporating facades at both ends with a monoclastic shape is considered as one single variant next the monoclastic, anticlastic and synclastic shape without the facades. The facades could however be applied in combination with all of these shapes. Both the anticlastic shape and facades were found to reduce the deformation and bending moments in the structure. It would therefore be recommended to analyse what happens to the internal forces and deformation in case a combination of the facades with an anticlastic shape is applied. Finally, a variant that incorporates only one façade could be analysed.

Structural optimization

As explained in Chapter 4, do the elements in the grid variants which are vertically projected have to connect in a certain way at the supports. This only happens at certain grid sizes. For the grid variant which is created by dividing the base shape in equal parts this limitation doesn't apply. The division in the primary and secondary direction can be adjusted, changing the grid's appearance but not causing any impracticalities. Therefore, this grid allows for a material density optimization. This can be done with the Generic solver Galapagos which was also used for the arch shape optimization. If the cross-section dimensions of the timber elements can be estimated using the internal forces or deflections that result from Karamba3D, the total amount of timber of the structure can be estimated. As explained in Chapter 3 does the generic solver require genes that can be adjusted to maximize or minimize a certain problem which's value depends on the genes. This problem could be the total amount of timber that has to be minimized, based on the grid division as genes. This method could be used to find a grid division that requires the least amount of timber creating a more material-effective design.

The variant utilizing the lattice system had a significantly smaller horizontal deformation due to wind than the variant utilizing the arch system. It may be interesting to analyse what the effect of semi-rigid supports and the segmentation of the arches due to transportation limits is on the deformation of this variant. When the appearance of the structure becomes a more important criterium this variant may become more interesting as it could lead to a structure that deviates less from the architectural design, considering the height difference for the anticlastic shape.

LITERATURE

Abu-Zidan, Y., Mendis, P., & Gunawardena, T. (2021). Optimising the computational domain size in CFD simulations of tall buildings. *Heliyon, 7*(4), e06723. https://doi.org/10.1016/j.heliyon.2021.e06723

Benthem Crouwel Architects. (2020). *Brno main station (CZ)*. Benthem Crouwel - Brno Main Station. https://www.benthemcrouwel.com/projects/brno-main-station

Blackmore, P., & Tsokri, E. (2006). Wind loads on curved roofs. *Journal of Wind Engineering and Industrial Aerodynamics*, 94(11), 833–844. https://doi.org/10.1016/j.jweia.2006.06.006

Bradley, R.A., Gohnert, M., Goliger, A.M., & Mistry, Y. (2016). Wind loading on catenary vault structures. *Journal of the South African Institution of Civil Engineering, 58*(4), 29-47. https://dx.doi.org/10.17159/2309-8775/2016/v58n4a4

Blass, H.J., & Sandhaas, C. (2017). *Timber Engineering - Principles for Design*. KIT Scientific Publishing.

Blok, R. (2014). *Tabellen: voor bouwkunde en waterbouwkunde*. ThiemeMeulenhoff bv.

Blumer-Lehmann AG. (n.d.). Cambridge Mosque opens. *Blumer-Lehmann*. https://www.blumer-lehmann.com/en/news-and-media/news/cambridge-mosque.html

Carlson, C. (2021, January 20). *Marks Barfield Architects designs Cambridge Central Mosque to be "place of tranquility"*. Dezeen. https://www.dezeen.com/2021/01/20/cambridge-central-mosque-marks-barfield-architects/

České vysoké učení technické v Praze. (n.d.). *ČSN EN 1991-1-4 Zatížení větrem* [Presentationslides]. Leonardo.cvut.cz. http://www.leonardo.cvut.cz/download/4b_Zatizeni-klimaticka-vitr.pdf

Cóstola, D. D., & Alucci, M. P. (2007). Pressure coefficient simulated by CFD for wind-driven ventilation analysis. *Building Simulation 2007, BS 2007*, 999–1006.

Chilton, J., & Tang, G. (2017). *Timber Gridshells: Architecture, Structure and Craft*. Routledge.

D'Amico, B., Kermani, A., & Zhang, H. (2014). Form finding and structural analysis of actively bent timber grid shells. *Engineering Structures, 81*, 195–207. https://doi.org/10.1016/j.engstruct.2014.09.043

D'Amico, B., Kermani, A., Zhang, H., Shepherd, P., & Williams, C. (2015). Optimization of cross-section of actively bent grid shells with strength and geometric compatibility constraints. *Computers & Structures, 154*, 163–176. https://doi.org/10.1016/j.compstruc.2015.04.006

Crocetti, R., Mårtensson, A., Pousette, A., Norlin, B., Lidelöw, H., Johansson, M., & Kliger, R. (2016). *Design of timber structures: Structural aspects of timber construction* (2nd edition, Vol. 1). Swedish Forest Industries Federation, Swedish Wood.

Dröscher, J., Augustin, M., & Schickhofer, G. (2016). *Comparison of verification and reinforcement concepts for timber beams with large round holes*. WCTE 2016 World Conference on Timber Engineering August 22-25, 2016, Vienna, Austria.

EPSRauthor. (2014, April 10). *Weights and dimensions of road vehicles in the EU*. Epthinktank. https://epthinktank.eu/2014/04/10/weights-and-dimensions-of-road-vehicles-in-the-eu/

Fan, F., Ma, H., Cao, Z., & Shen, S. (2011). A new classification system for the joints used in lattice shells. *Thin-Walled Structures 49 (2011) 1544–1553*. https://doi.org/10.1016/j.tws.2011.08.002

Franke, L., Stahr, A., Dijoux, C., & Heidenreich, C. (2017). How does the Zollinger Node really work?: A Structural Experimental Investigation to a Better Understanding of the Nodal Behavior. Proceedings of the IASS Annual Symposium 2017 “Interfaces: architecture.engineering.science” 25 - 28th September, 2017, Hamburg, Germany.

Gonchar, J. (2019, December 2). *A Closer Look at the Gridshell Roof of Swatch Headquarters by Shigeru Ban*. 2019-12-02 | Architectural Record. https://www.architecturalrecord.com/articles/14393-a-closer-look-at-the-gridshell-roof-of-swatch-headquarters-by-shigeru-ban

Glentleiten Open Air Museum. (n.d.). *Exploring tour*. Glentleiten. https://www.glentleiten.de/The-Glentleiten/Our-buildings/Exploring-tour/?La=2

Javanroodi, K., Mahdavinejad, M., & Nik, V. M. (2018). Impacts of urban morphology on reducing cooling load and increasing ventilation potential in hot-arid climate. *Applied Energy*, *231*, 714–746. https://doi.org/10.1016/j.apenergy.2018.09.116

Jongtien, D., Benthem, J., Biewenga, M., Benthem International B.V., & West 8. (n.d.). *Axonometric view of the structure of the entrance hall*. Brno City Chief Architect‘s Office. https://kambrno.com/competitions/brno-new-main-train-station/

Kilian, A., & Ochsendorf, J. (2005). Particle-spring systems for structural form finding. *Journal of the International Association for Shell and Spatial Structures, 46*(148), 77–84. http://designexplorer.net/newscreens/cadenarytool/KilianOchsendorfIASS.pdf

Larsson, S. (2018). *Design Implications of Rigid Timber Gridshells* [Master thesis]. Chalmers University Of Technology.

L’Express. (2010). *Découvrez l’architecture du Centre-Pompidou Metz*. Le Centre Pompidou-Metz en cinq points - L’Express. https://www.lexpress.fr/culture/art/le-centre-pompidou-metz-en-cinq-points_848555.html

Maraveas, C. (2020). Wind Pressure Coefficients on Greenhouse Structures. *Agriculture*, *10*(5), 149. https://doi.org/10.3390/agriculture10050149

Medvecká, S., Ivánková, O., & Macák, M. (2017). Pressure Coefficients Acting Upon the Cylinder Obtained by Numerical and Experimental Analysis. *Civil and Environmental Engineering, 13*(2), 149–155. https://doi.org/10.1515/cee-2017-0020

Nafisi Poor, P., & Javid, P. (2021). Philosophy, Geometry, and Purpose in Islamic and Gothic Architecture as Two Religious-Based Styles. *International Journal of Architectural and Environmental Engineering, 15*(2). https://www.researchgate.net/publication/349916440_Philosophy_Geometry_and_Purpose_in_Islamic_and_Gothic_Architecture_as_Two_Religious-Based_Styles

NEN-EN 1990:2002+A1:2019+NB:2019 – Basis of structural design.

NEN-EN 1991-1-4:2005+C2:2011+NB:2019 - General actions - Wind actions.

NEN-EN 1991-1-3:2003+A1:2019+NB:2019 - General actions - Snow loads.

NEN-EN 1993-1-1:2006+A1:2014+NB:2016 Design of steel structures - General rules and rules for buildings.

NEN-EN 1993-1-8:2006+C11:2016+NB:2011 Design of steel structures - Design of joints.

NEN-EN 1995-1-1:2005+A2:2014+NB:2013 Design of timber structures - Common rules and rules for buildings.

NEN-EN 14080:2013 – Glued laminated timber and glued solid timber.

Rani, N., Pratap, A., Ahuja, A.K. (2022). Wind Pressure Distribution on Multi-span Semi-circular Canopy Roofs. In: Marano, G.C., Ray Chaudhuri, S., Unni Kartha, G., Kavitha, P.E., Prasad, R., Achison, R.J. (eds) Proceedings of SECON'21. SECON 2021. *Lecture Notes in Civil Engineering, vol 171*. Springer, Cham. https://doi.org/10.1007/978-3-030-80312-4_71

Rutten, D. (2013). Galapagos: On the Logic and Limitations of Generic Solvers. *Architectural Design, 83*(2), 132–135. https://doi.org/10.1002/ad.1568

Shu, Z., Li, Z., He, M., Chen, F., Hu, C., & Liang, F. (2020). Bolted joints for small and medium reticulated timber domes: experimental study, numerical simulation, and design strength estimation. *Archives of Civil and Mechanical Engineering, 20*, 73 (2020). https://doi.org/10.1007/s43452-020-00073-7

Tzbinfo. (n.d.). *Mapa sněhových oblastí na území České republiky*. Stavba.tzb-info.cz. https://stavba.tzb-info.cz/tabulky-a-vypocty/143-mapa-snehovych-oblasti-na-uzemi-ceske-republiky

Van Vooren, T.G.J. (2018). *Optimization of 3D concrete printed arch structures* [Master Thesis]. Eindhoven University of Technology.

Vector Foiltec. (2023). *Waitomo Caves Visitor Centre*. https://www.vector-foiltec.com/projects/waitomo-caves-visitor-center/?cn-reloaded=1

Wooddays. (2020). *Multihalle Mannheim* (From ProHolz Austria). https://www.wooddays.eu/en/architecture/best-practice-architecture/detail/multihalle-mannheim/index.html

Young, W. C., & Budynas, R. G. (2001). *Roark's Formulas for Stress and Strain* (7th edition). McGraw-Hill Companies.

APPENDIX A: LOAD CASES

A-1: Snow load
A-2: Wind load
A-3: Load combinations
A-3 Internal force distributions

A.1 Snow load

The snow load on the entrance hall's roof is calculated in accordance with EN 1991-1-3, taking into account various load cases. Two of these load cases are imposed in the middle of the roof arches, and one load case results from snow drift accumulation between the various roof parts. A certain characteristic value depending on the location of the structure is required to determine the snow load. This characteristic value is shown in the map presented in Figure A.1.

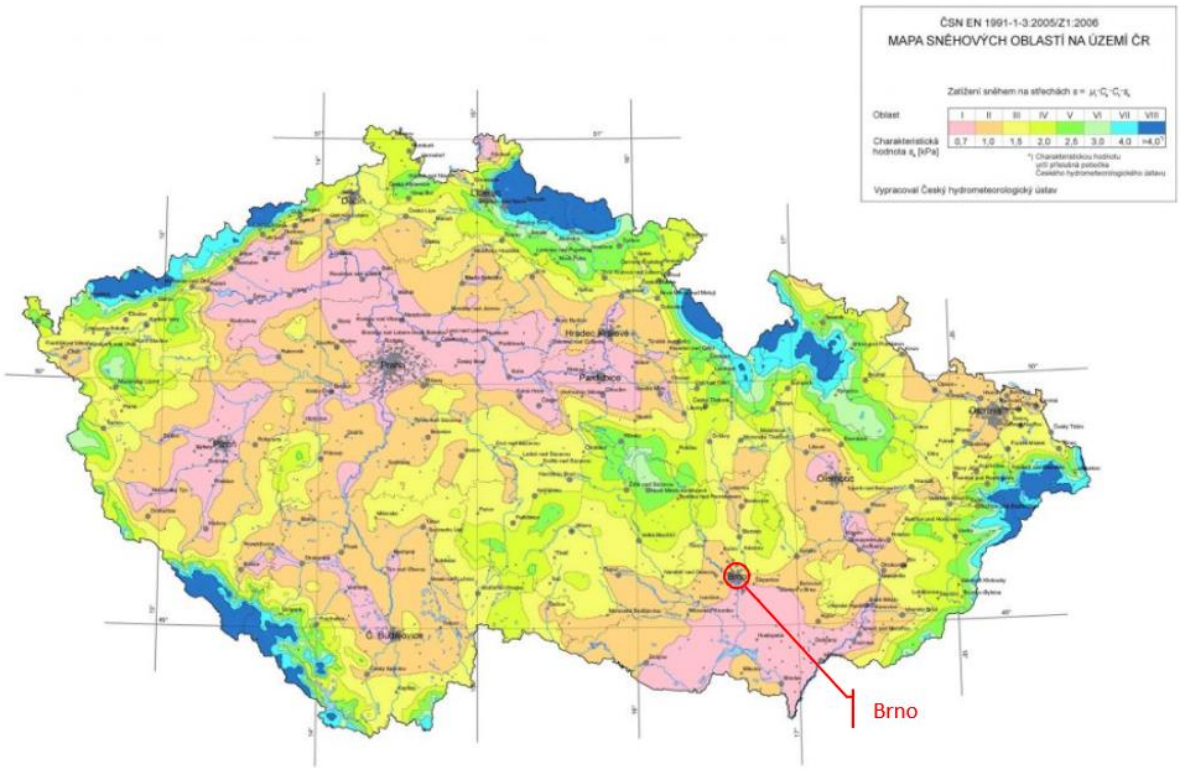

Figure A. 1 Snow areas Czech Republic, image from: Tzbinfo (n.d.)

A.1.1 Snow on curved roof

The snow load on the roof is calculated according to the general equation given in EN 1991-1-3 section 5.2. The characteristic value s_k is dependent on the location of the structure, with Brno being located in area II and thus having a value of 1,0 kN/m^2 (Figure A.1). The snow load shape coefficient μ_i is specific to the shape of the roof on which the load is acting. For the entrance hall, μ_i is determined according to EN 1991-1-3 section 5.3.5.

$$s = \mu_i * C_e * C_t * s_k \qquad \text{(A.1) (EN 1991-1-3, eq. 5.1)}$$

- Characteristic value s_k = 1,00 kN/m^2
- Exposure coefficient C_e = 1,00
- Thermal coefficient C_t = 1,00
- Snow load shape coefficient μ_i

The two load cases resulting from the snow load on the roof are illustrated in Figure A.2. As depicted, the snow load acts along the length l_s, which is the length where the slope of the arch (β) is less than 60 degrees. The value for the shape coefficient μ4 is calculated as follows:

$$For\ \beta > 60^o, \mu_4 = 0 \qquad \text{(A.2) (EN 1991-1-3, eq. 5.4)}$$

$$For\ \beta < 60^o, \mu_4 = 0{,}2 + 10\ \ h/b \qquad \text{(A.3) (EN 1991-1-3, eq. 5.5)}$$

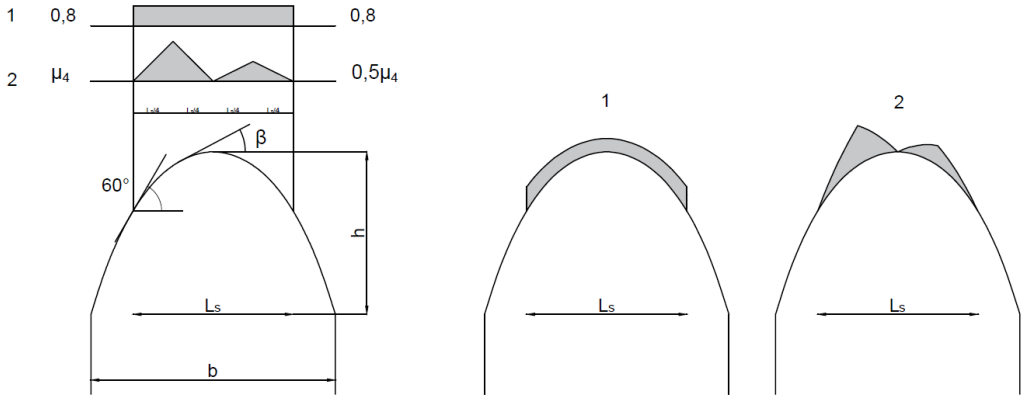

Figure A. 2 Snow load cases on a cylindrical roof, source: EN 1991-1-3

The slope β varies depending on the shape of the arch. To account for this, the Grasshopper model automatically measures β and subsequently adjusts the values of l_s and μ_4 when the arch shape is adjusted.

A.1.2 Snow drift

Roofs with multiple spans may experience snow drift accumulation between spans. In such cases, the snow load is calculated according to EN 1991-1-3 Annex B.2. These load cases are considered exceptional and therefore it can be assumed that no snow load is present on the remaining part of the roof. The following equation, as specified in the Eurocode, is used to determine the snow drift load:

$$s = \mu_i * s_k \qquad \text{(A.4) (EN 1991-1-3, eq. 5.3)}$$

For this load case the snow load is applied as shown in Figure A.3. The shape coefficient μ_1 is the minimum of the following values:

$$\mu_1 = 2h/s_k$$

$$\mu_1 = 2b_3/(l_{s1} + l_{s2})$$

$$\mu_1 = 5$$

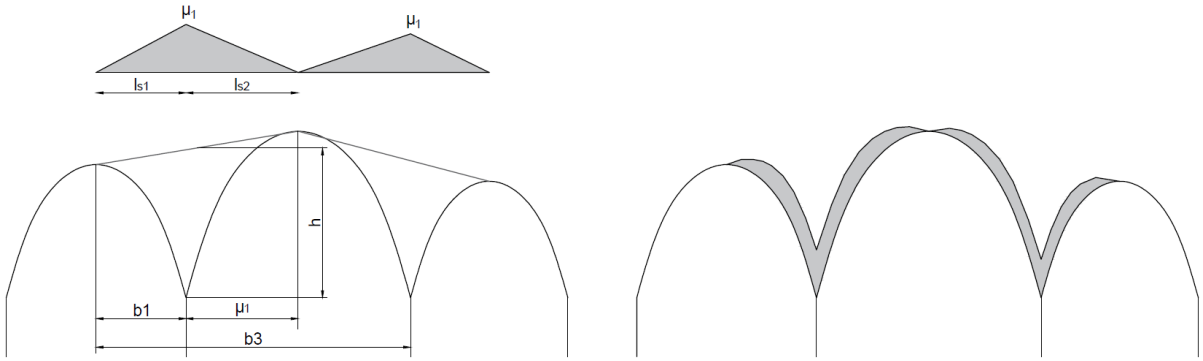

Figure A. 3 Snow drift for multiple spanning roofs, source: EN 1991-1-3

According to Annex B.2, the horizontal dimension b_3 is typically set to 1,5 times the span when the various parts of the roof are almost symmetrical and have similar shapes. However, if this is not the case, careful consideration is advised when determining b_3 as the larger section of the roof may function as an obstacle for the distribution of snow. In this case, b_3 is determined by adding the largest span to half of the smaller span.

A.2 Wind load

The wind load on the entrance hall's roof is determined by a peak velocity pressure and pressure coefficients. The peak velocity pressure is calculated according to EN 1991-1-4. Due to the unique shape of the entrance hall, no pre-existing external pressure coefficients that exactly match the structure are available. Therefore, a Computational Fluid Dynamics (CFD) analysis has been carried out. The results of the CFD analysis, which can be found in Appendix B, are compared to available pressure coefficients for similar structures in this appendix. Based on this comparison, it is determined whether the results from the CFD analysis provide a safe approximation of the wind load on the entrance hall's structure.

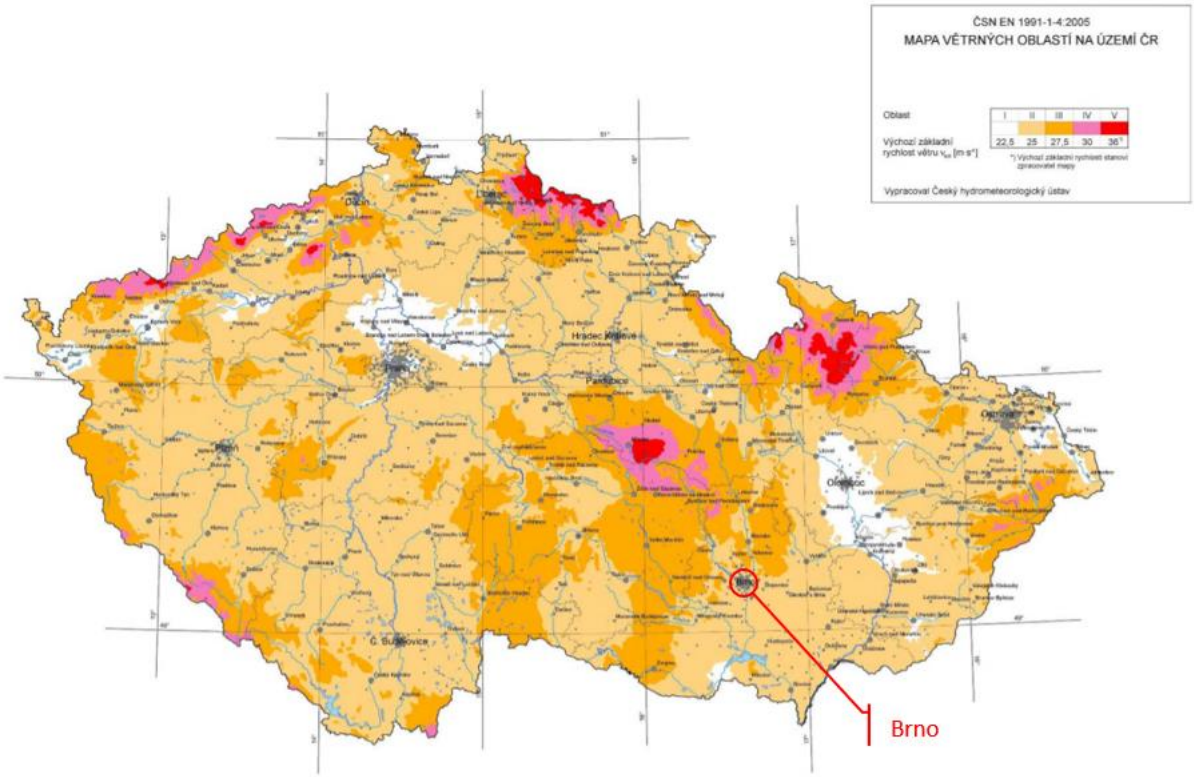

Figure A. 4 Wind load Czech Republic (České vysoké učení technické v Praze, n.d.)

The wind load is based on the peak velocity pressure q_p. This parameter depends on several factors like the location of the structure and the type of terrain. The peak velocity pressure is determined according to EN 1991-1-4 section 5. The procedure is presented below.

Wind area II (see figure A.4)

Wind direction factor	C_{dir}	= 1,0	
Season factor	C_{season}	= 1,0	
Fundamental wind velocity	$v_{b,0}$	= 25,0 m/s	
Basic wind velocity:	$v_b = v_{b,0} \cdot C_{dir} \cdot C_{season}$		(A.5) (EN 1991-1-4, eq. 4.1)

Terrain category III

Roughness length:	z_o	= 0,5 m
Minimum height:	z_{min}	= 7 m
Maximum height:	z_{max}	= 200 m
Structure height:	z	= 26,5 m

Roughness length II: $z_{o,II}$ = 0,05 m

Terrain factor: $k_r = 0{,}19 \cdot \left(\frac{z_0}{z_{0,II}}\right)^{0{,}07}$ (A.6) (EN 1991-1-4, eq. 4.5)

Turbulence factor: k_I = 1,0

Standard dev. Turbulence: $\sigma_v = k_r \cdot v_b \cdot k_I$ (A.7) (EN 1991-1-4, eq. 4.6)

Roughness factor: $c_r(z) = k_r \cdot \ln\frac{z}{z_0}$ (A.8) (EN 1991-1-4, eq. 4.4)

Orography factor: $c_0(z) = 1{,}0 \quad (assumption)$

Mean wind velocity: $v_m(z) = c_r(z) \cdot c_0(z) \cdot v_b$ (A.9) (EN 1991-1-4, eq. 4.3)

Turbulence intensity: $I_v(z) = \frac{\sigma_v}{v_m(z)} = \frac{k_I}{c_o(z)\cdot\ln(z/z_0)}$ (A.10) (EN 1991-1-4, eq. 4.7)

Air density $\rho = 1{,}25\ kg/m^3$

Peak velocity pressure: $q_p(z) = \left(1 + 7 \cdot I_v(z)\right) \cdot \frac{\rho \cdot v_m^2(z)}{2}$ (A.11) (EN 1991-1-4, eq. 4.8)

The peak velocity pressure q_p depends on the height of the structure. The highest point of the structure will be used for the determination of q_p which results in the most conservative loads.

A.2.1 Wind load on curved roofs

The general formula which is used to calculate the external wind load is given by EN 1991-1-4 section 5.2.

$w_e = q_p(z_e) \cdot c_{pe}$ (A.12) (EN 1991-1-4, eq. 5.1)

As seen in the formula, the wind load on the roof depends on an external pressure coefficient $C_{pe,10}$. For structures with a common shape, these coefficients can be obtained from relevant building codes. However, for structures with a complex shape, such as the entrance hall, suitable coefficients can be obtained through a wind tunnel test, a CFD simulation, or by using test results from structures with a similar shape. A wind tunnel test is over-scoped for this project, so the coefficients will be obtained through test results from structures with a similar shape as the entrance hall, or through a CFD simulation. Several options are considered to obtain realistic and safe values for the external pressure coefficients $C_{pe,10}$. Below, an overview is given for wind loads on curved roofs according to different building codes and test results from literature. This overview includes test results for catenary vault structures and a multi-spanning curved roof.

EN 1991-1-4

Coefficients for external pressure on curved roofs are provided by EN 1991-1-4 for a range of rise height to span ratios, from 0,05 to 0,5, and for side wall height to span ratios of 0 or greater than 0,5. For side wall height to span ratios between 0 and 0,5, coefficients must be determined through linear interpolation (Blackmore & Tsokri, 2006).

EN 13031-1

Data is given by EN 13031 which is applicable for greenhouses, both with and without side walls. For greenhouses with sidewalls, the code provides data for a rise height to span ratio ≤ 0,4 and ≥ 0,6 (Blackmore & Tsokri, 2006).

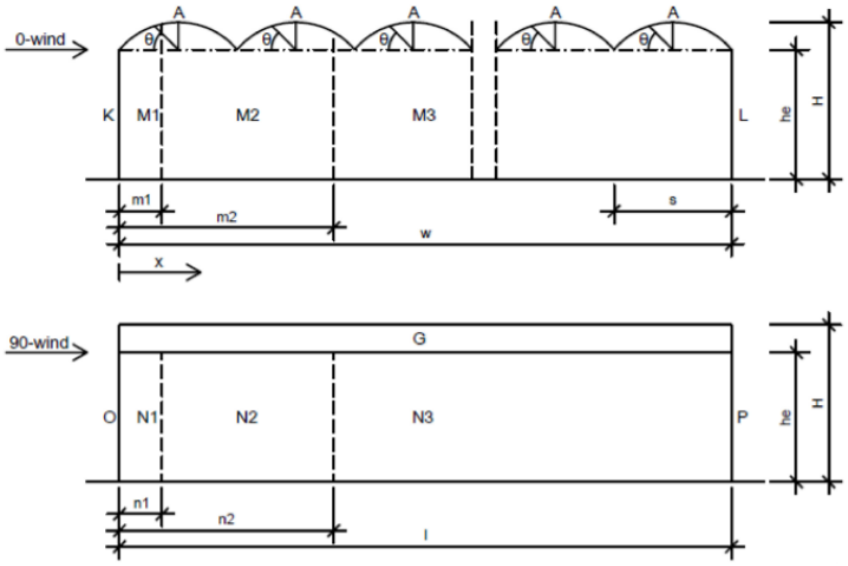

Figure A. 5 Wind pressure coefficients on circular roofs according to EN 13031 (Maraveas, 2020)

Bradley et al. (2016)

A series of simulations has been performed by Bradley et al. (2016) for catenary vault structures with rise height to span ratio up to 0,8. The test objects did not have side walls and are not multi-spanning. Coefficients are given for a wind direction of $\alpha = 0^o$, 45^o and 90^o.

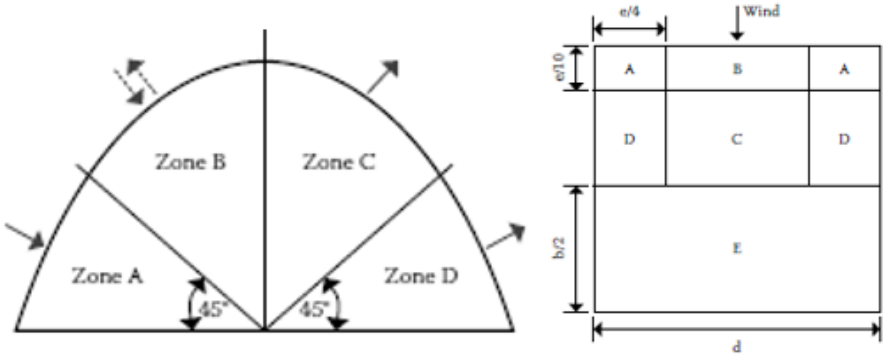

Figure A. 6 Wind pressure coefficients for a catenary vault structure from Bradley et al. (2016)

Rani et al. (2022)

An experiment using a wind tunnel has been carried out by Rani et al. (2022) for a single-, two-, and three span curved canopy roof. The rise height to span ratio is 0,5.

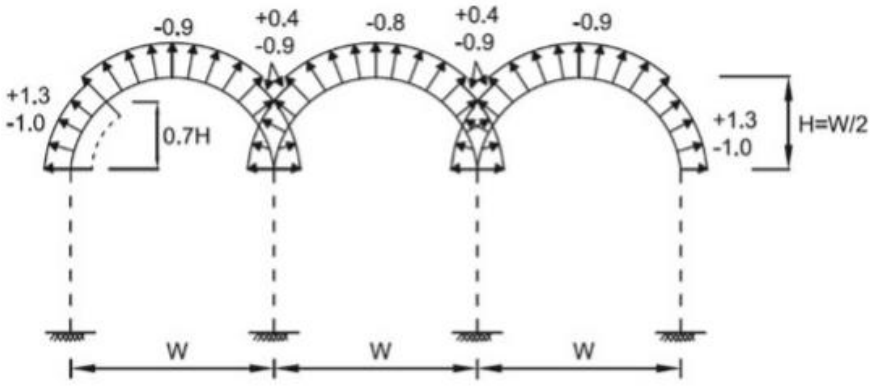

Figure A. 7 Wind pressure coefficients for multi-spanning roof from Rani et al. (2022)

A.2.2 Computational Fluid Dynamic analysis

The structure has a high rise height to span ratio and multi-spanning design. It is expected that both of these factors have a significant effect on the wind load. Given the differences with the pre-existing options, it was decided to conduct a simple CFD analysis using the program Ansys Fluent. The analysis was performed for five different wind directions and the results can be found in Appendix B. The wind load cases acting on the large section of the entrance hall, resulting from the CFD analysis are illustrated in Figure A.8. The pressure coefficients obtained by the CFD simulation were compared to those provided by the other options. It should be noted that in most options, wind directions from the side and front of the structure are described as 0° and 90°, which are more comparable to 45° and 135° in the CFD analysis. These notations for wind directions are also used in Table A.1.

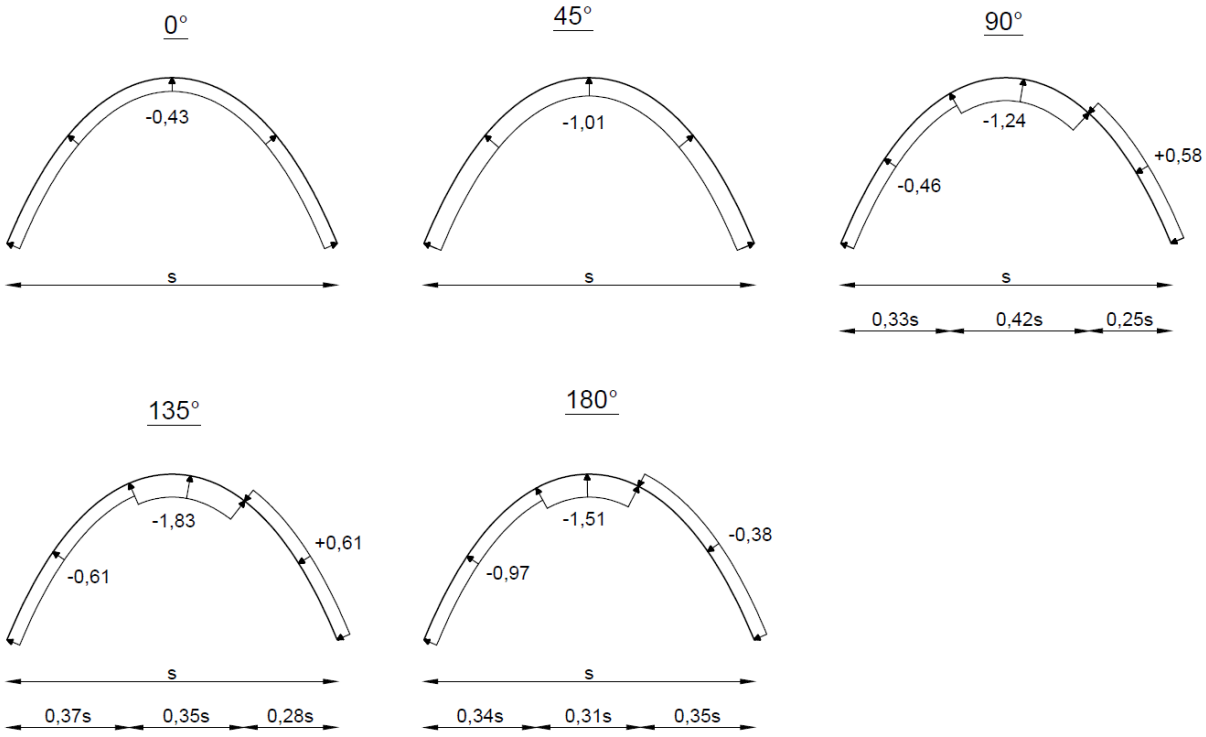

Figure A. 8 External pressure coefficients according to Ansys Fluent

Table A. 1 Comparison coefficients

		0°	45°	90°	135°	180°
Bradly et al. (2016)	-		-0,91	-0,88	-0,52	
	+				0,62	
Rani et al. (2022)	-				-1,00	
	+				1,30	
EN 1991-1-4	-				-1,20	
	+				0,80	
EN 13031-1	-		-1,20		-1,00	
	+					
Ansys Fluent	-	-0,70	-1,01	-1,24	-1,83	-1,51
	+	0	0	0	0,61	0

As depicted in the table, the coefficients obtained through the CFD analysis using Ansys Fluent are generally higher than those provided by the other options. However, there are two coefficients that are higher than those obtained by Ansys Fluent. The figures in Appendix B show that the pressure given by Rani et al. (2022) at that location won't occur at the entrance hall. The wind suction coefficient given by EN 13031-1 is dependent on the height of the structure.

A.2.3 Wind façade

The wind pressure on the façade is determined using Eurocode 1991-1-4 section 7.2.2, which corresponds to vertical facades of structures with a rectangular top view. However, as seen in Figure A.9, the top view of the entrance hall is not exactly a rectangle but rather a trapezoidal shape. When the wind direction (α) is 90 degrees, the use of either the length of the long side or the short side will result in the same coefficients and wind zones. Additionally, there is no wind zone E for this wind direction as the back side of the structure is connected to the main station. To determine the wind zones, the factor e is calculated as:

$$e = min[b; 2h] = [77{,}4; 53] = 53 \rightarrow e \geq d \tag{A.13}$$

For wind direction α = 0°, the wind is determined by article 7.2.2, and is coming from the right as viewed from the top in the figure. This is because the leftmost part of the entrance hall is an open structure without a façade. The value of e is determined as follows for this wind direction:

$$e = min[b; 2h] = [60; 53] = 53 \rightarrow e < d \tag{A.14}$$

The wind loads that act on the façade for wind direction 0° and 90° are based on the values for e and the measurements of the entrance hall. The wind zones for both wind directions are given in Figure A.9. In this figure also the facades are drawn in red and the front view is given. The external pressure coefficients for each wind zone are given in Table A.2.

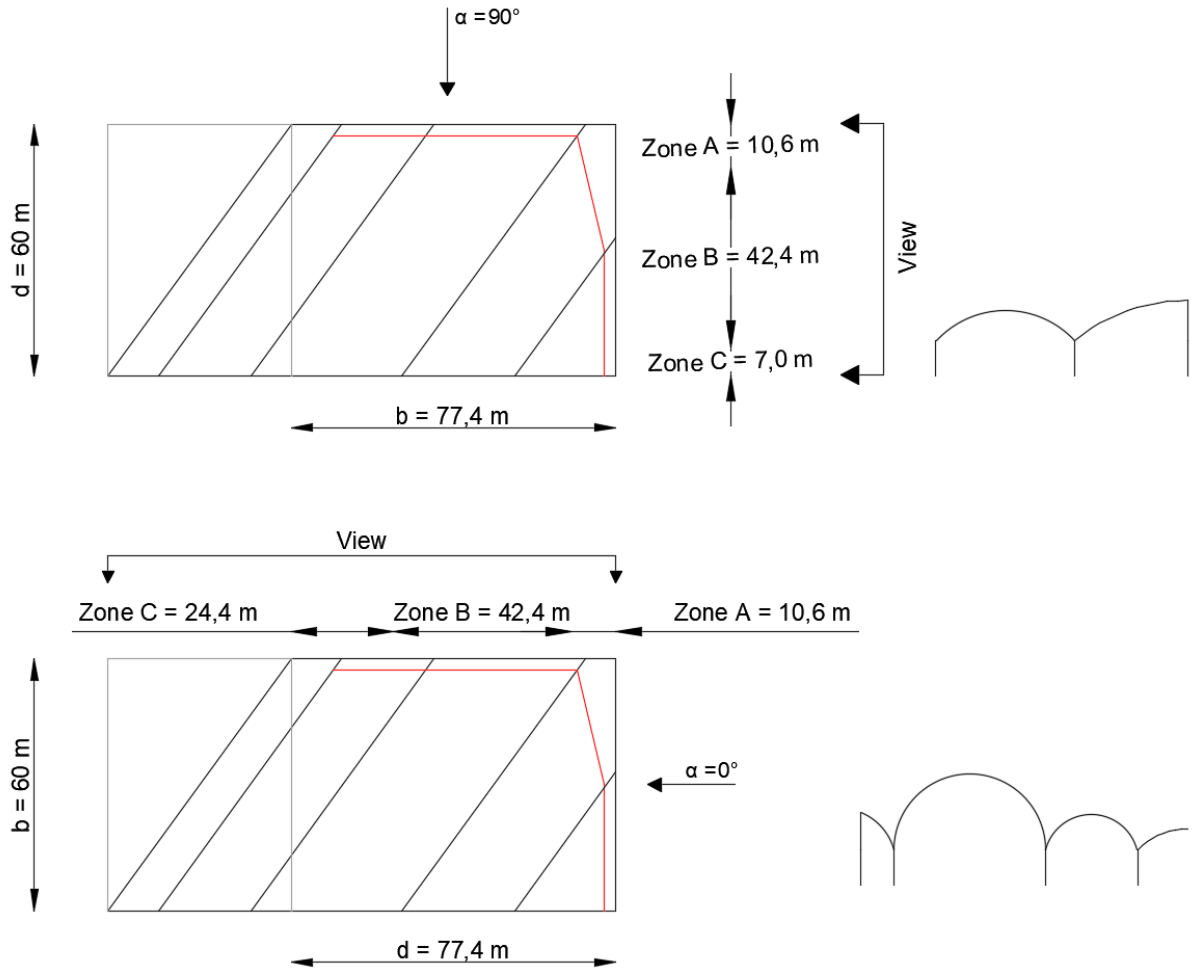

Figure A. 9 Wind zones facade

Table A. 2 External pressure coefficients wind façade according to EN 1991-1-4 Table 7.1

Zone	**A**		**B**		**C**		**D**		**E**	
h/d	$C_{pe,10}$	$C_{pe,1}$	$C_{pe,10}$	$C_{pe,1}$	$C_{pe,10}$	$C_{pe,1}$	$C_{pe,10}$	$C_{pe,1}$	$C_{pe,10}$	$C_{pe,1}$
≤ 1	-1,2	-1,4	-0,8	-1,1	-0,5	-0,5	+0,8	+1,0	-0,5	-0,5

From the CFD simulations in Ansys fluent pressure coefficients on the facades were obtained as well. However, it was decided to use the coefficients from the Eurocode. The validation of the results showed that the wind pressure was slightly overestimated and the wind suction underestimated when comparing the Ansys Fluent results to the Eurocode. The maximum wind pressure on the facades given by Ansys Fluent ranges between +0.83 and +0.92, but it should be noted that this maximum pressure only occurs on a part of the façade. Therefore, a global wind pressure coefficient of +0.8 was considered to be safe. For the wind suction that occurs on facades not perpendicular to the wind direction, the coefficients from the Eurocode were found to be larger. Additionally, because the validation showed that the wind suction may be underestimated, the coefficients from the Eurocode were considered to be more safe.

A.2.4 Internal wind

Detailed information about the openings in the entrance hall structure is not available. However, the structure will be accessible from all sides and the openings are assumed to be permanent since the entrance hall has a public function. Based on article 7.2.9 of Eurocode 1, the internal pressure coefficients C_{pi} applied will be -0.3 and +0.2, as the openings are assumed to be permanent.

A.2.5 Wind friction

De load resulting from wind friction is determined by

$$q_{fr} = q_p(z_e) \cdot C_{fr} \qquad \text{(A.15) (EN 1991-1-4, eq. 5.7)}$$

The factor C_{fr} is assumed to be 0,04 based on table 7.10 in Eurocode 1991-1-4. Also a reference surface A_{fr} is determined on which the load has to be applied. Based on Art. 7.5 from Eurocode 1991-1-4 this is determined to be the full surface of the roof. In the formula $q_p(z_e)$ is the peak velocity pressure which is determined earlier.

A.3 Load combinations

In this section, the load combinations corresponding to the Ultimate Limit State (ULS) and Serviceability Limit State (SLS) are given.

Consequence class

The consequence class which is assumed for the structure is consequence class 2 (CC2). This is determined based on NEN-EN 1990 table NB.24 – B1. The structure has a public function and does not belong to the examples given for CC3 and CC1. The following partial factors correspond to CC2.

Permanent loads:
γ_G: 1,35 (combination 6.10a)
γ_G: 1,20 (combination 6.10b)
γ_G: 0,90 (favourable load)

Variable loads:
γ_G: 1,50 (combination 6.10b)
γ_G: 0,90 (favourable load)

1.1.1 Factors

Category H roofs:

Ψ_0: 0
Ψ_1: 0
Ψ_2: 0

1.1.2 Ultimate limit state

The load combinations in the ULS are in accordance with EN 1990 chapter 6. The load combinations are given in table A.3 and A.4.

$$\sum_{j\geq 1}\gamma_{G,j}G_{k,j} + \gamma_p P + \gamma_{Q,1}\psi_{0,1}Q_{k,1} + \sum_{j>1}\gamma_{Q,i}\psi_{0,i}Q_{k,i} \quad \text{(A.16) (EN 1990, 6.10a)}$$

Table A. 3 Load combinations ULS 6.10a

LC	Permanent	Variable							
		Snow I $\Psi_0 = 0$	Snow II $\Psi_0 = 0$	Snow III $\Psi_0 = 0$	Wind 0° $\Psi_0 = 0$	Wind 45° $\Psi_0 = 0$	Wind 90° $\Psi_0 = 0$	Wind 135° $\Psi_0 = 0$	Wind 180° $\Psi_0 = 0$
ULS-1	1,50	-	-	-	-	-	-	-	-

$$\sum_{j\geq 1}\xi_j\gamma_{G,j}G_{k,j} + \gamma_p P + \gamma_{Q,1}Q_{k,1} + \sum_{j>1}\gamma_{Q,i}\psi_{0,i}Q_{k,i} \quad \text{(A.17) (EN 1990, 6.10b)}$$

Table A. 4 Load combinations ULS 6.10b

LC	Permanent	Variable							
		Snow I $\Psi_0 = 0$	Snow II $\Psi_0 = 0$	Snow III $\Psi_0 = 0$	Wind 0° $\Psi_0 = 0$	Wind 45° $\Psi_0 = 0$	Wind 90° $\Psi_0 = 0$	Wind 135° $\Psi_0 = 0$	Wind 180° $\Psi_0 = 0$
ULS-2	1,20	1,50	-	-	-	-	-	-	-
ULS-3	1,20	-	1,50	-	-	-	-	-	-
ULS-4	1,20	-	-	1,50	-	-	-	-	-
ULS-5	1,20	-	-	-	1,50	-	-	-	-
ULS-6	1,20	-	-	-	-	1,50	-	-	-
ULS-7	1,20	-	-	-	-	-	1,50	-	-
ULS-8	1,20	-	-	-	-	-	-	1,50	-
ULS-9	1,20	-	-	-	-	-	-	-	1,50

A.3.1 Servicability limit state

The load combinations for the SLS are in accordance with EN 1990 chapter 6. The corresponding load combinations can be seen in table A.5 to A.7.

$$\sum_{j\geq 1}G_{k,j} + P + Q_{k,1} + \sum_{j>1}\psi_{0,i}Q_{k,i} \quad \text{(A.18) (EN 1990, 6.14b)}$$

Table A. 5 Load combinations SLS 6.14b

LC	Permanent	Variable							
		Snow I $\Psi_0 = 0$	Snow II $\Psi_0 = 0$	Snow III $\Psi_0 = 0$	Wind 0° $\Psi_0 = 0$	Wind 45° $\Psi_0 = 0$	Wind 90° $\Psi_0 = 0$	Wind 135° $\Psi_0 = 0$	Wind 180° $\Psi_0 = 0$
SLS-1	1,0	1,0	-	-	-	-	-	-	-
SLS-2	1,0	-	1,0	-	-	-	-	-	-
SLS-3	1,0	-	-	1,0	-	-	-	-	-
SLS-4	1,0	-	-	-	1,0	-	-	-	-
SLS-5	1,0	-	-	-	-	1,0	-	-	-
SLS-6	1,0	-	-	-	-	-	1,0	-	-
SLS-7	1,0	-	-	-	-	-	-	1,0	-
SLS-8	1,0	-	-	-	-	-	-	-	1,0

Frequent load combination:

$$\sum_{j\geq 1} G_{k,j} + P + \psi_{1,1} Q_{k,1} + \sum_{j>1} \psi_{2,i} Q_{k,i} \quad \text{(A.19) (EN 1990, 6.15b)}$$

Table A. 6 Load combinations SLS 6.15b

LC	Permanent	Variable							
		Snow I	Snow II	Snow III	Wind 0º	Wind 45º	Wind 90º	Wind 135º	Wind 180º
SLS-9	1,0	0,2	-	-	-	-	-	-	-
SLS-10	1,0	-	0,2	-	-	-	-	-	-
SLS-11	1,0	-	-	0,2	-	-	-	-	-
SLS-12	1,0	-	-	-	0,2	-	-	-	-
SLS-13	1,0	-	-	-	-	0,2	-	-	-
SLS-14	1,0	-	-	-	-	-	0,2	-	-
SLS-15	1,0	-	-	-	-	-	-	0,2	-
SLS-16	1,0	-	-	-	-	-	-	-	0,2

Quasi permanent load combination

$$\sum_{j\geq 1} G_{k,j} + P + \sum_{j>1} \psi_{2,i} Q_{k,i} \quad \text{(A.20) (EN 1990, 6.16b)}$$

Table A. 7 Load combinations SLS 6.16b

LC	Permanent	Variable							
		Snow I	Snow II	Snow III	Wind 0º	Wind 45º	Wind 90º	Wind 135º	Wind 180º
SLS-17	1,0	-	-	-	-	-	-	-	-

A.4 Internal force distributions

On the next pages the distributions of the bending moment, shear force and normal forces are added for a 2D catenary arch. The distributions result from the load combinations according to the ULS as presented in Table A.3 and A.4.

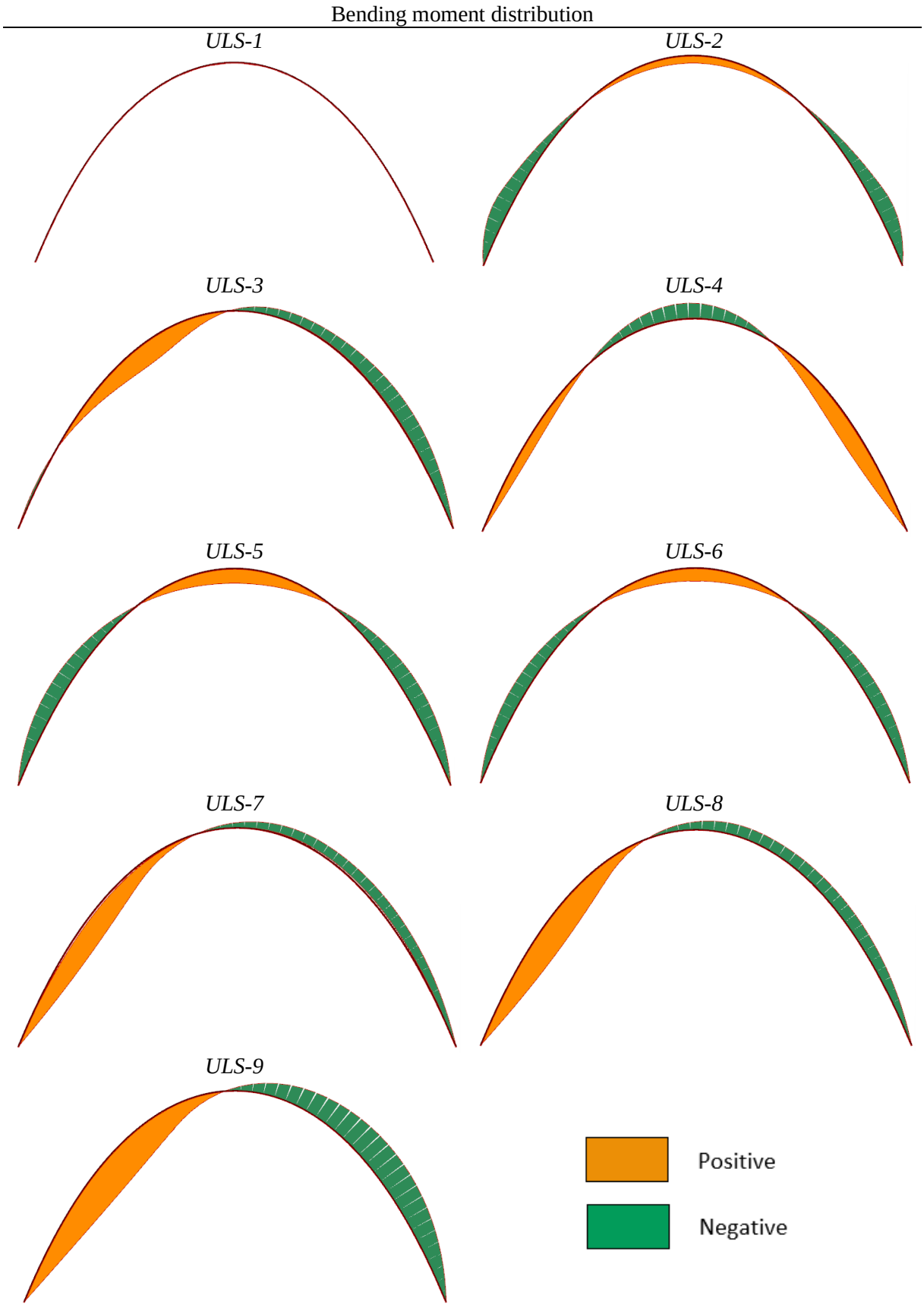

Figure A. 10 Bending moment distribution resulting from ULS load combinations for a catenary arch

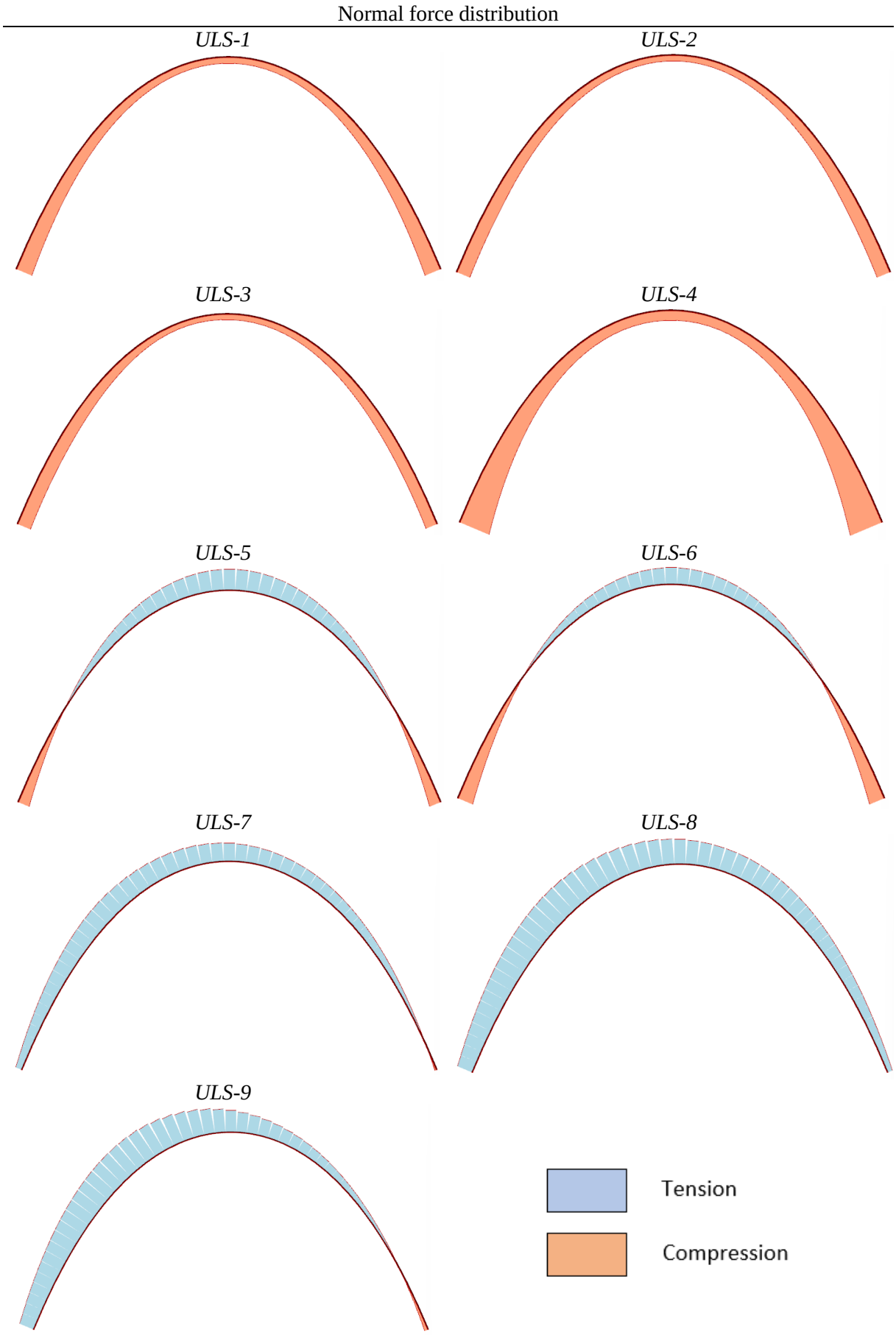

Figure A. 11 Normal force distribution resulting from ULS load combinations for a catenary arch

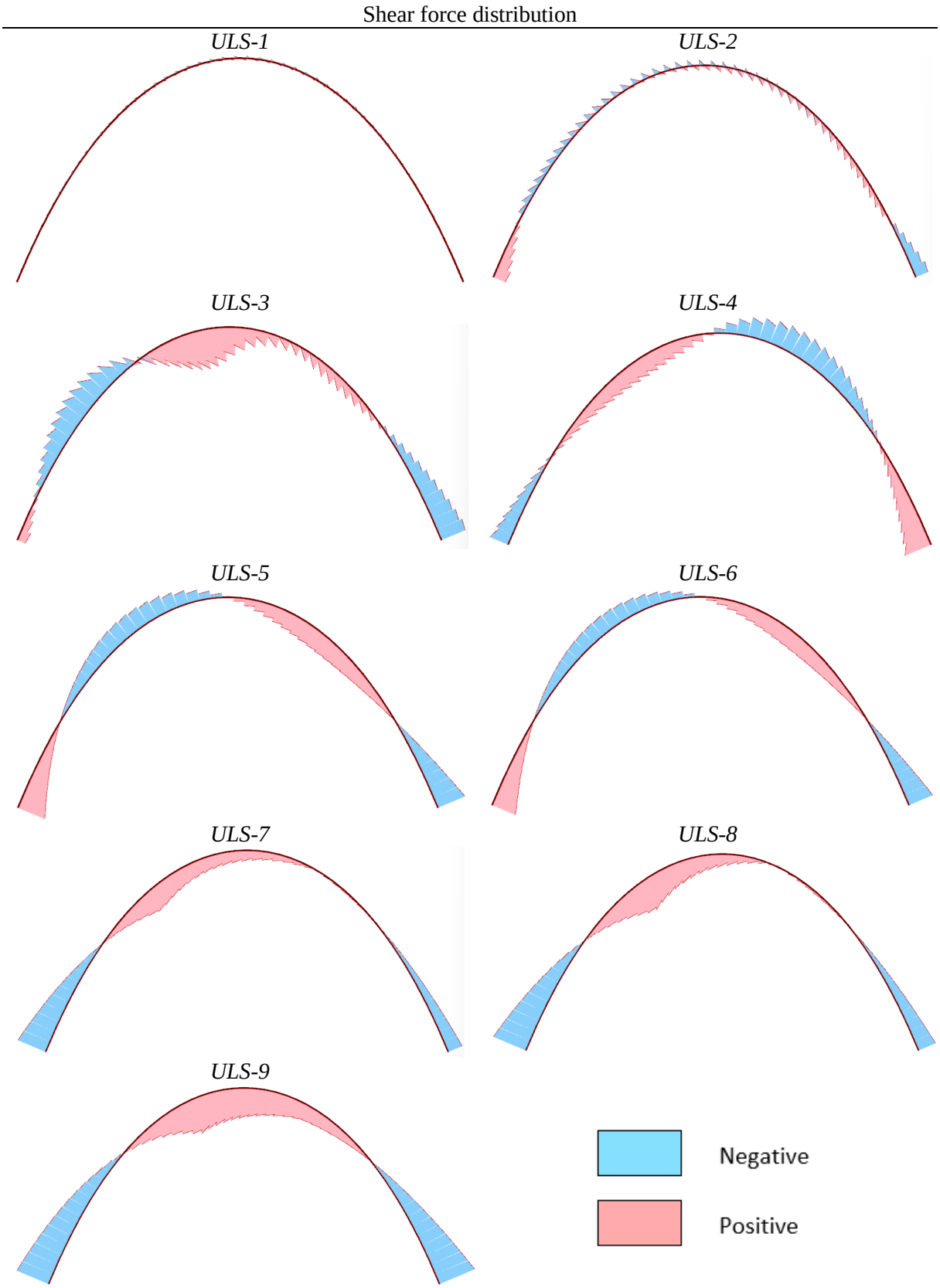

Figure A. 12 Shear force distribution resulting from ULS load combinations for a catenary arch

Appendix B: CFD analysis Ansys Fluent

B-1: Starting points
B-2: Results CFD analysis
B-3: Validation of results

B CFD ANALYSIS ANSYS FLUENT

As no pressure coefficients for a structure similar to the Brno main station's entrance hall are available, it was deemed necessary to conduct a Computational Fluid Dynamics (CFD) analysis. This analysis was carried out using the Ansys Fluent software. In this appendix, the methodology, results, and validation of the results are presented.

B.1 Starting points

In order to determine the wind pressure on the structure, five different wind directions surrounding the structure were taken into account. These wind directions are depicted in the figure below.

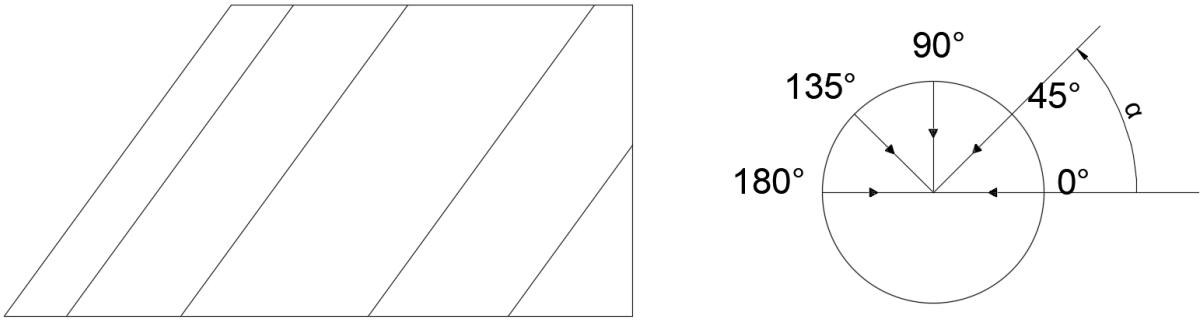

Figure B. 1 Analysed wind directions

The geometry was created using Rhino3D. As depicted in the figure below, a box has been placed behind the entrance hall to take into account the effect of the main building of the station. Additionally, it can be seen that the entrance hall geometry is not entirely accurate, as certain details have been left out. This is due to the use of a student version of Ansys Fluent, which has a limited number of elements that can be applied to the mesh. Using more elements would result in a coarse mesh in other areas, or a mesh that is too coarse to obtain reliable results for the detailed regions.

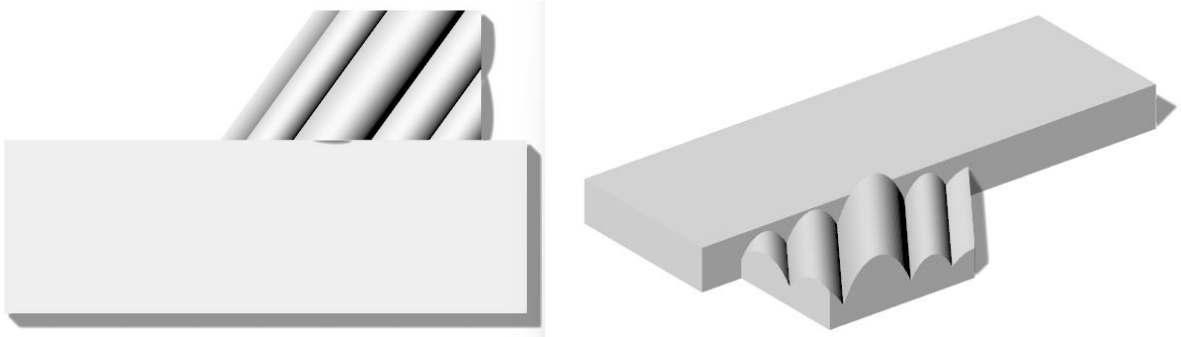

Figure B. 2 Geometry for CFD analysis

The dimensions of the fluid domain are based on the recommended values of 5H for the upstream, 15H for the downstream and 5H for the lateral distances (Abu-Zidan et al. 2021). In this case, H represents the maximum height of the geometry. The upstream distance refers to the area in front of the structure on the side from which the wind is coming, while the downstream distance is located behind the structure. Lateral distances refer to the distance above the structure and the distance between the sides and the end of the fluid domain. For the simulation, a standard K-epsilon model is used. This is the most commonly used model to simulate turbulence effects.

B.2 Results Ansys Fluent

α=0º

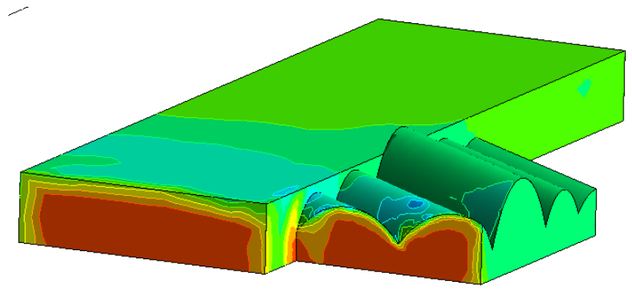

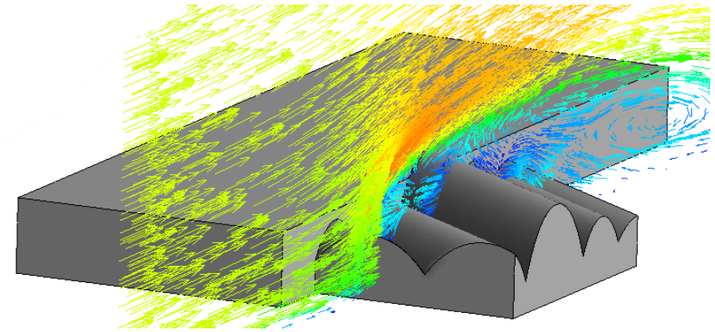

α=45º

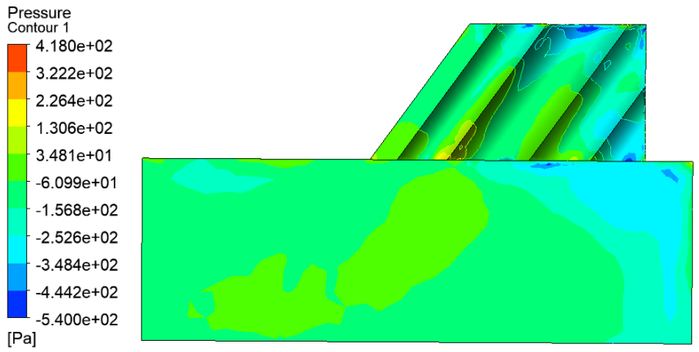

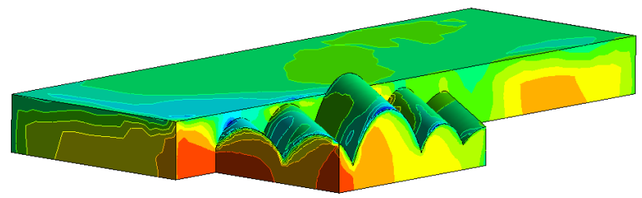

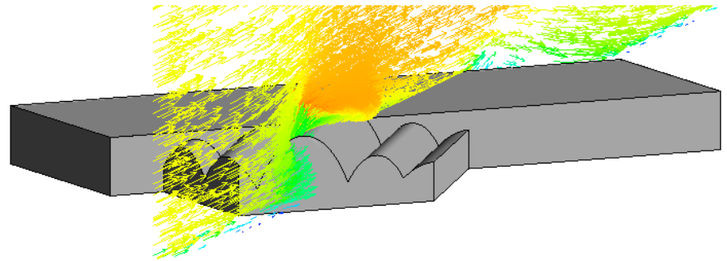

α=90º

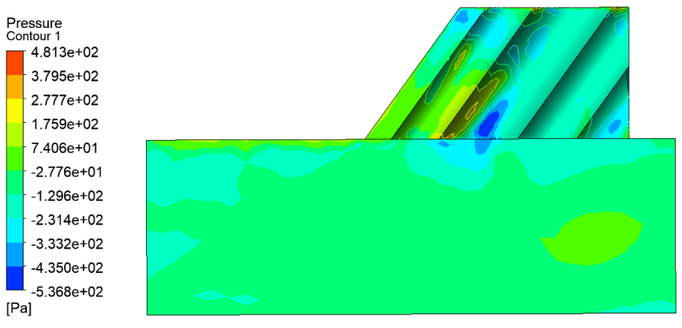

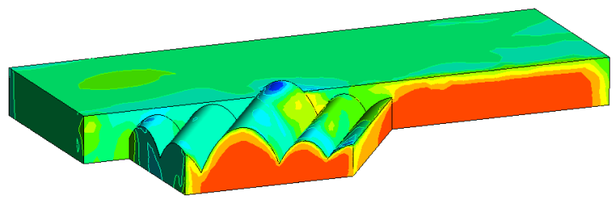

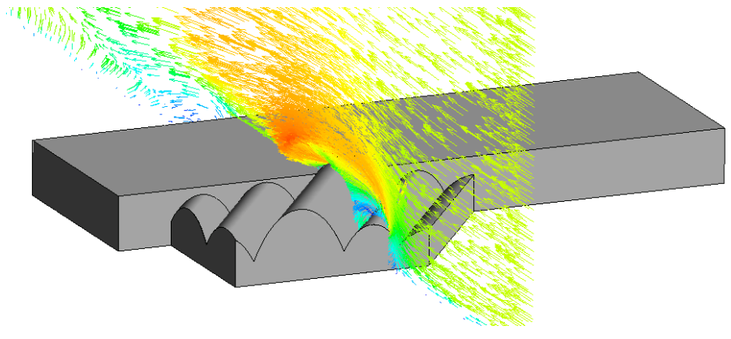

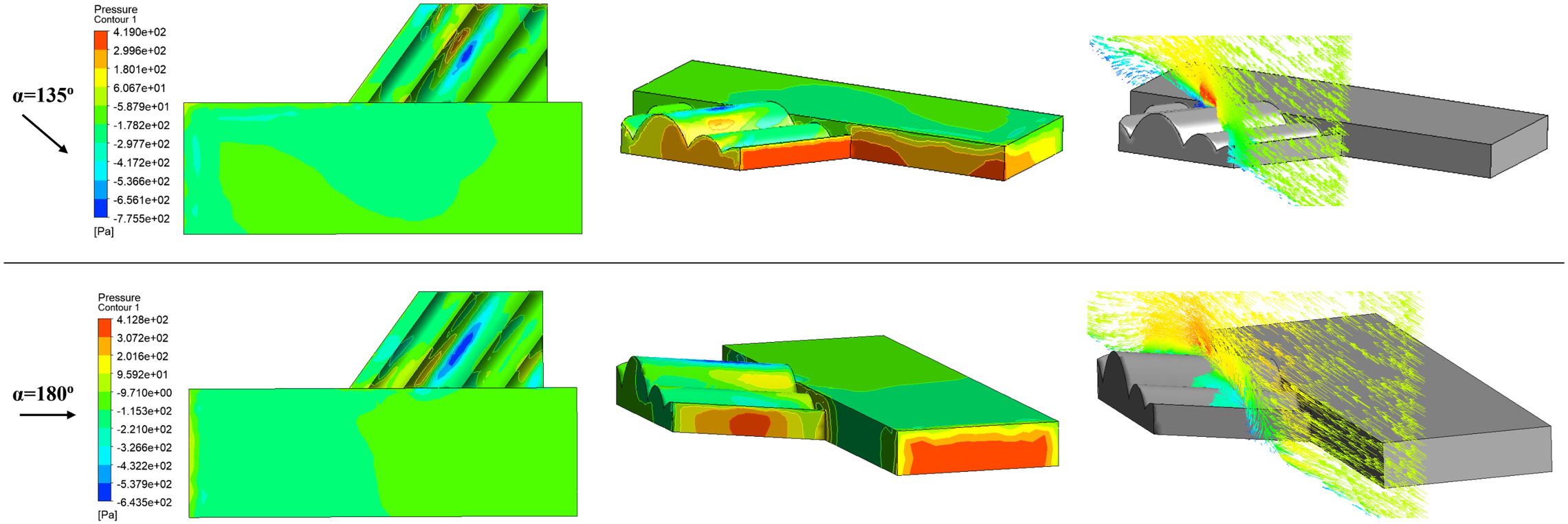

Figure B. 3 Wind pressure on entrance hall resulting from Ansys Fluent

As depicted in Figure B.3, the pressure on the roof of the entrance hall can be observed. However, the pressure values shown in the figures will not be used as the wind load. Instead, they will be used to calculate the pressure coefficients. According to Costola & Alucci (2007), the pressure coefficients can be calculated using the following formulas:

$$C_p = \frac{P_x}{P_d} \tag{B.1}$$

In which P_x is the wind pressure at a certain point and P_d is the reference pressure at a location which is not disturbed by any obstacles.

$$P_d = \frac{\rho \cdot V_{ref}^2}{2} \tag{B.2}$$

In this formula, ρ represents the air density, for which a value of 1,25 kg/m^3 will be used, and V_{ref} represents the reference velocity. In Ansys Fluent, a reference velocity of 25 m/s is assumed. Using these formulas, the pressure coefficients are calculated. The wind zones and corresponding pressure coefficients for both wind directions are presented in Figure. B.4. The measurements of the wind zones can be found in Table B.1. where b represents the span of the roof section in which the wind zone is located.

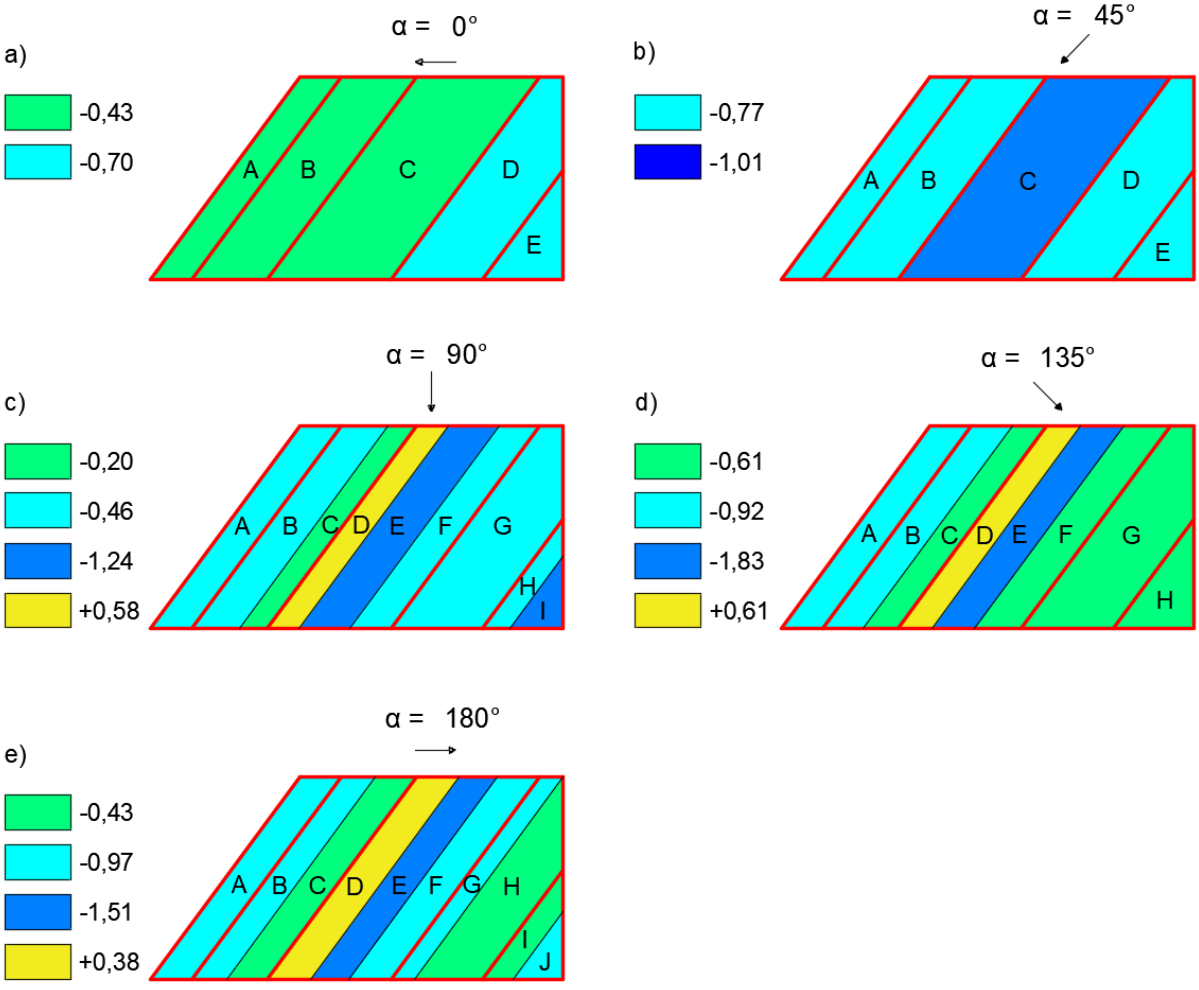

Figure B. 4 Wind zones and pressure coefficients for: (a) wind direction 0o, (b) wind direction 45o, (c) wind direction 90o, (d) wind direction 135o, (e) wind direction 180o

Table B. 1 Wind zone dimensions

Zone	α = 0°	α = 45°	α = 90°	α = 135°	α = 180°
A	-	-	-	-	-
B	-	-	0,66 x b	0,55 x b	0,45 x b
C	-	-	0,34 x b	0,45 x b	0,55 x b
D	-	-	0,25 x b	0,28 x b	0,35 x b
E	-	-	0,42 x b	0,35 x b	0,31 x b
F	-	-	0,33 x b	0,37 x b	0,34 x b
G	-	-	-	-	0,25 x b
H	-	-	0,33 x b	-	0,75 x b
I	-	-	0,67 x b	-	0,33 x b
J	-	-	-	-	0,67 x b

B.3 Validation of results

To validate the accuracy of the results obtained from Ansys Fluent with the current settings, a CFD analysis is conducted using a simple cube and cylinder. These results are then compared to pressure coefficients for a cube and cylinder from literature. The same settings, proportions for the fluid domain, and mesh type are used for the simulation.

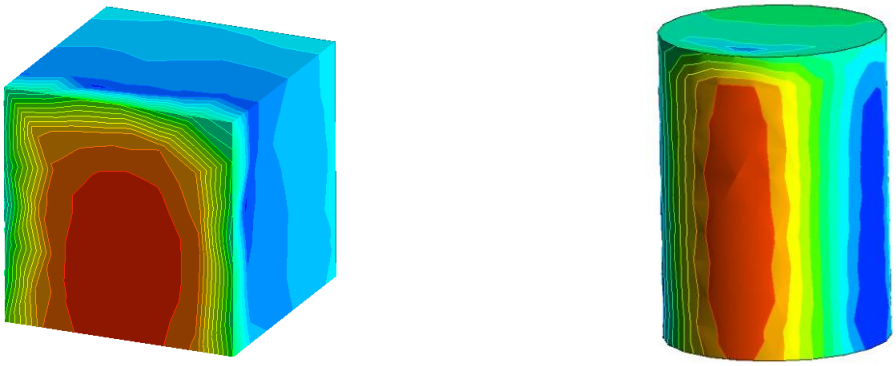

Figure B. 5 Wind pressure on a cube and a cylinder

Comparison cube

The results from the simulation in Ansys Fluent for the cube have been compared to those from Javanroodi, et al. (2018). To evaluate the pressure coefficients on the cube from various methods, in their research, the front, upper, and back side of the cube were divided into points, and the pressure coefficient was plotted for each point. The same process was applied to the results from the Ansys Fluent simulation. The pressure coefficients are calculated with Formula B.1 and B.2. As can be seen in the added graphs, the contours of the plotted results are similar to those of the Ansys Fluent results. However, the pressure coefficients presented by Javanroodi, et al. (2018) vary among the different methods. It is worth noting that the pressure on the facades, according to Ansys Fluent, is higher than the other results and even much higher than the results from their CFD with Ansys Fluent. On the other hand, the wind suction on the leeward side of the cube, according to Ansys Fluent, is lower than the other results. Only the Silsoe cube gives similar pressure coefficients. On the roof, all methods show a large peak in wind suction. Here, the wind suction given by Ansys Fluent seems to be lower than most results as well, except when compared to those of Autodesk CFD.

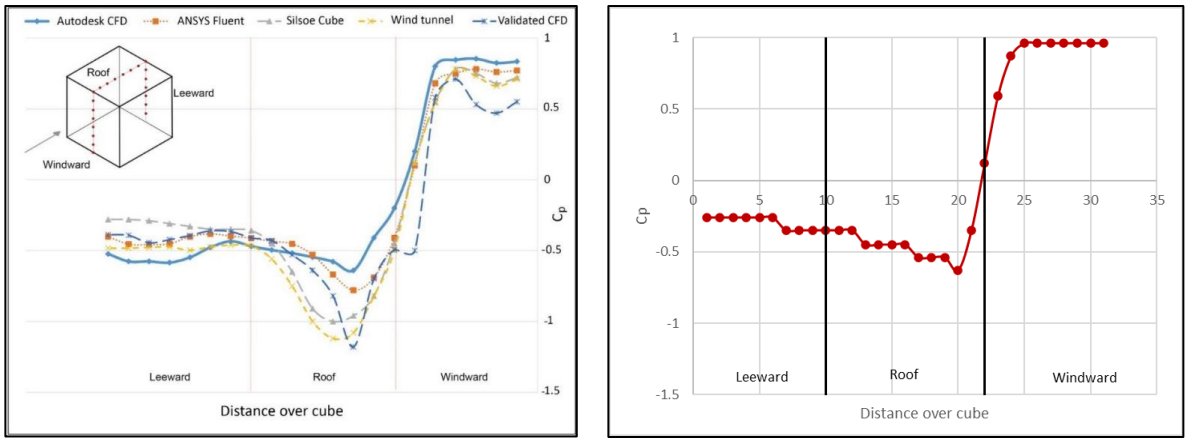

a) b)

Figure B. 6 a) Wind pressure cube from: Javanroodi et al. (2018); b) Wind pressure cube Ansys Fluent

Comparison Cylinder

The same settings are applied for the cylinder as the ones used for the cube and entrance hall roof. For this geometry the pressure coefficients have been compared to results from Medvecká, Ivanková, & Macák (2017). In their research the pressure coefficients are given for a cylinder with a diameter of 0,11 m and a height of 0,30 m. These pressure coefficients are obtained through a wind tunnel test, the Eurocode and a CFD simulation for which they also used Ansys Fluent. Their results are derived from a graph, and are added in the graph below, together with the results from Ansys Fluent.

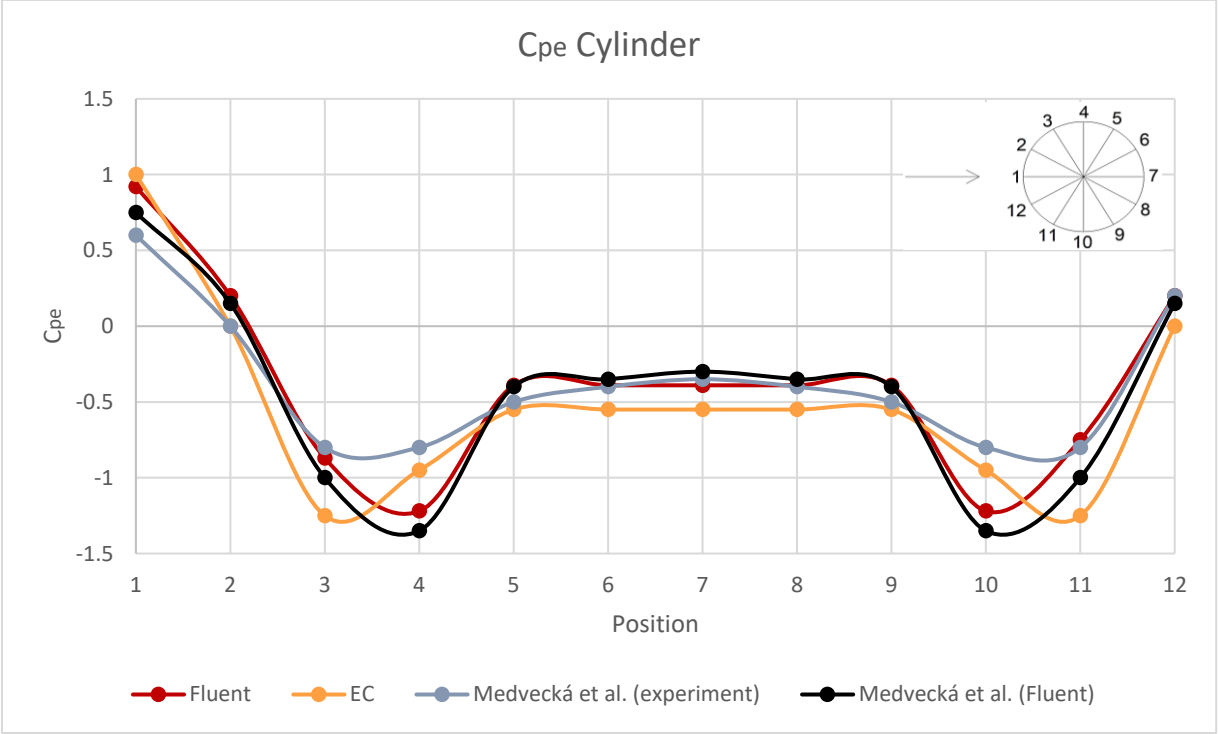

Figure B. 7 Wind pressure cylinder

The results from Ansys Fluent are represented by the red line in the graph. It can be observed that the contours are similar to the contours of the Ansys Fluent results by Medvecká et al. (2017). However, the results appear to be underestimated. This was observed with the cube as well. Additionally, the contours of the results from the Eurocode and wind tunnel test are similar to each other. Nevertheless, the pressure coefficients given by the Eurocode are higher than the results from the wind tunnel test and are comparable to the Ansys Fluent results. Assuming that the wind tunnel test results are accurate, it can be concluded that Ansys Fluent overestimates the pressure and suction on the cylinder.

The results of the cylinder comparison indicate that the contours of the results are significantly influenced by the method or software used. Additionally, it appears that wind pressure is consistently overestimated while wind suction is underestimated. Several settings were adjusted to determine the cause of these differences. This includes adjusting the dimensions of the enclosure, changing the wind speed constant from 25 m/s to 10 m/s, and increasing the number of iterations from 200 to 400. However, these adjustments had a minimal influence on the results. It is possible that the differences may be caused by the mesh size, but it is not possible to apply a finer mesh with the student version of Ansys Fluent.

Simpiflied situation

In addition to simulating a cube and a cylinder, two simplified variants of the entrance hall were simulated as well in order to gain a deeper understanding of the results. One of the geometries consisted of three arches placed next to each other, all of which have the same height. The other geometry also includes three arches placed next to each other, but the middle arch is significantly larger than the outer two. The wind flow is depicted in Figure B.8 and B.9, in which the red arrows indicate higher wind velocities and the blue arrows indicate lower wind velocities.

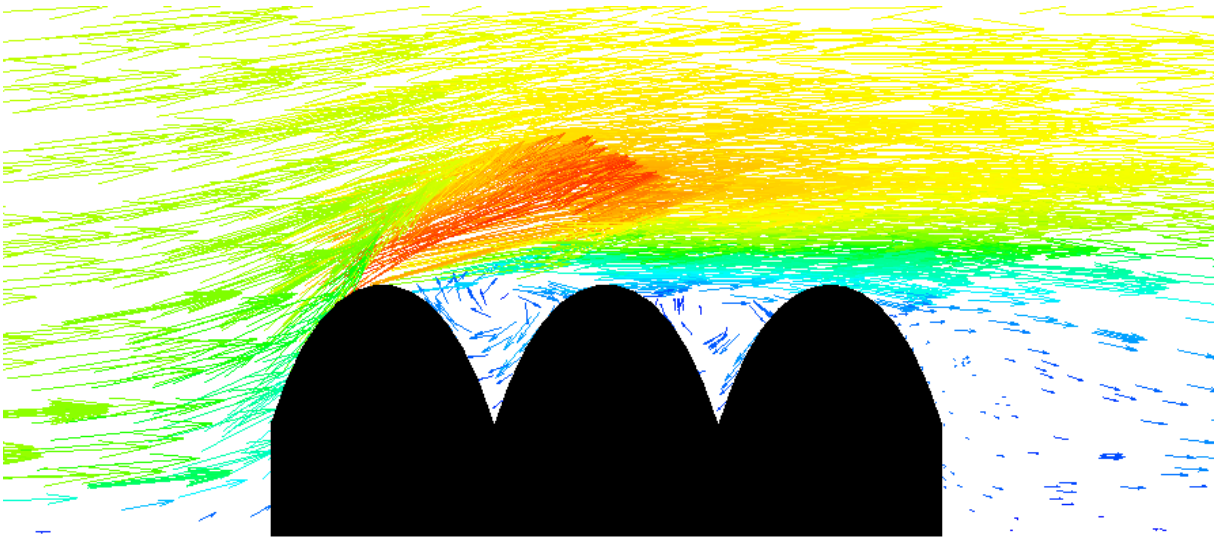

Figure B. 8 Wind flow over multi-spanning roof with equal heights

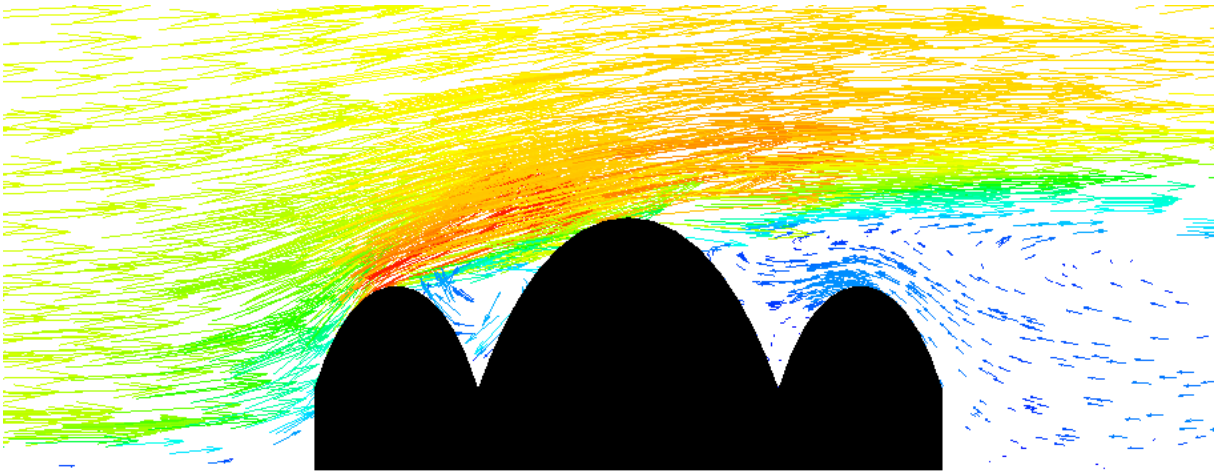

Figure B. 9 Wind flow over multi-spanning roof with varying heights

The figures above demonstrate that the first object in relation to the wind direction plays a significant role in determining the wind flow on the remaining parts of the roof. If the first object has sufficient height, only wind suction will occur on the other parts, as seen in the case of a wind direction of $\alpha = 0^{o}$. However, if the first object does not have sufficient height, wind pressure may still occur on the next

part. This effect can also be observed in the results for the wind direction of α = 135°. In the geometry used for the entrance hall, all facades were made flat. Given the importance of the first object, an additional simplified simulation was conducted with a flat façade. The results of this simulation can be seen in the figure below.

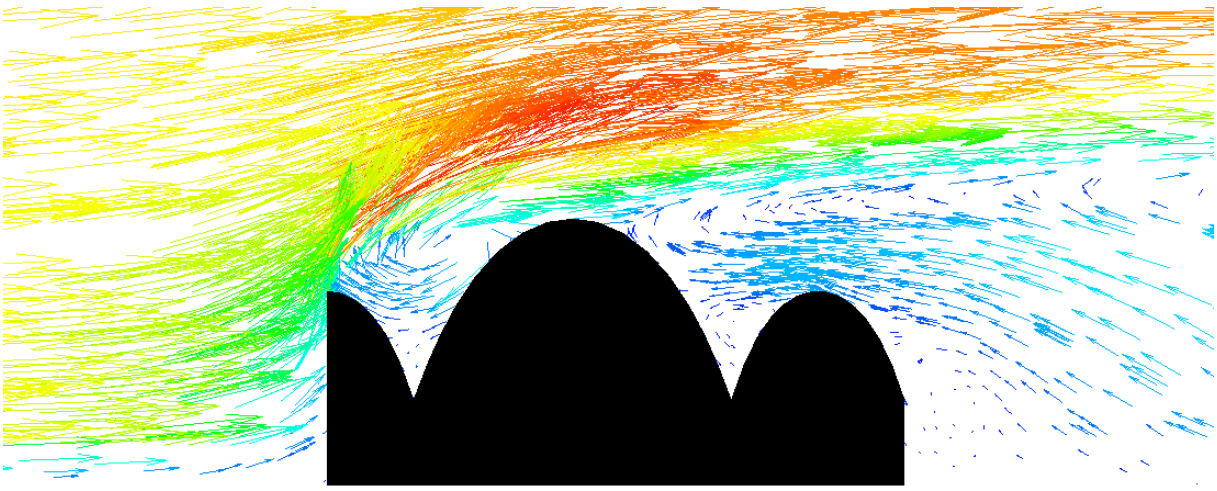

Figure B. 10 Wind flow over multi-spanning roof with varying heights and flat facade

The results of the simulation with a flat façade indicate that it directs the wind flow upwards as it is less aerodynamic. This is consistent with the observation that there is mainly wind suction on the roof of the entrance hall. Wind pressure is only observed on the largest part when the wind direction is 90°, 135° and 180°. For these wind directions the wind flows between the adjacent parts onto the large part of the entrance hall. Also the part on the left has the lowest height out of the different entrance hall parts.

Conclusion

Observing the results from the CFD analysis, it becomes clear that the entrance hall segments will mainly experience wind suction, as the wind flow is directed upwards due to the facades. Wind pressure only appears on the largest part for certain wind directions. The result validation showed that Ansys Fluent predicts the occurrence of wind pressure and suction at specific locations well. The pressure coefficients however, deviate among the applied methods used to predict the wind pressure. Other factors may decrease the accuracy of the results as well. The 3D model is not a fully detailed representation of the structure, a maximum mesh size could be applied, and the final design may have a different arch shape and/or double curvature. Therefore, the results should be viewed as a general estimation rather than an accurate prediction of the wind load.

Appendix C: Calculation and dimensioning procedures

C-1: Dimensioning of timber elements
C-2: Dimensioning of steel elements
C-3: Slotted in steel plate joint

C.1 Dimensioning of timber elements

In this section of the appendix relevant information concerning the dimensioning of timber elements is given. This includes criteria for the Ultimate Limit State (ULS) and Serviceability Limit State (SLS). Furthermore, the procedures for determining the design stresses for regular, curved and build-up elements is described.

C.1.1 Material factors timber

For the unity checks of the timber elements, several material safety factors need to be taken into account.

Material factor γ_m

The timber elements in the grid-structure of the roof will be made with Glued Laminated Timber (Glulam). A material factor γ_m has to be taken into account for the design strength of the material. The corresponding material factor γ_m for glulam is 1,25 according to NEN-EN 1995-1-1 table 2.3.

Height factor k_h

Timber is a natural material and therefore weak spots may be present in the element. An element with more volume has a higher chance to contain such a weak spot. To take this probability into account a height factor k_h needs to be considered. This only applies for bending and tension since timber shows brittle failure in tension. For Glulam the height factor can be determined with:

$$k_h = 1{,}0 \leq \left(\frac{600}{h}\right)^{0{,}1} \leq 1{,}1 \qquad \text{(C.1) (EN 1995-1-1, eq. 3.2)}$$

Height factor k_{mod}

Finally a modification factor k_{mod} has to be considered which depends on the load duration and climate class. Climate class 2 and a short load duration will be assumed for all timber elements. This leads to a modification factor of 0,90 according to table 3.1 of EN 1995-1-1.

C.1.2 Design strength

With the material factors described above the material strength for different types of internal forces can be determined for the timber elements.

Bending strength: $$f_{m,d} = \frac{f_{m,k}}{\gamma_m} \cdot k_{mod} \cdot k_h \qquad \text{(C.2)}$$

Shear strength: $$f_{v,d} = \frac{f_{v,k}}{\gamma_m} \cdot k_{mod} \qquad \text{(C.3)}$$

Tension strength parallel to grains: $$f_{t,0,d} = \frac{f_{t,0,k}}{\gamma_m} \cdot k_{mod} \cdot k_h \qquad \text{(C.4)}$$

Compressive strength parallel to grains: $$f_{c,0,d} = \frac{f_{c,0,k}}{\gamma_m} \cdot k_{mod} \qquad \text{(C.5)}$$

C.1.3 ULS criteria timber

The criteria for timber elements for the ULS are described by EN 1995-1-1 chapter 6. The criteria for the different types of stresses are given in this section.

Tension parallel to the grains

$$\sigma_{t,0,d} \leq f_{t,0,d} \qquad \text{(C.6) (EN 1995-1-1, eq. 6.1)}$$

Compression parallel to the grains

$$\sigma_{c,0,d} \leq f_{c,0,d} \qquad \text{(C.7) (EN 1995-1-1, eq. 6.2)}$$

Bending

$$\frac{\sigma_{m,y,d}}{f_{m,y,d}} + k_m \cdot \frac{\sigma_{m,z,d}}{f_{m,z,d}} \leq 1{,}0 \qquad \text{(C.8) (EN 1995-1-1, eq. 6.11)}$$

$$k_m \cdot \frac{\sigma_{m,y,d}}{f_{m,y,d}} + \frac{\sigma_{m,z,d}}{f_{m,z,d}} \leq 1{,}0 \qquad \text{(C.9) (EN 1995-1-1, eq. 6.12)}$$

The factor k_m takes into account the redistribution of the stresses and the heterogeneity of the material in the cross-section (NEN-EN 1995-1-1: 2005 section 6.1.6). The value of k_m depends on the shape of the cross-section:

$$k_m = \begin{cases} 0{,}7 & rectangular\ cross\ section \\ 1{,}0 & other\ shapes \end{cases}$$

Shear

$$\tau_d \leq f_{v,d} \qquad \text{(C.10) (EN 1995-1-1, eq. 6.13)}$$

Torsion

The criterium concerning the torsional stresses is given in EN 1995-1-1 chapter 6.1.8. This criterium is described by the following expression:

$$\tau_{tor,d} \leq k_{shape} f_{v,d} \qquad \text{(C.11) (EN 1995-1-1, eq. 6.14)}$$

With:

$$k_{shape} = min \begin{cases} 1 + 0{,}05\frac{h}{b} & for\ rectangular\ cross-sections \\ 1{,}3 \end{cases} \qquad \text{(C.12) (EN 1995-1-1, eq. 6.15)}$$

In which:

$\tau_{tor,d}$ is the design shear stress due to torsion
$f_{v,d}$ is the design shear strength
k_{shape} is a factor depending on the shape of the cross-section
h is the height of the cross-section
b is the width of the cross-section

For determining the maximum shear stresses which result from torsion in a solid rectangular cross section the following equation is used (Young & Budynas, 2001):

$$\tau_{max} = \frac{3T}{8ab^2}\left[1 + 0{,}6095\frac{b}{a} + 0{,}8865\left(\frac{b}{a}\right)^2 - 1{,}8023\left(\frac{b}{a}\right)^3 + 0{,}9100\left(\frac{b}{a}\right)^4\right] \qquad \text{(C.13)}$$

In which:

h is half of the short side of the rectangle
b is half of the long side of the rectangle

Combined stresses

In the structure normal forces and bending moments occur simultaneously. The normal force can be a compressive force as well as a tensile force. For a compressive normal force and bending moment in the weak and strong axis, EN 1995-1-1 chapter 6.3.2 gives the following expression:

$$\left(\frac{\sigma_{c,0,d}}{f_{c,0,d}}\right)^2 + \frac{\sigma_{m,y,d}}{f_{m,y,d}} + k_m \cdot \frac{\sigma_{m,z,d}}{f_{m,z,d}} \leq 1{,}0 \qquad \text{(C.14) (EN 1995-1-1, eq. 6.19)}$$

$$\left(\frac{\sigma_{c,0,d}}{f_{c,0,d}}\right)^2 + k_m \cdot \frac{\sigma_{m,y,d}}{f_{m,y,d}} + \frac{\sigma_{m,z,d}}{f_{m,z,d}} \leq 1{,}0 \qquad \text{(C.15) (EN 1995-1-1, eq. 6.20)}$$

In the case of a tensile normal force and bending moment in the weak and strong axis EN 1995-1-1 chapter 6.3.2 gives the following expression:

$$\frac{\sigma_{t,0,d}}{f_{t,0,d}} + \frac{\sigma_{m,y,d}}{f_{m,y,d}} + k_m \cdot \frac{\sigma_{m,z,d}}{f_{m,z,d}} \leq 1{,}0 \qquad \text{(C.16) (EN 1995-1-1, eq. 6.17)}$$

$$\frac{\sigma_{t,0,d}}{f_{t,0,d}} + k_m \cdot \frac{\sigma_{m,y,d}}{f_{m,y,d}} + \frac{\sigma_{m,z,d}}{f_{m,z,d}} \leq 1{,}0 \qquad \text{(C.17) (EN 1995-1-1, eq. 6.18)}$$

C.1.4 Curved elements

The bending stresses in a curved beam are not distributed linearly over the cross-section. Therefore Eurocode 5 includes a k_ℓ factor to determine the bending stress in the outer fibres (NEN-EN 1995-1-1: 2005 section 6.4). In the top zone of the curved elements the bending stresses have to meet the following requirement:

$$\sigma_{m,d} \leq k_r f_{m,d} \qquad \text{(C.18) (EN 1995-1-1, eq. 6.41)}$$

In which the factor k_r takes into account the reduction of strength which results from the bending of the lamella's during the production process. For curved elements this factor can be determined with the following expression:

$$k_r = \begin{cases} 1 & for\ \frac{r_{in}}{t} \geq 240 \\ 0{,}076 + 0{,}001\frac{r_{in}}{t} & for\ \frac{r_{in}}{t} < 240 \end{cases} \qquad \text{(C.19) (EN 1995-1-1, eq. 6.49)}$$

In which r_{in} is the radius of curvature and t is the thickness of one individual lamella. For the bending stress in the top-zone the following equation is given:

$$\sigma_{m,d} = k_\ell \frac{M_{ap,d} \cdot z}{I_y} \qquad \text{(C.20) (EN 1995-1-1, eq. 6.42)}$$

With:

$$k_\ell = k_1 + k_2\left(\frac{h_{ap}}{r}\right) + k_3\left(\frac{h_{ap}}{r}\right)^2 + k_4\left(\frac{h_{ap}}{r}\right)^3 \qquad \text{(C.21) (EN 1995-1-1, eq. 6.43)}$$

$$k_1 = 1 + 1{,}4\ \tan\alpha_{ap} + 5{,}4\ \tan^2\alpha_{ap} \qquad \text{(C.22) (EN 1995-1-1, eq. 6.44)}$$

$$k_2 = 0{,}35 - 8\ \tan\alpha_{ap} \qquad \text{(C.23) (EN 1995-1-1, eq. 6.45)}$$

$$k_3 = 0{,}6 + 8{,}3\ \tan\alpha_{ap} - 7{,}8\ \tan^2\alpha_{ap} \qquad \text{(C.24) (EN 1995-1-1, eq. 6.46)}$$

$$k_4 = 6\ \tan^2\alpha_{ap} \qquad \text{(C.25) (EN 1995-1-1, eq. 6.47)}$$

$$r = r_{in} + 0{,}5 h_{ap} \qquad \text{(C.26) (EN 1995-1-1, eq. 6.48)}$$

In wich:

$M_{ap,d}$ is the design value for the bending moment
h_{ap} is the height of the cross-section
b is the width of the cross-section
r_{in} is the radius of curvature
α_{ap} is the angle of the tapered beam (= 0 for a curved element)

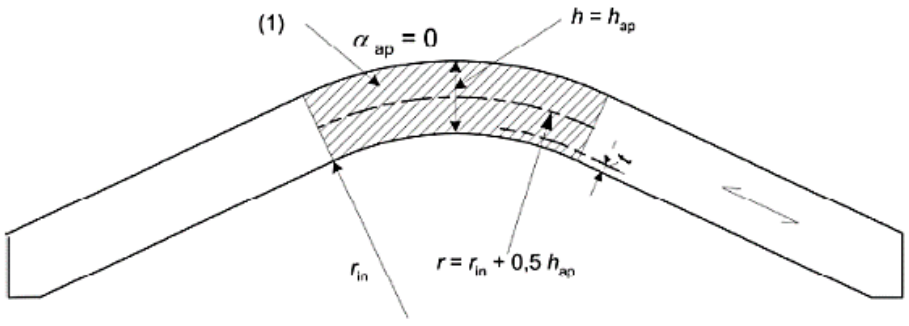

Figure C. 1 Topzone curved timber element, NEN-EN 1995 Figure 6.9

Furthermore, the bending of curved beams induces stresses perpendicular to the grains of the timber. This is because when a glulam curved element bends downwards, the lamellas tend to be pulled apart from each other. These stresses have to meet the following requirement:

$$\sigma_{t,90,d} \leq k_{dis} k_{vol} f_{t,90,d} \quad \text{(C.27) (EN 1995-1-1, eq. 6.50)}$$

With:

$$k_{vol} = \left(\frac{V_0}{V}\right)^{0,2} \quad \text{for glulam and LVL} \quad \text{(C.28) (EN 1995-1-1, eq. 6.51)}$$

$$k_{dis} = 1,4 \quad \text{for curved beams} \quad \text{(C.29) (EN 1995-1-1, eq. 6.52)}$$

In which:

k_{dis} is a factor which takes the stress distribution in the top-zone into account;
k_{vol} is a volume factor;
$f_{t,90,d}$ is the design value for the tension strength of the timber perpendicular to the grains;
V_0 is the reference volume of 0,01 m^3;
V is the volume of the stressed top-zone in m^3 and should not be bigger than $2V_b/3$ in which V_b is the total volume of the beam.

The design tension stress perpendicular to the grains can be calculated according to the following equation:

$$\sigma_{t,90,d} = k_p \frac{6M_{ap,d}}{bh_{ap}^2} \quad \text{(C.30) (EN 1995-1-1, eq. 6.54)}$$

With:

$$k_p = k_5 + k_6\left(\frac{h_{ap}}{r}\right) + k_7\left(\frac{h_{ap}}{r}\right)^2 \quad \text{(C.31) (EN 1995-1-1, eq. 6.56)}$$

$$k_5 = 0,2 \tan \alpha_{ap} \quad \text{(C.32) (EN 1995-1-1, eq. 6.57)}$$

$$k_6 = 0,25 - 1,5 \tan \alpha_{ap} + 2,6 \tan^2 \alpha_{ap} \quad \text{(C.33) (EN 1995-1-1, eq. 6.58)}$$

$$k_7 = 2,1 \tan \alpha_{ap} - 4 \tan^2 \alpha_{ap} \quad \text{(C.34) (EN 1995-1-1, eq. 6.59)}$$

Eurocode 5 also provides an expression for the combination of tension stresses perpendicular to the grains and shear stresses:

$$\frac{\tau_d}{f_{v,d}} + \frac{\sigma_{t,90,d}}{k_{dis} k_{vol} f_{t,90,d}} \leq 1 \quad \text{(C.35) (EN 1995-1-1, eq. 6.55)}$$

In which:

τ_d is the design value of the shear stress
$f_{v,d}$ is the design strength for shear force
$\sigma_{t,90,d}$ is the design stress perpendicular to the grains
k_{dis} is a factor which takes the stress distribution in the top-zone into account
k_{vol} is a volume factor

C.1.5 Serviceability limit state

Concerning the deformations of the structure, the Eurocode provides criteria for the maximum vertical and horizontal deformation, caused by the characteristic load combinations (Appendix A). For the vertical deformation the following criterium applies:

$$w_{vertical} \leq \frac{l}{250} \qquad \text{(NEN-EN 1990 art. A.1.4.3 (3))}$$

For a non-industrial building that utilizes one building layer the following criterium applies for the horizontal deformation:

$$w_{horizontal} \leq \frac{h}{300} \qquad \text{(NEN-EN 1990 art. A.1.4.3 (7))}$$

In which:

l is the span of the roof
h is the height of the roof

C.1.6 Build-up elements

One of the structural systems which is considered in this project is the lattice system. Differently from the other systems for which the elements have a rectangular cross-sections, is the cross-section in this system build-up from two layers with shear blocks in between. The shear blocks are connected to the layers by connectors such as bolts or nails. Therefore the elements in this system are considered to be mechanically connected beams, for which Appendix B of Eurocode 5 provides several design rules.

Stresses in a build-up element

In the cross-section of the elements, stresses occur from shear forces, normal forces and bending moments in both the strong and weak axis. To calculate the maximum design stresses in the cross-section, first the moment of inertia for both the strong and weak axis has to be determined. In a lattice grid-shell, shear blocks are applied to make the layers work together as one single cross-section. The degree of composite action can be taken into account by a factor C_s. When $C_s = 0$ there is no composite action and when $C_s = 1$ the layers fully work together (D'Amico et al., 2015). This leads to the following equations for the moment of inertia in the strong and weak axis:

$$I_y = c_s \frac{1}{6} bh^3 + 2bhe^2 \; ; \; C_s \in [0,1] \qquad \text{(C.38)}$$

$$I_z = \frac{1}{6} hb^3 \qquad \text{(C.39)}$$

An estimation of the connection efficiency factor C_s could be made based on finite element simulations or bending tests (D'Amico et al., 2014). The value of the factor Cs depends on the distance between each shear block, their cross-sectional area and how they are connected to the layers (D'Amico et al., 2015). A formula to estimate the connection efficiency factor Cs is provided by EC5 annex B.2:

$$C_s = [1 + \pi^2 E_i A_i s_i / (k_i L^2)]^{-1} \qquad \text{(C.40) (EN 1995-1-1, eq. B.5)}$$

In which:

E_i is the modulus of elasticity
A_i is the cross-sectional area ($A = bh$)
s_i is the spacing between the shear blocks. For a varying distance EC5 states that $s_{max} \leq 4s_{min}$.
k_i is the shear stiffness which can be calculated according to EC5 table 7.1
L is the rod's length

In Eurocode 5 the factor c_s is noted as γ_i. However in other literature about lattice grid-shells the notation c_s is used. Therefore for this report also this notation will be used. Furthermore it should be mentioned that the design rules provided by Eurocode 5 are for beams with pinned ends. However because information about this factor for curved elements or grid structures is limited, the equation provided by

Eurocode 5 will be used as an estimation. Finally the length which is needed for determining this factor varies within the grid-structure. The forces that appear in the primary arches are however significantly larger than in the elements in the secondary direction. Furthermore is the radius of curvature substantially smaller in the primary elements which is disadvantageous for curved elements. Therefore, for the variant study in Chapter 8 the length of the primary arches will be used for determining this factor. For a more detailed calculation every element could be considered individually.

Bending stresses
With the moment of inertia known, the maximum bending stress can be calculated for both the y- and z-direction. Note that in case the elements are curved, the following bending stress has to be multiplied with the factor k_ℓ.

$$\sigma_{m,d} = \frac{E_i Z_0 M}{(EI)_{ef}} \tag{C.41}$$

Shear stresses
The maximum shear stress occurs in the shear blocks. The Eurocode provides a formula to determine this shear stress.

$$\tau_{2,max} = \frac{\gamma_3 E_3 A_3 a_3 + 0{,}5 E_2 b_2 h^2}{b_2 (EI)_{ef}} V \tag{C42) (EN 1995-1-1, eq. B.9}$$

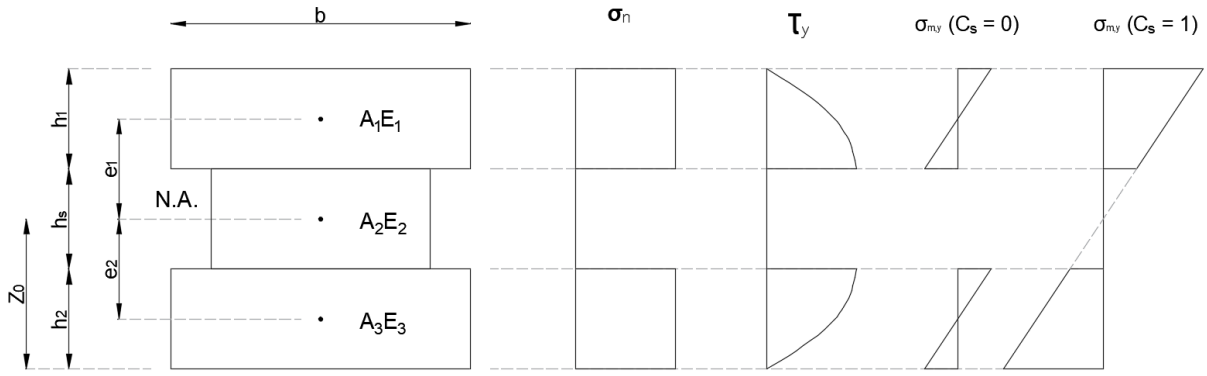

Figure C. 2 Dimensions of build-up element

Force on the connectors
The shear blocks can be connected to the outer layers of the elements by gluing or for example dowel-type fasteners. The force on the fasteners can be calculated according to the formula below which is provided by EC5 annex B.5.

$$F = \frac{c_s E_i A_i e_i s_i}{(EI)_{ef}} V \tag{C.43) (EN 1995-1-1, eq. B.10}$$

C.1.7 Material properties

For the calculation in the Ultimate Limit State and Serviceability Limit State, the material properties for Glulam according to EN 14080 will be used. The material properties are given in Table C.1 and C.2.

Table C. 1 Material properties homogenous Glulam EN 14080

		Glulam strength class (homogenous)						
Property	**Symbol**	**GL20h**	**GL22h**	**GL24h**	**GL26h**	**GL28h**	**GL30h**	**GL32h**
Bending strength	$f_{m,g,k}$	20	22	24	26	28	30	32
Tensile strength	$f_{t,0,g,k}$	16	17.6	19.2	20.8	22.3	24	25.6
	$f_{t,90,g,k}$	0.5						
Compression strength	$f_{c,0,g,k}$	20	22	24	26	28	30	32
	$f_{c,90,g,k}$	2.5						
Shear strength (shear and torsion)	$f_{v,g,k}$	3.5						
Rolling shear strength	$f_{r,g,k}$	1.2						
Modulus of elasticity	$E_{0,g,mean}$	8400	10500	11500	12100	12600	13600	14200
	$E_{0,g,05}$	7000	8800	9600	10100	10500	11300	11800
	$E_{90,g,mean}$	300						
	$E_{90,g,05}$	250						
Shear modulus	$G_{g,mean}$	650						
	$G_{g,05}$	540						
Rolling shear modulus	$G_{r,g,mean}$	65						
	$G_{r,g,05}$	54						
Density	$\rho_{g,k}$	340	370	385	405	425	430	440
	$\rho_{g,mean}$	370	410	420	445	460	480	490

Table C. 2 Material properties combined Glulam EN 14080

		Glulam strength class (combined)						
Property	**Symbol**	**GL20c**	**GL22c**	**GL24c**	**GL26c**	**GL28c**	**GL30c**	**GL32c**
Bending strength	$f_{m,g,k}$	20	22	24	26	28	30	32
Tensile strength	$f_{t,0,g,k}$	15	16	17	19	19.5	19.5	19.5
	$f_{t,90,g,k}$				0.5			
Compression strength	$f_{c,0,g,k}$	18.5	20	21.5	23.5	24	24.5	24.5
	$f_{c,90,g,k}$				2.5			
Shear strength (shear and torsion)	$f_{v,g,k}$	3.5						
Rolling shear strength	$f_{r,g,k}$	1.2						
Modulus of elasticity	$E_{0,g,mean}$	10400	10400	11000	12000	12500	13000	13500
	$E_{0,g,05}$	8600	8600	9100	10000	10400	10800	11200
	$E_{90,g,mean}$	300						
	$E_{90,g,05}$	250						
Shear modulus	$G_{g,mean}$	650						
	$G_{g,05}$	540						
Rolling shear modulus	$G_{r,g,mean}$	65						
	$G_{r,g,05}$	54						
Density	$\rho_{g,k}$	355	355	365	385	390	390	400
	$\rho_{g,mean}$	390	390	400	420	420	430	440

C.1.8 Manufacturing process

One of the main benefits of Glulam is the possibility to create curved elements. During the manufacturing process, individual lamellas are bend in the desired shape and are then glued together. The realizable curvature depends on the thickness of the lamellas, whereas thinner lamellas can be used to create a smaller radius. The thickness of the lamellas depends on the stresses occurring during the bending process as well, as described by Crocetti et al. (2016). The following equations can be applied to determine these stresses:

$$\sigma = \frac{E \cdot t}{2 \cdot r_{in}} \tag{C.44}$$

In which:

E is the modulus of elasticity
t is the thickness of the individual lamella's
r_{in} is the radius of curvature of the timber element

It can be assumed that the stresses are not present anymore during the assembly of the structure due to relaxation. However depending on the ratio between the radius of curvature and the thickness of the lamella's, a reduction in the bending strength has to be applied. According to Eurocode 5 this is the case when this ratio is $r_{in}/t \leq 240$ (Crocetti et al., 2016).

Furthermore are limitations for the lamella thicknesses given by EN 14080. These limitations are shown in the table below, and depend on the service class of the structure.

Table C. 3 Limitations for the lamella thickness according to EN 14080

	Service class (SC) according to EN 1995-1-1	
	SC 1 or 2	**SC 3**
Glued laminated timber	$6 \leq t \leq 45$	$6 \leq t \leq 35$
Glued solid timber	$45 \leq t \leq 85$	-

C.3 Dimensioning of steel elements

This section of the appendix covers the ULS criteria concerning steel elements. The steel elements in the roof structure of the entrance hall are the steel bracing elements, facades and connection parts like bolts and plates.

C.3.1 Material factors steel

EN 1993-1-1 section 6.1 provides three partial factors which should be taken into account for determining the resistance of the steel elements. The partial factors can be read from the table below.

Table C. 4 Partial factors for the resistance of steel elements according to EN 1993-1-1

Partial factor:	γ_{m0}	γ_{m1}	γ_{m2}
	1,00	1,00	1,25

C.3.2 ULS criteria steel

The resistance of steel elements to individual internal forces is in accordance with EN 1993-1-1. These unity checks are used for determining the resistance of the steel bracing elements and the steel tube of the connection between the primary and secondary beams in the final design. The expressions for the resistances are as follows:

Tension
The design rule for the tensile axial force is:

$$\frac{N_{Ed}}{N_{t,Rd}} \leq 1{,}0 \qquad \text{(C.45) (EN 1993-1-1, eq. 6.5)}$$

$$N_{t,Rd} = \frac{Af_y}{\gamma_{M0}} \qquad \text{(C.46) (EN 1993-1-1, eq. 6.6)}$$

Compression
The design rule for the compressive axial force is:

$$\frac{N_{Ed}}{N_{c,Rd}} \leq 1{,}0 \qquad \text{(C.47) (EN 1993-1-1, eq. 6.9)}$$

For cross-section class 1 to 3 the design resistance of the compressive normal force is:

$$N_{c,Rd} = \frac{Af_y}{\gamma_{M0}} \qquad \text{(C.48) (EN 1993-1-1, eq. 6.10)}$$

Bending
The design rule for the bending moment is:

$$\frac{M_{Ed}}{M_{c,Rd}} \leq 1{,}0 \qquad \text{(C.49) (EN 1993-1-1, eq. 6.12)}$$

The design value for the bending moment resistance for cross-section class 1 and 2 is:

$$M_{c,Rd} = M_{pl,Rd} = \frac{W_{pl}f_y}{\gamma_{M0}} \qquad \text{(C.50) (EN 1993-1-1, eq. 6.13)}$$

Shear
The design rule for the shear force is:

$$\frac{V_{Ed}}{V_{c,Rd}} \leq 1{,}0 \qquad \text{(C.51) (EN 1993-1-1, eq. 6.17)}$$

For cross-section class 1 and 2 a plastic stress distribution can be assumed. In this case the shear resistance is calculated with:

$$V_{pl,Rd} = \frac{A_v \frac{f_y}{\sqrt{3}}}{\gamma_{M0}} \quad \text{(C.52) (EN 1993-1-1, eq. 6.18)}$$

The shear area of an I-section is determined with:

$$A_v = A - 2bt_f + (t_w + 2r)t_f \quad \text{(C.53) (EN 1993-1-1, eq. 6.2.6(3))}$$

C.3.3 Plates

Several connections in the structure such as the slotted in steel plate joints contain steel plates, which are connected to the timber elements with bolts. The tensile resistance of the plates depends on the yielding of the gross cross-section or rupture of the net cross-section. The net cross-section is the cross-section of the plate including the bolt holes, which can be calculated as follow:

Net cross-section: $A_{net} = bt - nd_0t$ (C.54)

The plate's resistance for both failure mechanisms can be calculated by the following equations:

Yielding of the gross cross-section: $N_{t,Rd} = \frac{Af_y}{\gamma_{m0}}$ (C.55) (EN 1993-1-1, 6.6)

Rupture of the net cross-section: $N_{t,Rd} = \frac{0{,}9A_{net}f_u}{\gamma_{m2}}$ (C.56) (EN 1993-1-1, 6.7)

In which:

b	is the width of the plate
t	is the thickness of the plate
d_0	is the diameter of the bolts
n	is the number bolt rows
f_y	is the yielding strength
f_u	is the ultimate strength
γ_{mo}, γ_{m1}	are partial factors for the cross-sectional resistance, $\gamma_{mo} = 1{,}0$ and $\gamma_{mo} = 1{,}25$

For the axial compression resistance of the plate also the net cross-section should be applied. This is done with the following equation:

$$N_{c,Rd} = \frac{A_{net}f_y}{\gamma_{m0}} \quad \text{(C.57) (EN 1993-1-1, 6.7)}$$

C.3.4 Bolts

For bolts there are several standard sizes which are shown in the table below. The M in the name stands for metric screw-thread. The number is the diameter of the bolt in millimetres.

Table C. 5 Standard bolt sizes (Blok, n.d.)

	M12	**M16**	**M20**	**M22**	**M24**	**M27**	**M30**
Shaft cross-section A	113	201	314	380	452	573	707
Stress cross-section A_s	84,3	157	245	303	353	459	561

Furthermore are bolts divided in different classes. Each class has a corresponding yield strength and tensile strength. The yield strength is ten times the first number in the name multiplied with the second number. The tensile strength is the first number multiplied with one hundred.

Table C. 6 Bolt strength properties according to EN 1993-1-8 table 3.1

Bolt classification	**4.6**	**4.8**	**5.6**	**5.8**	**6.8**	**8.8**	**10.9**
f_{yb} (N/mm^2)	240	320	300	400	480	640	900
f_{ub} (N/mm^2)	400	400	500	500	600	800	1000

Bolts loaded in tension
For non-preloaded bolts loaded in tension, the tensile capacity can be calculated with the following equation:

$$F_{t,Rd} = \frac{k_2 f_{u,b} A_s}{\gamma_{m2}} \quad \text{(C.58) (EN 1993-1-8, table 3.4)}$$

In which:

$f_{u,b}$ is tensile strength of the bolt
k_2 is a calibrated factor which is 0,9 and is valid if the thread complies with EN 1090-2

Bolts loaded in shear
The shear resistance of the bolt depends on whether the shear plane runs though the shaft or thread of the bolt. The resistance is calculated by the following equations:

Shear plane running through the shaft: $F_{v,Rd} = \frac{0{,}6 f_{ub} A}{\gamma_{M2}}$ (C.59) (EN 1993-1-8, table 3.4)

Shear plane running through the thread: $F_{v,Rd} = \frac{\alpha_v f_{ub} A_s}{\gamma_{M2}}$ (C.60) (EN 1993-1-8, table 3.4)

In which:

$\alpha_v = 0{,}6$ for bolt class 4.6, 5.6 and 8.8
$\alpha_v = 0{,}5$ for bolt class 6.8 and 10.9

Bolts loaded in shear and tension
Often a bolt loaded in tension is also loaded in shear. This could for example be the case for the bolts at the nodes in the lattice grid-shell variant. In this case the following requirement applies:

$$\frac{F_{v,Ed}}{F_{v,Rd}} + \frac{F_{t,Ed}}{1{,}4 F_{t,Rd}} \leq 1{,}0 \quad \text{(C.61) (EN 1993-1-8, table 3.4)}$$

C.3.5 Steel pin joint

The Eurocode provides certain rules that apply to a steel pin connection. The resistance of the pin connections in the supports are checked according to EN 1993-1-8 article 3.13. Also rules are given for the geometry which can be seen below.

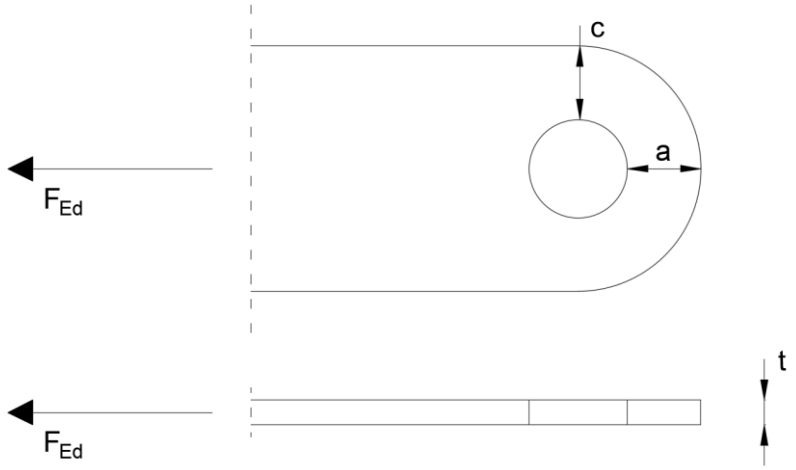

Figure C. 3 Dimensions of a steel pin joint according to EN 1993-1-8, table 3.9

$$a \geq \frac{F_{Ed} \gamma_{M0}}{2 t f_y} + \frac{2 d_0}{3} \quad \text{(C.62) (EN 1993-1-8, table 3.9)}$$

$$c \geq \frac{F_{Ed} \gamma_{M0}}{2 t f_y} + \frac{d_0}{3} \quad \text{(C.63) (EN 1993-1-8, table 3.9)}$$

The joint has to be checked on several different failure modes. The design rules for a pin joint are given by EN 1993-1-8 art. 3.13 table 3.10 and are given below:

Shear resistance pin: $$F_{v,Rd} = \frac{0{,}6Af_{up}}{\gamma_{M2}} \geq F_{v,Ed} \quad \text{(C.64)}$$

Bearing resistance plate and pin: $$F_{b,Rd} = \frac{1{,}5tdf_y}{\gamma_{M0}} \geq F_{b,Ed} \quad \text{(C.65)}$$

If the pin should be replaceable the following applies: $$F_{b,Rd,ser} = \frac{0{,}6tdf_y}{\gamma_{M6,ser}} \geq F_{b,Ed,ser} \quad \text{(C.66)}$$

Bending moment resistance pin: $$M_{Rd} = \frac{1{,}5W_{el}f_{yp}}{\gamma_{M0}} \geq M_{Ed} \quad \text{(C.67)}$$

If the pin should be replaceable the following applies: $$M_{Rd} = \frac{0{,}8W_{el}f_{yp}}{\gamma_{M6,ser}} \geq M_{Ed,ser} \quad \text{(C.68)}$$

Combined shear and bending resistance pin: $$\left[\frac{M_{Ed}}{M_{Rd}}\right]^2 + \left[\frac{F_{v,Ed}}{F_{v,Rd}}\right]^2 \leq 1 \quad \text{(C.69)}$$

In which:

d is the pin diameter
f_y is the lowest yield strength of the pin or connected part
f_{up} is the tensile strength of the pin
f_{yp} is the yield strength of the pin
t is the thickness of the connected part
A is the surface of the cross-section of the pin
W_{el} is the moment of resistance of the pin calculated with $W_{el} = \pi/32 \cdot d^3$

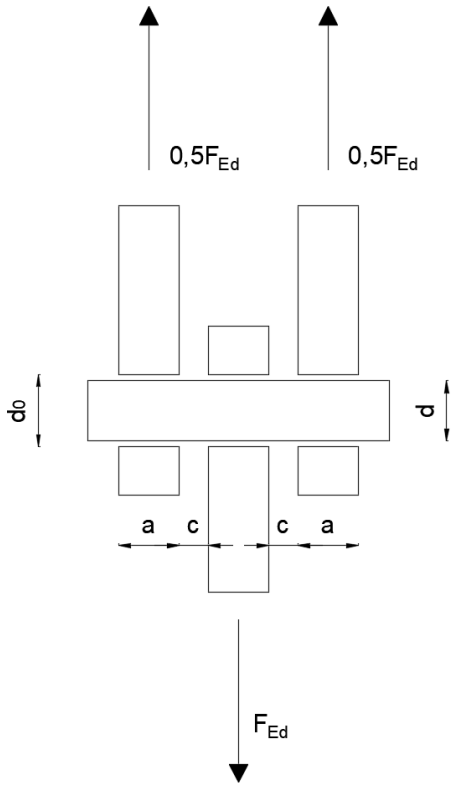

Figure C. 4 Bending moment in pin connection according to EN 1993-1-8, figure 3.11

The bending moment which occurs in the pin caused by the design load can be calculated according to the following equation:

$$M_{Ed} = \frac{F_{Ed}}{8}(b + 4c + 2a) \qquad \text{(C.70) (EN 1993-1-3 art. 3.13 Figure. 3.11)}$$

C.3.6 Welds

The stresses in a welded joint can be checked by the directional method. This method is based on the Von Mises yield criterium . In the directional method the following criteria apply:

$$\sqrt{\sigma_{\perp}^2 + 3(\tau_{\perp}^2 + \tau_{\parallel}^2)} \leq \frac{f_u}{\beta_w \gamma_{M2}} \quad \text{and} \quad \sigma_{\perp} \leq \frac{0{,}9 f_u}{\gamma_{M2}} \qquad \text{(C.71) (EN 1991-1-8, eq. 4.1)}$$

In which:

β_w	is a correlation factor
f_u	is the tensile strength of the weakest connected element
γ_{M2}	is the diameter of the bolts

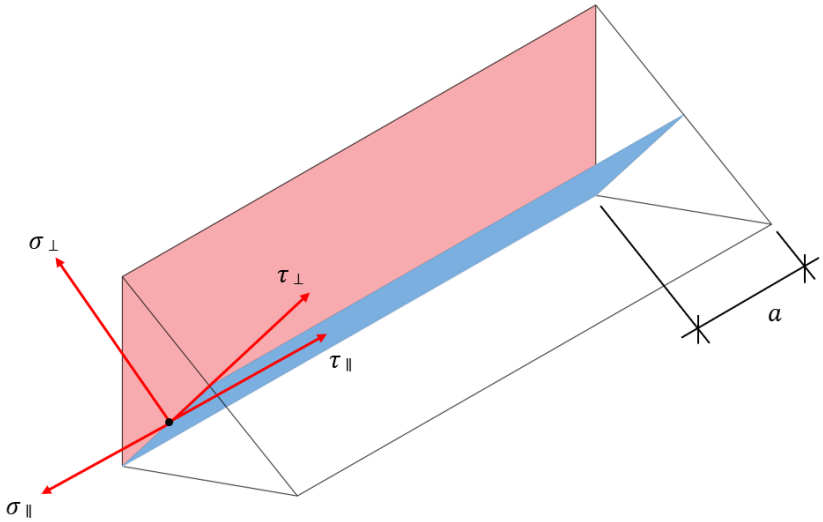

Figure C. 5 Stresses in fillet weld

The correlation factor β_w depends on the parent material and can be read from EN 1991-1-8 table 4.1. The values for steel grade S235 up to S460 are given below:

Table C. 7 Correlation factor for different steel grades

Steel grade	B_w
S235	0,80
S275	0,85
S355	0,90
S420	1,00
S460	1,00

When l_{eff} is longer than 150a the weld should be considered as a long weld. In this case the stresses are not distributed equally. Therefore a reduction factor $\beta_{Lw.1}$ should be taken into account. This factor is determined as follows:

$$\beta_{Lw.1} = 1{,}2 - 0{,}2L_j/(150a) \text{ and } \beta_{Lw.1} \leq 1{,}0 \qquad \text{(C.72) (EN 1991-1-8, eq. 4.9)}$$

In which:

L_j is the length of the overlay in the direction of the force transmission

As an alternative to the directional method, the simplified method may be used according to EN 1991-1-8 section 4.5.3.3. In this method it can be assumed that the weld has sufficient capacity if the following criterium is met:

$$F_{w,Ed} \leq F_{w,Rd} \quad \text{(C.73) (EN 1991-1-8, eq. 4.2)}$$

In which:

$F_{w,Ed}$ Is the design value of the acting force per unit length

$F_{w,Rd}$ Is the design value of resistance of the weld per unit length

Independently of the orientation of the plane of the throat section with respect to the acting force, the resistance per unit length $F_{w,Rd}$ can be determined according to:

$$F_{w,Rd} = f_{vw,d}\,a \quad \text{(C.74) (EN 1991-1-8, eq. 4.3)}$$

In which $f_{vw,d}$ is the design value of the shear resistance of the weld. The shear resistance can be calculated as follows:

$$f_{vw,d} = \frac{f_u/\sqrt{3}}{\beta_w \gamma_{m2}} \quad \text{(C.75) (EN 1991-1-8, eq. 4.4)}$$

C.3.7 Material properties

The table below shows the yield strength and the ultimate strength for hot-rolled construction steel according to EN 1993-1-1 table 3.1.

Table C. 8 Material properties steel strength grades

	Thickness: t ≤ 40 mm		**Thickness: 40 mm < t ≤ 80 mm**	
	f_y (N/mm^2)	f_u (N/mm^2)	f_y (N/mm^2)	f_u (N/mm^2)
S235	235	360	215	360
S275	275	430	255	410
S355	355	490	335	470
S450	440	550	410	550

Furthermore are values for other material properties given by EN 1993-1-1 section 3.2.6. These material properties are listed below.

Modulus of elasticity: $E = 210000\ N/mm^2$

Shear modulus: $G = \frac{E}{2(1+v)} \approx 81000\ N/mm^2$

Poisson's ration: $v = 0{,}3$

Thermal coefficient: $\alpha = 12 \cdot 10^{-6}$

C.4 Slotted in steel plate joint

As described earlier, a common type of joint for timber grid structures is a slotted in steel joint. This joint utilizes a rectangular configuration of connectors such as bolts and dowels. In this appendix, the determination of the strength and stiffness properties for this joint is presented. First the Johansen Meyer equations are used by which the load capacity per shear plane can be calculated. The embedment strength $f_{h,\alpha,k}$ of the timber should be calculated using the following equations:

$$f_{h,\alpha,k} = \frac{f_{h,0,k}}{k_{90} \cdot sin^2\alpha + cos^2\alpha} \quad \text{(C.76) (EN 1995-1-1, eq. 8.31)}$$

$$f_{h,0,k} = 0{,}082 \cdot (1 - 0{,}01 \cdot d) \cdot \rho_k \quad \text{(C.77) (EN 1995-1-1, eq. 8.14)}$$

$$k_{90} = 1{,}35 + 0{,}015 \cdot d \text{ (for coniferous timber)} \quad \text{(C.78) (EN 1995-1-1, eq. 8.33)}$$

$$k_{90} = 0{,}90 + 0{,}015 \cdot d \text{ (for deciduous timber)} \quad \text{(C.79) (EN 1995-1-1, eq. 8.33)}$$

Yield moment of bolds:

$$M_{y,Rk} = 0{,}3 \cdot f_{u,k} \cdot d^{2,6} \quad \text{(C.80) (EN 1995-1-1, eq. 8.14)}$$

The Johansen Meyer equations include different failure modes for different connection types. The failure modes which have been taken into account are meant for a steel to timber connection with a steel plate, regardless of the thickness, in a double shear plane connection as a middle element. This is exactly the situation for a slotted in steel plate joint. In this situation three different failure modes have to be taken into account. The first failure mode is yielding of the timber fibres. The second failure mode is yielding of the steel bolt with a plastic hinge occurring in the middle of the bolts. The final failure mode is also yielding of the steel bolt where two plastic hinges occur. The failure modes are illustrated in Figure C.6.

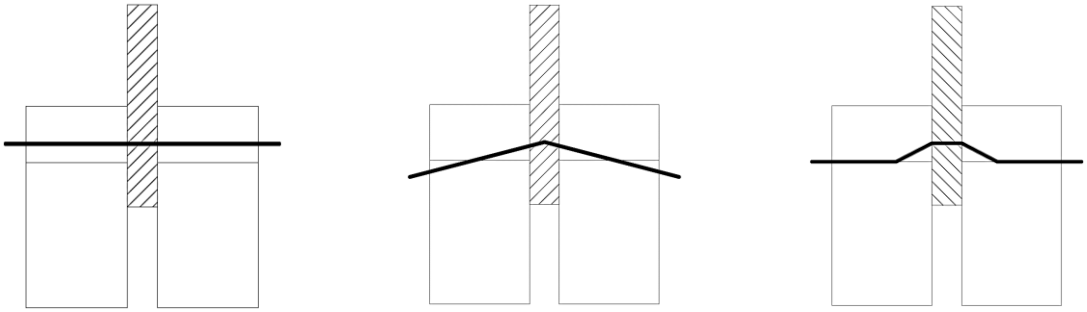

Figure C. 6 Failure mechanisms

With the embedment strength the ultimate load $F_{v,Rk}$ can be calculated. The corresponding equations for each failure mode, shown in Figure C.6 is provided by Eurocode 5 and given in Formula C.81. The failure load is the minimum value of the three equations.

$$F_{v,Rk} = min \begin{cases} f_{h,1,k} t_1 d & (I) \\ f_{h,1,k} t_1 d \left[\sqrt{2 + \frac{4 M_{y,Rk}}{f_{h,1,k} d t_1^2}} - 1 \right] + \frac{F_{ax,Rk}}{4} & (II) \\ 2{,}3 \sqrt{M_{y,Rk} f_{h,1,k} d} + \frac{F_{ax,Rk}}{4} & (III) \end{cases} \quad \text{(C.81) (EN 1995-1-1, eq. 8.11)}$$

$$F_{v,Rd} = \frac{k_{mod}}{\gamma_m} F_{v,Rk} \quad \text{(C.82)}$$

To determine the total strength of the joint, a group effect of the connectors should be taken into account. According to the Eurocode the total strength can be calculated as follows:

$$n_{ef} = min\begin{Bmatrix} n \\ n^{0.9^4}\sqrt{\frac{a_1}{13d}} \end{Bmatrix} \quad \text{(C.83) (EN 1995-1-1, eq. 8.34)}$$

In which n is the number of connectors in one row in the joint, a_1 is the distance between the connectors (Figure C.7) and d is the diameter of the connectors. The axial strength of the joint then becomes:

$$N = n_{ef} n_{collumns} F_{v,Rd} \quad \text{(C.84)}$$

C.4.1 Plate resistance

For the axial capacity of the node, also the tensile and compressive resistance of the plates should be determined. The procedure for determining the resistance of the plate is presented in Chapter C.3.3.

C.4.2 Axial stiffness

Eurocode 5 table 7.1 provides equations for the shear modulus (K_{ser}) for different types of fasteners per shear plane. The shear modulus of bolts in the SLS can be calculated with the equations presented below. For the ULS, the shear modulus K_u is obtained by multiplying K_{ser} with 2/3. Because the connection is a steel to timber connection, the stiffness can be doubled according to Eurocode 5. The stiffness can be doubled again since the connection has two shear planes. This leads to the following equation:

$$K_{ser} = n \cdot 2 \cdot 2 \cdot \frac{\rho_m^{1,5} \cdot d}{23} \quad \text{(C.85) (EN 1995-1-1, table 7.1)}$$

$$\rho_m = \rho_k \cdot 1{,}2 \quad \text{(C.86)}$$

C.4.3 Rotational stiffness

A general method to determine the rotational stiffness of a joint that exists of dowels or bolts in a rectangular configuration is presented by Blass & Sandhaas (2017). The rotational stiffness is determined according to Formula C.87 and C.88. Relevant properties of the joint can be seen in the figure below.

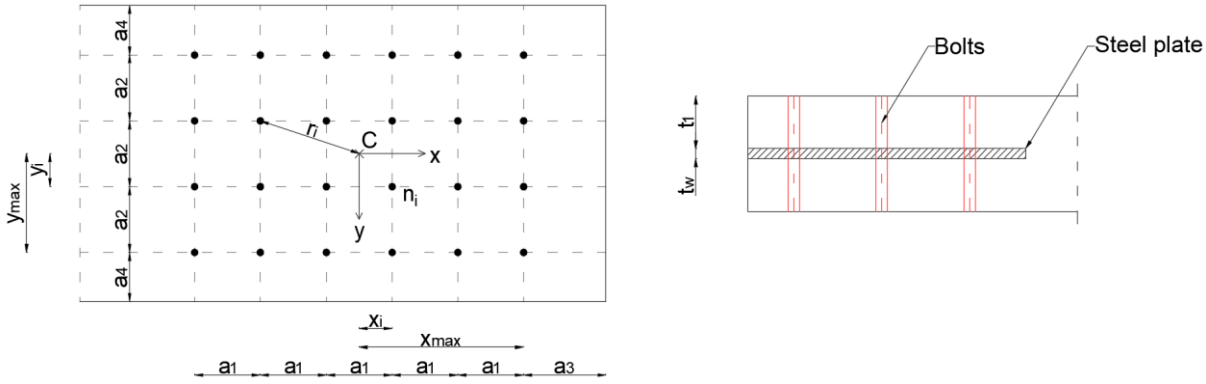

Figure C. 7 Slotted in steel plate joint layout

$$K_r = \sum_{j=1}^{n} K_j \cdot r_i^2 \quad \text{(C.87)}$$

In which r_i is the distance from the centre point to bolt n_i and K_i is the slip modulus K_{ser} of bolt n_i. For a rectangular configuration as shown in the figure above, the rotational stiffness can be calculated as follows:

$$K_r = K_{ser} \cdot \left(\sum_{i=1}^{n} x_i^2 + \sum_{i=1}^{n} y_i^2\right) \quad \text{(C.88)}$$

According to Shu et al. (2020) however, this method cannot be used to directly estimate the rotational stiffness, if this type of joint is applied to a structure like a dome structure. This is because this method does not take into account the large axial force and arch effect. Therefore, the writers have performed tests and present a different analytical method to estimate the stiffness more accurately.

The ultimate design moment M_d is calculated, which is the summation of the moment resistance of the individual bolts. This is multiplied with two factors Φ_{an} and Φ_{ax}. Values for these coefficients are given by Shu et al. (2020) for an angle of 4^o and 8^0 between the steel part and timber element of the joint. For calculating Φ_{an} as shown in Formula C.90, a_1 is the axial forces distributed over a single hole of the joint. A value of 1,3 can be applied if no information about the axial force is available.

$$M_d = \Phi_{an}\Phi_{ax}\sum_{i=1}^{n} F_i \cdot r_i \tag{C.89}$$

$$\Phi_{an} = \begin{cases} 1, & a_1/F \leq 20\% \\ x, & a_1/F > 20\% \end{cases} \tag{C.90}$$

The moment resistance (M_{ave}) of the slotted in steel plate joint is calculated by multiplying the design bending moment (M_d) with the factor γ_m/k_{mod}. It is described that the bolts in the outermost layer in the tension side usually not reach their full capacity. Therefore these axial forces need to be multiplied with a factor that depends on the number of rows of bolts, as shown in Formula C.91. The centre of rotation (CoR) is not located exactly in the middle of the bolts in this situation. From their FEM calibrations it is determined the the CoR is located 2/3 of the distance between the outer rows of the bolts. If there are more than two rows the moment arm should be linear interpolated for the bolts in the middle row(s).

$$M_{ave} = \Phi_{an}\Phi_{ax}\frac{\gamma_m}{k_{mod}}\sum_{i=1}^{n} F_i \cdot r_i \tag{C.91}$$

$$F_t = \begin{cases} 0{,}40\ F & 2\ horizontal\ rows \\ 0{,}65\ F & 3\ horizontal\ rows \\ 0{,}90\ F & 4\ or\ more\ horizontal\ rows \end{cases} \tag{C.92}$$

The ultimate rotation, when the ultimate load is reached, can roughly be estimated according to Formula C.93. With the ultimate rotation and bending moment, a linear model which estimates the mechanical behaviour of the slotted in steel plate joint is obtained.

$$\theta_u = \beta \cdot \left(\frac{0{,}07}{\Phi_{ax}} - 0{,}0005 \cdot d\right) \tag{C.93}$$

$$\beta = \begin{cases} 1{,}0\ t_w \leq 200\ mm \\ 1{,}1\ t_w > 200\ mm \end{cases} \tag{C.94}$$

Applying the analytical method presented by Shu et al. (2020), results in a rotational stiffness that is significantly lower than the analytical method presented by Blass & Sandhaas (2017). The test provided by Shu et al. (2020) show that their analytical method is a safer and better estimation of the rotational stiffness for a structure that experiences large axial forces. Therefore, this method will be used in this project for determining the stiffness and strength properties of this type of joint.

C.4.4 Rotational stiffness weak axis

According to Shu et al. (2020), an advantage of this type of joint is that it can provide some rotational stiffness in the weak direction. The bending moment resistance in this direction is obtained through interaction between the steel plate and timber. As no bolts are applied in this direction, the rotational stiffness can be described by a linear model. This behaviour is shown by their test results, from which a rotational stiffness of approximately 87 kNm/Rad can be estimated. The results are however for a specific joint layout, and no analytical method is available for the rotational stiffness in this direction.

C.4.5 Bolt spacing

For the design of the slotted in steel plate joint, the minimum bolt spacing has to be taken into account. The minimum distances are given by EN 1995-1-1 table 8.4 and shown in Table C.9.

Table C. 9 Minimum bolt spacing timber connection

Spacing and end/edge distances	Angle	Minimum spacing or distance
α_1 (parallel to grain)	$0^o \leq \alpha \leq 360^o$	$(4 + \lvert\cos\alpha\rvert)d$
α_2 (perpendicular to grain)	$0^o \leq \alpha \leq 360^o$	$4d$
$\alpha_{3,t}$ (loaded end)	$-90^o \leq \alpha \leq 90^o$	$\max(7d; 80\ mm)$
$\alpha_{3,c}$ (unloaded end)	$90^o \leq \alpha \leq 150^o$ $150^o \leq \alpha \leq 210^o$ $210^o \leq \alpha \leq 270^o$	$\max[(1 + 6\sin\alpha)d; 4d]$ $4d$ $\max[(1 + 6\sin\alpha)d; 4d]$
$\alpha_{4,t}$ (loaded end)	$0^o \leq \alpha \leq 180^o$	$\max[(2 + 2\sin\alpha)d; 3d]$
$\alpha_{4,c}$ (unloaded end)	$180^o \leq \alpha \leq 360^o$	$3d$

Appendix D Validation results Karamba3D

D-1: Comparison results Karamba3D and SCIA-Engineer

D.1 Comparison results Karamba3D and SCIA-Engineer

To validate the internal forces which are obtained by performing the structural analysis with Grasshopper plug-in Karamba3D, a validation is done using software SCIA-Engineer. To perform the structural analysis with SCIA-Engineer, the geometry from the Grasshopper script is exported to SCIA-Engineer by using Grasshopper plug-in Koala. The loads, constraints, material and cross-sections are manually entered in SCIA. The structure which is analysed is the large part of the entrance hall's roof with a parabolic shape for the arches, grid variant 3 and no bracing elements are applied. The load combinations applied for the analysis are ULS-1 which includes only permanent load, and ULS-9 which includes a wind load where wind pressure acts at one side, and wind suction acts on the other side of the structure. The internal forces given by Karamba3D and SCIA-Engineer can be observed in the tables below.

Table D. 1 Comparison results Karamba3D and SCIA-Engineer ULS-1

	M_y [kNm]	M_z [kNm]	M_t [kNm]	V_y [kN]	V_z [kN]	N_t [kN]	N_c [kN]
Karamba3D	16.67	4.64	0.66	3.76	5.81	12.16	93.21
SCIA	16.58	4.19	0.72	3.48	5.82	9.15	91.47

Table D. 2 Comparison results Karamba3D and SCIA-Engineer ULS-9

	M_y [kNm]	M_z [kNm]	M_t [kNm]	V_y [kN]	V_z [kN]	N_t [kN]	N_c [kN]
Karamba3D	224.45	52.34	9.28	35.92	42.26	166.10	210.50
SCIA	228.32	53.44	10.52	36.48	43.30	152.40	176.89

The internal forces which are caused by load combination ULS-1 are very similar between both Karamba3D and SCIA-Engineer. Between the normal forces however, a relatively large difference can be observed. This is the case for both load combinations. For both calculations GL24h is applied with the same specific weight (420 kg/m^3). The differences may be explained due to the fact that the analysis performed with SCIA-Engineer is linear, whereas the analysis with Karamba3D is non-linear. Furthermore are the distributions for all internal forces resulting from ULS-9 given in the figures below. The plots at the left side are from Karamba3D and the right plots are from SCIA-Engineer. As can be seen are the distributions very similar for all internal forces.

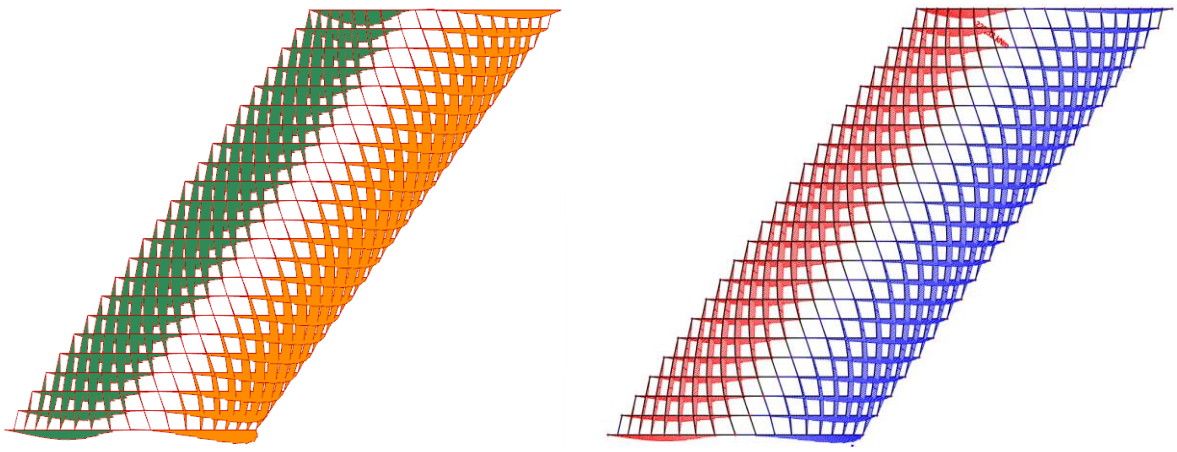

Figure D. 1 Bending moment My caused by ULS-9

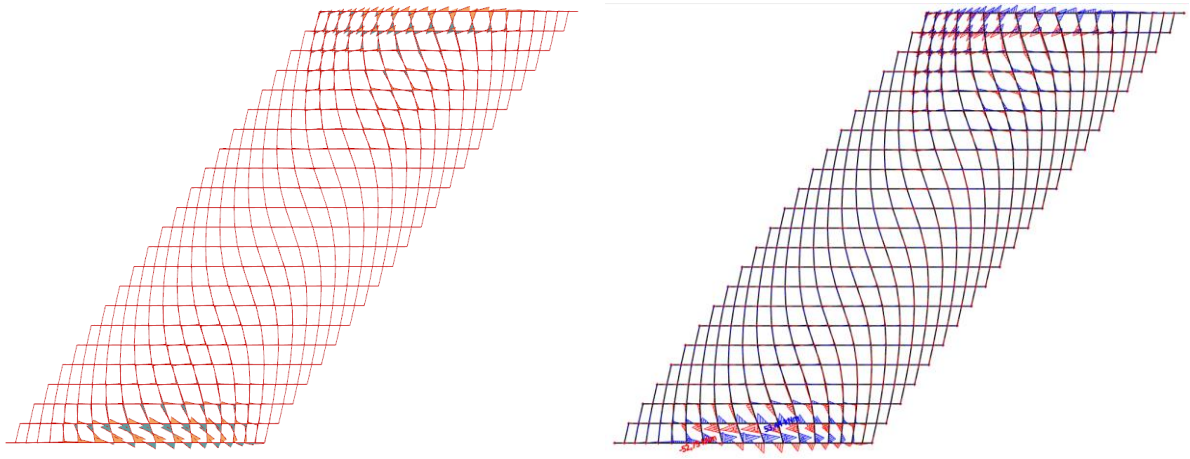

Figure D. 2 Bending moment Mz caused by ULS-9

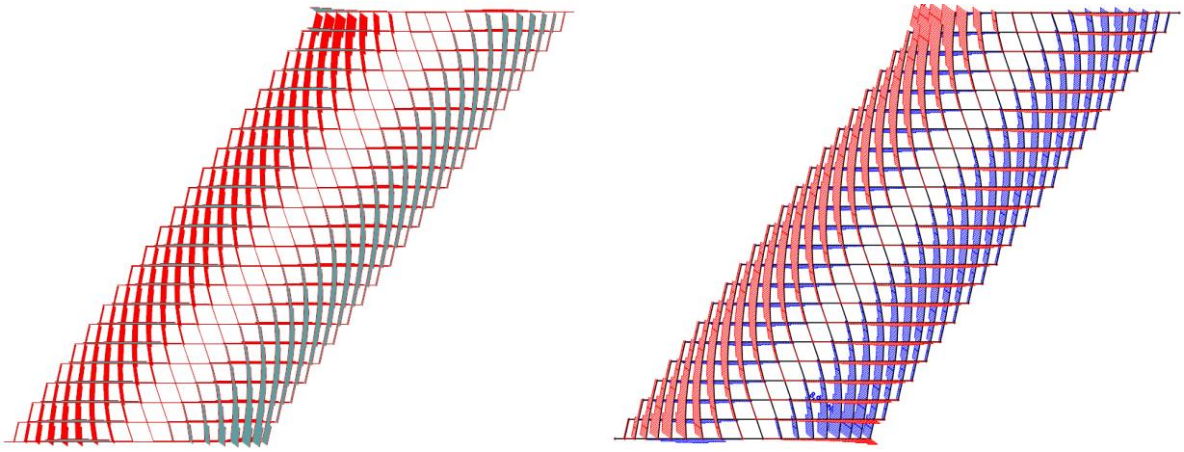

Figure D. 3 Torsional moment M_t caused by ULS-9

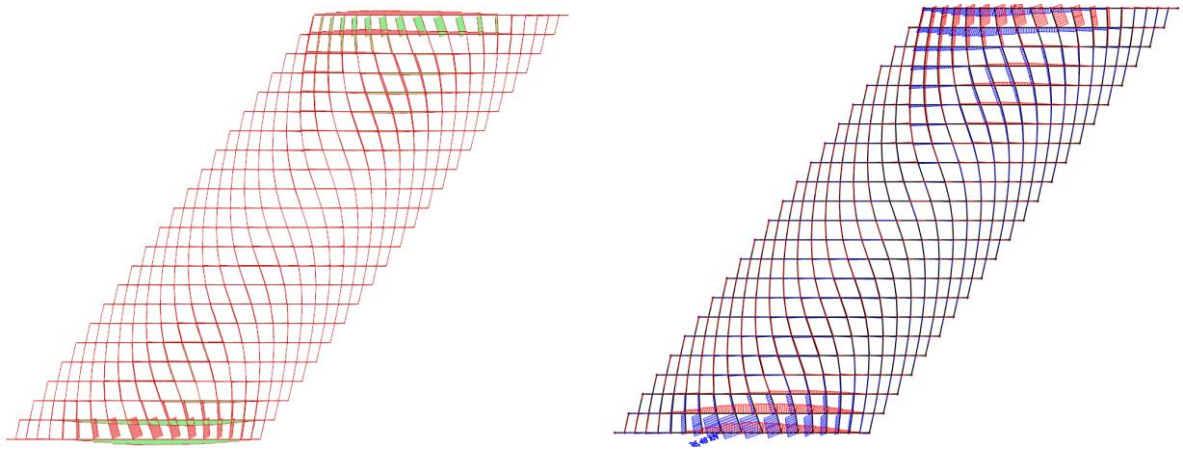

Figure D. 4 Shear force V_y caused by ULS-9

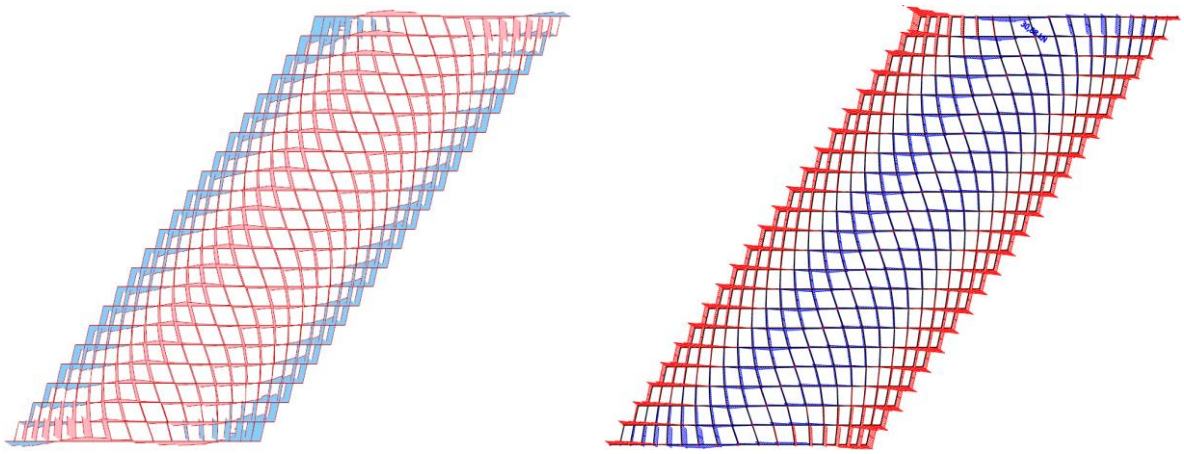

Figure D. 5 Shear force Vz caused by ULS-9

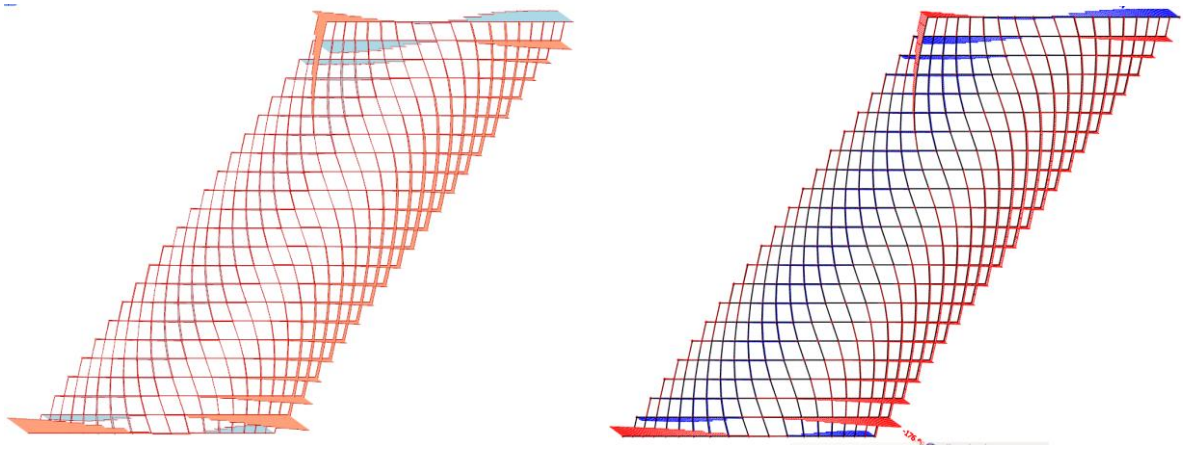

Figure D. 6 Normal force caused by ULS-9

Appendix E: Spreadsheets

E-1: Spreadsheets for variant study
E-1: Spreadsheets for final design

E.1 Spreadsheets variant study

Variant:	*Segmented system*
Part:	*Unity checks cross-sections*

Cross-section		
b	240	[mm]
h	660	[mm]
Wy	17424000	[mm3]
Wz	6336000	[mm3]
I_y	5749920000	[mm4]
I_x	760320000	[mm4]
A	158400	[mm2]

Strength class		GL24h
(ULS)	$f_{m,k}$	24
	$f_{t,0,k}$	19.2
	$f_{t,90,k}$	0.5
	$f_{c,0,k}$	24
	$f_{c,90,k}$	2.5
	$f_{v,k}$	3.5
	ρ_k	385
	$E_{m,0,k}$	9600
(SLS)	$E_{m,0,mean}$	11500
	$E_{m,90,mean}$	300
	G_{mean}	650

Characteristic strength		
$f_{m,d}$	17.116	[N/mm2]
$f_{v,d}$	2.52	[N/mm2]
$f_{c,0,d}$	17.28	[N/mm2]
$f_{t,0,d}$	13.69	[N/mm2]
k_h	0.991	[-]
k_{mod}	0.9	[-]
γ_m	1.25	[-]
k_m	0.7	[-]
k_{shape}	1.14	[-]

	LC1	LC2	LC3	LC4	LC5	LC6	LC7	LC8	LC9	
My	9.07	17.52	26.98	70.54	45.45	80.12	51.26	69.81	81.73	[kNm]
Mz	1.71	4.36	6.56	11.23	8.79	12.95	20.20	27.44	26.55	[kNm]
Mt	0.83	1.42	2.03	5.37	3.60	6.26	4.08	5.53	6.41	[kNm]
Nc	179.85	244.66	271.94	405.36	329.62	495.45	419.54	486.22	798.85	[kN]
Nt	1.32	5.83	11.03	173.25	54.92	155.88	239.58	319.96	291.93	[kN]
Vy	5.57	9.59	13.13	22.32	13.89	24.35	15.11	20.08	25.56	[kN]
Vz	1.45	2.82	4.66	6.71	3.51	4.90	7.32	9.74	9.44	[kN]

$\sigma_{m,y,d}$	0.52	1.01	1.55	4.05	2.61	4.60	2.94	4.01	4.69	[N/mm2]
$\sigma_{m,z,d}$	0.27	0.69	1.04	1.77	1.39	2.04	3.19	4.33	4.19	[N/mm2]
τ_x	8.35E-02	1.42E-01	2.03E-01	5.38E-01	3.60E-01	6.26E-01	4.08E-01	5.54E-01	6.42E-01	[N/mm2]
$\sigma_{c,0,d}$	1.14	1.54	1.72	2.56	2.08	3.13	2.65	3.07	5.04	[N/mm2]
$\sigma_{t,0,d}$	0.01	0.04	0.07	1.09	0.35	0.98	1.51	2.02	1.84	[N/mm2]
τ_y	5.28E-02	9.08E-02	1.24E-01	2.11E-01	1.32E-01	2.31E-01	1.43E-01	1.90E-01	2.42E-01	[N/mm2]
τ_z	1.37E-02	2.67E-02	4.41E-02	6.35E-02	3.32E-02	4.64E-02	6.93E-02	9.23E-02	8.94E-02	[N/mm2]

UC: Mt	2.9E-02	5.0E-02	7.1E-02	1.9E-01	1.3E-01	2.2E-01	1.4E-01	1.9E-01	0.22	OK
UC: M	0.04	0.09	0.13	0.31	0.21	0.35	0.31	0.42	0.45	OK
UC: Vy	2.09E-02	3.60E-02	4.93E-02	8.39E-02	5.22E-02	9.15E-02	5.68E-02	7.54E-02	0.10	OK
UC: Vz	5.45E-03	1.06E-02	1.75E-02	2.52E-02	1.32E-02	1.84E-02	2.75E-02	3.66E-02	4E-02	OK
UC: Nc	0.07	0.09	0.10	0.15	0.12	0.18	0.15	0.18	0.29	OK
UC: Nt	0.00	0.00	0.01	0.08	0.03	0.07	0.11	0.15	0.13	OK
UC: M+C	0.05	0.09	0.14	0.33	0.22	0.39	0.33	0.45	0.53	OK
UC: M+T	0.04	0.09	0.14	0.39	0.23	0.42	0.42	0.56	0.58	OK

Variant:	*Segmented system*
Part:	*Slotted in steel plate joint*

Design loads			**Geometry**			**Material**					
Maximum loads in nodes			*Cross-section and joint*			*Timber:*	*GL24h*		*Bolt:*	*6.8*	
$M_{y,Ed}$	81.73	kNm	h	660	mm	$f_{m,g,k}$	24	N/mm2	f_{yb}	480	N/mm2
$M_{z,Ed}$	27.44	kNm	b	240	mm	$f_{t,0,g,k}$	19.2	N/mm2	f_{ub}	600	N/mm2
$F_{c,Ed}$	798.85	kN	t	12	mm	$f_{t,90,g,k}$	0.5	N/mm2			
$F_{t,Ed}$	319.96	kN	d	22	mm	$f_{c,0,g,k}$	24	N/mm2	*Plate:*	*S235*	
V_{Ed}	25.56	kN	Rows	7	-	$f_{c,90,g,k}$	2.5	N/mm2	f_y	235	N/mm2
			Columns	8	-	$f_{v,g,k}$	3.5	N/mm2	f_u	360	N/mm2
						$f_{r,g,k}$	1.2	N/mm2			
						$E_{0,g,mean}$	11500	N/mm2	*Material factors:*		
			Bolt spacing			$E_{0,g,05}$	9600	N/mm2	α	0	-
			α1	110	mm	$E_{90,g,mean}$	300	N/mm2	kmod	0.9	-
			α2	88	mm	$E_{90,g,05}$	250	N/mm2	γm	1.25	-
			α3,t	154	mm	$G_{g,mean}$	650	N/mm2	γm0	1.00	-
			α4,t	66.00	mm	$G_{g,05}$	540	N/mm2	γm2	1.25	-
			Check	GOOD	-	$G_{r,g,mean}$	65	N/mm2			
			h_{req}	660.00	mm	$G_{r,g,05}$	54	N/mm2			
			l_{plate}	924	mm	$\rho_{g,k}$	385	kg/m3			
						$\rho_{g,mean}$	420	kg/m3			

Joint resistance						**Stability elements**			**Axial stiffness**		
Unity check bolts			*Unity check plate*			N_{ed}	197.5	kN	Kser	2127677.62	N/mm
k_{90}	1.68	-	A_{net}	6072	mm2	Material:	S235	-	Ku	1418451.75	N/mm
$f_{h,0,k}$	24.62	N/mm2	$N_{t,Rd1}$	1861200	N	fy	235	N/mm2			
$f_{h,\alpha,k}$	24.62	N/mm2	$N_{t,Rd2}$	1573862	N	A_{min}	840.43	mm2			
$M_{y,Rk}$	556636.24	Nmm	$N_{c,Rd}$	1426920	N	D	26	mm			
Fv,Rk	32233.18	N	U.C. (t)	0.20		$A_{1,cable}$	530.66	mm2			
I	61758.50	N	U.C. (c)	0.56		$A_{2,cables}$	1061.32	mm2			
II	32233.18	N									
III	39940.13	N									
n_{ef}	5.12	-									
Fv,Rd	831325.91	N									
U.C.	0.96										

Variant:	*Lattice system*
Part:	*Unity checks cross-sections*

Cross-section		
b	240	[mm]
h	250	[mm]
h_s	250	[mm]
z	375	[mm]
t	18	[mm]
I_y	7740950172	[mm4]
I_x	576000000	[mm4]
A	120000	[mm2]

Strength class		GL24h
(ULS)	$f_{m,k}$	24
	$f_{t,0,k}$	19.2
	$f_{t,90,k}$	0.5
	$f_{c,0,k}$	24
	$f_{c,90,k}$	2.5
	$f_{v,k}$	3.5
	ρ_k	385
	$E_{m,0,k}$	9600
(SLS)	$E_{m,0,mean}$	11500
	$E_{m,90,mean}$	300
	G_{mean}	650

Characteristic strength		
$f_{m,d}$	16.899	[N/mm2]
$f_{v,d}$	2.52	[N/mm2]
$f_{c,0,d}$	17.28	[N/mm2]
$f_{t,0,d}$	13.52	[N/mm2]
k_h	0.978	[-]
k_{mod}	0.9	[-]
γ_m	1.25	[-]
k_m	1	[-]
kshape	1.16	[-]

	UGT-1	UGT-2	UGT-3	UGT-4	UGT-5	UGT-6	UGT-7	UGT-8	UGT-9	
My	4.91	26.58	55.57	99.42	72.41	112.58	147.82	180.35	187.21	kNm
Mt	0.07	0.24	0.72	1.55	0.83	1.57	1.93	2.48	2.62	kNm
Mz	1.55	2.48	5.80	18.40	8.81	13.80	21.09	25.85	26.47	kNm
Nc	100.27	156.85	158.12	308.13	108.22	238.74	186.52	202.79	149.07	kN
Nt	1.65	9.50	17.62	20.68	36.96	114.99	104.99	131.54	166.29	kN
Vy	3.30	7.66	14.32	22.81	19.47	26.86	27.61	33.44	38.93	kN
Vz	1.74	3.18	5.85	12.84	5.61	8.66	13.17	16.09	16.50	kN

$\sigma_{m,y,d}$	0.24	1.30	2.71	4.85	3.54	5.50	7.22	8.81	9.14	N/mm2
$\sigma_{m,z,d}$	0.32	0.52	1.21	3.83	1.83	2.87	4.39	5.39	5.52	N/mm2
τ_{tor}	6.05E-03	2.03E-02	6.19E-02	1.33E-01	7.17E-02	1.35E-01	1.66E-01	2.13E-01	2.25E-01	N/mm2
$\sigma_{c,0,d}$	0.84	1.31	1.32	2.57	0.90	1.99	1.55	1.69	1.24	N/mm2
$\sigma_{t,0,d}$	0.01	0.08	0.15	0.17	0.31	0.96	0.87	1.10	1.39	N/mm2
τ_y	0.03	0.06	0.12	0.18	0.16	0.22	0.22	0.27	0.31	N/mm2
τ_z	4.54E-05	8.28E-05	1.52E-04	3.34E-04	1.46E-04	2.26E-04	3.43E-04	4.19E-04	4.30E-04	N/mm2

UC: Mt	2.1E-03	7.0E-03	2.1E-02	4.6E-02	2.5E-02	4.6E-02	5.7E-02	7.3E-02	7.7E-02	OK
UC: M	0.03	0.11	0.23	0.51	0.32	0.50	0.69	0.84	0.87	OK
UC: Vy	0.01	0.02	0.05	0.07	0.06	0.09	0.09	0.11	0.12	OK
UC: Vz	0.00	3.29E-05	6.04E-05	1.33E-04	5.80E-05	8.95E-05	1.36E-04	1.66E-04	1.71E-04	OK
UC: Nc	0.05	0.08	0.08	0.15	0.05	0.12	0.09	0.10	0.07	OK
UC: Nt	0.00	0.01	0.01	0.01	0.02	0.07	0.06	0.08	0.10	OK
UC: M+C	0.04	0.11	0.24	0.54	0.32	0.51	0.70	0.85	0.87	OK
UC: M+T	0.03	0.11	0.24	0.53	0.34	0.57	0.75	0.92	0.97	OK

Bending stress (0)	
r_{in}	11137
α_{ap}	0
t	18
h_{ap}	250
r	11262
k1	1
k2	0.35
k3	0.6
k4	0
kl	1.01
kr	1.00

Bending stress (90)	
My	112.6
$\sigma_{m,y,d}$	5.50
Vb	6.39
V	4.26
k5	0
k6	0.25
k7	0
kp	0.00554964
$\sigma_{t,90,d}$	0.03
k_{dis}	1.4
k_{vol}	0.30
$f_{t,90,d}$	0.35
U.C	0.33

Manufacturing	
σ_m	9.29
U.C	0.55

Variant:	*Lattice system*
Part:	*Shear blocks*

Design load			*Material:*			*Geometry*		
V	38926.97	N	Bolt	4.6		Rows	4	
			fu,k	400	N/mm2	Columns	2	
Bolt	M12		Kmod	0.9		d	12	mm
A	113	mm2	ym	1.25		A	120000	mm2
A_s	84.3	mm2	ρk	385	kg/m3	A1	60000	mm2
y_{m2}	1.25		ρm	462	kg/m3	e1	250	
			E	9600	N/mm2	Si	700	mm
						L	53850	mm
			Zb	375	mm	h1	250	mm
			b2	240	mm	h2	250	mm
			b0	230	mm	Cs	0.95	
			I	7.74E+09	mm4			

Shear and connector resistance			*Minimum bolt spacing*			*Axial stiffness*		
σv,Ed	1.41	N/mm2	α1	60	mm	Kser	82896.5308	N/mm
fv,Rd	2.52	N/mm2	α2	48	mm	Ku	55264.3539	N/mm
U.C	0.56		α3,t	84	mm			
			α4,t	36.00	mm			
F	6288.20	N	min. b	228	mm			
Fv,Rd,1	21696	N	min. d	216	mm			
Fv,Rd,2	16185.6	N						
U.C.	0.39							

Variant:	*Arch system*
Part:	*Unity checks cross-sections primary beams*

Cross-section		
b	240	[mm]
h	610	[mm]
W_y	14884000	[mm3]
W_z	5856000	[mm3]
t	18	[mm]
I_y	4.54E+09	[mm4]
I_x	7.03E+08	[mm4]
A	146400	[mm2]

Strength class		GL24h
(ULS)	$f_{m,k}$	24
	$f_{t,0,k}$	19.2
	$f_{t,90,k}$	0.5
	$f_{c,0,k}$	24
	$f_{c,90,k}$	2.5
	$f_{v,k}$	3.5
	ρ_k	385
	$E_{m,0,k}$	9600
(SLS)	$E_{m,0,mean}$	11500
	$E_{m,90,mean}$	300
	G_{mean}	650

Characteristic strength		
$f_{m,d}$	17.251	[N/mm2]
$f_{v,d}$	2.52	[N/mm2]
$f_{c,0,d}$	17.28	[N/mm2]
$f_{t,0,d}$	13.80	[N/mm2]
k_h	0.998	[-]
k_{mod}	0.9	[-]
γ_m	1.25	[-]
k_m	0.7	[-]
k_{shape}	1.13	[-]

	UGT-1	UGT-2	UGT-3	UGT-4	UGT-5	UGT-6	UGT-7	UGT-8	UGT-9	
My	5.70	29.33	69.92	122.00	77.50	116.58	122.31	162.43	221.99	kNm
Mt	0.68	4.29	8.04	16.40	12.55	17.55	14.85	19.45	27.42	kNm
Mz	0.19	0.83	2.33	4.42	2.46	3.90	4.45	5.90	8.43	kNm
Nc	90.02	139.83	140.42	323.64	163.62	128.32	97.95	93.67	154.97	kN
Nt	0.00	0.00	0.00	0.00	86.41	164.93	143.82	155.57	123.02	kN
Vy	4.59	9.28	18.66	32.83	19.06	25.12	19.08	24.49	36.60	kN
Vz	0.16	0.95	1.90	3.45	5.06	7.05	4.74	6.06	7.94	kN

$\sigma_{m,y,d}$	0.38	1.97	4.70	8.20	5.21	7.83	8.22	10.91	14.91	N/mm2
$\sigma_{m,z,d}$	0.03	0.14	0.40	0.76	0.42	0.67	0.76	1.01	1.44	N/mm2
τ_{tor}	0.04	0.23	0.43	0.88	0.68	0.94	0.80	1.05	1.48	N/mm2
$\sigma_{c,0,d}$	0.61	0.96	0.96	2.21	1.12	0.88	0.67	0.64	1.06	N/mm2
$\sigma_{t,0,d}$	0.00	0.00	0.00	0.00	0.59	1.13	0.98	1.06	0.84	N/mm2
τ_y	0.05	0.10	0.19	0.34	0.20	0.26	0.20	0.25	0.38	N/mm2
τ_z	1.65E-03	9.72E-03	1.94E-02	3.53E-02	5.18E-02	7.23E-02	4.85E-02	6.20E-02	8.14E-02	N/mm2

UC: Mt	0.01	0.08	0.15	0.31	0.24	0.33	0.28	0.37	0.52	OK
UC: M	0.02	0.12	0.29	0.51	0.32	0.48	0.51	0.67	0.92	OK
UC: Vy	0.02	0.04	0.08	0.13	0.08	0.10	0.08	0.10	0.15	OK
UC: Vz	0.00	3.86E-03	7.71E-03	1.40E-02	2.06E-02	2.87E-02	1.93E-02	2.46E-02	3.23E-02	OK
UC: Nc	0.04	0.06	0.06	0.13	0.06	0.05	0.04	0.04	0.06	OK
UC: Nt	0.00	0.00	0.00	0.00	0.04	0.08	0.07	0.08	0.06	OK
UC: M+C	0.02	0.12	0.29	0.52	0.32	0.48	0.51	0.67	0.93	OK
UC: M+T	0.02	0.12	0.29	0.51	0.36	0.56	0.58	0.75	0.98	OK

Bending stress (0)	
r_{in}	11137
α_{ap}	0
t	18
h_{ap}	610
r	11442
k1	1
k2	0.35
k3	0.6
k4	0
kl	1.02
kr	1.00

Bending stress (90)	
My	98
$\sigma_{m,y,d}$	6.58
Vb	7.79
V	5.20
k5	0
k6	0.25
k7	0
kp	0.013328
$\sigma_{t,90,d}$	0.09
k_{dis}	1.4
k_{vol}	0.29
$f_{t,90,d}$	0.36
U.C	0.76

Manufacturing	
σ_m	9.29
U.C	0.54

Variant:	*Arch system*
Part:	*Unity checks cross-sections secondary beams - conservative*

Cross-section		
b	120	[mm]
h	120	[mm]
Wy	288000	[mm3]
Wz	288000	[mm3]
I_y	17280000	[mm4]
I_x	17280000	[mm4]
A	14400	[mm2]

Critical load		
Lcr	4000	[mm]
Fcr	102.3279	[kN]

Strength class		GL24h
(ULS)	$f_{m,k}$	24
	$f_{t,0,k}$	19.2
	$f_{t,90,k}$	0.5
	$f_{c,0,k}$	24
	$f_{c,90,k}$	2.5
	$f_{v,k}$	3.5
	ρ_k	385
	$E_{m,0,k}$	9600
(SLS)	$E_{m,0,mean}$	11500
	$E_{m,90,mean}$	300
	G_{mean}	650

Characteristic strength		
$f_{m,d}$	20.297	[N/mm2]
$f_{v,d}$	2.52	[N/mm2]
$f_{c,0,d}$	17.28	[N/mm2]
$f_{t,0,d}$	16.24	[N/mm2]
k_h	1.175	[-]
k_{mod}	0.9	[-]
γ_m	1.25	[-]
k_m	0.7	[-]
k_{shape}	1.05	[-]

	ULS-1	ULS-2	ULS-3	ULS-4	ULS-5	ULS-6	ULS-7	ULS-8	ULS-9	
My	0.17	0.17	0.17	0.17	0.17	0.17	0.17	0.17	0.17	[kNm]
Mz	0.00	0.00	0.00	0.00	0.00	0.00	0.00	0.00	0.00	[kNm]
Mt	0.00	0.00	0.00	0.00	0.00	0.00	0.00	0.00	0.00	[kNm]
Nc	0.25	3.93	14.95	13.85	30.64	98.28	67.64	75.96	39.92	[kN]
Nt	2.61	7.51	13.10	39.79	30.18	8.36	12.93	17.32	47.45	[kN]
Vy	0.18	0.18	0.18	0.18	0.18	0.18	0.18	0.18	0.18	[kN]
Vz	0.00	0.00	0.00	0.00	0.00	0.00	0.00	0.00	0.00	[kN]

$\sigma_{m,y,d}$	0.61	0.61	0.61	0.61	0.61	0.61	0.61	0.61	0.61	[N/mm2]
$\sigma_{m,z,d}$	0.00	0.00	0.00	0.00	0.00	0.00	0.00	0.00	0.00	[N/mm2]
τ_x	0.00E+00	0.00E+00	0.00E+00	0.00E+00	0.00E+00	0.00E+00	0.00E+00	0.00E+00	0.00E+00	[N/mm2]
$\sigma_{c,0,d}$	0.02	0.27	1.04	0.96	2.13	6.82	4.70	5.27	2.77	[N/mm2]
$\sigma_{t,0,d}$	0.18	0.52	0.91	2.76	2.10	0.58	0.90	1.20	3.30	[N/mm2]
τ_y	1.88E-02	1.88E-02	1.88E-02	1.88E-02	1.88E-02	1.88E-02	1.88E-02	1.88E-02	1.88E-02	[N/mm2]
τ_z	0.00E+00	0.00E+00	0.00E+00	0.00E+00	0.00E+00	0.00E+00	0.00E+00	0.00E+00	0.00E+00	[N/mm2]

UC: My	0.03	0.03	0.03	0.03	0.03	0.03	0.03	0.03	0.03	OK
UC: Mt	0.0E+00	0.0E+00	0.0E+00	0.0E+00	0.0E+00	0.0E+00	0.0E+00	0.0E+00	0.00	OK
UC: Mz	0.00	0.00	0.00	0.00	0.00	0.00	0.00	0.00	0.00	OK
UC: Vy	7.46E-03	7.46E-03	7.46E-03	7.46E-03	7.46E-03	7.46E-03	7.46E-03	7.46E-03	0.01	OK
UC: Vz	0.00E+00	0.00E+00	0.00E+00	0.00E+00	0.00E+00	0.00E+00	0.00E+00	0.00E+00	0E+00	OK
UC: Nc	0.00	0.02	0.06	0.06	0.12	0.39	0.27	0.31	0.16	OK
UC: Nt	0.01	0.03	0.06	0.17	0.13	0.04	0.06	0.07	0.20	OK
UC: M+C	0.03	0.03	0.03	0.03	0.04	0.19	0.10	0.12	0.06	OK
UC: M+T	0.04	0.06	0.09	0.20	0.16	0.07	0.09	0.10	0.23	OK

E.2 Spreadsheets for final design

Variant:	*Final design*
Part:	*Unity checks cross-sections primary beams*

Cross-section		
b	240	[mm]
h	720	[mm]
W_y	20736000	[mm3]
W_z	6912000	[mm3]
t	33	[mm]
I_y	7.46E+09	[mm4]
I_x	8.29E+08	[mm4]
A	172800	[mm2]

Strength class		GL28h
(ULS)	$f_{m,k}$	28
	$f_{t,0,k}$	22.3
	$f_{t,90,k}$	0.5
	$f_{c,0,k}$	28
	$f_{c,90,k}$	2.5
	$f_{v,k}$	3.5
	ρ_k	425
	$E_{m,0,k}$	10500
(SLS)	$E_{m,0,mean}$	12600
	$E_{m,90,mean}$	300
	G_{mean}	650

Characteristic strength		
$f_{m,d}$	19.796	[N/mm2]
$f_{v,d}$	2.52	[N/mm2]
$f_{c,0,d}$	20.16	[N/mm2]
$f_{t,0,d}$	15.77	[N/mm2]
k_h	0.982	[-]
k_{mod}	0.9	[-]
γ_m	1.25	[-]
k_m	0.7	[-]
k_{shape}	1.15	[-]

	UGT-1	UGT-2	UGT-3	UGT-4	UGT-5	UGT-6	UGT-7	UGT-8	UGT-9	
My	8.50	24.34	75.29	111.71	47.29	76.60	83.16	111.74	148.63	kNm
Mt	0.13	0.25	0.67	2.08	2.38	3.47	3.00	3.31	2.17	kNm
Mz	0.57	2.00	3.36	7.20	10.58	13.65	12.69	14.02	11.77	kNm
Nc	99.63	155.31	164.74	332.25	187.33	81.06	71.52	60.66	153.84	kN
Nt	0.00	0.00	0.00	0.00	19.45	188.82	168.43	183.48	63.91	kN
Vy	5.62	11.02	19.81	47.60	18.15	23.36	26.92	34.03	39.03	kN
Vz	0.21	0.74	1.13	2.65	7.73	11.20	10.56	12.02	9.45	kN

$\sigma_{m,y,d}$	0.42	1.20	3.72	5.52	2.34	3.78	4.11	5.52	7.34	N/mm2
$\sigma_{m,z,d}$	0.08	0.29	0.49	1.04	1.53	1.97	1.84	2.03	1.70	N/mm2
τ_{tor}	0.00	0.01	0.03	0.08	0.09	0.13	0.12	0.13	0.08	N/mm2
$\sigma_{c,0,d}$	0.58	0.90	0.95	1.92	1.08	0.47	0.41	0.35	0.89	N/mm2
$\sigma_{t,0,d}$	0.00	0.00	0.00	0.00	0.11	1.09	0.97	1.06	0.37	N/mm2
τ_y	0.05	0.10	0.17	0.41	0.16	0.20	0.23	0.30	0.34	N/mm2
τ_z	1.86E-03	6.39E-03	9.82E-03	2.30E-02	6.71E-02	9.72E-02	9.17E-02	1.04E-01	8.21E-02	N/mm2

UC: Mt	0.00	0.00	0.01	0.03	0.03	0.05	0.04	0.04	0.03	OK
UC: M	0.02	0.07	0.21	0.32	0.17	0.26	0.27	0.35	0.43	OK
UC: Vy	0.02	0.04	0.07	0.16	0.06	0.08	0.09	0.12	0.13	OK
UC: Vz	0.00	2.54E-03	3.90E-03	9.11E-03	2.66E-02	3.86E-02	3.64E-02	4.14E-02	3.26E-02	OK
UC: Nc	0.03	0.04	0.05	0.10	0.05	0.02	0.02	0.02	0.04	OK
UC: Nt	0.00	0.00	0.00	0.00	0.01	0.07	0.06	0.07	0.02	OK
UC: M+C	0.02	0.07	0.21	0.32	0.18	0.26	0.27	0.35	0.43	OK
UC: M+T	0.02	0.07	0.21	0.32	0.18	0.33	0.33	0.42	0.45	OK

Bending stress (0)	
r_{in}	11137
α_{ap}	0
t	33
h_{ap}	720
r	11497
k1	1
k2	0.35
k3	0.6
k4	0
kl	1.02
kr	1.00

Bending stress (90)	
My	83.2
$\sigma_{m,y,d}$	4.01
Vb	9.20
V	6.13
k5	0
k6	0.25
k7	0
kp	0.015656
$\sigma_{t,90,d}$	0.06
k_{dis}	1.4
k_{vol}	0.28
$f_{t,90,d}$	0.35
U.C	0.62

Manufacturing	
σ_m	18.67
U.C	0.94

Variant:	*Final design*
Part:	*Unity checks cross-sections secondary beams*

Cross-section		
b	200	[mm]
h	280	[mm]
Wy	2613333	[mm3]
Wz	1866667	[mm3]
I_y	3.66E+08	[mm4]
I_x	1.87E+08	[mm4]
A	56000	[mm2]

Critical load		
Lcr	4000	[mm]
Fcr	1105.394	[kN]

Strength class		GL24h
(ULS)	$f_{m,k}$	24
	$f_{t,0,k}$	19.2
	$f_{t,90,k}$	0.5
	$f_{c,0,k}$	24
	$f_{c,90,k}$	2.5
	$f_{v,k}$	3.5
	ρ_k	385
	$E_{m,0,k}$	9600
(SLS)	$E_{m,0,mean}$	11500
	$E_{m,90,mean}$	300
	G_{mean}	650

Characteristic strength		
$f_{m,d}$	18.648	[N/mm2]
$f_{v,d}$	2.52	[N/mm2]
$f_{c,0,d}$	17.28	[N/mm2]
$f_{t,0,d}$	14.92	[N/mm2]
k_h	1.079	[-]
k_{mod}	0.9	[-]
γ_m	1.25	[-]
k_m	0.7	[-]
k_{shape}	1.07	[-]

	ULS-1	ULS-2	ULS-3	ULS-4	ULS-5	ULS-6	ULS-7	ULS-8	ULS-9	
My	0.00	0.00	0.00	0.00	0.00	0.00	0.00	0.00	0.00	[kNm]
Mz	0.00	0.00	0.00	0.00	0.00	0.00	0.00	0.00	0.00	[kNm]
Mt	0.00	0.00	0.00	0.00	0.00	0.00	0.00	0.00	0.00	[kNm]
Nc	1.83	4.64	11.90	61.65	45.99	102.84	83.85	95.26	71.73	[kN]
Nt	7.87	20.67	39.31	9.17	25.24	14.78	2.45	3.29	42.68	[kN]
Vy	0.00	0.00	0.00	0.00	0.00	0.00	0.00	0.00	0.00	[kN]
Vz	0.00	0.00	0.00	0.00	0.00	0.00	0.00	0.00	0.00	[kN]

$\sigma_{m,y,d}$	0.00	0.00	0.00	0.00	0.00	0.00	0.00	0.00	0.00	[N/mm2]
$\sigma_{m,z,d}$	0.00	0.00	0.00	0.00	0.00	0.00	0.00	0.00	0.00	[N/mm2]
τ_x	0.00E+00	0.00E+00	0.00E+00	0.00E+00	0.00E+00	0.00E+00	0.00E+00	0.00E+00	0.00E+00	[N/mm2]
$\sigma_{c,0,d}$	0.03	0.08	0.21	1.10	0.82	1.84	1.50	1.70	1.28	[N/mm2]
$\sigma_{t,0,d}$	0.14	0.37	0.70	0.16	0.45	0.26	0.04	0.06	0.76	[N/mm2]
τ_y	0.00E+00	0.00E+00	0.00E+00	0.00E+00	0.00E+00	0.00E+00	0.00E+00	0.00E+00	0.00E+00	[N/mm2]
τ_z	0.00E+00	0.00E+00	0.00E+00	0.00E+00	0.00E+00	0.00E+00	0.00E+00	0.00E+00	0.00E+00	[N/mm2]

UC: My	0.00	0.00	0.00	0.00	0.00	0.00	0.00	0.00	0.00	OK
UC: Mt	0.0E+00	0.0E+00	0.0E+00	0.0E+00	0.0E+00	0.0E+00	0.0E+00	0.0E+00	0.00	OK
UC: Mz	0.00	0.00	0.00	0.00	0.00	0.00	0.00	0.00	0.00	OK
UC: Vy	0.00E+00	0.00E+00	0.00E+00	0.00E+00	0.00E+00	0.00E+00	0.00E+00	0.00E+00	0.00	OK
UC: Vz	0.00E+00	0.00E+00	0.00E+00	0.00E+00	0.00E+00	0.00E+00	0.00E+00	0.00E+00	0E+00	OK
UC: Nc	0.00	0.00	0.01	0.06	0.05	0.11	0.09	0.10	0.07	OK
UC: Nt	0.01	0.02	0.05	0.01	0.03	0.02	0.00	0.00	0.05	OK
UC: M+C	0.00	0.00	0.00	0.00	0.00	0.01	0.01	0.01	0.01	OK
UC: M+T	0.01	0.02	0.05	0.01	0.03	0.02	0.00	0.00	0.05	OK

Variant:	*Final variant*
Part:	*Connections between arch segments*

Design loads			**Geometry**			**Material**					
Maximum loads in nodes			*Cross-section and joint*			*Timber:*	*GL28h*		*Bolt splice:*	*4.6*	
F_{Ed}	185.2	kN	h	720	mm	$f_{m,g,k}$	28	N/mm2	f_{yb}	240	N/mm2
			b	240	mm	$f_{t,0,g,k}$	22.3	N/mm2	f_{ub}	400	N/mm2
			t	12	mm	$f_{t,90,g,k}$	0.5	N/mm2			
			d	24	mm	$f_{c,0,g,k}$	28	N/mm2	*Plate splice:*	*S235*	
			Rows	7	-	$f_{c,90,g,k}$	2.5	N/mm2	f_y	235	N/mm2
			Columns	8	-	$f_{v,g,k}$	3.5	N/mm2	f_u	360	N/mm2
						$f_{r,g,k}$	1.2	N/mm2			
						$E_{0,g,mean}$	12600	N/mm2	*Material factors:*		
			Bolt spacing			$E_{0,g,05}$	10500	N/mm2	α	0	-
			α1	120	mm	$E_{90,g,mean}$	300	N/mm2	kmod	0.9	-
			α2	96	mm	$E_{90,g,05}$	250	N/mm2	γm	1.25	-
			α3,t	168	mm	$G_{g,mean}$	650	N/mm2	γm0	1.00	-
			α4,t	72.00	mm	$G_{g,05}$	540	N/mm2	γm2	1.25	-
			Check	GOOD	-	$G_{r,g,mean}$	65	N/mm2			
			h_{req}	720.00	mm	$G_{r,g,05}$	54	N/mm2			
			l_{plate}	1008	mm	$\rho_{g,k}$	425	kg/m3			
						$\rho_{g,mean}$	460	kg/m3			

Joint resistance						**Axial stiffness**		
Unity check bolts			*Unity check plate*			Kser	2692072.11	N/mm
k_{90}	1.71	-	A_{net}	6624	mm2	Ku	1794714.74	N/mm
$f_{h,0,k}$	26.49	N/mm2	$N_{t,Rd1}$	2030400	N			
$f_{h,\alpha,k}$	26.49	N/mm2	$N_{t,Rd2}$	1716941	N			
$M_{y,Rk}$	465297.24	Nmm	$N_{c,Rd}$	1556640	N			
Fv,Rk	35634.47	N	U.C. (t)	0.11				
I	72465.70	N	U.C. (c)	0.12				
II	35634.47	N						
III	39555.50	N						
n_{ef}	5.12	-						
Fv,Rd	919048.52	N						
U.C.	0.20							

Variant:	*Final variant*
Part:	*Connections primary beams at supports*

Design loads			**Geometry**			**Material**					
Maximum loads in nodes			*Cross-section and joint*			*Timber:*	*GL28h*		*Bolt splice:*	*4.6*	
F_{Ed}	332.75	kN	h	720	mm	$f_{m,g,k}$	28	N/mm2	f_{yb}	240	N/mm2
			b	240	mm	$f_{t,0,g,k}$	22.3	N/mm2	f_{ub}	400	N/mm2
			t	12	mm	$f_{t,90,g,k}$	0.5	N/mm2			
			d	24	mm	$f_{c,0,g,k}$	28	N/mm2	*Plate splice:*	*S235*	
			Rows	7	-	$f_{c,90,g,k}$	2.5	N/mm2	f_y	235	N/mm2
			Columns	8	-	$f_{v,g,k}$	3.5	N/mm2	f_u	360	N/mm2
						$f_{r,g,k}$	1.2	N/mm2			
						$E_{0,g,mean}$	12600	N/mm2	*Material factors:*		
			Bolt spacing			$E_{0,g,05}$	10500	N/mm2	α	0	-
			α1	120	mm	$E_{90,g,mean}$	300	N/mm2	kmod	0.9	-
			α2	96	mm	$E_{90,g,05}$	250	N/mm2	γm	1.25	-
			α3,t	168	mm	$G_{g,mean}$	650	N/mm2	γm0	1.00	-
			α4,t	72.00	mm	$G_{g,05}$	540	N/mm2	γm2	1.25	-
			Check	GOOD	-	$G_{r,g,mean}$	65	N/mm2			
			h_{req}	720.00	mm	$G_{r,g,05}$	54	N/mm2			
			l_{plate}	1008	mm	$\rho_{g,k}$	425	kg/m3			
						$\rho_{g,mean}$	460	kg/m3			

Joint resistance						**Axial stiffness**		
Unity check bolts			*Unity check plate*			Kser	2692072.11	N/mm
k_{90}	1.71	-	A_{net}	6624	mm2	Ku	1794714.74	N/mm
$f_{h,0,k}$	26.49	N/mm2	$N_{t,Rd1}$	2030400	N			
$f_{h,\alpha,k}$	26.49	N/mm2	$N_{t,Rd2}$	1716941	N			
$M_{y,Rk}$	465297.24	Nmm	$N_{c,Rd}$	1556640	N			
$F_{v,Rk}$	35634.47	N	U.C. (t)	0.19				
I	72465.70	N	U.C. (c)	0.21				
II	35634.47	N						
III	39555.50	N						
n_{ef}	5.12	-						
$F_{v,Rd}$	919048.52	N						
U.C.	0.36							

Variant:	*Final*
Part:	*Supports - connection secondary beams*

Design loads			**Geometry**			**Material**					
Maximum loads in nodes			*Cross-section and joint*			*Timber:*	*GL24h*		*Bolt:*	*4.6*	
$F_{c,Ed\ arch}$	102.84	kN	h	280	mm	$f_{m,g,k}$	24	N/mm2	f_{yb}	240	N/mm2
			b	200	mm	$f_{t,0,g,k}$	19.2	N/mm2	f_{ub}	400	N/mm2
			t	8	mm	$f_{t,90,g,k}$	0.5	N/mm2			
			d	20	mm	$f_{c,0,g,k}$	24	N/mm2	*Pin:*	*6.8*	
			Rows	3	-	$f_{c,90,g,k}$	2.5	N/mm2	f_{yb}	480	N/mm2
			Columns	3	-	$f_{v,g,k}$	3.5	N/mm2	f_{ub}	600	N/mm2
						$f_{r,g,k}$	1.2	N/mm2			
						$E_{0,g,mean}$	11500	N/mm2	*Plate:*	*S235*	
Pin			*Bolt spacing*			$E_{0,g,05}$	9600	N/mm2	f_y	235	N/mm2
t	10	mm	α1	100	mm	$E_{90,g,mean}$	300	N/mm2	f_u	360	N/mm2
d	40	mm	α2	80	mm	$E_{90,g,05}$	250	N/mm2			
d0	43	mm	α3,t	140	mm	$G_{g,mean}$	650	N/mm2	*Material factors:*		
a	50.55	mm	α4,t	60.00	mm	$G_{g,05}$	540	N/mm2	α	0	-
c	36.21	mm	Check	GOOD	-	$G_{r,g,mean}$	65	N/mm2	kmod	0.9	-
A	628.32	mm^2	h_{req}	280.00	mm	$G_{r,g,05}$	54	N/mm2	γm	1.25	-
			l_{plate}	340	mm	$\rho_{g,k}$	385	kg/m3	γm0	1.00	-
						$\rho_{g,mean}$	420	kg/m3	γm2	1.25	-

Connection at support											
Unity check bolts			*Unity check plate*			*Unity check pin*			*Axial stiffness*		
k_{90}	1.65	-	A_{net}	1760	mm2	$F_{v,Rd}$	180955.58	N	Kser	310861.99	N/mm
$f_{h,0,k}$	25.26	N/mm2	$N_{t,Rd1}$	526400	N	U.C.	0.57		Ku	207241.33	N/mm
$f_{h,\alpha,k}$	25.26	N/mm2	$N_{t,Rd2}$	456192	N	$F_{b,Rd}$	141000.00	N			
$M_{y,Rk}$	289640.46	Nmm	$N_{c,Rd}$	413600	N	U.C.	0.73				
Fv,Rk	24227.58	N	U.C. (t)	0.23		W_{el}	6283.18				
I	48491.52	N	U.C. (c)	0.25		M_{Rd}	4523889.6	Nmm			
II	24227.58	N				M_{Ed}	3290260.04				
III	27819.85	N				U.C.	0.73				
n_{ef}	2.12	-				M+V	0.85				
Fv,Rd	110771.90	N									
U.C.	0.93										

Variant:	*Final variant*
Part:	*Connections between primary and secondary beams*

Design loads			**Geometry**			**Material**					
Maximum loads in nodes			*Cross-section and joint*			*Timber:*	*GL24h*		*Bolt splice:*	*4.6*	
$F_{Ed,sec}$	102.84	kN	h	280	mm	$f_{m,g,k}$	24	N/mm2	f_{yb}	240	N/mm2
$F_{Ed,stab}$	36.83	kN	b	200	mm	$f_{t,0,g,k}$	19.2	N/mm2	f_{ub}	400	N/mm2
			t	8	mm	$f_{t,90,g,k}$	0.5	N/mm2	*Bolt tube:*	*8.8*	
			d	20	mm	$f_{c,0,g,k}$	24	N/mm2	f_{yb}	640	N/mm2
			Rows	3	-	$f_{c,90,g,k}$	2.5	N/mm2	f_{ub}	800	N/mm2
			Columns	3	-	$f_{v,g,k}$	3.5	N/mm2	*Plate splice:*	*S235*	
						$f_{r,g,k}$	1.2	N/mm2	f_y	235	N/mm2
						$E_{0,g,mean}$	11500	N/mm2	f_u	360	N/mm2
			Bolt spacing			$E_{0,g,05}$	9600	N/mm2	*Plate tube:*	*S355*	
			α1	100	mm	$E_{90,g,mean}$	300	N/mm2	f_y	355	N/mm2
			α2	80	mm	$E_{90,g,05}$	250	N/mm2	f_u	490	N/mm2
			α3,t	140	mm	$G_{g,mean}$	650	N/mm2	*Material factors:*		
			α4,t	60.00	mm	$G_{g,05}$	540	N/mm2	α	0	-
			Check	GOOD	-	$G_{r,g,mean}$	65	N/mm2	kmod	0.9	-
			h_{req}	280.00	mm	$G_{r,g,05}$	54	N/mm2	γm	1.25	-
			l_{plate}	480	mm	$\rho_{g,k}$	385	kg/m3	γm0	1.00	-
						$\rho_{g,mean}$	420	kg/m3	γm2	1.25	-

Joint resistance						**Stability elements**			**Axial stiffness**		
Unity check bolts			*Unity check plate*			Material:	S355	-	K_{ser}	310861.99	N/mm
k_{90}	1.65	-	A_{net}	1760	mm2	f_y	355	N/mm2	K_u	207241.33	N/mm
$f_{h,0,k}$	25.26	N/mm2	$N_{t,Rd1}$	526400	N	A_{min}	103.75	mm2			
$f_{h,\alpha,k}$	25.26	N/mm2	$N_{t,Rd2}$	456192	N	D	12	mm			
$M_{y,Rk}$	289640.46	Nmm	$N_{c,Rd}$	413600	N	$A_{1,cable}$	113.04	mm2			
$F_{v,Rk}$	24227.58	N	U.C. (t)	0.23		$N_{t,Rd}$	40.13				
I	48491.52	N	U.C. (c)	0.25		U.C.	0.92				
II	24227.58	N									
III	27819.85	N									
n_{ef}	2.12	-									
$F_{v,Rd}$	110771.90	N									
U.C.	0.93										

Tube connection											
Unity check bolts			*Unity check plate*			*Unity check CHS*			*Weld*		
Bolt	M16	-	t	8.00	mm	D	60.30	mm	Stell	S235	N/mm2
A	201	mm2	A_{net}	322.4	mm2	t	3.20	mm	fu	360	N/mm2
A_s	157	mm2	$N_{t,Rd1}$	171.25	kN	A	574.03	mm2	βw	0.8	-
a_v	0.60	-	$N_{t,Rd2}$	113.74	kN	F_{cRd}	134.90	kN	a	5	mm
$F_{v,Rd}$ (I)	154.37	kN	$N_{c,Rd}$	114.45	kN	F_{tRd}	134.90	kN	fvw,d	207.85	N/mm2
$F_{v,Rd}$ (II)	120.576	kN	U.C. (t)	0.90		U.C.	0.76		Fw,Rd	125.33	kN
U.C	0.85		U.C. (c)	0.90					U.C.	0.82	

Appendix F: Additional information model

F.1: Loads
F.2: Semi-rigid supports
F.3: Bracing elements
F.4: Lattice system joint mechanism
F.5: Arch shape definition

F.1 Loads

All loads are applied to the primary beams (arches) of the grid. The load cases that result from snow and wind are unsymmetrical and in some cases are not applied over the full length of the arches. As described in appendix A, do several snow loads act on a length which depends on the slope of the arches. This slope varies depending on the shape of the arch. To account for this, a part is included in the Grasshopper script that measures the slope of the arch over its length. Based on this information it determines the length on which the snow loads should act. Therefore the snow load is corrected every time the arch shape is adjusted. In the Grasshopper model the loads are defined by a polyline. On each element a part of the load is vertically projected as a polylinear load. This load requires a relative position t (0<t<1) with a corresponding force. The positions are the end points of the element (0 and 1) and in some cases a position for a change of the force magnitude which is read from the polyline. The magnitude of the force is determined by the height difference of a point and a reference height. This force is than multiplied with factors concerning the beam-to-beam distance and the load combinations

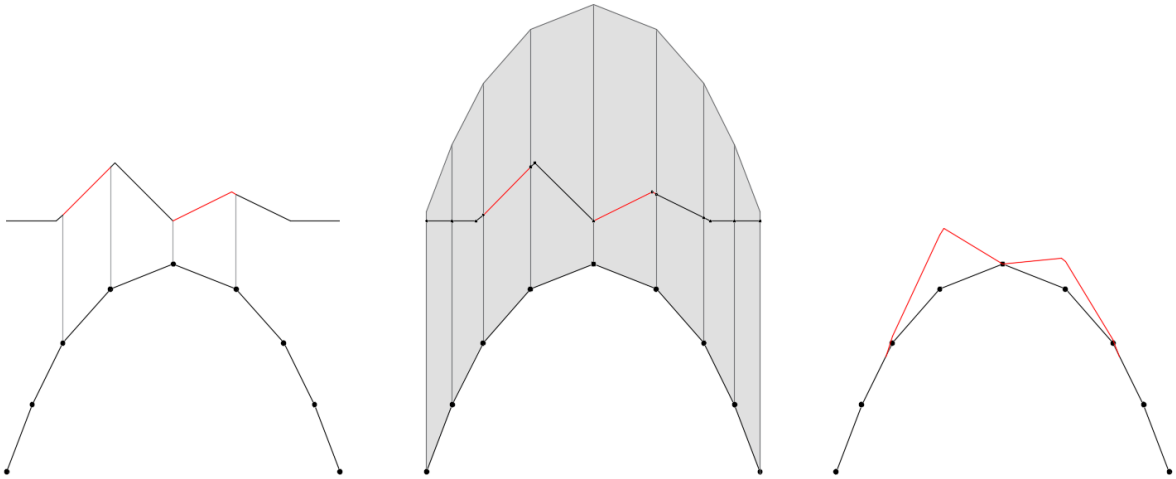

Figure F. 1 Vertical projection of load cases in Grasshopper/Karamba3D

The figure above illustrates the process for one of the snow loads as an example. The figure below shows the results of what it looks like in Grasshopper/Karamba3D. In this case the load has a global orientation. For wind the orientation is according the base surface normal.

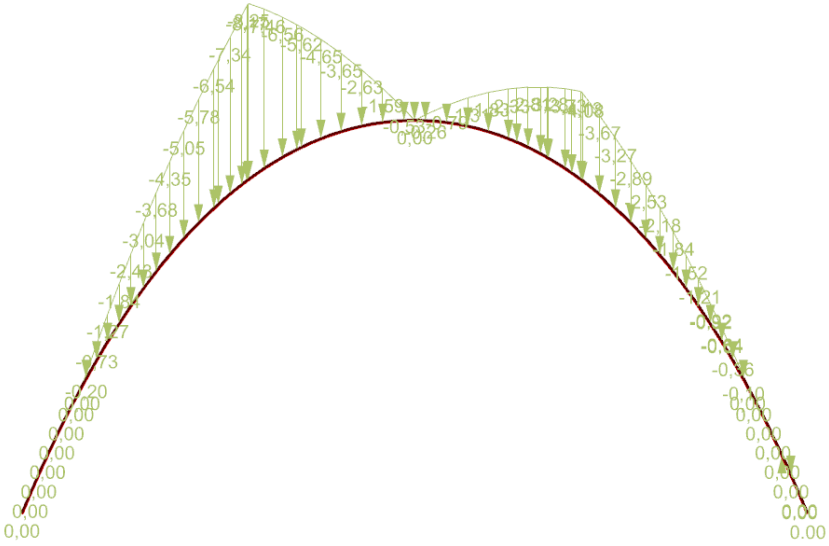

Figure F. 2 Load applied snow load in Karamba3D

F.2 Semi-rigid supports

Karamba3D does not contain a component by which the supports can be given a rotational stiffness. Therefore a beam is applied at the supports which is rigidly connected to the arch at the support, as depicted in the figure below.

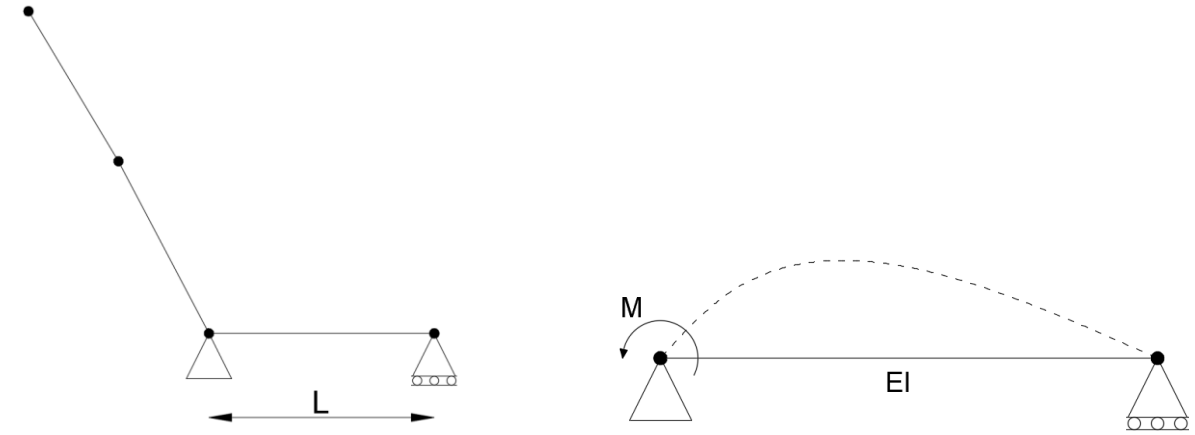

Figure F. 3 Modelling of semi-rigid supports

For a simply supported beam with a bending moment at the support, the rotation at the support where the bending moment acts can be calculated with:

$$\varphi = \frac{ML}{3EI} \tag{F.1}$$

By putting this equation in the general relation between the rotation, bending moment and rotational stiffness, this leads to the following rotational stiffness.

$$\varphi = \frac{M}{c_r} \rightarrow c_r = \frac{3EI}{L} \tag{F.2}$$

In the Grasshopper model, the beam which gives the rotational stiffness is modelled as a steel beam with a circular hollow profile. The beam's length is fixed at one meter and the wall thickness is fixed at 5 mm. The rotational stiffness is adjusted by changing the diameter of the cross-section.

F.3 Bracing elements

Between the timber grid elements, cross bracing is applied. These bracing elements are modelled in the Grasshopper model as cables, meaning that the bracing elements are only able to resist tensile normal forces. In Grasshopper the bracing elements are initially modelled as normal elements. Then using the 'modify element' component, the bending stiffness is turned off creating truss elements. Then another component is used called 'Tension/compression eliminator'. This component eliminates all elements of a certain group in which compressive or tensile normal forces appear. In this case it eliminates all bracing elements experiencing compressive normal forces.

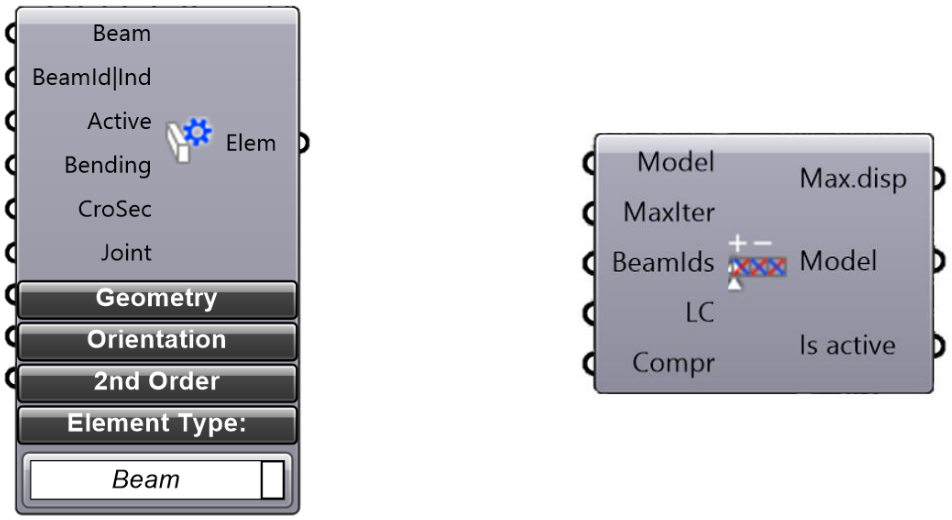

Figure F. 4 Components for creating tension-only elements

For every load combination, the elements which are eliminated is different. Therefore this process is done separately for each load combination.

F.4 Lattice system joint mechanism

In a lattice grid-shell the crossing elements can rotate along their length freely from each other. This mechanism is comparable to two scissor blades, and therefore this mechanism is called a scissor mechanism. To analyse the effect of this mechanism on the stability and internal forces in the structure this mechanism is modelled in Karamba3D. How this is done is presented in Figure F.5. First, an offset between the layers is created. The direction of this offset is in the direction of the normal vector of the base surface. At the location where the elements cross each other, another element is placed which connects the two layers. This connecting element is then divided in two parts creating a node in the middle. At his node, a hinge is applied with a rotational freedom along the z-axis. This way the elements in both directions are able to rotate along their length independently from each other.

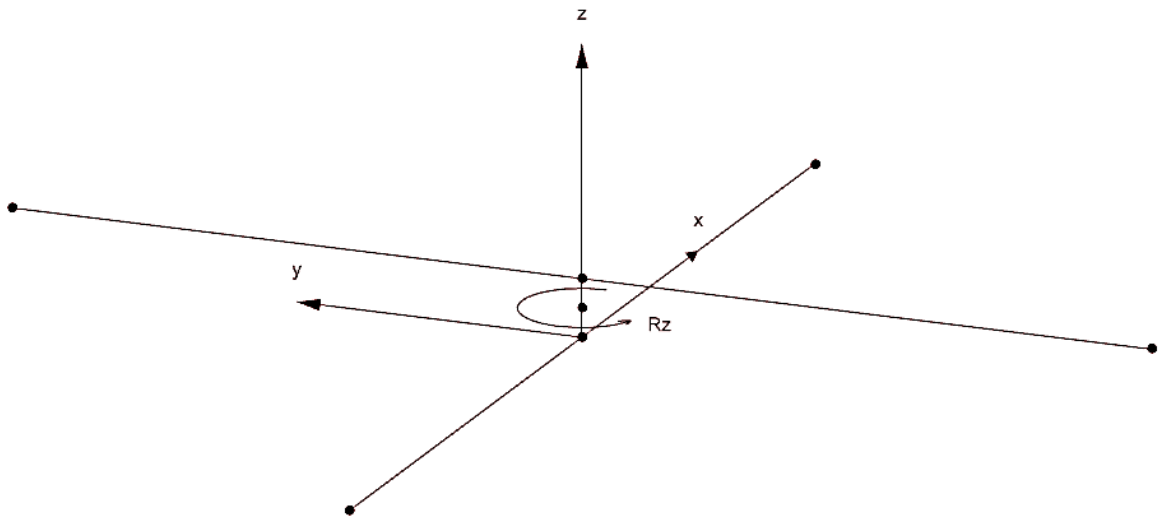

Figure F. 5 Modelling of scissor mechanism for lattice system

F.5 Arch shape definition

In this project, three common shapes for the arches have been analysed. Each of this shape is defined by an equation that have been used to model the shapes in Grasshopper. The equation corresponding to each shape is given in this section.

Catenary shape:

$$y = \frac{a}{2}\left(e^{\frac{x}{a}} + e^{-\frac{x}{a}}\right) \tag{F.3}$$

a is a parameter that determines the height of the arch

Ellipse:

$$\frac{x^2}{a^2} + \frac{y^2}{b^2} = 1 \tag{F.4}$$

In which:

a is the height of the arch
b is halve of the arch's span

Parabola:

$$y = a(x - h)^2 + k \tag{F.5}$$

In which:

a is the height of the arch
b is halve of the arch's span